U.S. Department
of Transportation
National Highway
Traffic Safety
Administration

NHTSA

DOT HS 813 740

December 2025

Safety Implications of Potential Advanced Driver Assistance Systems Sensor Degradation

This page is intentionally left blank.

DISCLAIMER

This publication is distributed by the U.S. Department of Transportation, National Highway Traffic Safety Administration, in the interest of information exchange. The opinions, findings, and conclusions expressed in this publication are those of the authors and not necessarily those of the Department of Transportation or the National Highway Traffic Safety Administration. The United States Government assumes no liability for its contents or use thereof. If trade or manufacturers' names or products are mentioned, it is because they are considered essential to the object of the publication and should not be construed as an endorsement. The United States Government does not endorse products or manufacturers.

NOTE: This report is published in the interest of advancing motor vehicle safety research. While the report may provide results from research or tests using specifically identified motor vehicle models, it is not intended to make conclusions about the safety performance or safety compliance of those motor vehicles, and no such conclusions should be drawn.

Suggested APA Format Citation:

Stowe, L., Alcazar, J., Huggins, S., Beale, G., Palmer, M., & Doerzaph, Z. (2025, December). *Safety implications of potential advanced driver assistance systems sensor degradation* (Report No. DOT HS 813 740). National Highway Traffic Safety Administration. doi:doi.org/10.21949/87jb-q591

This page is intentionally left blank.

Technical Report Documentation Page

1. Report No.	2. Government Accession No.	3. Recipient's Catalog No.
DOT HS 813 740		

4. Title and Subtitle	5. Report Date
Safety Implications of Potential Advanced Driver Assistance Systems Sensor Degradation	December 2025
	6. Performing Organization Code

7. Authors	8. Performing Organization Report No.
Loren Stowe, Javier Alcazar, Steven Huggins, Gregory Beale, Matt Palmer, Zachary Doerzaph	

9. Performing Organization Name and Address	10. Work Unit No. (TRAIS)
Virginia Tech Transportation Institute 3500 Transportation Research Plaza (0536) Blacksburg, VA 24061	11. Contract or Grant No. Contract No. DTNH2214D00328L / 693JJ919F000194

12. Sponsoring Agency Name and Address	13. Type of Report and Period Covered
National Highway Traffic Safety Administration 1200 New Jersey Avenue SE Washington, DC 20590	14. Sponsoring Agency Code

15. Supplementary Notes

Stephen Stasko was NHTSA's contracting officer's representative for this report.

Digital Object Identifier: https://doi.org/10.21949/87jb-q591

16. Abstract

The project examined the impact of degradations on advanced driver assistance system (ADAS) perception sensor performance. Sensor degradation refers to the gradual decline in a sensor's performance over time, resulting in deviations from its nominal or expected output. The scope included permanent and semi-permanent cumulative degradations affecting camera, radar, and LiDAR sensors. Degradation types were identified through a literature review and stakeholder interviews. Methods were developed to create, test, and evaluate degradations using static tests with various targets, enabling consistent assessment of different material and degradation combinations. Results helped identify the most impactful degradations and guided the selection of samples for component and vehicle-level testing. Each degradation was tested at three severity levels (high, medium, and low). Camera, radar, and LiDAR sensors and a ground truth system were mounted on a vehicle for data collection in dynamic scenarios using a target vehicle. Sensor data with and without degraded conditions were compared. While all degradations affected sensor signal paths, impacts varied. Occlusions reduced sensor response, and road grime or improper repairs significantly decreased sensor range and point returns. System level evaluation of a vehicle's ADAS with degraded sensors introduced additional challenges. Depending on how the ADAS processed degraded sensor signals and the level of redundancy (e.g., sensor fusion), system behavior ranged from feature shutdown, to ADAS performance degradation, or no impact.

17. Key Words	18. Distribution Statement
advanced driver-assistance systems, ADAS, sensor, self-diagnostics, sensor fusion, degradation, automotive sensor, radar, camera, ultrasonic, lidar	Document is available to the public from the DOT, BTS, National Transportation Library, Repository & Open Science Access Portal, https://rosap.ntl.bts.gov/

19. Security Classif. (of this report)	20. Security Classif. (of this page)	21. No. of Pages	22. Price
Unclassified	Unclassified	248	

Form DOT F 1700.7 (8-72) Reproduction of completed page authorized

This page is intentionally left blank.

Table of Contents

List of Figures

List of Tables

Acknowledgements

The research team at Virginia Tech Transportation Institute would like to thank all the people who made information gathering for this project possible. The list includes project managers, directors, subject matter experts, service and maintenance experts, and outreach personnel. These people generously donated tremendous amounts of time and were willing to share information in an effort to find ways to improve ADAS performance and to increase safety.

List of Abbreviations and Acronyms

ACC	adaptive cruise control
ADAS	advanced driver assistance system
ADS	automated driving systems
AEB	automatic emergency braking
BSW	blind spot warning
DAS	data acquisition system
dBsm	decibel square meters
DGPS	differential Global Positioning System
DOE	design of experiments
DTC	diagnostic trouble codes
ELK	emergency lane keeping
EMR	electromagnetic radiation
ESFR	edge spatial frequency response
FCW	forward collision warning
FFT	fast Fourier transform
FOV	field of view
GVT	global vehicle target
IIHS	Insurance Institute for Highway Safety
ISO	International Organization for Standardization
LCA	lane centering assist
LDW	lane departure warning
lidar	light detection and ranging
LKA	lane keep assist
LOS	line-of-sight
LRR	long range radar
MRR	medium range radar
MTF	modulation transfer function
NCAP	New Car Assessment Program
PCA	principal components analysis
POV	principal other vehicle
RCS	radar cross-section
RCSsm	radar cross section in square meters
ROS	robot operating system
SDE	standard error
SME	subject matter expert
SNR	signal to noise ratio
SRE	steel-reinforced epoxy
SRR	short range radar
STD	standard deviation
SV	subject vehicle
SVC	surround view camera
TV	target vehicle
VTTI	Virginia Tech Transportation Institute

This page is intentionally left blank.

Executive Summary

The American Automobile Association (NewsRoom.AAA.com, 2019) reported that nearly 93 percent of all new vehicle models in 2019 had at least one advanced driver assistance system ADAS are systems that help the human driver operate a vehicle with warnings, active safety assistance, and driving assistance. These include technologies such as forward collision warning, automatic emergency braking, adaptive cruise control, blind spot warning, lane departure warning, lane keep assist, and surround view cameras. In addition, the average age of vehicles on the road has increased in the last decade, reaching 12.1 years as of 2021 (IHS Markit, 2021). This combination of the prevalence of ADAS technology in the fleet and the average age of vehicles led to this project's goal of understanding the effects of long-term degradations on sensor performance and how degraded sensor performance may affect ADAS performance.

To evaluate how degradation may affect sensor performance, the study's approach is outlined in Figure 1, focusing on degradation development and component testing.

Figure 1. Project approach

The study first looked at existing research and engaged industry stakeholders to identify what long-term degradations to consider. To this set, the project team added additional degradations based on experience and technical knowledge of the sensors, perception systems, and the vehicle driving environment. The team then developed and tested a range of simulated degradations designed to replicate those degradations for a sensitivity experiment. The set included those degradations associated with cumulative effects such as scratches, dirt and debris buildup between a radar and bumper, or hard-to-remove occlusions such as tree sap or road tar.

During this phase, the researchers and NHTSA identified and procured the sensors used in the evaluation. The research focused on three primary types of sensors that represent those technologies most prevalent for more dynamic driving conditions (camera and radar) or that are emerging (lidar). We selected different sensor models that had varying price points, technologies, or, in the case of radar, operated at different frequencies. While vehicles may use other sensor technology for driver assist technology such as ultrasonic for backup assist, these tend to be short-range and low-speed applications and were not considered for evaluation.

Testing during degradation development involved static tests using a variety of targets to enable repeatable evaluation of the many combinations of base materials and degradations used. Results identified the degradations that most affected sensor performance and narrowed the degradation samples for use in component and ADAS-equipped vehicle testing.

For component testing, we designed a series of dynamic tests to evaluate sensor response while the vehicle(s) were moving. The team developed a set of test procedures using both the lateral and longitudinal subject vehicle position relative to the target vehicle. For these tests, we collected data simultaneously from two cameras, five radars, four lidars, and a ground truth

system (differential GPS). This gave common inputs for the different test conditions. Based on the results from the degradation development, we created high, medium, and low levels of each degradation of interest. The results of this collection showed varying levels of response depending on the way a degradation affected the signal path. As expected, degradations that occluded the signal path (e.g., sandblasting to simulate heavy pitting and scratching) reduced the response of the camera and lidar sensors. However, in some instances, the uncertainty in the sensor responses counterintuitively improved with the application of the degradation, likely because the degradation filtered out small signals and left signals from the most salient features of the target vehicle under the specific test conditions. For those occlusions that altered the paths of the signals, such as silicone sealant to simulate tree sap, the degradation effect was not as severe. In some instances it was observed that the sealant could potentially increase the signal return due to a lensing effect.

During stakeholder outreach, several manufacturers told us these systems were assist systems (i.e., ADAS) and that drivers were responsible for safe operation of their vehicles. As such, if a system health check revealed degraded performance, the system would be disabled. The limited system level testing reinforced this claim, particularly for FCW and AEB.

We developed several processes and procedures that may be applicable to other studies. In addition, we identified long-term degradations that may be important to consider for system level performance. That said, the way a system processes sensor signals and the level of redundancy for a system (e.g., sensor fusion) may make ADAS robust enough for the overall performance to remain unaffected by partial degradation of one sensor.

Chapter 1. Introduction

In 2019 more than 90 percent of new vehicles included some form of ADAS (AAA, 2019). Although sometimes considered convenience features, many modern ADAS technologies offer potential positive safety benefits by augmenting driver capabilities via vehicle technology (*Figure **2***). For example, AEB, which helps drivers avoid crashes by applying the brakes prior to impact, is scheduled for widespread availability across most production vehicles by 2023, per the voluntary agreement by 20 manufacturers. The National Highway Traffic Safety Administration reported that 95 percent of vehicles made by half the manufacturers offered AEB as an option. These safety-related ADAS perceive the driving environment by applying signal-processing methods to data captured by vehicle-mounted sensors. ADAS performance relies on both the quality of the raw sensor data and the ability of downstream algorithms to accurately identify and respond to objects of interest. Thus, safety depends on reliable sensor data as well as robust ADAS algorithms.

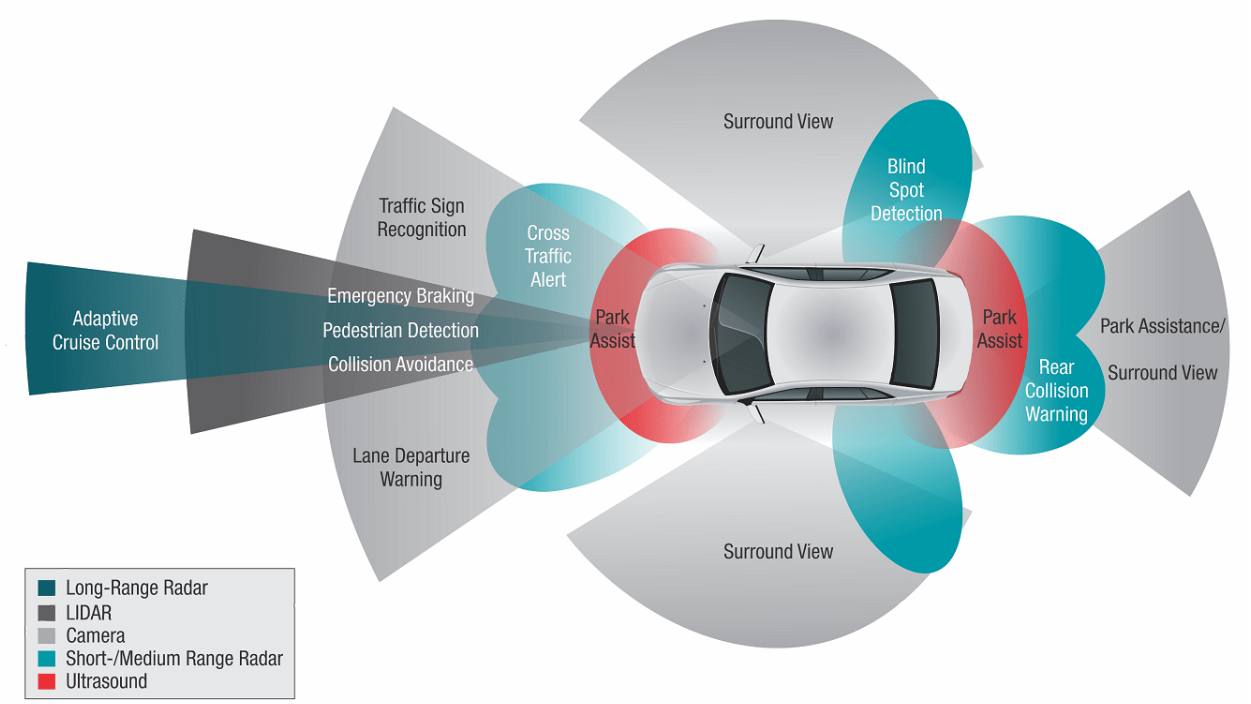

Figure 2. Typical ADAS sensors (AAA, 2018)

The names and zones in Figure 2 correspond to the sensor's job or function (AAA, 2018). For example, the function "collision avoidance" corresponds to the ADAS "forward collision warning." The function "emergency braking" is related to ADAS "automatic emergency braking," and the function "pedestrian detection" is related to ADAS "pedestrian automatic emergency braking." It is worth mentioning that AEB makes the vehicle brake, as compared to forward collision warning, which is only intended to alert the driver. Although some FCW systems briefly pulse the brakes as part of their alert cascade, they do so with the intention of notifying the driver of a safety critical event, not to provide a meaningful speed reduction.

Once ADAS technologies are deployed in the fleet, sensor output may be affected by degradation from temporary conditions (e.g., debris on the sensor), cumulative wear and tear (e.g., scratches and lens discoloration), and sudden degradation (e.g., collisions that affect alignment and/or calibration). These degradations may adversely impact system performance. However, there is not much publicly available, robust research about degradation and best practices to proactively mitigate its potential effect on safety. Given the proliferation of ADAS-equipped vehicles, characterizing the impact that sensor degradation might have on ADAS performance is an important step in ensuring safe ADAS operation throughout the service life of the vehicle.

This project's goal was to increase understanding of the operational, performance, reliability, and maintenance issues associated with ADAS sensors. ADAS used to be found on high-end, luxury vehicles, but the rapid proliferation of ADAS across vehicles available in the 2019/20 model years is apparent (Sinclair, 2019). Advanced features such as blind spot detection and lane departure warning are now standard on many entry-level vehicles, and 20 automakers are working to make AEB a standard feature by 2022. Even cutting-edge features such as lane centering assist coupled with adaptive cruise control are providing SAE Level 2 driving automation (SAE, 2018) at accessible price points. Thus, it is important to investigate the role of sensor degradation on ADAS performance.

Scope and Assumptions

Working with NHTSA and stakeholders, who provided insight into particular areas of industry interest, we defined the project scope and assumptions as follows. The project:

- Focuses on perception sensors rather than more traditional sensors such as wheel speed and throttle position that also provide input for ADAS but tend to be better understood and have more deterministic outputs.
- Investigates radar and camera sensors as the primary sensors used in currently deployed ADAS and those likely to be deployed in the near future. Lidar is also examined as it is a sensor entering production and being deployed in a growing number of vehicle platforms. Ultrasonic and infrared sensors are not included in the scope of this study.
- Is primarily interested in permanent degradations that accumulate over time rather than those that are more transient. We were particularly interested in degradation that occurs from real-world exposure that may not be captured in typical component durability testing, such as environmental chambers for water intrusion, vibration, and heat.
- Excludes the following degradations

  (1) low voltage or other upstream signal inputs feeding the sensor (e.g., the speed signal into a radar);
  (2) electronic degradations due to incorrect calibration and remote software updates (e.g., those distributed over-the-air without proper validation);
  (3) factors that are easy to self-diagnose and are already addressed by industry (e.g., complete sensor malfunction); and
  (4) potential interference between sensors on several equipped vehicles. These sources of degradation were beyond the project scope.

- Focuses on sensor performance rather than perception performance. Sensor performance does not necessarily correlate directly to ADAS performance. How the system processes sensor data and what additional inputs it uses also determines ADAS performance. Each manufacturer has different ADAS implementations it installs in vehicles. Though the study did test some ADAS features, evaluating the performance of all the ADAS systems on the market to assess the general effect of degradations on ADAS was beyond the scope of the project.

Project Structure

Chapter 2 discusses the project's literature review, and Chapter 3 presents results from stakeholder engagement, which provided information on the current state of knowledge on degraded sensor performance, test methods, and industry areas of interest, including degradations, test conditions, and general project insights. We defined a three-tiered approach to evaluate the effect of degradations on ADAS (Figure 3):

- degradation development (Chapter 4),
- degraded sensor component-level testing (Chapter 5), and
- degraded system-level testing (Chapter 6).

Chapter 7 lists conclusions from the research. To be flexible and resource-efficient, each step was informed by the activities in the prior step. For example, if component-level testing showed a sensor was not affected by a given degradation, the degradation was not tested during the system-level testing step. We focused primarily on the first two steps of degradation development and component testing.

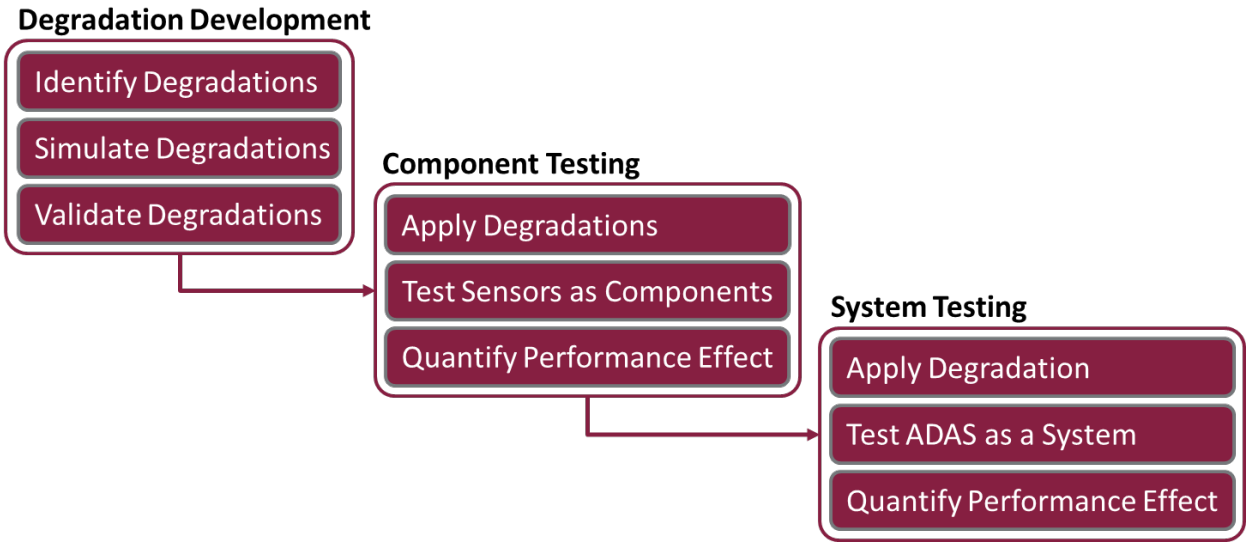

Figure 3. Overall test approach

This page is intentionally left blank.

Chapter 2. Literature Review

Literature Review

The literature review evaluated published knowledge about sensor degradation. These sources we reviewed are listed in the Bibliography section. This section presents the major findings of the literature review and discusses how these findings were applied to the sensor degradation project as a whole.

Market Survey

The market survey focused on current ADAS technologies and sensors available in the market. First, a generic overview of ADAS features and sensors found in the literature is provided. Then the material is presented from two perspectives, sensor-based and system-based. The sensor-based approach focuses on the capabilities of the sensors and the ADAS functions they support. The system-based approach looks at specific ADAS from an overall feature perspective.

Overview: ADAS Features and Sensors

More and more vehicles coming onto the market are equipped with ADAS features. Figure 2 shows an example of several vehicle functions and their associated sensors. Table 1 lists vehicle functions along with the set of exemplary sensors used and the area the sensors cover. The names and zones in Figure 2 correspond to the sensor's job or function (AAA Automotive, 2018).

Table 1. Vehicle Functions, Typical Sensors Used, and Areas Covered by Sensor

Vehicle Function	Common Sensors Used	Areas Sensed
Adaptive Cruise Control	Radar	Front
	Camera	
Lane Departure Warning	Camera	
	Lidar	
Traffic Sign Recognition	Camera	
Park Assist	Ultrasonic	Front, Rear
Blind Spot Detection	Camera	Rear
	Radar	Rear
Surround View	Camera	Front, Rear, Sides
Emergency Braking	Radar	Front
	Camera	
Pedestrian Detection	Camera	
	Radar	
Collision Avoidance	Radar	
	Camera	
	Lidar	

Automotive suppliers build production sensors to meet durability specifications that are sometimes, but not always, defined by vehicle manufacturers. These specifications are evaluated using standard test methods such as those of ASTM International, Institute of Electrical and Electronics Engineers, and SAE International, as well as novel test methods based on internal company practices.

Through the literature review below and preliminary conversations with industry stakeholders, we confirmed that real-world performance of sensors may degrade for reasons not anticipated under current development and testing methods, just like other cutting-edge technology. However, the research indicated that the implications of degraded sensors were not well understood, particularly when output of several sensor systems are fused together. There is concern that appropriate ADAS sensors may not function for the duration of a vehicle's increasing service life, which could affect safety and increase repair costs. This concern formed the motivation for this research.

Sensors

From a sensor perspective, typical ADAS sensors are radar, camera, and ultrasonic. The demand for more technically advanced sensors has recently brought new suppliers to the market. *Automotive News* (Chappell, 2019) reported the top 100 suppliers ranked by sales of original equipment parts but did not report sales by the type of sensor. Due to this lack of information, it is challenging to select a representative sample for each type of sensor without additional input from the industry.

Therefore, for each sensor type a small reasonably representative sample based on publicly available information is listed. This list is not complete, nor does it represent the sensors we selected for testing. A sample of vehicle manufacturers along with the ADAS features they support is also listed. Specifications for sensors were acquired from data sheets (footnoted below) when available on the company's webpage. These specifications were used to frame the discussion in the Test Methods and Metrics section. We emphasize that our market search was not exhaustive, as this would require efforts that are beyond the project's scope or resources.

There are many other ADAS sensors we don't discuss in this literature review. For example, ADAS may use engine control sensors, wheel-speed sensors, and other comparable "traditional" sensing systems. Consideration of them was beyond the scope of this work, which is specifically focused on the sensors that enable perception of the outside environment, not something inside the vehicle. This decision was made after discussions with members of the automotive industry and based on an assumption that degradation of the more traditional sensors is well understood, and the industry is already aware of the consequences of their degradation.

Radar

An automotive radar is an active sensor. It sends out an electromagnetic wave that is reflected back by objects in its surroundings. The time of flight is used to estimate the distance to objects, and the doppler effect is used to estimate object motion.

According to MarketsandMarkets Research (2019):

> The automotive radar market consists of various major system and chip manufacturers. Companies such as Robert Bosch GmbH (Germany), HELLA KGaA (Germany), Continental AG (Germany), Denso Corporation (Japan), Delphi Automotive PLC (U.K.), Autoliv Inc. (Sweden), and Valeo S.A. (France) are the system manufacturers and companies such as Infineon Technologies AG (Germany), NXP Semiconductors N.V. (The Netherlands) are the chip manufacturers in this market.

Depending on sensing range, radars can be classified into long-range radars, mid-range radars, and short-range radars. A sample of automotive radar suppliers, types, models, and associated supported ADAS features are shown in Table 2.

Table 2. Sample of Automotive Radars

Maker	Subtype	Model	ADAS Features	Source
Robert Bosch GmbH	LRR	LRR4	Predictive Emergency Braking System Adaptive Cruise Control Traffic Jam Assist Left Turn Assist Integrated Cruise Assist Evasive Steering Support	Fourth generation long-range radar sensor LRR4[1] (2014 Datasheet)
	MRR	MRR	Predictive Emergency Braking System Adaptive Cruise Control Heading Distance Indicator	Mid-range radar sensor (MRR) for front and rear applications[2] (2015 Datasheet)
		MRR-rear	Lane Change Assist Rear Cross Traffic Alert	
Continental AG	LRR	ARS441	Adaptive Cruise Control Emergency Brake Assist Forward Collision Warning	ARS 441 Long Range Radar (2020 Datasheet)
		ARS510	Adaptive Cruise Control Emergency Brake Assist Traffic Continuous Indication Traffic Jam Assist (combined with camera)	ARS 510 Long Range Radar (2020 Datasheet)
		ARS540	Highly Automated Driving Classification of Traffic Participants and Infrastructure Vulnerable Road User Detection	ARS 540 Long Range Radar[3] (2020 Datasheet)
	SRR	SRR520	Blind Spot Warning Lane Change Assist Rear Cross Traffic Alert Front Cross Traffic Alert Rear Pre-Crash Sensing	SRR 520 Short Range Radar[4] (2020 Datasheet)

[1] https://fccid.io/ANATEL/00716-15-03745/Manual-LRR4/31C2FFEF-4EE5-4249-953F-247858F6FF0F/PDF
[2] https://www.atleducation.org/wp-content/uploads/curriculum/adas/product-data-sheet-mid-range-radar-sensor-(mrr-rear).pdf
[3] https://www.continental-automotive.com/en/components/radars/long-range-radars/advanced-radar-sensor-ars540.html
[4] https://www.continental-automotive.com/en-gl/Trucks-Buses/Vehicle-Chassis-Body/safety-topics/Product-Portfolio/SRR520-Short-Range-Radar-CV

Camera

Current automotive cameras used in ADAS are passive sensors. They monitor and capture electromagnetic waves in the visible range for further processing.

According to Allied Market Research (2020):

> The key market players … are Automation Engineering Inc., Robert Bosch GmbH, Continental AG, Aptiv PLC, Stonkam Co., Ltd., Mobileye N.V., Autoliv Inc., Magna International Inc., OmniVision Technologies, and Valeo.

ADAS cameras can be classified into mono and stereo camera categories. Mono cameras, as the name implies, use a single camera to sense the environment. Stereo cameras typically use two cameras to resolve depth in a manner similar to that of human vision. Subaru (2012) introduced this technology in the United States for ADAS features in 2012. From the reported key market players (Allied Market Research, 2020), a sample of automotive cameras available to the market is shown in Table 3.

Table 3. Sample of Automotive Cameras

Maker	Subtype	Model	ADAS Features	Source
Robert Bosch GmbH	Mono	Multi-Purpose Camera	Lane Departure Warning Lane Keeping Assist Road Sign Assistant Intelligent Headlight Control Automatic Emergency Braking Predictive Pedestrian Protection Traffic Jam Assist Highway Assist Left Turn Assist	Multi-purpose camera.[5] (Web page)
	Mono	Near Range Camera	Rear View System Multi-Camera System	Near-range camera systems[6] (Web page)
	Stereo	Stereo Video Camera	Lane Departure Warning Lane Keeping Assist Road Sign Assistant Intelligent Headlight Control Automatic Emergency Braking	Stereo video camera[7] (Web page)

[5] www.bosch-mobility.com/en/solutions/camera/multi-purpose-camera/
[6] www.bosch-mobility.com/en/solutions/camera/near-range-camera/
[7] www.bosch-presse.de/pressportal/de/en/stereo-video-camera-125253.html

Maker	Subtype	Model	ADAS Features	Source
Continental AG	Mono	MFC500	Lane and Road Departure Protection Emergency Brake Assist Adaptive Cruise Control Head Light Assist Traffic Sign Assist Traffic Light Recognition Unsteady Driving Warning	Cameras MFC500[8] (2020 Datasheet)
Mobileye Global, Inc.	Mono	8 Connect EyeQ4	Forward Collision Warning Urban Forward Collison Warning Lane Departure Warning Pedestrian and Cyclist Collision Warning Headway Monitoring and Warning Speed Limit Indication	The Mobileye 5-Series Technical Specifications[9] (2011 Datasheet)

Thermal Camera

Thermal cameras are designed to capture images in the infrared range of the electromagnetic spectrum and can provide heat maps from surrounding objects.

Thermal cameras are emerging as a potential sensing technology for ADAS. They have been used in vehicles to improve situational awareness for the drivers, but none were identified in current production vehicles. However, the company FLIR[10] does offer a thermal vision automotive development kit (FLIR, 2020) and is facilitating testing and development of ADAS leveraging thermal cameras.

Ultrasonic

Ultrasonic sensors are active sensors. They transmit a sound wave that is reflected from objects encountered in its surroundings. The time of flight of the emitted sound wave is used to estimate distance to objects. Ultrasonic sensors are considered good short distance sensors, and a typical application involves parking functions. A sample of automotive ultrasonic sensors and ADAS features implemented on the market is provided in Table 4.

[8] www.continental-automotive.com/en/components/cameras/multi-function-mono-camera-mfc527.html
[9] http://tracksurveying.com/sensorica/pdf/Mobileye%205%20-%20Full%20Technical%20Spec%20v0.3.pdf
[10] Founded in 1978, FLIR Systems acquired companies such as Agema (Sweden), Inframetrics (Boston, MA), and Indigo Systems, before becoming acquired by Teledyne Technologies in 2021. It was then rebranded as Teledyne FLIR.

Table 4. Sample of Automotive Ultrasonic Sensors

Maker	Model	ADAS Features	Source
Texas Instruments	TIDA-00151	Blind Spot Detection Park Assist	Automotive Ultrasonic Sensor Interface for Park Assist or Blind Spot Detection Systems. TIDA-00151[11] (2014 Datasheet)
Robert Bosch GmbH	Generation 6	Maneuver Assist (With Camera) Remote Park Assist (With Camera) Homezone Park Assist (With Camera or Radar)	Ultrasonic-Base Driver Assistance Systems.[12] (2018 Datasheet)
Valeo Service	Beep & Park Park Vision	Parking Assistance System Parking Assistance System (With Rear Camera)	Parking Assistance Sensors: O.E. Ultrasonic Technology Available for the International Aftermarket[13] (Web page)

Lidar

Lidar is an active sensor that emits a light and measures the time of flight to return to its source. The time measured is used to estimate distance to surrounding objects. Radars, cameras, and ultrasonic sensors are readily identifiable as primary data sources empowering ADAS features in current vehicles on the market. Lidar systems, on the other hand, are a dominant data source being tested on prototypes and concept vehicles aiming for higher levels of automation (i.e., SAE driving automation Level 4 and Level 5).

Fueled primarily by the potential ADS market for advanced perception sensors, there are more than 200 lidar startups in the automotive industry (Tracxn, 2020). As of December 4, 2019, the top 10 automated vehicle lidar startups were: Velodyne Acoustics GmbH;[14] LeddarTech Holdings, Inc.; Luminar Technologies, Inc.; Innoviz, Ouster, Inc., Quanergy, AEye, Blacksmore, TriLumina and Cepton. The top seven were selected to constitute a sample of lidar sensors for automotive use, as shown in Table 5.

[11] TIDA-00151 reference design | TI.com
[12] https://atleducation.org/wp-content/uploads/curriculum/adas/product-data-sheet-ultrasonic-sensors-generation-6.pdf
[13] www.valeoservice.com/en-com/passenger-car/switches-and-detection-systems/valeo-parking-assistance-sensors-oe-ultrasonic
[14] In February 2023 Velodyne merged with Ouster, with the combined company keeping the name Ouster.

Table 5. Sample of Automotive Lidar

Maker	Model	Notes	Source
Velodyne Acoustics GmbH	Puck VLP-16	Mechanical	Four Puck datasheets[15] (2020 Datasheets)
LeddarTech	LCA2	Solid State	LCA2 LeddarCore[16] (2021 Datasheet)
Luminar Technologies	Iris Hydra		Luminar Technologies[17,18] (Web Page and 2020 Datasheet)
Innoviz	InnovizPro	MEMS	InnovizPro High Performance Solid State Lidar SOP[19] (2020 Datasheet)
Ouster	OSO OS1 OS2	Ultra-wide view Mid-range Long-range	OS0 Ultra-Wide View[20], OS1 Mid Range[21], and OS2 Long Range High-Resolution Imaging Lidars[22], (2025 Datasheets)
Quanergy	M8	Solid State	Quanergy[23] (2022 Datasheet)
AEye	AE110 AE200	Solid State	AEye Lidar Products[24] (Web page)

From a production ADAS perspective, as of the writing of this report, there were only a few vehicles offered to the general public with lidar technology, and vehicle manufacturers have expressed differing predictions regarding future implementations.

ADAS

The perception sensors described in the previous section are part of broader vehicle systems that enable ADAS features. These ADAS features incorporate numerous additional system

[15] https://data.ouster.io/downloads/datasheets/velodyne/Puck%20Datasheets.zip
[16] https://leddartech.com/app/uploads/dlm_uploads/2021/03/Data-Sheet_LCA2-SoC_V4.0_EN.pdf
[17] https://levelfivesupplies.com/product/luminar-iris-lidar/
[18] https://levelfivesupplies.com/wp-content/uploads/2020/08/Luminar-Hydra-Datasheet.pdf
[19] https://innoviz.tech/wp-content/uploads/dlm_uploads/InnovizPro-datasheet_12-19.pdf
[20] https://data.ouster.io/downloads/datasheets/datasheet-rev7-v3p1-os0.pdf
[21] https://data.ouster.io/downloads/datasheets/datasheet-rev7-v3p1-os1.pdf
[22] https://data.ouster.io/downloads/datasheets/datasheet-rev7-v2p5-os2.pdf
[23] https://quanergy.com/wp-content/uploads/M8-Prime-Series-2022.pdf
[24] www.aeye.ai/products/

components such as traditional sensing technologies (e.g., wheel speed sensors) and control systems (e.g., throttle, brakes). For the purpose of the project, and this associated literature review, all components are considered as a single system. Our focus is developing an understanding of how the degradation of one of the aforementioned perception sensors impacts the performance of the entire ADAS.

Depending on the ADAS implementation, one or more perception sensors may be involved. ADAS features involving two or more sensors are more likely to run sensor fusion. "Sensor fusion is the process of merging data from multiple sensors to reduce the amount of uncertainty that may be involved in a robot navigation motion or task performing. Sensor fusion helps in building a more accurate world model in order for the robot to navigate and behave more successfully" (Tzafestas, 2014).

In many instances fundamentally comparable ADAS features have numerous brand names, which can lead to confusion regarding the functionality of a given feature. The names and acronyms for some ADAS features, such as ACC, has converged to form a relatively common vernacular among researchers. In other examples such as a lateral control ADAS feature, the examples of those presently used include lane centering, lane keep assist, Autopilot, Super Cruise, Blue Cruise, ProPILOT Assist, traffic jam assist, etc. In addition, even though it may seem to those less familiar with the technology that these systems have similar functionality, their actual operation may differ in significant ways.

Thus, of all the ADAS technologies on the market, this report focuses on prevalent ADAS features that generally behave the same (i.e., have similar goals). We use common names to describe ADAS features that are also supported by the standards community (SAE International, 2015b) when possible. ADAS features on the market along with sample vehicle manufacturers and models are listed below.

FCW

An FCW system detects an impending collision and alerts the driver. Most FCW systems focus on vehicle-to-vehicle collision, although some might include pedestrian or other object detection but present a comparable warning to the driver regardless of the object sensed. The typical sensor used is radar and depending on the implementation one or more cameras may be used. Many vehicles on the market are equipped with FCW; Table 6 shows 10 representative cars with low-cost FCW available from most major manufacturers for some time (Krome, 2016).

Table 6. Market Survey of Vehicles With FCW (Krome, 2016)

Make	Model	Year
Chevrolet	Spark	2016
Chrysler	200	
Dodge	Challenger	
Mazda	3	
Ford	Taurus	
Volkswagen	Golf	
Nissan	Altima	
Toyota	Prius	
Kia	Soul	
Hyundai	Elantra	2017

AEB

AEB detects an impending forward crash and brakes the vehicle in time to avoid or mitigate the crash. If the driver does not respond or the response is insufficient to an FCW alert to avoid the crash, AEB may automatically apply the brakes to help prevent or reduce the severity of the crash. Most AEB systems are designed to address lead vehicles; however, as with FCW, they may also address pedestrians and other objects. The typical sensors are camera-based; however, depending on implementation, they could also use radar. There are many vehicles on the market with AEB. Table **7** shows the percentage of vehicles that have AEB as reported by NHTSA (2020) at the end of 2020.

Table 7. Percentage of Vehicles With AEB (NHTSA, 2020)

Manufacturer	% Reported in 2020	Manufacturer	% Reported in 2020
Tesla	100	Honda	94
Volvo	100	Nissan	93
BMW	99	Ford	91
Audi	99	Kia	75
Subaru	99	Porsche	55
Volkswagen	98	Maserati	48
Mercedes-Benz	97	General Motors	47
Toyota	97	Mitsubishi	39
Mazda	96	FCA	14
Hyundai	96	Jaguar Land Rover	0

ACC

ACC is a relatively mature ADAS feature that maintains a set speed and automatically adjusts the vehicle speed to maintain a safe distance from vehicles ahead. This technology uses sensor information from onboard sensors such as radar or cameras, allowing the vehicle to brake and accelerate to maintain a constant headway to a lead vehicle (SAE International, 2014). Newer vehicles tend to have the full speed range variant of ACC, which can bring the vehicle to a full stop during stop-and-go traffic. Many vehicles have ACC, and virtually all with ACC will also have FCW. Table 8 shows a sample of 2019 vehicle models supporting ACC down to a stop (Mays, 2019).

Table 8. Market Survey of 2019 Vehicles With ACC Down to a Stop (Mays, 2019)

Make	2019 Models
Alfa Romeo	Giulia, Stelvio
Audi	A3/S3/RS3
BMW	I3, X1, X6, Z4
Buick	Enclave, Envision, LaCrosse, Regal, Regal TourX
Cadillac	ATS, CTS, Escalade, Escalade ESV, XT4, XT5, XTS
Chevrolet	Blazer, Equinox, Impala, Malibu, Malibu Hybrid, Traverse, Volt
Chrysler	300, Pacifica, Pacifica Hybrid
Dodge	Charger, Durango

Make	2019 Models
Ford	Expedition, Fusion, Fusion Energi, Fusion Hybrid, F150
GMC	Arcadia, Terrain
Hyundai	Elantra GT, Ioniq Electric, Santa Fe, Santa Fe XL, Sonata, Sonata Hybrid, Sonata Plug-in Hybrid, Tucson
Infiniti	Q70, QX30, QX60, QX80
Jaguar	XE, XF, XJ, E-Pace
Jeep	Cherokee, Compass, Grand Cherokee, Wrangler
Kia	Cadenza, Optima, Optima Hybrid, Optima Plug-in Hybrid, Sedona, Sorento
Land Rover	Discovery Sport, Range Rover Evoque
Lexus	LX, NX, NX Hybrid
Lincoln	Continental, MKZ, MKZ Hybrid, Navigator
Mazda	3, 6, CX-3, CX-5, CX-9
Mercedes-Benz	CLA-Class, GLA-Class, G-Class, SLC-Class
Mini	Clubman, Countryman, Cooper S E Countryman plug-in hybrid
Mitsubishi	Outlander, Outlander PHEV, Eclipse Cross
Nissan	Armada, Maxima, Murano, Pathfinder, Sentra
Porsche	718 Boxster, 718 Cayman, 911, Panamera, Panamera E-Hybrid, Panamera Sport Turismo, Panamera Sport Turismo E-Hybrid, Macan
Ram	1500, 2500, 3500
Subaru	Ascent, Crosstrek, Forester, Impreza, Legacy, Outback, WRX
Toyota	Avalon, Avalon Hybrid, Camry, Camry Hybrid, C-HR, Prius, Prius Prime
Volkswagen	Arteon, Atlas, e-Golf, Golf, Golf Alltrack, Golf GTI, Golf SportWagen, Jetta, Tiguan

Blind Spot Detection

Most blind spot detection ADAS use sensors mounted near a vehicle's side view mirrors to monitor the blind spots beside the vehicle. Blind spot detection sensors may include ultrasonic, cameras, radar, or a combination. Many vehicles on the market have blind spot detection. Table 9 shows 10 cars with blind spot warning systems (Threewitt, 2020).

Table 9. Market Survey of 2016 Vehicles With Blind Spot Detection (Threewitt, 2020)

Make	Model
Hyundai	Genesis
Mazda	Mazda3
Chevrolet	Cruze
Mercedes-Benz	E-Class
Ford	Focus
Honda	Fit
Volvo	S60
Dodge	Charger
Nissan	Maxima
Cadillac	ATS

LDW, LKA, and LCA

LDW monitors the vehicle's lane position and alerts the driver when departure from the lane boundaries has occurred or is imminent. Both LKA and LCA add active lateral control of the vehicle. LKA provides control inputs to help prevent departures over the lane edges (SAE International, 2015b). In contrast, LCA is designed to keep the vehicle centered in the lane. Coupled with ACC, LCA may allow Level 2 driving automation, as defined by SAE International (2021). SAE L2 driving automation requires the driver to remain attentive and in control of the vehicle at all times. Most systems evaluate driver attentiveness through the steering wheel, thereby requiring the driver keep their hand(s) on the steering wheel at all times. While cameras are the most common sensor used to implement LKA and LCA, there are many vehicles on the market with some variant of LCA. Table 10 shows a sample of vehicles with lane centering and ACC, both down to a stop (Mays, 2019).

Table 10. Market Survey of Vehicles With Lane Centering and ACC Down to a Stop (Mays, 2019)

Make	2019 Models
Acura	RLX, RLX Sport Hybrid
Audi	A4/S4, A5/S5/RS5, A6, A7, A8, e-tron, Q5/SQ5, Q7, Q8
BMW	5 Series, 5 Series plug-in hybrid (530e), 6 Series, 7 Series, 7 Series plug-in hybrid (740e), X3, X4
Ford	Edge
Hyundai	Nexo
Infiniti	QX50
Kia	Niro EV, K900
Lexus	GS, RX, RX Hybrid, LC, LC Hybrid, ES, ES Hybrid, LS, LS Hybrid, UX, UX Hybrid
Lincoln	Nautilus
Maserati	Ghibli, Levante, Quattroporte
Mercedes-AMG	GT 4-Door
Mercedes-Benz	A-Class, C-class, C-Class Plug-in Hybrid (C350e), E-class, S-Class, CLS-Class, GLC-Class, GLC-Class Plug-in Hybrid (GLC350e), GLE-Class, GLS-Class, SL-Class
Nissan	Altima, Leaf, Rogue, Rogue Sport
Porsche	Cayenne, Cayenne E-Hybrid
Tesla	Model 3, Model S, Model X
Toyota	Corolla Hatchback, RAV4, RAV4 Hybrid
Volvo	S60, S90, V60, V90, V90 Cross Country, XC40, XC60, XC90

Parking Assist System

Parking assistance is an ADAS feature that aids the driver during parking maneuvers. Depending on the sensors and algorithms employed, the level of assistance can range from low (driver inside vehicle being assisted via auditory sounds) to fully self-parking (driver able to step out of the vehicle and command the vehicle to park itself). The preferred short distance sensor used for parking ADAS features is ultrasonic due to its low cost and high reliability. There are many

vehicles on the market with parking assist systems. Table 11 shows 10 cars with active park assist (Gold, 2016).

Table 11. Market Survey of 2019 Vehicles With Park Assist (Gold, 2016)

Make	Model(s)
Lincoln	MKC
Lincoln	Navigator
Jeep	Cherokee
Lexus	LS 460
Toyota	Prius
Ford	Focus Titanium
Jaguar	XE
Land Rover	Range Rover
Cadillac	CTS
Volvo	S90

Rear Cross Traffic Alert

Rear cross traffic alert warns the driver if one or more vehicles are about to enter their backing path via sounds or images. Rear cross traffic alert systems typically activate when the driver puts the vehicle's transmission into reverse gear. Rear cross traffic alert sensors include ultrasonic, camera, and radar. Table 12 shows vehicles with rear cross traffic alert (Cartelligent, 2018).

Table 12. Market Survey of 2018 Vehicles With Rear Cross Traffic Alert (Cartelligent, 2018)

Make	2019 Models
Acura	TLX, ILX, RLX, RDX, MDX, NSX
Audi	A3, A4, A5, A6, A7, A8, Q3, Q5, Q7, TT
BMW	2 Series, 3 Series, 4 Series, 5 Series, 7 Series, X1, X2, X3, X4, X6, I3, I8
Buick	Lacrosse, Encore, Envision, Enclave, Regal
Chevrolet	Cruze, Malibu, Impala, Volt, Bolt EV, Trax, Equinox, Traverse, Tahoe, Suburban, Camaro, SS
Dodge	Charger, Challenger, Durango, Grand Caravan
Ford	Focus, Fusion, Ecosport, Escape, Edge, Flex, Explorer, Expedition, F-150
Genesis	G90, G80
Infiniti	Q50, Q60, Q70, QX50, QX60, QX80
Jaguar	I-Pace, XF, XJ
Jeep	Wrangler, Compass, Renegade
Land Rover	Discover, Range Rover, Range Rover Sport, Evoque
Lexus	IS, ES, GS, LS, NX, RX, GX, LX, RC, LC
Mercedes-Benz	C-Class, E-Class, S-Class, GLS
Nissan	Sentra, Altima, Maxima, Leaf, Rogue Sport, Murano, Pathfinder, Titan
Subaru	Impreza, Legacy, Crosstrek, Forester, Outback, WRX
Toyota	Camry, Avalon, Sienna, Tundra, C-HR, RAV4, Highlander, Sequoia, Land Cruiser, Prius

Make	2019 Models
Volkswagen	Tiguan, Jetta, Passat, Golf, Golf Alltrack, Beetle
Volvo	XC90, XC60, XC40, V60, V90, S90, S60

Sensor Degradation

The following sections synthesize our understanding of ADAS sensor degradation and its associated effects across the sources in this literature review. The team did not identify a robust body of research to provide a clear understanding of the ADAS sensor degradation space. This outcome suggests research is needed to better understand the domain. Therefore, this section expands beyond simply reporting the existing literature and includes information about the study's approach to sensor degradation. This approach was further refined after discussions with industry during stakeholder interviews and was validated during test plan development.

Degradation Sources

Several factors can cause sensor degradation. Weather conditions are one of the most studied degradations that reduce sensor performance. For instance, long-range infrared-based, and millimeter-wave radar sensors have difficulty in adverse weather such as mist, rain, freezing rain, ice pellets, snow, hail, and fog due to the interaction of electromagnetic waves with water particles in the surrounding environment. The build-up of materials, such as grit, dirt, snow, and water films on sensor surfaces can also interfere with electromagnetic waves (Arage Hassen, 2006).

Vehicle sensors may also be exposed to harsh working conditions such as extreme temperatures, high humidity, adverse chemical exposure, strong vibration, electromagnetic interference, and exposure to environmental pollution, depending on their mounting locations (Wang et al., 2008) and operational environment. These conditions can cause sensors to abruptly malfunction due to issues such as loss of power or communications from corroded contacts, and sensing element wear can result in problems such as drift and precision deterioration (Jiang et al., 2007). Beyond environmental and working conditions, other causes of sensor degradation include physical damage to the sensors from scratches, pitting, yellowing, fogging, contamination, or low-impact collisions.

Degradation can negatively affect sensor performance. In general, vehicles rely on sensor measurements as inputs to the control logic that determine the state of the vehicle and its surroundings before relying on the appropriate commands to control the vehicle systems. If sensor degradation causes sensor faults, incorrect information could be sent to the control logic, resulting in suboptimal vehicle responses. In the case of adverse weather conditions and debris on the sensor surface, the sensor may not be able to accurately detect other vehicles and objects on the road (Seppelt et al., 2005).

A key aspect of this project was identifying variables and metrics related to sensor and system evaluation, as well as characterizing the general relationship between sensor performance and system performance. As described in the Market Survey section, the primary sensors in use today are camera, radar, and ultrasonic sensors, which are non-contact sensors using propagating electromagnetic radiation to estimate the physical attributes of objects surrounding the vehicle. The propagation of EMR may be attenuated and/or deflected as it travels through different mediums or comes into contact with the interface between media. For radar and ultrasonic

sensors, the sensor transmits a known signal and then receives the signals reflected back from objects that do not allow the continued transmission of the wave. Typical automotive cameras receive EMR signals from external sources (e.g., sun and headlights) directly or after reflection by other objects. As the EMR travels through, to, and from an object, the medium that it travels through affects the quality of the signal. Because each sensor is sensitive to EMR of different frequencies, different media often have different effects on sensor performance. For example, a radar transmitting a signal at 24 or 76.5 GHz can easily propagate through a plastic cover that blocks all visible light and renders a camera useless. Consequently, the identification of the media that influence sensors was performed based on sensor type. As an example, consider a sensor mounted on a vehicle, which will encounter several propagation media, as shown in Figure 4.

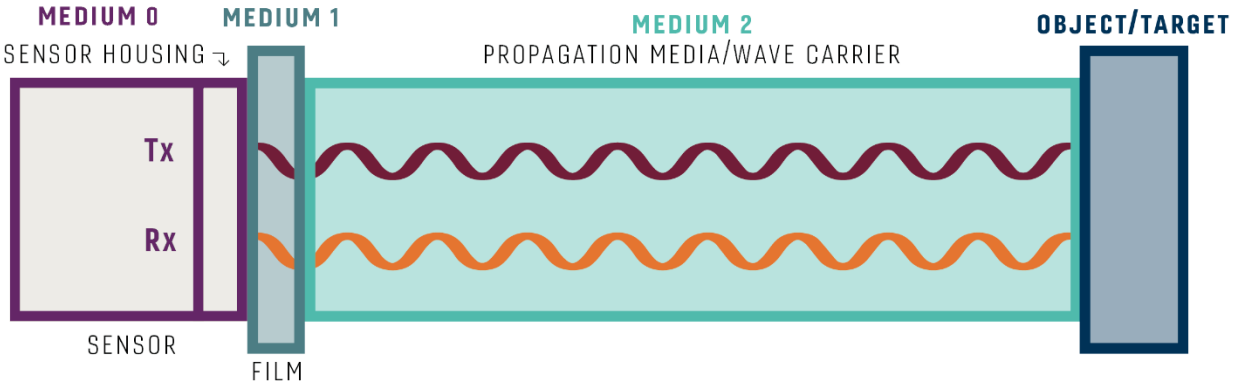

Figure 4. Example schematic showing a typical set of media encountered during sensor operation

In normal operation, a vehicle sensor might be covered by a film of mud or water (medium 1 in Figure 4). In addition, the EMR could be traveling through snow, rain, or hail (medium 2 in Figure 4). As the EMR travels from the object to the sensor, it passes through the same media. Since the carrier or medium encountered by the EMR could negatively affect its propagation, the sources of sensor degradation due to propagation influences can be split into two classifications.

1. Static degradation, or film degradation, due to an alteration to the fixed medium in front of the sensor that the signal passes through (medium 1 in Figure 4). This could come in the form of natural obstructions (snow, dirt, bugs, water, etc.) or unnatural obstructions (scratches, changes in opacity, or light damage, etc.). This latter category can be cumulative over time and may affect the baseline performance of the sensor in ideal conditions. The sensor signal is degraded due to a film on the surface of the sensor, as shown as medium 1 in Figure 4.

2. Dynamic or environmental degradation due to changes to the medium(s) the EMR passes through as it travels to and/or from the vehicle, such as rain, snow, dust, bugs, etc. (medium 2 in Figure 4). These tend to be transient and are beyond the control of the operator to improve the sensor performance.

In addition to these, design and maintenance-related degradation could also affect the quality and robustness of a sensor over the life of the system. The categories of degradation listed above are

a framework for identifying the key sources of degradation. Table 13 lists of items that could degrade the sensor output based on our overall synthesis of literature reviewed.

Table 13. Examples of Sensor Degradation

Medium 0	Medium 1	Medium 2	Object	Interference
• Scratches • Damage • Lens/fascia clarity • Mounting/ alignment • Calibration • Aging	• Water • Snow • Ice • Dirt • Mud • Bugs	• Rain/water • Snow • Hail/freezing rain • Fog • Dust • Bugs	• Reflectivity • Occlusion • Camouflage with background	• Light • Extremal sensor noise

Effects of Degradation

Degradation at a high level, affects the strength of the signal from the object of interest relative to the strength of the signal returned from objects not of interest. Medium 1 degradations are the most easily understood as they often block or deflect the transmission of the signal. For weather-related degradation (medium 2), the EMR is often scattered or attenuated as it propagates through the different fluids or mediums. As a specific example, for lidar, rain can be its own object, reflecting the signal back and thus creating additional noise in the data that the perception system has to disregard. Degradation of the object of interest also has the effect of reducing the strength of the signal returned to the sensor.

Interference as a degradation does not affect the signal strength as much as it injects noise into the system, thereby reducing the signal to noise ratio. In the case of sunlight shining in a camera, the sensor can be saturated by the noise (sunlight) so that it is unable to distinguish the target.

Operational Considerations

This section reviews literature related with the operation of ADAS and their associated sensors. The goal is to extract public information regarding the impacts of degradation and approaches that are in use to mitigate such impacts. This includes discussions of sensor reliability in deployed systems, diagnostic mechanisms for identifying degraded sensors and ADAS features, maintenance that is applied to reduce degradation, and the implications of servicing degraded systems to return performance to acceptable levels.

Sensor Reliability

Sensor reliability can be defined as the probability of meeting specification requirements (Granig et al., 2018). However, the specification requirements are a function of the system requirements, including operational life. For example, the same sensor used in two different ADAS systems could have different sensor reliability if the ADAS requirements for the two system were different (i.e., AEB may have more stringent requirements than FCW). Similarly, the acceptance criteria for this reliability parameter are typically defined by an OEM based on their specific vehicle and system, rather than broadly applied by the industry. We were not able to find robust research to describe requirements or measures of ADAS sensor reliability post deployment.

Vehicle lifetime also continues to increase, and as more vehicles incorporate ADAS features, which drivers are beginning to rely on, it is important that all components of the features function properly. The average age of light vehicles in operation in the United States was 12.1 years in 2021 and continues to increase as the quality of vehicles also increases (IHS Markit, 2021). According to a specifications sheet by Continental, one of the leading automotive suppliers and manufacturing companies, some long-range radars in passenger cars are only expected to have a lifetime of 10,000 hours or 10 years (Continental Engineering Services, 2018). A vehicle remaining in service longer than the life expectancy of the sensor could result in a malfunctioning system, requiring effective diagnostics and subsequent service of a vehicle component to regain ADAS functionality.

Diagnostics

Currently, several methods exist for vehicles to self-diagnose and report sensor degradation. One of the most common is based on the incorporation of onboard diagnostics, which allow vehicles to self-diagnose and report issues, assisting automotive technicians in troubleshooting faulty components. However, as newer vehicles become more complex, it is more difficult for technicians to identify issues because of the several interactions between components. This increases the time required to diagnose issues, adding to service and warranty costs, and contributing to customer dissatisfaction. Self-diagnosis may be improved through automated methods, including physics-based modeling and data-driven approaches. Physics-based modeling checks for consistency between the sensed measurements and the outputs of a mathematical model; large discrepancies between the measured and modeled values indicate sensor faults. The data-driven approach requires the knowledge of system monitoring data for no-fault and faulty conditions (Mathew et al., 2016). Another option is the hardware redundancy or sensor fusion approach, in which several sensors measure the same variable, and the consistency between the sensor measurements is assessed (Jiang et al., 2007). A relatively new way to diagnose ADAS performance is through remote vehicle diagnostics, in which a vehicle's performance parameters and trouble codes are accessed using a wireless network. If any type of malfunction is detected, the necessary support services can be provided (Taie et al., 2016).

In the case of a vehicle self-diagnosing an issue with a sensor or ADAS feature, there are several ways the vehicle can alert a user to the issue. Typically, a warning light or message will show on the instrument panel to indicate there is a problem and that maintenance is required. Diagnostic trouble codes (DTC) may also be stored in the vehicle's computer memory to notify a user about any malfunctions. In some vehicles, performance could be affected by the malfunctioning of an ADAS or sensor function, the steering pulling in a certain direction, or increased steering effort required to operate the vehicle or physical cues such as the vehicle issuing a steering wheel vibration (AAA Automotive, 2018). These cues may be signs for a vehicle owner to know when to maintain and get their vehicle serviced if a DTC is not available; however, they may also imply a dangerous condition is present as a consequence of degradation.

Maintenance

Just like legacy vehicles, new vehicles with ADAS need to be maintained to ensure continued optimal performance. ADAS, including their sensors, should be continually monitored to ensure that they are performing properly. Any damaged sensors need to be repaired or replaced. According to literature from AAA (2018), vehicle owners should be alerted of malfunctioning

features or sensors by the vehicle system through warning lights or messages on the instrument panel, or through other vehicle actions. However, sometimes a system will not notify a user that a feature is not working properly if it cannot detect any issues with the sensors. These issues tend to be related to miscalibration of the sensors rather their functionality. Therefore, the user should be aware that any event that occurs that could disturb the aim of a sensor may also result in calibration issues, therefore leading to decrements in ADAS feature performance.

Additionally, literature from AAA (2018) highlights some events that can disturb sensors: collisions even as minor as a fender bender, windshield replacement, suspension repair, or wheel alignment. Additionally, the removal or replacement of sensors or their mounting brackets; changes in tire size; front air bag deployment; or roof repairs may also call for sensor recalibration. Sensor recalibration will also be required if there is a DTC in the car's computer memory or an automaker releases a technical service bulletin calling for recalibration, potentially because of some other required alternation or repair to the vehicle. In the case of any of these events, a user should avoid using the ADAS feature until the vehicle can be inspected by a professional who will determine if the sensors require recalibration.

Related to recalibration, specific sensor types also require maintenance. Camera sensors view objects through the windshield and are designed for "specific rates of light transmission through glass that has minimal imperfections and distortions" (AAA Automotive, 2018). Therefore, vehicle owners need to keep their windshields clean and get any cracks or chips fixed. Windshield repairs or replacements may also be necessary in certain instances, in which case, AAA recommends that the owner have this performed by an OEM to ensure that the camera sensor will interface properly with the windshield and provide accurate information (AAA Automotive, 2018).

Radar sensors can either be centrally mounted or offset, but they are generally near or in the bumper facia, so it is important to check that their positions are not disturbed (AAA Automotive, 2018). Any damage to the bumper will also require inspection of the radar sensor underneath. Repairs to areas of the bumper that are in front of a radar sensor may affect performance due to changes in the medium through which the signal propagates. OEM bumper covers are recommended to ensure that the bumper materials do not interfere with the sensor signals. Excessive bumper cover paint and bumper stickers can also cause problems with the radar sensors, which vehicle owners should be aware of. Finally, while ultrasonic sensors do not require calibration, they are designed to be in precise positions on the vehicle in certain orientations, so any misalignment may affect their performance. Additionally, aftermarket vehicle parts are not recommended by AAA for use as they can cause these sensors to be oriented incorrectly (AAA Automotive, 2018).

Aside from ensuring that sensors are calibrated and functioning properly, it is advisable that vehicle owners regularly maintain the sensors for the ADAS features. This primarily includes cleaning the sensors. Some vehicle companies, such as Ford, General Motors, Cadillac, Volvo, Nissan, Seeva Technologies, 3M, and Continental, have ADAS features with self-cleaning capabilities for their camera sensors. Lasers, fluids, or compressed air may be used to keep the sensors clean (Linkov, 2018; Abuelsamid, 2019). Owners can also manually clean the sensors with the appropriate tools but need to be careful not to move the sensors out of position or cause damage by using an improper cleaning tool. Radar sensors typically do not need to be cleaned as they are located behind a bumper cover or grille on the vehicle; however, there are currently no

vehicles that have technology to remove dirt or ice from a grille, which may obstruct the view of a radar sensor (Linkov, 2018).

Serviceability

ADAS features may sometimes require professional repair or replacement. Just like a legacy vehicle, a vehicle with ADAS can be taken to a dealership service center or autobody shop to be serviced. The type of service will depend on the extent of the repairs. Table 14 illustrates the typical repair costs for select sensors associated with specific ADAS features.

Table 14. Repair Costs for Damaged ADAS Cameras and Sensors (AAA Automotive, 2018)

Sensor	ADAS Features	Repair Cost
Front radar sensors	AEB ACC	$900 to $1,300
Rear radar sensors	BSM Rear cross traffic alert	$850 to $2,050
Front camera sensors	AEB ACC LDW LKA	$850 to $1,900
Front, side mirror, or rear camera sensors	Around-view systems	$500 to $1,100
Front or rear ultrasonic sensors	Parking assist	$500 to $1,300
Windshield replacement	AEB ADD LDW	Aftermarket glass: $1,200 to $1,600 Factory glass: $1,300 to $1,650

According to literature from AAA (2018), aside from replacing damaged sensors, sensors may need to be calibrated even when they are not affected. As ADAS sensors are precisely aimed to detect objects that can be some distance down a road, any misalignment will significantly affect what the sensors detect as well as their capability and effectiveness. If there is a disturbance to their position, such as from a collision, windshield replacement, suspension repair, or removal/replacement, sensors will need to be recalibrated. Sensor recalibration can also be required when there is a DTC in a vehicle's computer memory, or when technical service bulletins recommending recalibration as part of a repair are released by automakers.

Because most vehicles have onboard diagnostics, service shops can perform complete diagnostic scans before and after the repairs to understand the issues with the vehicle and identify any malfunctioning sensors (AAA Automotive, 2018). It is then possible to confirm that the issues have been resolved, the ADAS sensor calibrations are complete, and the vehicle control systems are communicating properly.

Recalibrating ADAS sensors can be complex and time-consuming depending on the sensor and ADAS feature calibration requirements (AAA Automotive, 2018). Calibration also requires the dealership or service center to have the proper equipment to calibrate the sensors, such as a computer scan tool to support ADAS sensor calibration; a proper calibration environment; and a wheel alignment rack to ensure that the vehicle thrust line points straight down the road when the steering wheel is centered. Prior to the calibration tests, unnecessary or heavy items are removed from the vehicle or trunk, the tires are properly inflated, the front and rear vehicle ride height are

within specifications, the fuel tank is full, the windshield is cleaned in front of any camera sensors, the protective cover are removed from the radar sensor, and the wheel alignment is performed.

According to AAA (2018), the two types of calibration methods are static and dynamic. Procedures vary based upon vehicle make and model. Generally, static calibration first involves determining the vehicle thrust line.[25] Next, aiming targets are positioned in precise locations relative to the thrust line and the sensor at a specified height, with any offsets to the sensor taken into consideration for the positioning of the target. The targets are typically 3 to 6 meters from the vehicle. Camera targets are typically black and white images, and radar targets include metal elements that reflect the radio waves back to the sensor. The sensors may need to be leveled. Finally, the aiming process is initiated using a factory scan tool to indicate whether the alignment was performed completely. For some sensors, dynamic follow-up tests are required. These consist of driving the vehicles on relatively straight roads with clear lane markings for 5 to 30 minutes until the scan tool indicates that the calibration is complete. The amount of traffic may also affect the time needed to calibrate the sensors. Calibration cannot be performed in harsh or degraded weather conditions.

Test Methods and Metrics

The following sections are an overview of sensor and system level tests that could be used for performance characterization. Understandably, the tests for ADAS performance are more readily available in the literature (e.g., New Car Assessment Program and the Insurance Institute for Highway Safety) than the sensor tests used to evaluate specific ADAS sensors. Therefore, testing of sensors both in and outside the automotive industry were reviewed to expand the knowledge acquired.

Sensor Test Methods

The sensors previously identified in the Market Survey section can be lumped into two primary sensing categories: active and passive. The active sensors operate primarily by emitting a signal and then measuring the response time of the received signal as opposed to cameras, which are passive sensors and just receive information. Radar, lidar, and ultrasonic sensors work on this general principle, though the specific implementation can vary based on the form of the transmitted signal. For these types of sensors, there are common parameters to characterize performance. Birdsong et al. (2005) presented generic test methods for the following sensors: ultrasonic, laser, and radar. Some of these metrics can also be extended to vision-based sensors. Test methods were classified into two categories: static and dynamic.

Static tests measure the performance of the sensors keeping targets and sensors stationary. These tests aim to measure the optimal sensor performance and are based on range, field of view, accuracy, reliability, and sensitivity.

Dynamic tests measure the performance of the sensors while keeping sensors stationary and the targets moving during the test, or vice versa. Dynamic tests are performed with controlled

[25] The vehicle thrust line is an imaginary line drawn perpendicular to the rear axle's centerline. The term “thrust” refers to the direction in which the rear wheels are pushing. The imaginary line compares the direction that the rear axle is aimed with the centerline of the vehicle. It also confirms if the rear axle is parallel to its front axle and that the wheelbase on both sides of the vehicle is the same.

velocities of the target (or sensor) object. Measurements include sensitivity to direction of motion, near misses, and detection time. Several objects are used to characterize sensor performance.

Radar

Radar creates a challenge in performance evaluation due to the architecture of the sensor for automotive applications. Typical metrics for radar performance characteristics include power budget (which is a function of SNR), range resolution and accuracy, and static target suppression (IEEE, 2017; Stove & Hurd, 2003; Wasserzier et al., 2019; Watts et al., 2002). The returned raw signal is heavily processed to identify objects of interest in the sensor's FOV. This abstracted data typically includes a target list, which may include object recognition information (e.g., sedan, tractor trailer, guardrail, pedestrian). For each object, an associated position and velocity are also reported (in either Cartesian or polar coordinates, depending on the sensor). Consequently, measuring the true SNR for the signal received by the radar sensor is often not possible without diagnostic tools and knowledge proprietary to the sensor manufacturer. Instead, the effect of degradation would be noted in parameters such as the number of objects and, if provided, an indication of the strength or confidence in the target.

Isolating the targets from surroundings when performing sensor testing is also a consideration. For example, National Instruments (2019) has offered a vehicle radar test system for the evaluation of automotive radar systems. The VRTS provides automated radar measurement and obstacle simulation capabilities for 76 GHz to 81 GHz automotive radar systems with 1 GHz and 4 GHz of bandwidth. Engineers can use VRTS to develop validation and production tests that are repeatable.

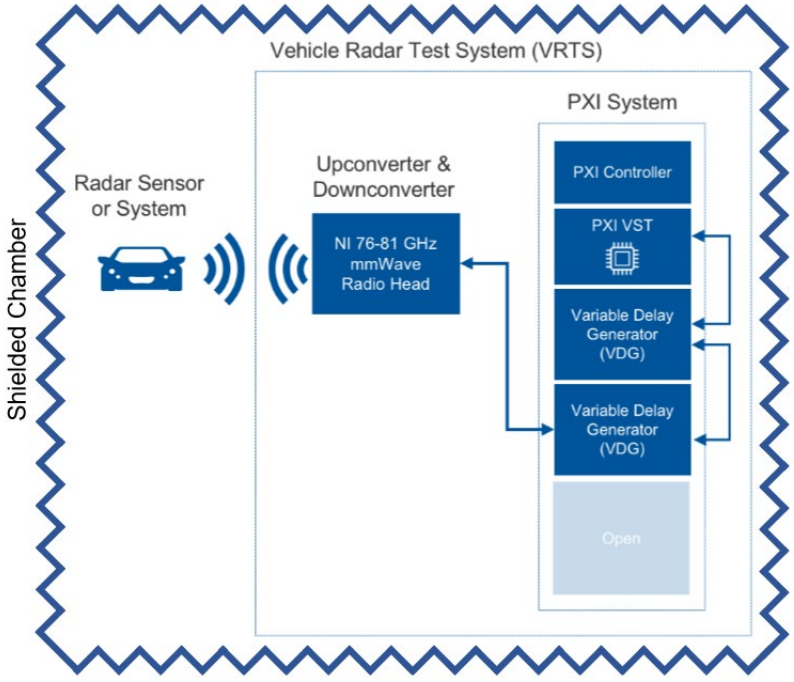

Figure 5. Block diagram of typical VRTS configuration (from National Instruments, 2019)

As shown in Figure 5, an automotive radar together with a VRTS are contained in a shielded chamber (National Instrument, 2019). The shielded chamber is an anechoic room that has radio-

wave absorbing materials applied to the walls. The shield is designed to stop reflections of electromagnetic waves. The first component of the VRTS is a millimeter wave radio head that interacts with the radar. It captures the chirps and then generates the objects back to the radar up and down, converting the radio frequency signals. A radio frequency downconverter converts high radio frequency signals to low radio frequency signals. The upconverter converts low radio frequency signals to high radio frequency signals. PXI stands for PCI eXtensions for Instrumentation. PCI is a bus technology that stands for peripheral component interconnect. The PXI system has the controller capable of running a subwoofer performing all the test. The variable delay generator grabs the signal capture from the sensor and object simulation. It provides quantities such as object distance, radar cross-section, and velocity. The obstacle generation is based on user-configured scenarios through optical delay lines supported by a second VDG. Finally, the vector signal transceiver (VST) performs relevant radio frequency measurements across the radar's FOV. It can have one or several VSTs depending on test needs for coverage and speed. The VRTS can simulate up to four objects and simulate common driving scenarios, including lane changes and an object crossing the street. The behavior of each scenario can be controlled via three key parameters, including range, velocity, and RCS. VRTS can be configured to simulate a wide range of objects and scenarios.

Camera

There are several common standards for characterizing the performance of cameras, such as from the International Organization for Standardization "Photography — Electronic still picture imaging — Resolution and spatial frequency responses" (ISO, 2017a). This specifies methods for measuring the resolution, which is a measure of the highest spatial frequency the camera can resolve, and the spatial frequency response, which measures contrast loss as a function of spatial frequency and can be used to derive sharpness and acutance. There are several methods to measure these values and associate applications to analyze the images used in the test. These applications typically compute the modulation transfer function that is equal to the SFR, or an equivalent measure. In addition to commercially available packages, there are several freeware applications. The software and test procedures were developed to support the performance analysis of fingerprint capture devices and printers for the Department of Justice and Federal Bureau of Investigation for product certifications (Nill, 2006; Nill et al., 2016). The targets used by MITRE have similar features to some of the calibration targets used by manufacturers shown in Figure 6 (AAA Automotive, 2018).

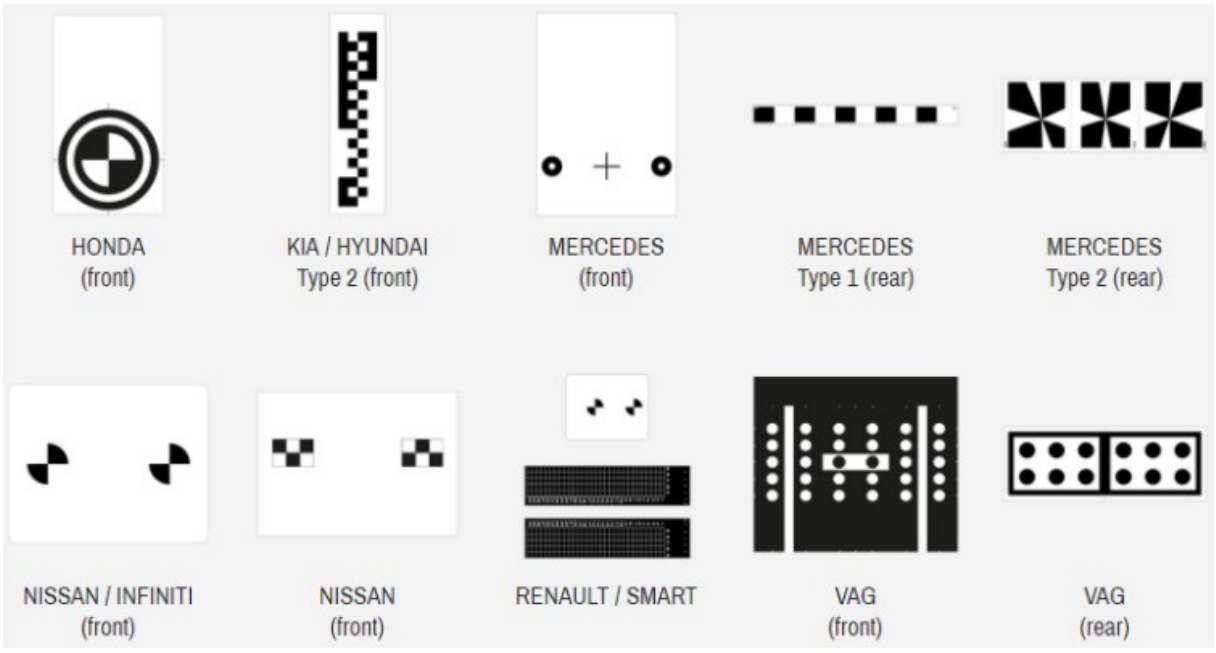

Figure 6. Typical ADAS camera aiming targets (AAA Automotive, 2018)

ASTM International E2566-17a, "Standard Test Method for Evaluating Response Robot Sensing: Visual Acuity," provides a test method to quantitatively measure visual acuity. Similar to a vision test, acuity is determined by identifying the smallest target (such as a quick response, or QR, code) that can accurately be read, or in the case of a QR code, interpreted.

In *Test Methodology for Vision-Based ADAS Algorithms With an Automotive Camera-in-the-Loop*, Reway et al. (2018) presented a methodology for vision-based ADAS algorithms using camera-in-the-loop to control the input to the sensor. In it, the authors described a process for creating a test matrix that includes environmental conditions (e.g., day, fog, night, and dusk) as well as unwanted effects at the camera such as occlusions, dirt, image distortion, and noise.

This shows there is no consistent industry approach to measure image quality. To address this, IEEE has established the IEEE P2020 Automotive Image Quality Working Group to address "the fundamental attributes that contribute to image and quality… as well as identify existing metrics and other useful information relating to these attributes" (IEEE, 2020).

Ultrasonic

Ultrasonic sensors have some of the same metrics as the other sensors including FOV, range accuracy, influence of angle of incidence and the SNR (Gamarra-Diezma et al., 2015). In *Testing Accuracy of Long-range Ultrasonic Sensors for Olive Tree Canopy Measurements*, Gamarra-Diezma et al. (2015) provided test methods to determine these values. The angle of incidence measure may be particularly interesting for this project as the off-axis measurements may be more sensitive to degradation. Birdsong et al. (2005) showed that ultrasonic sensors have a cone-shaped range-finding capability. Given the shape of the radiation pattern of ultrasonic sensors, measuring the range accuracy across the radiation pattern or FOV may be useful for assessing the effects of degradation. Ultrasonic sensors can also show sensitivity to different materials

(Adarsh, 2016; Birdsong et al., 2005), which may also provide an opportunity for more pronounced differences with different degradations.

Lidar

ASTM has two standards of interest related to lidar. ASTM E3125, *Standard test method for evaluating the point-to-point distance measurement performance of spherical coordinate 3D imaging systems in the medium range*, presents a method for evaluating point-to-point distance measurements and ASTM E2938-15, *Standard test method for evaluating the relative-range measurement performance of 3D imaging systems in the medium range*, describes a quantitative method for evaluating range measurement performance. In addition to distance measurements, SNR is critical in object detection (McManamon, 2019). In *Lidar Technologies and Systems*, McManamon presented a lengthy list of potential parameters of interest, including contrast, resolution, FOV, horizontal and vertical resolution, detector sampling, optical aberrations, dynamic range, noise characteristics, range resolution, and off-axis sensitivity. Some can be measured using similar metrics as are used for cameras such as MTF for resolution. In addition to these, quality metrics that are associated with automatic target detection, recognition, and identification are presented. Some are used for other applications (e.g., airborne imaging), but others may be relevant for ADAS applications that require not just the detection of an object (finding the area of interest that contains the target), but also its recognition (class of object, i.e., truck or tank) and identification (type of object, i.e., T-72 or M1 tank).

There are several studies that have looked at lidar performance in degraded states, particularly poor weather conditions, such as rain, fog, and snow. Jokela et al. (2019) developed and executed a test method using range measure performance for evaluating lidar. They used a fog chamber and optically calibrated plates with different reflectivity (90% and 5%, or white and black, respectively) similar to those used by manufacturers and then looked at the variation in range measurements for different environmental conditions. Birdsong et al. (2005) also applied tests identified by the study to lidar to look at such things as range measures and signal strength. In *Evaluating Complementary Strengths and Weaknesses of ADAS Sensors*, Xique et al. (2018) evaluated the strengths and weakness of ADAS sensors. Because the sensor they used did not return any scatter data from which they could compute SNR, the authors used the ratio of returns to the minimum detectable signal as an estimate for SNR. In addition to these parameters, velocity has also been used in the characterization of lidar, including under a degraded state like rain (Rasshofer et al., 2011).

National Instruments Sensor Fusion Scenario-Based HIL Tester

Sensor fusion is the mixture of information from various sensors. A typical example is the fusion of information provided by a front camera and a front radar into a single ADAS, such as AEB. As illustrated in Figure 7, the engineering consulting firm Capgemini Engineering (previously known as Altran Technologies, SA) has integrated an innovative radar object simulator based on National Instruments technologies (National Instruments, 2020) and a 3D virtual road scenario simulator into a hardware-in-the-loop setup in Italy to produce a scenario-based tester that fully synchronizes camera and radar data to validate sensor fusion algorithms.

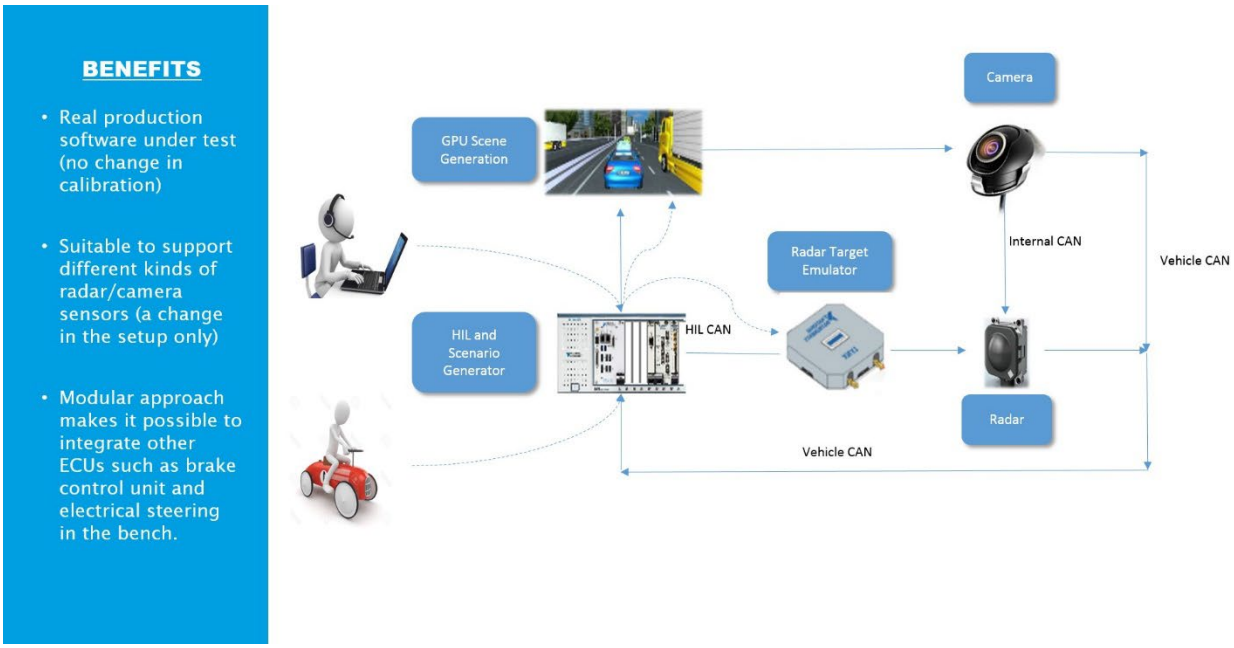

Figure 7. ALTRAN-NI ADAS HIL test solution (from National Instruments, 2020)

Accelerated Degradation & Simulation Techniques

Limited quantitative information was identified in the literature search to help determine how degradations can be simulated for sensor evaluation. While radar congestion and the effects of weather on sensors has been ongoing topics of research, as has discussion of lidar and the potential processing that can be used to mitigate these, much of the quantitative discussion is based on computer modeling rather than empirical testing. Consequently, there does not appear to be published methods in which these degradations are introduced or their effects measured. This is one of the areas in which stakeholders may be able to provide valuable insight into the primary sources of degradation that affect sensor performance, how these are quantified, and how they can be replicated.

ADAS Test Methods

The following test methods were identified in the literature for the common ADAS features described previously. This section addresses ADAS test procedures, particularly those procedures that are, or were, likely to lead to industry standardized practices. Such test procedures form the basis for the ADAS test for this project given that they are well documented and open to the industry for future refinement and replication.

FCW

According to the NHTSA (2013a) *Forward Collision Warning System Confirmation Test*, an FCW system confirmation test is used to evaluate the ability of a system to detect and alert drivers of hazards in the vehicle's path. There are three tests: a subject vehicle approaches a stationary principal other vehicle in the same lane of travel; an SV follows a POV at a constant speed, and the POV stops; and the SV approaches a slower moving POV, both vehicles traveling at constant speed. Whether the system passes the test depends upon when it issues the alert based

upon time-to-collision criteria, which varies based upon each of the three tests. The three tests can be seen in Figure 8, Figure 9, and Figure 10.

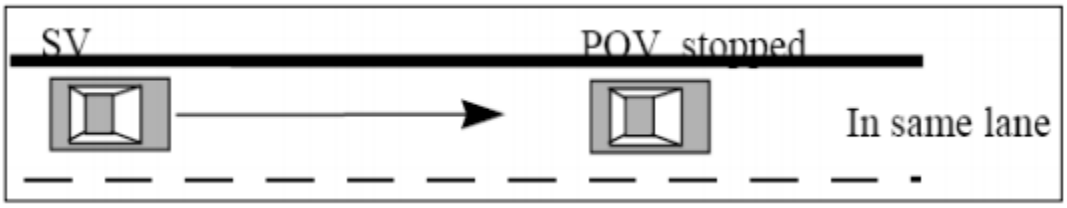

Figure 8. Test 1 – SV encounters stopped POV on a straight road (NHTSA, 2013a)

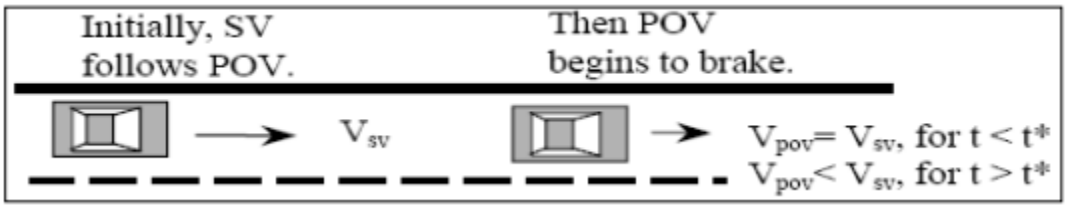

Figure 9. Test 2 – SV encounters decelerating POV (NHTSA, 2013a)

Figure 10. Test 3 – SV encounters slower POV (NHTSA, 2013a)

Overall, this section provided several potential testing procedures that were considered and leveraged in the project testing phase.

AEB

According to a November 5, 2015, notice published by NHTSA (80 FR 69604), AEB refers to either crash imminent braking, dynamic brake support (DBS), or both on the same vehicle. CIB automatically applies vehicle brakes if the vehicle sensing system anticipates a potential rear impact with the vehicle in front of it. DBS applies more brake power if the sensing system determines that the driver has applied the brakes prior to a rear-end crash but estimates that the amount of braking is not sufficient to avoid the crash.

According to the AEB test protocol from the European New Car Assessment Programme (Euro-NCAP, 2019) *Test Protocol – AEB systems*, the performance of AEB is assessed using the following scenarios: car-to-car rear stationary (CCRs), car-to-car rear moving (CCRm), and car-to-car rear braking (CCRb). Scenarios are shown in Figure 11. For testing purposes, the presented research used a modified car-to-car rear stationary scenario. A soft car was used as the target vehicle (EVT in Figure 11). The vehicle with AEB being tested traveled at the minimum speed that allowed AEB activation. A few dry runs were executed to determine the minimum speed of activation. Tests were then conducted with and without degradations.

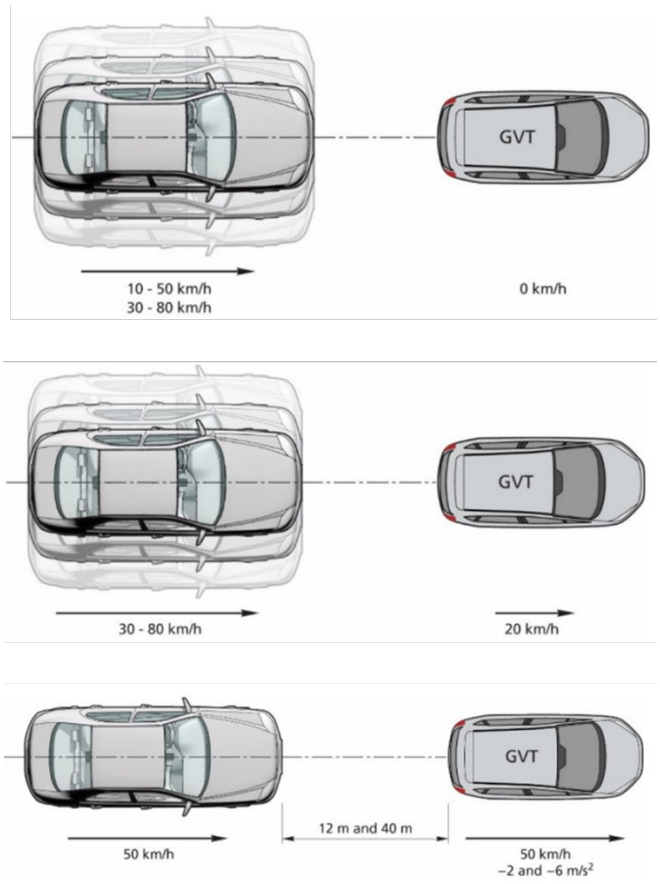

Figure 11. Testing scenarios for AEB (Euro-NCAP, 2021)

The IIHS (2013) has also developed an "Autonomous Emergency Braking Test Protocol". The AEB system is set to the default or normal setting, and the vehicle should perform a number of stops prior to the testing, with a few of the stops to activate the vehicle's antilock braking system. For the test, the target vehicle is placed in the center of the lane with the rear of the target facing the approaching vehicle. The test vehicle should approach the target at speeds of either 20 km/h or 40 km/h. The vehicle then either strikes the target or comes to a stop before affecting the target.

ACC

The ISO (2010, first edition) has been updated to standard ISO 15622 (third edition, 2018), *Intelligent transport systems – ACC systems – Performance requirements and test procedures.* The test targets should be representative based upon the technology being used (infrared lidar, millimeter wave radar).

The first test is a target acquisition range test, which is used to define how the given ACC system should be expected to function when a forward vehicle falls within a certain range from the SV. The subject and forward vehicles should either both be moving, or both be stationary. The forward vehicle is present at a prescribed distance from the SV. Based upon the range into which the forward vehicle falls, the ACC on the SV should either measure the range between the forward and SVs (farthest range), detect the presence of the vehicle but not measure the range or

relative speed between vehicles (middle range), or not detect the presence of a vehicle (closest range; ISO, 2010, first edition). This is represented by Figure 12.

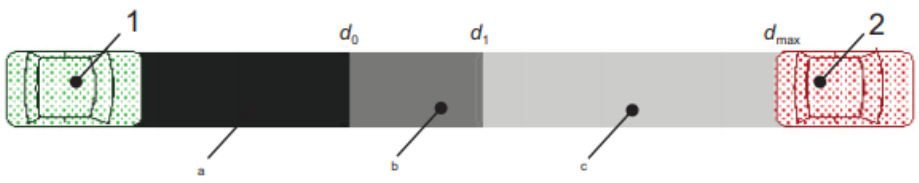

Key

1 subject vehicle
2 forward vehicle

a Detection not required.
b Detection of vehicles required.
c Determination of range required.

Figure 12. Target acquisition range test (ISO, 2010, first edition)

Lane Support Systems

NHTSA uses a system confirmation test to evaluate LDW performance for its NCAP. For the test, the vehicle is driven in a straight line at a constant speed. The driver then begins to manually input sufficient steering to cause a lane departure to occur at a defined lateral velocity. The test is complete once the vehicle has crossed at least 0.5 m over the lane edge boundary. There should also be two departures during a test, one to the left and one to the right, and there should be different roadway markings used. The LKA tests are performed in the same way in a series of separate tests, where the driver releases the steering wheel after initiating a heading change towards a lane line to emulate an imminent lane departure. The test is complete 10 seconds after the driver has released the steering wheel, regardless of whether the system prevents the lane departure (NHTSA, 2013).

There are specific instructions for the setup of the course, as well as the speed, lateral velocity, and yaw rate for the LDW and LKA tests. LDW performance is evaluated by the vehicle's proximity to the inside edge of a lane line at the time the alert is issued (NHTSA, 2013).

The Euro-NCAP (2017) also has test protocols for emergency lane keeping, LKA, and LDW. For ELK, there are road edge tests in which the driver will manually steer the car towards the road edge on the passenger side of the vehicle. In the oncoming vehicle scenario, a global vehicle target will follow a straight-line path in the adjacent lane to the test vehicle in the opposite direction. The paths of the vehicles will be synchronized so that when the test vehicle maneuvers toward the adjacent lane, the front edges of the vehicles will have overlapping lateral positions. In the overtaking vehicle scenario, the GVT will follow a straight-line path in the adjacent lane to the test vehicle in the same direction. The paths of the vehicles will be synchronized so that the longitudinal position of the leading edge of the GVT is equal to the position of the rear axle of the test vehicle when the test vehicle begins the maneuver into the adjacent lane (Euro NCAP, 2017).

For the LKA tests, the road edge tests are the same as for the ELK tests in which the driver will manually steer the car towards the road edge on the passenger side of the vehicle. There will also be dashed and solid line tests of the same manner. Testing of the LDW system can be assessed in conjunction with the ELK or LKA tests if the vehicle is equipped with both features; if not, the standalone tests are the same as for the LKA dashed and solid line tests (Euro NCAP, 2017).

This page is intentionally left blank.

Chapter 3. Stakeholder Outreach

Introduction

The stakeholder outreach was based on discussions with NHTSA. Subject matter experts from major domestic and international OEMs, Tier 1 suppliers, and automotive industry groups were interviewed between March and May 2020. A guided interview approach was selected because it provided opportunities for exploratory questioning about current sensor practices while also ensuring that a consistent set of topics were discussed. The study leveraged telecommunication methods for supporting the collaborative discussions. Project background was given to the interviewees using a set of slides, and discussion topics were navigated by displaying the list of questions to be discussed. The list of questions can be found in Appendix A.

Disclaimer

The comments reported represent the views of SMEs who were willing to provide information and might not represent the opinion across all organizations interviewed. Also, there were only a few organizations that provided information related to lidar.

Methods

Data Analysis

The interview data was primarily interrogated through content analysis methods. For this qualitative approach, we applied a modified framework methodology (Marshall & Rossman, 1999; Ritchie et al., 2003). This approach has been successful in several past VTTI research efforts (e.g., Blanco et al., 2015, 2020) and allows researchers to manage and analyze the data in a logical and complete manner. Using this iterative approach allows the data to be transformed from recorded audio to written transcripts, then to charts and data in a manner that is comprehensive, transparent, and traceable.

The digital recordings containing the qualitative feedback from the interviews were (1) compiled into transcripts with all personally identifying information removed; (2) categorized based on common themes and subthemes; and (3) prioritized based on needs, concerns, and other points of interests. Where appropriate, descriptive statistics were also used to summarize information from the surveys. All data collected was handled and stored securely according to VTTI data handling best practices to protect any PII.

Responses were aggregated for each organizational interview, which allowed several SMEs with direct involvement in the design and verification of sensors and ADAS systems to participate at one time. This approach also allowed us to benefit from each organization's collective hands-on sensor and system knowledge.

Findings

When summarizing the results of this effort, it is important to consider that, to ensure compliance with the Paperwork Reduction Act of 1995, nine organizations were engaged for interviews. They included four OEMs, four suppliers, and one automotive services association with a particular interest in ADAS. These were viewed as having the most important expertise relative to developing, deploying, and improving ADAS. As such, responses may not represent every

possible sensor degradation-related issue because the interviews did not reach deeply into supply or maintenance chains. Further, it is important to recognize that while each interview included a consistent set of open-ended questions (the discussion guide can be found in the stakeholder outreach in Appendix A), responses reflected issues most significant to the participating organizations and their representative SMEs. At times, proprietary information the SMEs asked not to be released may have been discussed to help we better understand the participant's approach to addressing sensor degradation.

Sensor Overview

Each interview began with a discussion of the sensors used and/or produced by each organization. Responses included vision (camera), thermal, radar, ultrasonic, and lidar (Figure 13).

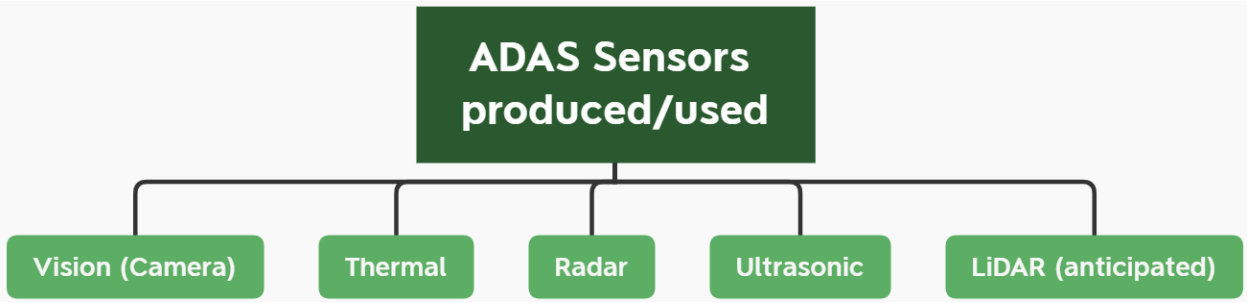

Figure 13. ADAS and/or sensors produced or used

When looking more closely at the sensors in production vehicles, the most commonly used sensors that organizations said they used or produced were radar- (eight organizations), vision- (eight organizations), and ultrasonic-based (six organizations). Less commonly used sensors were lidar- and thermal-based sensors, with the latter used primarily for animal detection and classification. While lidar is included in a limited capacity on some more progressive ADAS systems, most SMEs said that lidar was still in the development phase.

Sensor-System Specific Degradation Considerations

Additional questions prompted SMEs to consider the degradations of particular interest for each type of sensor previously identified as being produced or used. The following sections summarize the participants' comments and why those degradations were of particular interest.

Radar-Based Sensors

SMEs called attention to the environmental factors (e.g., snow, mud, dirt and debris, water) that could result in blockage-related degradation to the FOV associated with radar systems. These same environmental factors could also damage secondary/protective surfaces (e.g., stone cracking the cover). As a result, the secondary surface was cited as being of more concern than the sensor itself by one SME and implied by others. Changes to the radar antenna geometry were noted to result in degradations to the FOV. These changes could result from corrosion, changes in bumper position, and general degradation. Metallic objects on the roadway could also negatively affect radar systems, as could materials used in/on the vehicle. For example, humidity and moisture absorbed into plastics or an additional layer of paint or alternative paint blend

applied by a repair shop may result in degradations. In some cases, algorithms have been developed to indicate that the sensors are not functioning optimally. These could be developed through testing that simulates real-world conditions (e.g., using a high-pressure washer to simulate rain at speed).

Permanent Versus Temporary Radar-Based Sensor Degradation

Permanent degradations associated with radar-based sensor systems can broadly be attributed to degradation of the vehicle's physical condition. For example, radars may become misaligned due to significant bumper sagging. Repairs, such as those that incorporate a wire mesh, could block the radar, as could repainting of the bumper. A build-up of dirt or debris has the potential to block the sensor either in front of or behind the bumper, and debris may also damage or crack the surface of the radome (front portion of enclosure in which the radar signal is sent/received). Components themselves may have issues associated with humidity/moisture absorption into plastic, corrosion or rusting, and general aging of materials. General aging may also result in electrical degradation; however, one respondent noted that they are generally able to design this issue out of the component.

Temporary degradation can be associated with temporary blockages (e.g., anything the vehicle might see while driving, such as water droplets, rain, snow, ice, dust). Some ADAS mitigate blockages in forward-looking radar-based sensors (though not generally corner radar-based sensors) using heating elements in bumpers that can melt snow and ice. Ambient temperature can also affect performance (i.e., meets specifications at higher temperatures, but works better at lower temperatures). Misalignments can also be temporary, as over time the left-right axis can realign, thus correcting the degradation.

Vision-Based Sensors

With regard to vision-based sensors, SMEs noted degradations associated with ambient lighting and FOV. FOV could be affected by visibility and incorrect calibrations. Further, degradations, such as those resulting from environmental conditions (e.g., rain, ice, snow, mud, grime, and extreme temperature changes) were a common concern in terms of their effect on the range and FOV. At times, these environmental agents could result in a broken lens or damaged protective covering, causing defects or allowing for the intrusion of other environmental agents (e.g., when a rock cracks a lens covering or an extreme temperature change compromises a seal, which in turn permits moisture and water to degrade the sensor). SMEs noted several countermeasures for ensuring the integrity of the vision-based sensor. These could include, for example, locating cameras behind windscreens and using wipers and/or heating elements to clear blockages. It was noted that emblems and other components, which have the potential to create blockages, are subjected to a range of testing to ensure that this is not the case.

Incorrect calibration associated with the vision camera sensor could have a negative effect, such as on object or lane detection, due to degrading the longitudinal (i.e., angular) measures. The issue can be a problem even if there are several sensors used for sensor fusion; incorrect calibration can result in a malfunction when fusing data with another sensor. As an example, using an incorrectly calibrated vision camera could make another secondary sensor attempt to detect the position of an object, resulting in an object being mispositioned because calculations were based relative to the incorrectly calibrated sensor. Pre- and post-testing checks on image quality are used to detect potential degradation over time. Using special lenses, relative distance to an image is measured over time and monitored for focal shifts (i.e., blurriness), which could

also be the result of inconsistent degradation across the detected region. SMEs cited using engineering experience and dimensioning to bring vision-based sensors back to calibration and in-focus. Dimensioning is the process by which the vision camera estimates the area or the volume that an object occupies.

Permanent Versus Temporary Vision-Based Sensor Degradation

Interviews suggested that permanent degradations to vision-based sensors tend to result in malfunctioning system and diagnostic reports until a repair is made. These degradations include:

- Calibration-related degradations, such as misalignment, that result in auto calibration requirements that are out of range;
- Hardware-related damage that negatively impacts the FOV (e.g., cracked windscreen) or use of non-OEM specification materials (e.g., non-OEM glass that has a non-compliant coating); and
- Severe contamination from items like dirt or stickers.

Temporary degradations to vision-based sensors result from things like fogging (e.g., moisture on the camera screen) and weather-related degradation (e.g., rain, fog, snow, sunlight). In a case such as this, a driver may be informed that the function is not available until the system recovers, a topic discussed in more detail in the associated diagnostics section of this report.

Lidar-Based Sensors

Degradation in lidar systems was noted in association with water and other weather-related environmental concerns (e.g., reflections in raindrops). For example, when drops accumulate on the lidar window, performance — range, resolution, FOV size — can be affected. There was less discussion about lenses and other potential issues because participants noted that lidar sensors were prototypes and thus their durability had not been fully verified.

Permanent Versus Temporary Lidar-Based Sensor Degradation

Physical factors including vibration, collisions, and the impact of stone chips over time, can result in permanent degradation to lidar-based sensors. Temporary degradations noted included those associated with the cooling/heating system and weather conditions. Much as with the previous sensor systems discussed, rain can result in reflections that affect overall lidar performance and the sensor's range, resolution, and FOV size.

Ultrasonic-Based Sensors

The reflectivity of objects was noted in specific regard to ultrasonic-based sensors. Overall, there was much less discussion on ultrasonic sensors. This sensing technology is currently used for short range proximity sensing generally for low-speed applications.

Permanent Versus Temporary Ultrasonic-Based Sensor Degradation

Sensor degradation associated with ultrasonic-based sensors was noted as being permanent in nature and a result of aftermarket repairs, such as a non-OEM bumper with altered sensor positioning or coatings or paints. While follow-up questions were asked, SMEs did not specifically call out temporary degradations associated with ultrasonic-based sensors.

Forms of Degradations

Although sources of sensor degradation are presented, it is of particular interest to know which types of degradation studies could be more beneficial to suppliers and OEMs. On one hand, some degradations could be chosen based on the frequency or probability of encountering a particular scenario. Determining such probabilities may involve conducting experiments and/or observations of naturalistic driving. Additionally, some degradations could be more challenging for the technology to overcome such that the most impactful degradations should be the focus of testing. Such questions were included in the stakeholder interviews to reduce the current level of uncertainty with respect to applying degradation to ADAS sensors.

SMEs offered a range of insight into the types of degradation considered. Degradation was discussed in terms ranging from broad categorical classifications of degradations to specific examples of sensor-related degradation. Beginning with the broad categorical classifications, SMEs identified the following groupings.

- Mechanical, electrical, and chemical product degradations
- Degradations affecting the dependability of the sensor grouped according to functional safety, unintended functionality, and cybersecurity
- Hardware faults, communication faults, and sensor blindness

General examples of degradation included those associated with the lifecycle of the vehicle, including mechanical shock and vibration, thermal cycling, aging, and chemical resistance, along with environmental degradation resulting from temperature and humidity variations and other weather-related factors. Similarly, degradations can result from a compromised FOV due to blockage or position and orientation, especially over time (such as that associated with the corrosion or sagging of a bracket due to age or a minor crash).

Examples of radar-based sensor degradations that SMEs drew to researchers' attention included environmental factors like temperature, snow, rain, dirt, or mud; blockage degradations due to the FOV of the sensor being blocked by snow, rain, dirt, or mud; degradations on the radome or the secondary surface encountered in front of the radar (e.g. bumper) associated with a damaged surface, scratches or improper repairs, humidity absorption in plastic, or aging; improper sensor installation or alignment; and interference from other entities sharing the frequency band. SMEs noted that radar is also susceptible to "migration" out of position; minor collisions, relaxation or sagging over time, and effects from inappropriate wheel alignment could result in the radar pointing in the wrong direction.

General vision-based sensor degradations were associated with blocked FOV, misaligned sensors, and out-of-range calibration. The FOV may become blocked as a result of dirt or mud on the lenses, scratches, humidity/snow/ice/water, or any other factor that results in shifting images (i.e., blurriness) or reduced visibility of the external environment.

Other degradations noted were degradation caused by coating-related changes such as repainting over ultrasonic-based sensors or bumper fascia in front of radar and general degradation that occurs over the lifetime of a lidar-based sensor during prototype development (generally not described in detail, though lens discoloration due to exposure was mentioned).

The narrative above provides details from the interviews compiled across many SMEs. Figure 14 represents a possible mechanism by which to organize the associated sensor degradation factors captured during the interviews. The list of questions discussed can be found in Appendix A.

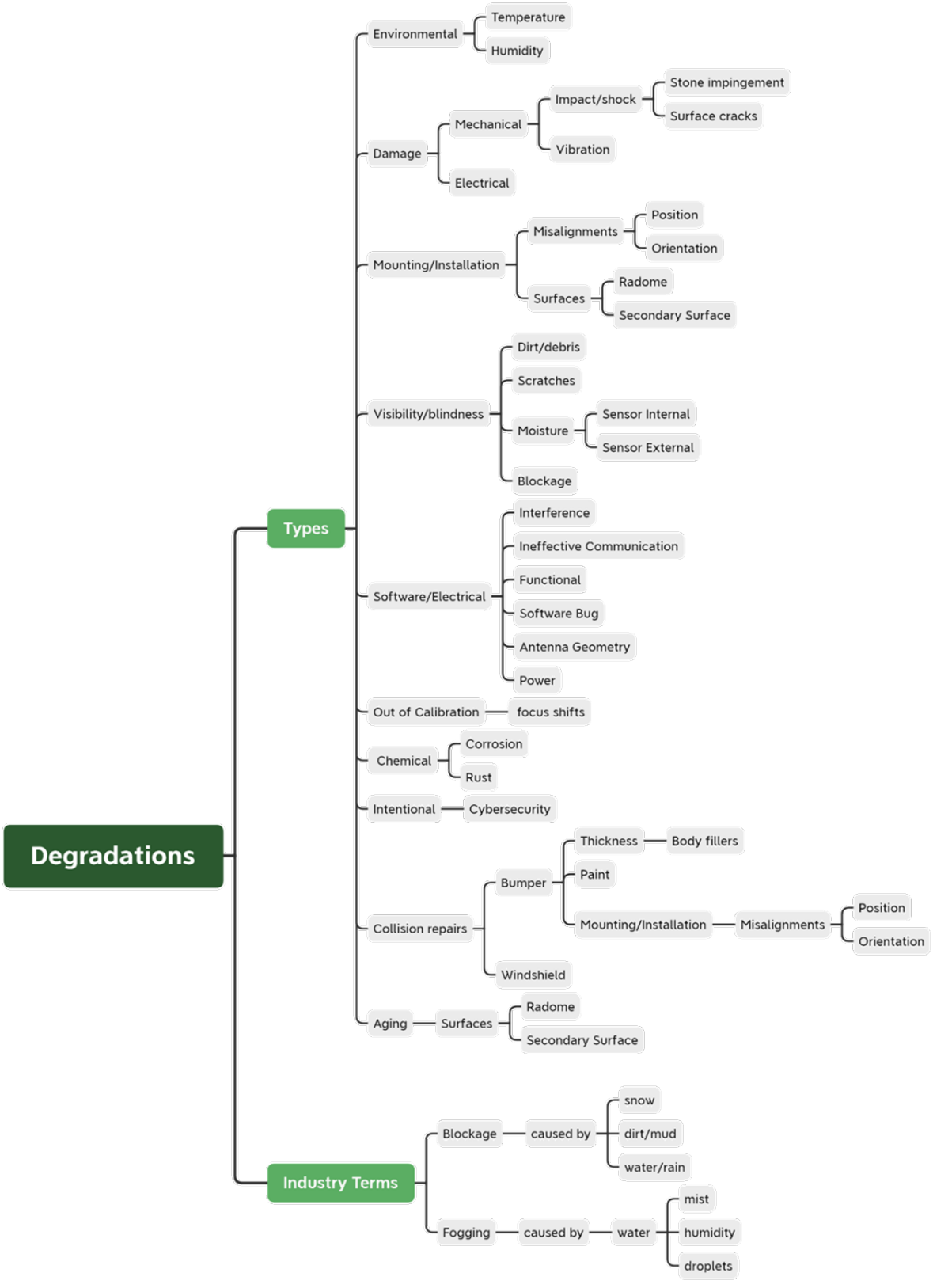

Figure 14. Forms of degradation

Design and Development Considerations

Several SMEs described a holistic or system-wide approach, taking into consideration all malfunctions; that is, considering anything that could be a potential malfunction and the resulting outcomes. One organization ranked potential malfunctions according to the impact on the system and associated side-effects of the malfunction. The malfunction is then designed out of the system, or a robust monitor is developed to detect it and take appropriate (e.g., diagnostic) actions. Others noted that mechanical shock testing (i.e., a generic set of tests performed for the sensors and electronic control units, depending on mounting placement in the vehicle) is done for every sensor. Still others emphasized the importance of design considerations. For example, design is critical in managing water around the sensor, developing the coverings to prevent the intrusion of foreign materials (e.g., dust), accounting for heat near the sensor, and identifying materials that might come between the sensor and the secondary surface in front of it (e.g., road grime between an emblem or bumper). Throughout the discussion, design considerations for potential degradations associated with stones, rocks, and pebbles was mentioned, particularly for radar and especially evaluated as part of durability drives at the systems level. Additional methods to deal with faults include:

- Turning hardware systems off when a malfunction mode is detected (due to an inability to pinpoint them); and

- Turning off affected portions of the system while leaving other functions on (e.g., if steering wheel input is lost, functions not requiring this input could remain active).

Noted challenges associated with the validation of sensor systems included the controllability of testing environment and external factors like water projection and ambient light impact as well as the general need to rely on simulation and/or controlled physical testing.

Considering repair and maintenance, SMEs noted that the focus was primarily on calibration, alignment, and orientation as opposed to repair. Guidance or maintenance recommendations were limited mainly to alignment or replacement of undamaged, older sensors.

The narrative above provides many details from the SME interviews. Figure 15 represents a possible way to organize part of the degradation-related elements captured during the interviews about designing the sensors.

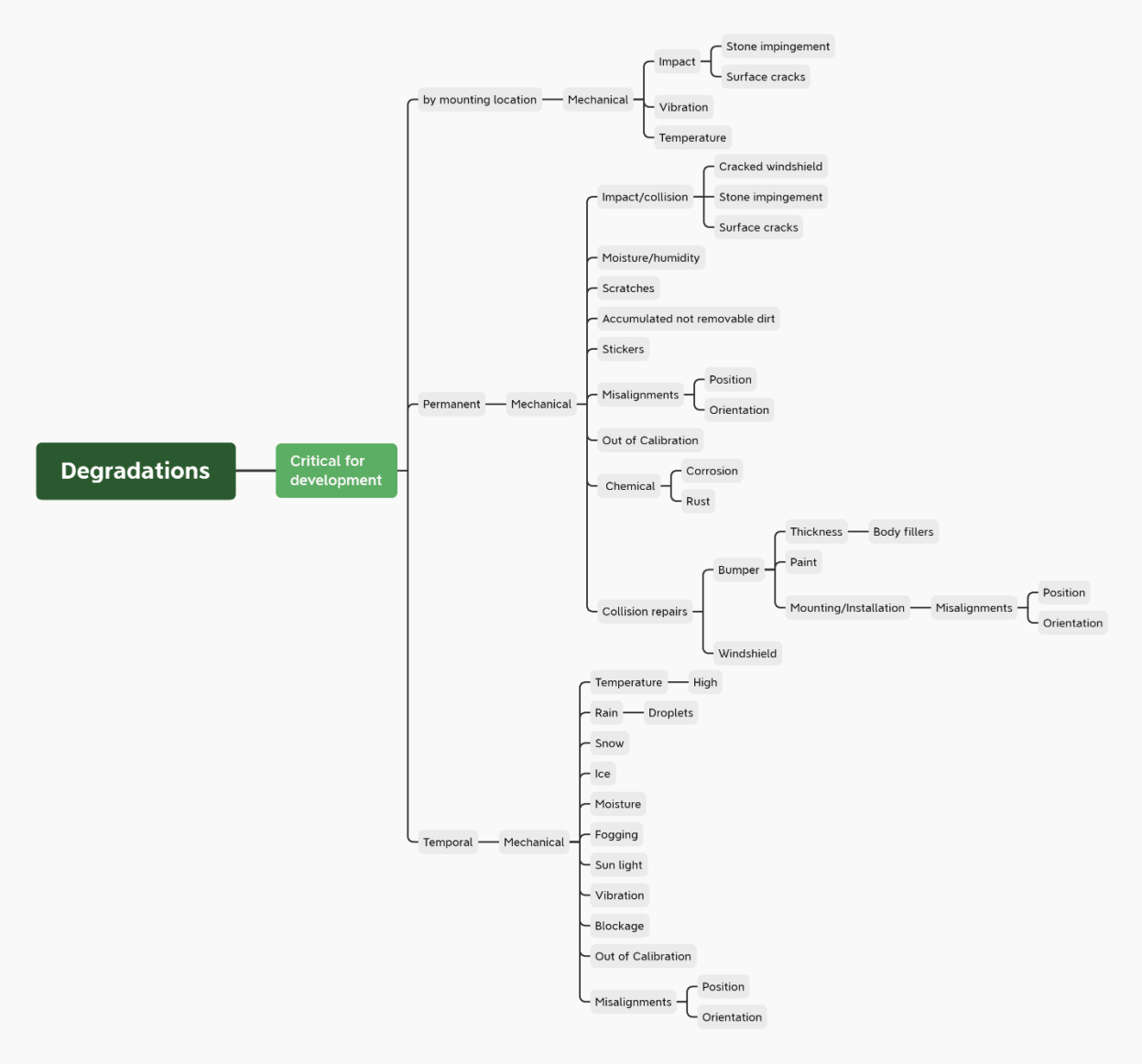

Figure 15. Degradations of interest

Sensor-Related Performance Requirements and Specifications

The next topic explored the performance requirements and specifications associated with sensors. Researchers expressed interest in determining whether the organization set the sensor requirements and specifications or if they were provided to them. Discussions revealed that the process appears to be collaborative and dynamic in nature.

Most OEMs interviewed set the performance requirements and specifications—either at the vehicle level or within a specific functionality. The suppliers then tended to respond to these requirements and specifications by developing the sensors to achieve the functionality from a sensing standpoint. In other instances, the supplier and the OEM worked collaboratively to discuss the sensor performance and parameters to identify realistic alternatives for market development. Industry leaders, through their innovations, may guide the development of specifications, for example, by identifying new features that they want to offer and the use cases for that feature to motivate shared development of sensors and ADAS. Thus, depending on the organization and the technology/project in development, the expertise needed to set the specifications may be in the organization or external and may require/benefit collaboration between the supply chain.

Feature specifications often consider international standards and latest industry directions. Suppliers work closely with OEMs to define the set of possible sensors to be used for a specific ADAS feature or system. All sensors are considered at the initial concept phase; then, sensor comparisons are run and a set of specific sensors, with particular parameters and performance measures, is defined. Further, different organizations may have different performance level definitions or features, requiring adjustment of the fault conditions. Global NCAP requirements are also monitored to ensure that specifications are consistent.

Both suppliers and OEMs perform validation testing; labs in these organizations used for the validation testing and certification process tended to be self-certified. Testing is done at many stages of development to validate the designs and the product, and engineers can be heavily involved in the test process, traveling to test sites, and overseeing the management of the tests. System engineers and functional safety engineers monitor this process and can intervene as appropriate. Suppliers may be required to develop additional internal validation specifications, which may then be reviewed by the OEM's validation experts. This ensures that the validation process is well understood, agreed upon, and transparent. Figure 16 is a graphical representation illustrating the entity that sets the requirements and the standards that are considered.

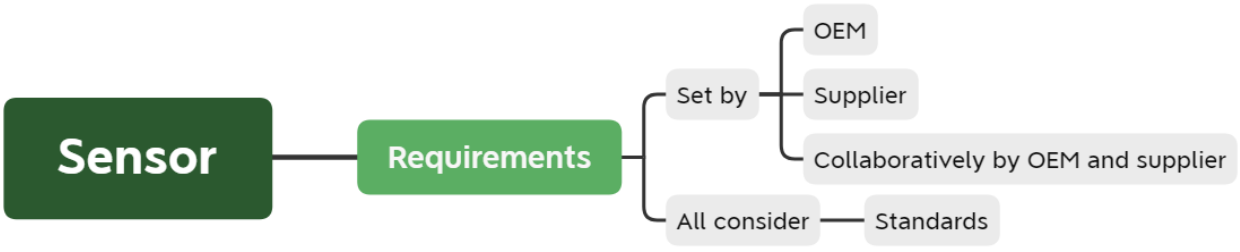

Figure 16. Sensor requirements

Sensor-Level Testing and Validation Approaches

This section provides a summary of the discussions held with SMEs regarding their processes and tests used to validate sensor performance and explore testing under degraded states and the metrics used to quantify those states.

According to one SME, measurement apparatuses (e.g., shake, salt, chambers), simulators, and proving grounds are used for sensor validation processes and tests. Another SME mentioned using a rain tunnel that can control the rain rate in millimeters, which allows radar performance to be precisely measured in real time. This SME emphasized the importance of distinguishing between droplets on a stationary bumper and wetness smeared across the bumper at speed, as the latter has a greater effect than the former. The same SME noted that snow on the bumper might make it difficult to see it but pointed out that the radar would still be able to see through the snow. The SME emphasized the importance of understanding the sensor capability limitations when designing durability tests to mitigate degradation effects.

Various SMEs also discussed using heat chambers and outdoor sites to expose sensors, such as lidar systems, to cold and snow as they work on developing new features. Calibration, alignment, positioning, pre-test scans, and diagnostics were also discussed. With regard to radar, the following were mentioned: confirming an array of parameters before and after validation tests, exposure to a broad array of environmental influences, blockage detection, misalignment detection, external influence detection, and tunnel detection (e.g., noisy reflective environment). For camera (vision) testing, pre- and post- comparisons can be used to ensure that the lens and imager focus scores are within a certain tolerance; even if there is some degradation (e.g., scratch on a lens), the algorithms may be able to tolerate the focal lens shifts. Humidity, shake, and reverse voltage power were also mentioned as testing areas.

Many standardized tests were noted to be on the vehicle level, such as those prescribed by the IIHS or NHTSA's NCAP. One SME mentioned that standardized tests are run based on ISO 26262, but the interviewee stated that some standards are not related to lidar, so adjustments need to be made as these sensors become more common. Testing standards mentioned for vision included product validation tests, endurance runs on the supplier side, hardware-in-the loop where the different components are on the software loop, and 3- or 9-point functional tests for temperature and advanced aging. Testing standards for radar included the closed loop control system for accurately measuring the radio frequency transmission and reception.

With regard to vision testing, Federal Motor Vehicle Safety Standard No. 108 was mentioned; this standard requires the electronic control unit to be put on a random vibration access. After the part being tested is shaken, the participant stated it was important to verify that the light source can still be detected within the same tolerance pre-test. Another vision system test involves exposing the camera to bright sun for a lengthy period to verify that the imager is not damaged by excessive natural light.

Some SMEs mentioned specialized testing. One noted that different vehicles will have different radar signatures due to integration factors such as production differences on the front facia of the vehicle. To address this, equipment can move different target types (e.g., a truck, a pedestrian) in the distance domain, and then the radar sensor can be rotated in the azimuth domain to evaluate the radar performance as a function of relative object location. Lidar specialized tests that were mentioned included test lines, scanning patterns, resolutions, and range tests. The effect of blockage was also noted in response to this question. In certain cases, a 75 percent blockage

might still result in the ability to see 50 percent of the range. In that specific situation, the 50 percent range is considered in the performance evaluation to determine if the function is turned off, indicating that some sensors may have capabilities well beyond the minimum requirements for the feature. One SME noted that specialized testing is conducted to ensure that foreign material does not build up between the sensor and the surface, which could create a false warning and confuse the user.

The narrative above details the SMEs. Figure 17 represents a possible way to organize part of the sensor validation methods captured during the interviews.

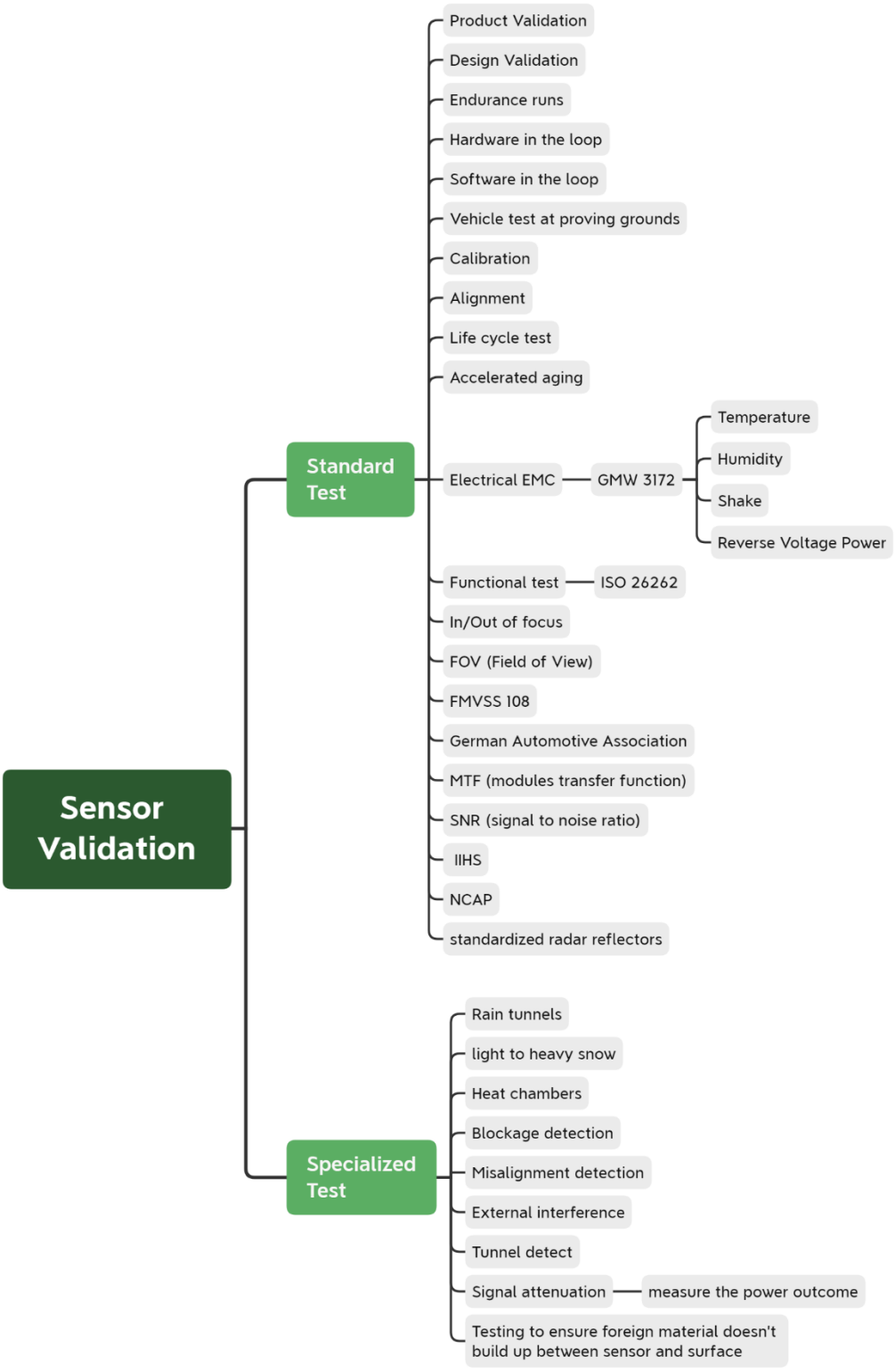

Figure 17. Sensor validation methods

Sensor Testing in Degraded States

All organizations interviewed said that they performed sensor testing under degraded states. Metrics used to quantify performance under degraded states varied based on the function and the sensor type in question. Further, when evaluating a sensor, its function in the system being examined may be taken into consideration, so there may be several performance requirements for the same sensor in different vehicle platforms/packages. For example, a vision-based system may have a higher standard for object detection than for lane detection depending on the feature(s) supported by the sensor. Metrics are then specified for the sensor function, and the sensor is tested at varying levels of degradation to see how serious the performance impact is from both a sensor and a system perspective.

Metrics Used to Quantify Performance

For radar-based sensors and vision-based sensors, metrics mentioned include system-level (e.g., false negatives) and sensor-level (e.g., object loss, received signal power, SNR, misalignment angle). Distance performance was also noted in relation to radar-based sensors. Shifting radar alignment (e.g., upward or downward) will modify the range of performance capabilities when compared to the vehicle in its new state. Additional general metrics used to assess degraded states are key performance indicators such as false positive and true positive rates and distance and speed measurement errors.

Methods Used to Simulate Degraded States

When asked how degraded states were simulated during testing, a variety of approaches were identified. For example, simulation was used to test algorithms associated with lidar-based sensors to save time and reduce effort. Some SMEs noted that they simulated scenarios by creating artificial conditions in a test environment, making it look like a real scenario (e.g., using ambient conditions like temperatures, heat chambers, the aforementioned weather/rainfall simulation, etc.). Others clarified that their tests were real outdoor winter tests in cold-weather facilities (e.g., testing for blockage due to snow and ice) as opposed to simulated environmental conditions. One SME noted that there are environmental and mechanical tests that are standardized from a sensor level that are meant to simulate the lifetime exposure of a sensor to the environment and the types of situations it would encounter. It was also said that pre- and post-functional testing is conducted to determine degradation and the associated impact. One SME also pointed out that they tested with aged conditions, but with unspecified aging characteristics (e.g., conducting testing with a tightly controlled scratch versus simply aged sensors with unmeasured levels of lens scratches from use).

When probed for additional details about testing that may be performed to evaluate sensors in degraded states, SMEs mentioned the difficulty in simulating real scenarios and testing corner cases given the breadth of potential test conditions. As a result, several types of testing are conducted (e.g., testing in heavy and light rain). In addition to winter test facilities, one SME noted spending time in a cold chamber with a focus on environmental testing related to snow and ice.

A few SMEs mentioned product validation testing followed by functional testing. For example, extended durability tests are conducted to ensure sensors are staying within specification. Pre- and post-testing is conducted to measure degraded state attenuation in angular error. Another example included taking advantage of the degraded sensor state following product validation testing to measure the functionality in the degraded state (e.g., sensor blockage due to snow,

misalignment, or improper positioning of sensors). In the misalignment case, sensor angles would be manipulated to determine the degradation's impact on performance.

Sensor Self-Diagnostics

The final discussion point in this section of questioning explored whether sensors performed self-diagnostics. Radar-based sensor systems were noted to incorporate self-diagnostics to monitor degradation. For example, algorithms are used so that the sensor can test itself to determine its typical object detection range estimates to identify when it is blocked. Further, these systems can determine the percentage of blockage to evaluate whether a function is still available and can compensate up to a certain number of degrees. Radar-based self-diagnostics were specifically cited as including detection for tunnel, blockage, misalignment, and "numerous" internal health monitoring parameters. Internal radar diagnostics monitor a large range of parameters that are communicated to a central controller and are then accessible by service personnel. The diagnostics also provide capability information to a system or subsystem used to guide actions of the ADAS under certain specified conditions.

Vision-based sensors were also reported to have considerable self-diagnostics capabilities. These may include algorithms that might be defined to identify critical blockages versus non-critical blockages. Calibration and self-calibration parameters can also change. The sensor may detect that it is not aligned correctly, in which case there are calibration processes to realign (both automatic and manual according to the severity).

Lidar-based sensors were noted to alert the system to automotive DTC and to detect blockages. As these sensors continue to mature, it was implied they lidar diagnostics would be comparable to a combination of diagnostics supported by radar and vision-sensing systems.

Redundancy in sensor-based systems was frequently mentioned and took a variety of forms, including validity comparisons across systems through overlapping FOVs (e.g., two radars in rear corners), and more comprehensive fusion between two sensors that provide a single combined output for increased measurement accuracy. Additional examples included redundancy that coupled vision with inertial measurement, where both light and motion are compared (used to detect blockages) and the use of pixel algorithms (e.g., to detect rain or road spray) to monitor the anticipated performance of the vision system. In some instances, the sensor will not provide any information through self-diagnostics unless there is a complete malfunction (e.g., voltage or ground supply), whereas in other cases the sensor provided degraded measures but paired them with a confidence attribute for downstream determination of ADAS feature availability.

Through the self-diagnostic process, faults are categorized as recoverable (e.g., communication malfunctions) or non-recoverable (e.g., hardware malfunctions such as electrical or mechanical damage). Recoverable malfunctions are temporary in that they could heal, while a non-recoverable fault would require service.

System-Level Testing and Validation Approaches

SMEs provided input on the tests performed for validating ADAS. One response said that all functions are tested under various conditions for 100,000+ km on proving grounds and in real-world traffic. Another SME said that many complete vehicle checks are conducted during development. A third SME stated that when a fault is noted in a system at the vehicle level, the source of the issue is identified and compared to the component-level testing. All feature validation is done at the vehicle level, according to another SME, since many subsystems must

work together to complete various tasks for the ADAS to function. Another SME said that a system verification test is critical and is where most of the validation testing occurs rather than at the component level.

When asked about standardized testing performed, SMEs said that their testing included electromagnetic compatibility, NCAP (e.g., AEB), IIHS, United Nations Economic Commission for Europe, Chinese National GB Standards, and the ISO. It was noted that testing depended on the feature and the country, as some features have standard performance requirements and legislative documentation on how the feature performs. NCAP (e.g., AEB) was cited as an example, as it specifies a test procedure on how to perform a test at the vehicle level. Speaking in general terms, the following types of standardized tests were mentioned: mechanical, electrical, consumer tests, functional, safety, and diagnostic tests on benches and hardware in the loop simulations.

SMEs were also asked to comment on specialized testing. One SME stated that integration of radar into a vehicle is a unique experience for each model due to variations on the facia and bumper. Another noted driving the vehicle for the accelerated lifetime of a vehicle under various conditions on highways and rough (e.g., gravel) roads to see the effects of aging on the systems. Encouraging extreme aging in corrosion with a high-humidity salt environment and testing for the impact of ice and snow were also mentioned by this SME. Another response regarding LKA noted that the system identifies the vehicle path to maintain and that the deviation from that path can be examined. In addition, studying how safe the test driver feels regarding any deviations in actual traffic was noted.

The narrative above provides details from the SMEs. Figure 18 represents a possible way to organize part of the system validation methods elements captured during the interviews.

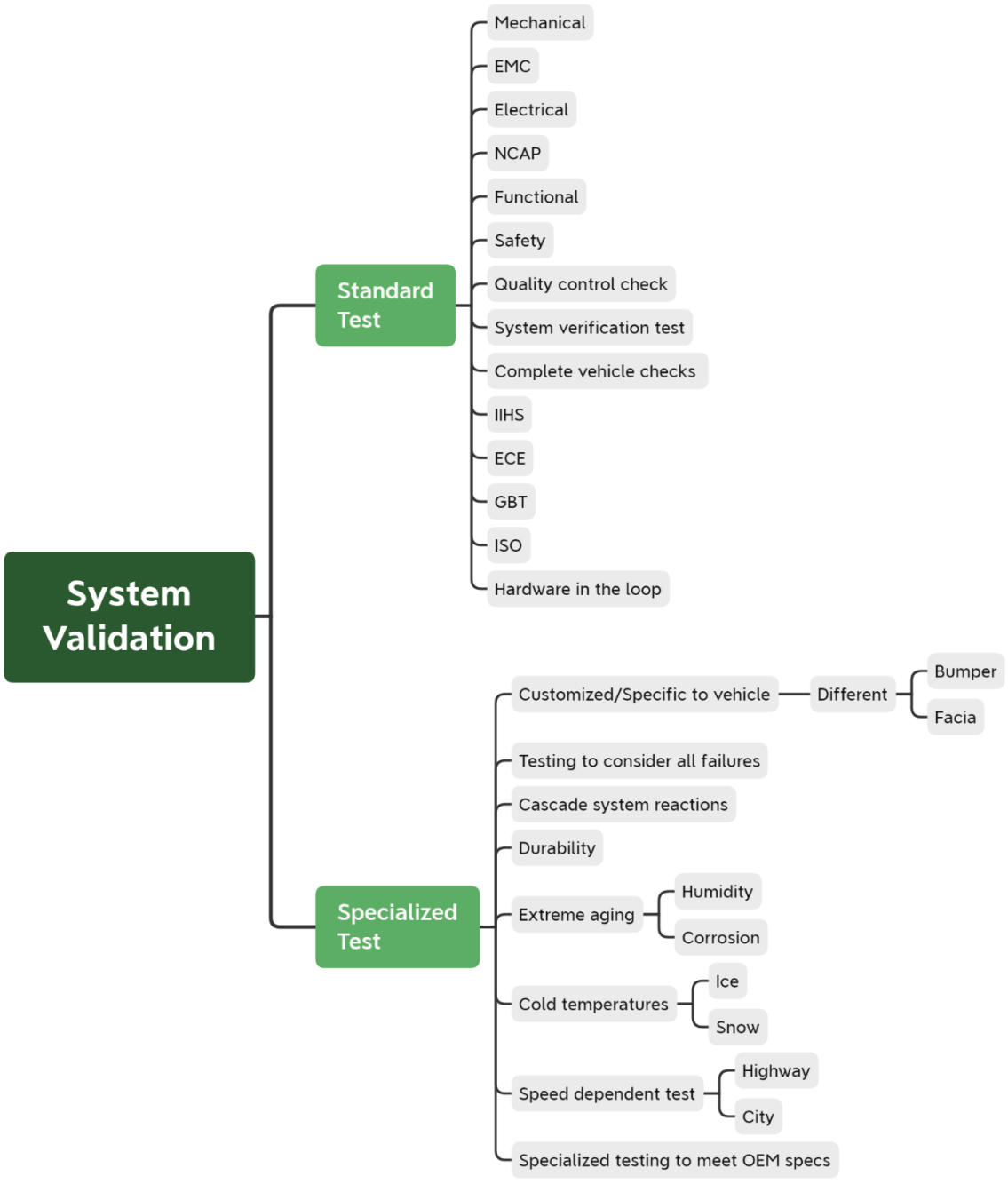

Figure 18. System validation methods

System Operation in Degraded State

SMEs were queried about system operation under degraded states, and they said that users are often informed of this state. Some examples of the notifications provided are specific as to where the malfunction exists; for example, “blind spot system isn’t functioning” or “parking sensor is blocked.” Some sensors in a degraded state will turn off the associated feature and notify the user

until the situation is resolved. Temporary states, such as a mud-covered sensor, are conveyed to the user so it is clearly presented that action is required (i.e., clean the affected area) to regain functionality. While some systems simply turn off due to degradation, others consider the level of degradation (e.g., how far the sensor can see) to determine whether the ADAS feature was still supported. In most cases, SMEs implied that ADAS features do not tend to run when performance is notably degraded; however, it was stated that in some instances ADAS may continue to operate, particularly if the extent of degradation is difficult to measure. Some systems perform self-diagnostics, and one SME noted that sensors self-align using software and that self-alignment runs all the time, constantly compensating for small changes due to aging. It was also noted that proving ground tests can be helpful in evaluating system performance in degraded states during system durability testing.

Information Given to Users

The degraded state information communicated to the user elicited many responses from the SMEs. All said that messages are conveyed to the user, but the extent of the transmitted information varied among respondents. The capability to provide general information (e.g., system is activated, deactivated, or in degraded mode) or specific details (e.g., sensor has become detached from the bracket) exists, but detailed and irrelevant information was not given because confusion and frustration of the driver was indicated as an undesired potential outcome. Each degradation source may warrant a different communication strategy based on the needed response (e.g., take vehicle for service versus clean sensor). While a message with detailed information might be appropriate when driving at low speed (e.g., in a driveway), such information may not be desirable when traveling on a busy highway due to the potential for eliciting driver distraction. The feedback received indicates that suppliers can provide various diagnostic functionalities, but the OEM will ultimately select what type and amount of communication they want the system to provide.

Use of Sensor Interaction and Fusion

When asked if their organization used interaction/fusion between sensors to address degradation concerns, most of the SMEs responded affirmatively, though not across all ADAS features or sensor packages. The reasons given referred to the benefits of redundancy and of bringing the complementary strengths of different sensors together. One SME mentioned sensor-specific diagnostics and system-level cross diagnostics, and the combination providing a multi-point check system. Fulfilling product liability was also cited by a different SMEs as a reason for this redundancy, though higher levels of automation were implied during this part of the discussion.

One SME who responded in the negative to this question said that the sensors function independently so as not to rely on another system to help identify when there is a problem with the sensor; instead, they self-diagnose for problems such that sensors could be packaged without requiring specific secondary fusion sensors for ADAS features and diagnostics to function appropriately.

It was also mentioned that the OEM sets the functional requirement for a feature allowing the supplier to use sensor fusion to meet that requirement. Thus, sometimes two systems (such as a camera and radar) are provided by the same supplier. In these instances, the sensor array may be packaged with a specification for fusion, even if the OEM does not request or require it. While interpreting the input of one SME, it appears that sensor fusion is used for accuracy improvement, not to mitigate or evaluate degradation. Thus, it appears overall that sensor fusion

is leveraged for different purposes across respondents, which may or may not improve resistance to the performance impacts of degradation.

Testing Recommendations

SMEs gave substantial input regarding where resources were focused for testing. Weather-related effects on radar, such as moisture, rain, snow, ice, and heat, were cited in several responses. It was noted that there is much potential for degradation due to wetness—of the sensor itself, of the air in between, or of the bumper in front of the sensor—and these situations warrant further study. It was mentioned that a possible test could be created, if and only if there is a controllable way to drive a route with water spraying the outside of the bumper to simulate the effect of rain. It would need to be reproducible and/or repeatable.

Blockage caused by dirt was cited as another issue that deserves investigation. Simulating the build-up of dirt (as well as snow and water) on all types of sensors can reveal the point at which the FOV is reduced past a certain level. With regard to radar, it was noted that it is easy to determine and clean the outside of the bumper when it is dirty, whereas it is difficult to detect level of dirtiness on the inside the bumper as well as hard to clean. One SME noted that transparent sticky tape can be used to collect samples of dirt that accumulate behind the bumper.

Tests on the distance performance of radar and lidar were mentioned in some interviews. This was acknowledged as a tricky area, but suggestions referred to measuring the distance that is accurately detected by a working sensor, and then testing the distance with a low-reflectivity measure delta prior to and after degradation of the sensor. A potential visibility test mentioned by one SME was partially to fully blocking the lens on the lower part of the camera and running an ADAS test on lane or marker detection. The same idea of visibility blocking could be used for testing object detection.

Several SMEs referred to the importance of the preventive measures that can be incorporated in sensors. With radar, brackets can be designed to hold the radar units, which also serve to keep the radar clean (e.g., first blocking and then limiting the space for accumulating of debris). The strategic positioning of radar can also allow for more accurate assessment of the thickness and type of dirt that accumulates over time. For example, a corner sensor that is 3.8 centimeters away from the bumper can allow for easy simulation and measurement, and the radar can indicate the loss resulting from the dirt.

One SME noted that certain manufacturers are very precise as to where the radar needs to be pointed, implying that with less precision comes a greater need for troubleshooting. Misalignment, mispositioning, and visibility issues were specifically mentioned with regard to camera (vision) systems, as was the resulting need for calibration—including online calibration—to make corrections to these problems when necessary.

One response addressed the challenge of making sure that the OEM-recommended procedures are followed for restoring the systems back to a safe, functional state when warranted. It was noted that since the insurance industry is interested in the safety features provided by advanced technology, they need to be agreeable to following OEM specifications when repairing a vehicle to prevent system degradation or possibly endangering consumers.

Even though there are no standard industry practices to test sensors under degraded states, there is some activity aimed at understanding how sensors perform under degradation. One SME

commented that there are many degradation-related assessments that have not been conducted, and thus there are opportunities for future work in these areas.

Test Plan Development Considerations

After conducting and analyzing all interviews, some information was extracted and used for test plan development. The following are test plan developments that were considered.

Vision Camera

Elements that appear inside and outside the vision camera lens are of particular interest when conducting testing. The effects from elements such as water and dirt and their physical forms were of special interest to most SMEs.

- Water droplets degrade the performance of vison cameras. Droplets could be found outside and inside the sensor lens (also referred to as moisture), which would block and reduce the vision camera's FOV.

- Dirt is another factor of particular interest. Its accumulation, particularly outside the vision camera, degrades the sensor performance.

- Mud created from the mixture of dirt and water outside and inside the sensor is also a sensor degradation factor.

Developing a test plan around the three elements above (water droplets, dirt, mud) that are permanently present in the sensor's FOV seemed of particular interest to all interviewed SMEs. In addition, the project considered other degradations (such as scratches) that could occlude or distort the signal coming into the camera. The amount of the elements and their location in the FOV would be the independent variables to be manipulated. The test plan would then measure their effects on the image captured, potentially considering the number of pixels affected and the region blocked as metrics of sensor degradation. Depending on the sensor output signals that could be accessed, the performance of the sensor could be measured in the form of (1) successes and malfunctions on object detection, (2) the amount of image distortion imposed by the degradation, and (3) report diagnostic information coming out of the degraded sensor, which in turn could be used for the vehicle function and to alert the driver.

Calibration is another effect of particular interest in the industry. The test plan considered vision cameras before and after calibration and measured performance quantities, such as FOV size, distance to focal area, and location of focal area (center of FOV, upper left, etc.). Depending on the accessibility of the output signals, this considered the successful identification and classification of objects of interest, such as pedestrians, lane markers, other vehicles, traffic control devices, etc.

Radar

Elements that appear outside the radar sensor housing are of particular interest in conducting testing. The following areas around the radar can be identified: (1) between sensor housing and the bumper, (2) the bumper itself, and (3) the front of the bumper. Area 1 is of interest, as in most cases such an area cannot be accessed to clean away any contaminants, such as dirt, mud, or ice. Area 2, the bumper, could absorb road elements, such as dirt, grease, and moisture. These

entrapped elements in Areas 1 and 2 can degrade sensor performance. Some of the industry approaches to overcome the issues related to Area 1 rely on designing mounting brackets that reduce, and could potentially eliminate, the gap. For the purposes of developing a test plan to simulate degradation on Areas 1 and 2, some suggestions from SMEs were to simulate the contamination using paper-thin layers on a bare sensor. The paper-thin layer could be wet, frozen, or greased to simulate entrapped moisture, ice, and dirt.

Another degradation of interest is sensor misalignment, which typically occurs due to "sagging" of the bumper or other slow deterioration of the vehicle (suspension sag, bracket loosening, etc.). This happens over time due to age, accumulated road vibrations, or minor impacts. Misalignments affect the sensor's FOV and therefore cause it to point away from the originally intended direction. Our test plan development involved radar misalignments and considered misalignments in the three angular quantities that can be measured to characterize its mounting orientation: roll, pitch, and yaw. Performance metrics considered the effects on the FOV and the effects on the main measurement provided by the radar–range to targets.

Lidar

Elements that appear outside the lidar sensor housing are of particular interest in conducting testing. Weather such as rain and snow are of note due to their blockage and reflective properties. SMEs suggested using a target with low reflectivity in particular for weather testing to emphasize the sensitivity.

Another test of interest is related to rain drops accumulating and adhering to the lidar window. This could affect the sensor performance in quantities such as range, resolution, and FOV (through lensing due to surface tension). One potential independent variable would be the amount of wetted surface area on a lidar window. One of the main quantities measured from lidar is the range. Range could be measured to quantify sensor degradation and, depending on accessibility of the sensor output signals, resolution and size of FOV could also be used.

Ultrasonic and Thermal

Through discussion with NHTSA and OEMs, it was agreed that ultrasonic and thermal sensor would not be included in the study.

Literature Review and Stakeholder Outreach Considerations

First, despite a lengthy search on ADAS sensors and features available on the market, the exact sensor or combination of sensors used on any given platform were not readily available. Even the features available on a given vehicle were difficult to determine with certainty. In addition, the knowledge of the sensor type and model, as well as whether a fusion architecture was being used by a given ADAS feature, was generally unknown. This lack of detailed ADAS information was further complicated by an inconsistent naming convention, a diversity of ADAS feature capabilities, and a plethora of sensors across vehicle manufacturers and models. These factors created an environment in which we had to dig deeper to identify sensor/vehicle test candidates and carefully consider selection to maximize relevance of the results. Fortunately, the direct collaboration from industry partners helped guide the selection. Further, the selection was partially motivated by the availability of stand-alone sensors, which were tested in isolation from the ADAS while also being available in a vehicle acquired for system-level testing.

It was clear that ADAS sensors have matured considerably enough in recent years that late model vehicles and their associated sensors were the focus of this work. Features such as FCW and lane change warning are maturing into AEB and LCA through refined sensing technology and automated vehicle control. The literature review showed that more advanced features leverage complex sensors and systems. The added complexity of these systems provides opportunity for faults, which could decrease the safety assurance provided by ADAS. Alternatively, these more capable and refined systems demonstrated performance and a resistance to degradation well beyond the entry-level systems. During the testing phase, it was found that ADAS systems that used sensor fusion were capable of providing the ADAS feature even when individual sensors were completely degraded and not functional.

Based on the literature review, it appears that vehicle service shops and owners are expected to understand and monitor some of the issues associated with sensor degradation. For example, sources reviewed (AAA Automotive, 2018; Börner & Isermann, 2003; Linkov, 2018; Grimaldi & Mariani, 2001; Arage Hassen, 2006) said that modification to vehicles with after-market components, minor body repairs, and aging may call for sensor calibration. The ADAS may not be capable of issuing a DTC when the sensor is not calibrated, which may imply a reduction in ADAS performance without awareness from the vehicle operator. The work in this project considered whether the DTC are tripped as a result of sensor degradation or if ADAS performance simply diminishes with little feedback to the driver.

Servicing ADAS systems can present a technical and cost challenge to individual repair shops (AAA Automotive, 2018), creating potential barriers to retaining ADAS performance when degradation occurs. Calibration of sensors involves specialized tools (AAA Automotive, 2018), and interviews revealed that there does not appear to be a standardized procedure that independent service centers may apply. Interviews also revealed that it is unclear whether frequent services, such as windshield replacements, are understood to have potential impacts on ADAS by service providers and vehicle owners.

Literature reviews and interviews do not constitute an exhaustive search, but they revealed a sample of the test methods and test equipment used to evaluate the performance of automotive sensors. Some sophisticated lab equipment and procedures are available for bench testing components (Gamarra-Diezma et.al., 2015; Jokela et al., 2019; Koopman et.al., 2016; SAE International 2017, 2019). These systems are intended for organizations that regularly test and validate system components. Some interviewees expressed that, for the testing of the real-world impacts of degradation, the focus should be on experiments that tend toward in situ environments rather than more sanitized laboratory environments.

Accepted sensor degradation metrics were not defined in the literature reviewed. A comprehensive list of potential degradations to sensor systems was not identified. Thus, an attempt to define metrics was included as part of synthesizing the literature to form a basis for developing a final list of degradations of interest moving into the test plan phase. The preliminary metrics were redefined according to inputs obtained from suppliers and OEMs during interviews. In addition, mechanisms for degrading perception sensors, particularly at an accelerated rate, were not identified in the literature. The study dedicated resources to developing methods for creating degradations that are valid and repeatable.

Fortunately, there is a foundation upon which the ADAS level testing may be developed. NCAP in both the United States and Europe, along with ISO, have proposed and documented several

tests for most of the common ADAS. These tests are generally repeatable and provided the resources available to the project. They may be expanded and refined to be appropriately specific to sensor degradation testing with input and collaboration from the appropriate stakeholders.

While the literature review report is not an exhaustive source of information for understanding the implications of sensor degradation, the level of effort put into locating information relative to the acquired information demonstrates the potential for impactful research in this area. The literature review suggests there is a limited body of knowledge on the implications of sensor degradation on the safety performance of ADAS over the lifetime of the vehicle. Interviews with OEMs and automotive suppliers were of great assistance in establishing the non-public level of awareness and readiness for sensor degradation as well as defining the test plan for this project.

This page is intentionally left blank.

Chapter 4. Degradation Development

The primary goal of the degradation development was to identify key degradations for different sensors, develop methods to replicate or simulate each degradation, and validate that the simulated degradation replicates the effect of the real-world degradation on sensor element performance. The secondary goals were to (1) identify the levels of degradation that may be of interest to test at the component level and (2) provide early insight into which degradations are likely to have the greatest impact on sensor and ADAS performance.

The following describes how the study identified, developed, tested, and evaluated the degradations.

Survey of Degradations

Degradations were initially selected based on the Literature Review. The initial list of degradations was grouped and organized as shown in Figure 14. Using the initial list of degradations, and discussions with NHTSA, Table 15 shows the list of degradations pursued for this project. Rain and lighting were not carried forward as part of this study because they are temporary and are being investigated as part of a separate NHTSA-funded sensor characterization study.

Table 15. Types of Degradations Identified

Degradations Pursued	Camera	Radar	Lidar
Mount displacement	x	x	x
Debris accumulation*	x	x	x
Repair not to OEM spec**	x	x	
Obstructions/blockage	x	x	
Pitting/scratches	x	x	x
Water absorption		x	
Discoloration	x		x

* Radar/lidar = road debris; Camera = off-gassing film.
** Radar = bumper repair; Camera = windshield replacement.

The researchers started the task of searching for real-world degradation samples supported by local searches around VTTI in collision repairs and junk yards and national searches supported by the Society of Collision Repair Specialists.

Degradation Replication and Testing

The researchers collected real-world degradation samples; some examples are shown in Figure 19. The left picture shows a bumper with scratches, and the right shows a slightly misaligned radar that also has insects stuck to it. The insects look like flies, bees, or similar.

Figure 19. Real-world degradation samples

The researchers then produced degradation samples to simulate those encountered in real-world situations. However, the survey of vehicles was limited in what it returned as far as variety and intensity of degradations. To ensure the scope of the research was adequate, the research replicated degradations that went above and beyond the collected samples. At this point in the research, there was not prior knowledge on the level of impact each degradation has; therefore, the intensity of these degradations was initially targeted at an extreme level. This first pass at degradation development was only a high/low test to check for existence of a sensitivity to degradation. In the component testing, this was expanded to three levels (low/medium/high) using the extreme sample made in degradation development to define a reasonable range of intensities.

To facilitate the application of the degradations to sensors in subsequent testing, the degradation used a base material to apply the simulated degradation. This allowed the degradation slides to be easily moved between sensors to reduce variability due to potential variations in the degradation treatments. The list of bases and degradations are included in Table 16. Degradations are grouped into those applicable to bumpers/radars and those that can be found on optical materials, such as windshields.

Table 16. List of Base Materials and Degradations (High Level) for Initial Evaluation

	Bumper (Radar) Degradations	Optical (Camera and Lidar) Degradations
Base Material	Polypropylene	Plate Glass
	Emblem 1, 2, 3	Polycarbonate
	Bumper (25, 30, and 35 mm thick)	Acrylic
	Aftermarket Bumper	Laminated Glass
		Windshield Sample
		Borosilicate
Degradations (high level)	Epoxy	Epoxy
	Blacktop Sealant	Clear Silicone Sealant
	Bondo	CA Glue
	Bondo and Mesh	Packing Tape
	3M Safety Walk Tape	Sanding (60-Grit 2-way)
	Foil Tape	Sandblasting (Laminated only)
	Steel Reinforced Epoxy	Cracked (Windshield only)
	Duct Tape	Tinted (Windshield only)
	Water (Polypropylene only)	Off Gassed Plastic (Borosilicate only)
	Scratches	Salt (Laminated only)
	Dirt	Epoxy (Laminated only)
	Organic (spruce needles)	Glue Primer (Laminated only)
	Salt	Shellac (Laminated only)

Base Material Validation

Sensors in automobiles are typically mounted behind a windshield, bumper, or similar materials. These materials are referred to as base materials in this project. Degradations are most likely to occur to the base materials because they are exposed to the environment. A naked sensor is one that is found exposed to the environment without an extra layer of protection (i.e., no base material in front). Therefore, a naked sensor with no additional degradations applied (e.g., no rain, snow, dirt) is referred to as baseline and it constitutes a reference for sensor performance in this report. Different materials are then placed in front of naked sensors aiming to find materials that provide the same output response as compared to the base materials typically found in automobiles such as windshields, bumpers, and similar. Finding materials that have the same sensor output allowed development of bases that can be used to simulate the originals. Then, the team took steps to ensure the same sensor outputs fall within the validation procedures. To validate the simulated bases, the study compared the sensor return with nothing (i.e., naked sensor), sensor returns with the typically found materials (i.e., windshields, bumpers), and sensor

return with the different simulated base materials (i.e., polypropylene, polycarbonate). The full list of base materials is in Table 16.

Figure 20 shows unmodified OEM parts that were used as baselines. The simulated baseline materials did not show any statistical differences from the sensor outputs. Sensor outputs (Table 25, Table 26, and Table 27), scores, and grouping (Table 28, Table 29, and Table 30) can be found in Appendix C. Therefore, simulated baseline materials were used to further develop the degradations.

Figure 20. Unmodified OEM samples to establish baselines (from left to right: bumper, emblems, windshield, laminated glass)

Three bumpers were obtained: two unmodified OEM bumpers and one unmodified aftermarket bumper. The OEM bumpers were acquired from the dealer parts shop. The aftermarket bumper was purchased from an online retailer not associated with the manufacturer. The first unmodified OEM bumper was divided into four numerical zones (i.e., 1, 2, 3, and 4), and the second unmodified OEM bumper was divided into five alphabetical zones (i.e., A, B, C, D, and E). Numerical zones contained paint treatments and alphabetical zones contained non-paint treatments, such as cuts, putty, mesh, Bondo, etc. as shown in Table 17.

Figure 20 also shows how blue tape was used to mark the zones on the bumper before treatments were applied. The list of treatments by zone is provided on Table 17. Painting treatments (zones 1 to 4) were done at an automotive shop. Non-painting treatments, as described in zones A to E, were done at VTTI's shop. Each of these zones was treated with the purpose of getting real-world samples of those treatments. Non-painting treatments included the use of a router tool with a bit shaped in the form of a "V" to simulate "scratches." The V-shape bit is also known as V-groove. The length of the superficial cut was 10.16 centimeters.

Table 17. Bumper Treatments by Zones

Zone 1	Zone 2	Zone 3
Standard surface preparation Primer only – One coat NO Paint coat NO Clear coat Constant thickness area Feather primer on one side	Standard surface preparation Primer White – Three coats Clear coat Constant thickness area Feather paint on one side	Standard surface preparation Primer White – One coat Clear coat Constant thickness area Feather paint on one side
Zone 4	**Zone A**	**Zone B**
Standard surface preparation Primer Metallic Red – Three coats Clear coat Constant thickness area Feather paint on one side	4-inch V-Groove (Not cut through) Repair with putty front face only Sand front face No Paint or primer	4-inch V-Groove and cut through Repair with epoxy and mesh on back face Repair putty front face Sand front face No Paint or primer

Zone C	Zone D	Zone E
4-inch V-Groove and cut through Repair with plastic weld Sand front face only No Paint or primer	No cuts “Repair” with putty front face only Sand front face No Paint or primer	No cuts “Repair” with epoxy and mesh on back face No work on front face No Paint or primer

The study collected data using a selection of targets and sensors. The targets included typical calibration targets as well as common targets found while driving (Figure 21). The left figure includes two radar calibration targets and the ISO chart used to determine camera characteristics. The right figure shows the four real-world targets consisting of a construction cone, pedestrian, speed signs, and sedan. The same pedestrian was used all along the study. During degradation development, data was captured from a real pedestrian, i.e., a human posing as a pedestrian, wearing the same clothes, as shown in Figure 21.

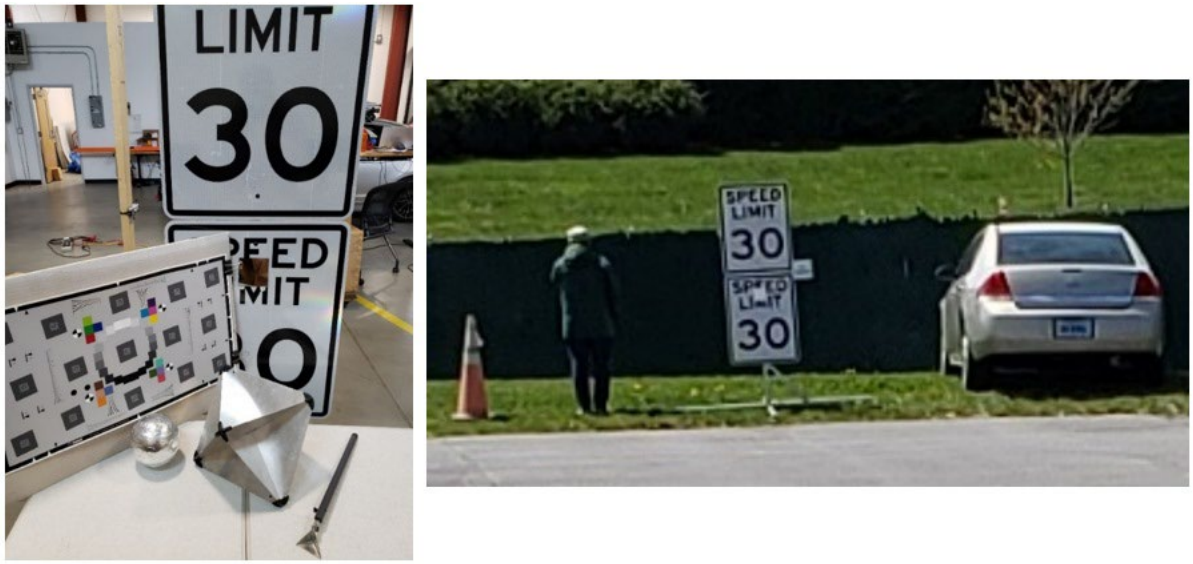

Figure 21. Targets used to compare the effect of base materials and degradations

The study collected data for analysis with different quality cameras (consumer grade and lab grade), a selection of radars (different sensing ranges, frequencies of 24 GHz and 77 GHz, and different manufacturers), and lidar with different point cloud densities and configurations. An overview of the procedures is provided in Appendix B. A set of data with no base material or degradations provided baseline performance. The study then collected and analyzed the data with the different base materials and degradations.

Initial Degradation Exploration

The effects of the individual degradation factors and their relative magnitudes compared to those of the other degradation factors was assessed through a stepwise design of experiments (DOE) with the outputs of each experiment informing the subsequent DOE. DOE matrices are efficient for testing effects of factors and their interactions. The DOE optimized the number of runs needed to determine the degradation factors with the greatest impacts on sensor performance. Therefore, the initial set of bases and degradations produced for simulation aims at severe (maximum) levels of degradations. Figure 22 shows examples of the test slides that consisted of

a base material and degradation treatment. The left picture shows bumper degradations and the right shows optical degradations. The slides, when placed in front of a sensor, acted as a filter to the sensor signal.

Figure 22. Samples of simulated degradations (left: bumper degradations; right: optical degradations)

To support the data collection of a multitude of sensors simultaneously, VTTI designed and built a custom data acquisition system that could interface to several sensors through a variety of interfaces. The DAS uses a robot operating system (ROS) to record the data from the sensors. Because not all sensors have a standard recording frequency, the DAS records the data channels asynchronously with a common time stamp so the signals can be aligned during analysis. A custom user interface allows the experimenter to record relevant data associated with the test conditions defined by the DOE.

Camera Mis-Calibration

The object camera was unmounted from a sedan vehicle and re-mounted on another sedan of similar size. The new mounting of the camera was mis-calibrated due to the differences on the windshield angle (i.e., angular tilt by a few degrees) and the slight variation on the vertical mounting locations (i.e., mounted height from the ground by a few centimeters). Data was collected under these two conditions: calibrated and mis-calibrated. A stationary vehicular object was used as a target during baseline lane slalom maneuvers. Our defined baseline lane slalom was executed by driving the SV with the following characteristics: 15 mph, moving in sinusoidal fashion at a frequency of 0.5 Hz, with defined amplitude of 50 percent (i.e., the center line of the SV moved laterally to sweep 50 percent of the width between the lane markers; 100 percent amplitude would be moving the SV laterally from lane marker to lane marker).

Figure 23 shows the reported relative position of the stationary target vehicle as the SV passed by in slalom fashion. A first slalom pass was performed with the camera calibrated, and then a second slalom pass was performed with the camera mis-calibrated. Since the same camera was used, two slalom passes were performed. Each slalom was executed by a human driver. The red line shows the location of the TV using differential GPS, and the blue line is the position as reported by the camera. To clearly show the effects of mis-calibration, the human driver performed a slalom with a bigger amplitude, as shown by the red line in Figure 23. The relative longitudinal position (x) and the relative lateral position (y) of the target is off by a few meters for the mis-calibrated case. Specifically, for the mis-calibrated camera, offsets persist across the slalom range and the object detection distance is shorter (i.e., in the mis-calibrated camera, the

blue line under the red line in the top figure indicates lower relative *x* position values on the detected object), and for the calibrated camera, its accuracy improves as the distance reduces between TV and SV. By having a mis-mounted sensor (i.e., one that was not mounted according to the specified [*x*, *y*, *z*] position and/or was not mounted according to the specified angular position [roll, pitch, yaw]), it was shown to report inaccurate target positions with offsets that were maximized as the distance between TV and SV increased. As shown in Figure 14, a form of degradation is "out of calibration" (i.e., mis-calibration) as stated during stakeholder interviews. A task in this research project was to investigate the effects of this specific form of degradation. This section reports mis-calibration effects, which is why mis-calibration does not appear in the list of degradations further studied in this research project.

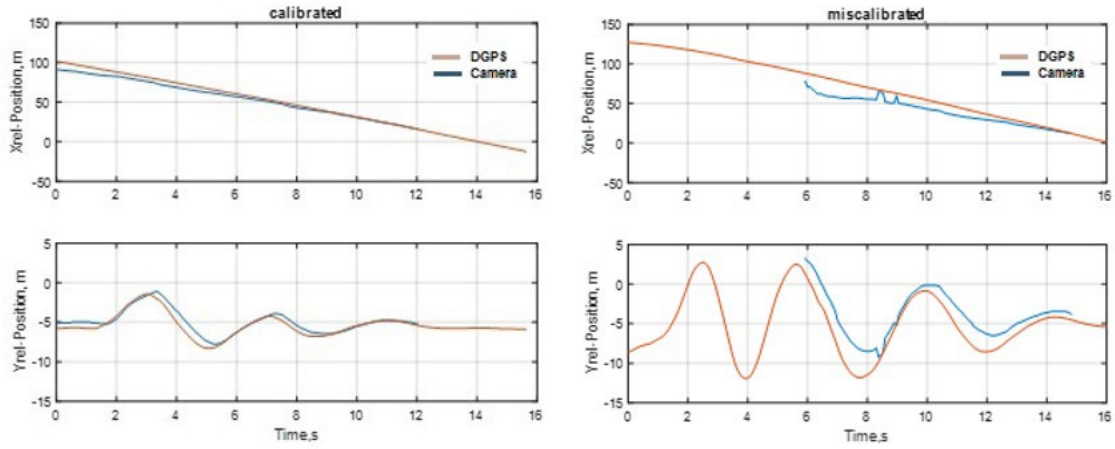

Figure 23. Relative x and y vehicle positions of stationary TV during lane slalom: Calibrated versus mis-calibrated camera

Analysis

The goal of the analysis was to identify the effect of the different base materials and degradations on sensor performance. The study investigated several sensor outputs and metrics (Table 25, Table 26, and Table 27) to identify those metrics that were relevant to a sensor type and sensitive to the effect of the degradations. The metrics had to be derived from the available sensor outputs because the sensors incorporated varying levels of preprocessing. For example, the output from one of the cameras (used later in the study during component testing) does not provide a raw video stream. Instead, it analyzes the video frames to identify objects of interest and then outputs relevant information about the objects. For this part of the project, we analyzed the most unprocessed output signal that the sensor provided. The cameras used during this phase output raw video. Similarly, the lidars output point cloud data. One of the radars output object-related data, while the other radars output point cloud-like data.

The metrics were basic statistical calculations, such as mean, standard deviation, and standard error for available signals from the sensor and applied to the bounded target data for lidar and radar. The metrics for the camera came from the edge spatial frequency response test chart (MATLAB Help Center, 2020a) processing in MATLAB; in other words, the chart is placed in front of the camera and data is captured and processed using MATLAB. Data analyzed included signals like edge aberration (MATLAB Help Center, 2020b) and chroma response (MATLAB Help Center, 2020c). A complete list of metrics used for the degradation development are

provided in Appendix C. The following provides an overview of the analysis steps to go from the collected raw signal data to a final selection of meaningful and unique degradation samples.

Unique Categories: Pie charts were used to ensure data categories are uniquely labeled. If the user assigns the word "Acrylic" and "acrylic" to refer to the same category, computer software will treat them as two different categories even though they represent the same category. Therefore, each category should have a unique label. To make sure that categories are unique, pie charts were created. Figure 24 shows the unique categories grouped by distance, target, base, and degradation in four pie charts. They represent the factors and variables used in degradation development. The first pie chart shows the distances used for initial testing (i.e., 20 m, 40 m, and 60 m) and their usage percentage. The second pie chart shows the four targets used (from cone to speed sign) and their usage percentage. The third pie chart shows that seven unique base materials were used. The labels under category (on the right-hand side) show the base materials. The pie chart also shows the percentage of times each base material was used. In a similar fashion, the last pie chart shows the 13 degradations used (from angled to tinted under category) and their usage percentage.

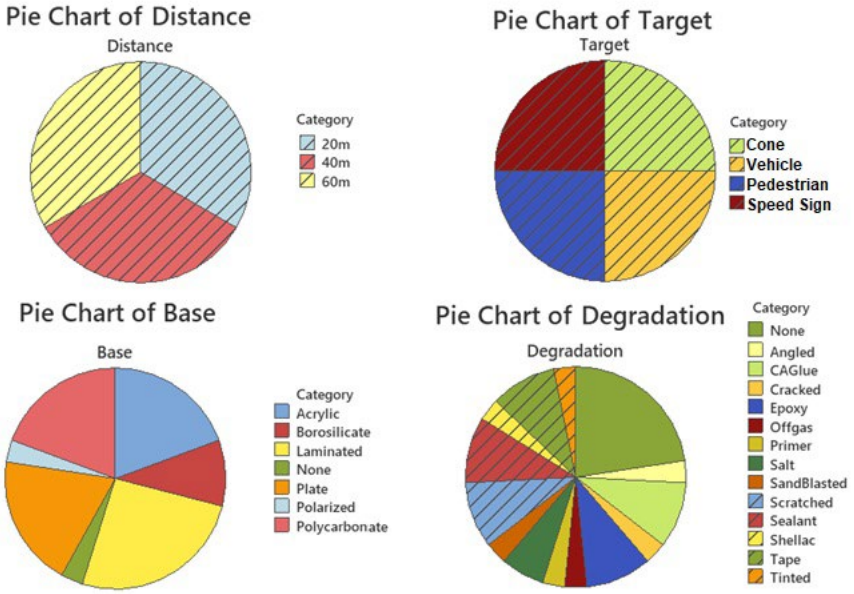

Figure 24. Unique categories showing factors and variables used in degradation development

Next, the analysis removed outliers for the metrics associated with the different sensors. The following boxplot (Figure 25) shows an example of the outlier identification. Figure 25 specifically shows the vertical variable, represented by the letter *z*, as measured by the solid-state lidar. Lidar provides a relatively large amount of data, in the form of point clouds, from objects found in its surroundings. The first boxplot (on the left) shows the five-number summary for the variable minimum *z* (min *z*). Minimum *z* is the minimum value read by the sensor on the vertical component from one of the targets from the previous pie chart. The following boxplot shows the variables maximum *z*, mean *z*, standard deviation of *z*, and standard error of *z*, respectively.

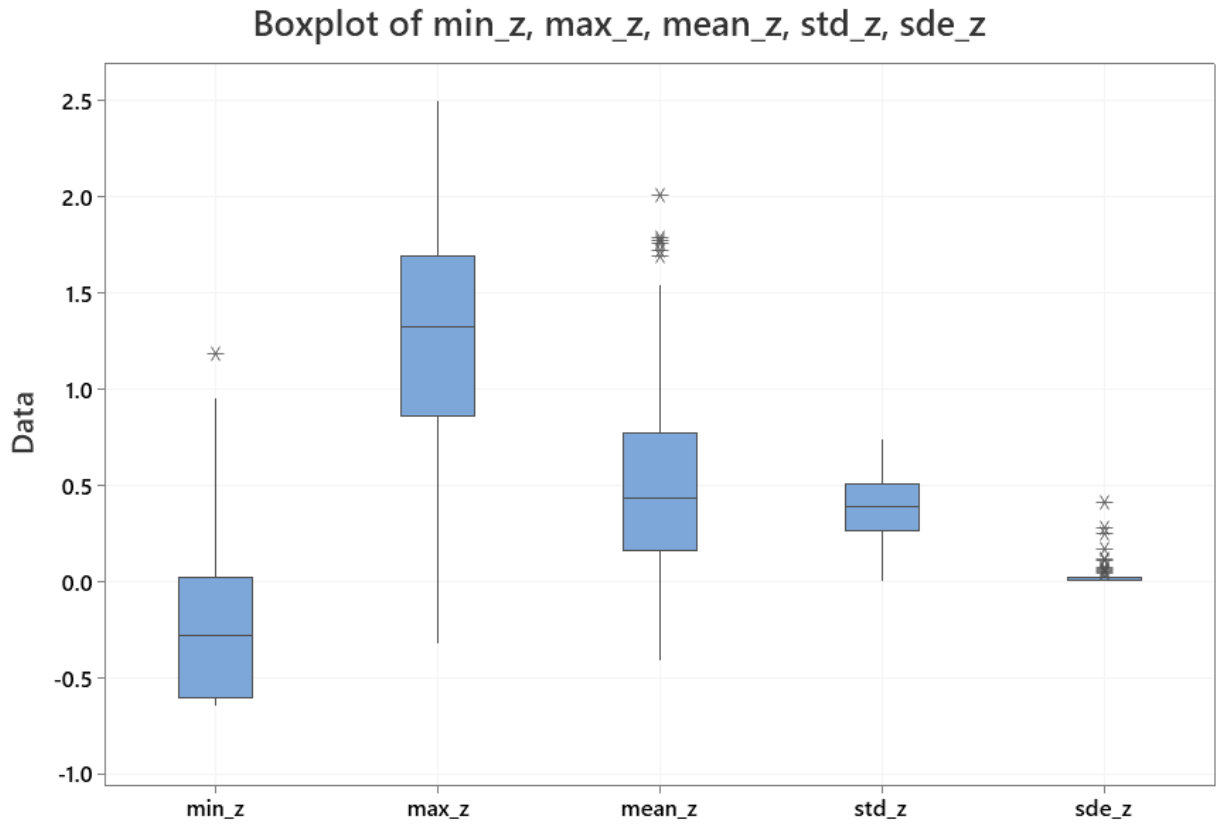

Figure 25. Boxplot showing results from outlier identification

Identify Main Metrics of Interest: Each sensor has a corresponding set of sensor outputs. Using lidar as an example, the sensor outputs (*x*, *y*, *z*) location and intensity form points that correspond to objects encountered in its surroundings. The following statistics can be calculated for each of the sensor outputs: minimum (min), maximum (max), mean, standard deviation (std), standard error (sde), and coefficient of variation (cov, i.e., standard deviation divided by the mean). In the case of lidar, points are grouped into objects, and then their statistics can be calculated for each of the following quantities: *x, y, z*, and intensity. Each of the statistics on each of the variables is treated as an independent variable. In other words, min, max, std, sde, and cov are computed on *x, y, z*, and intensity. The (*x, y, z*) points were also used to compute their equivalent in spherical coordinates, which corresponds to range I, azimuth (Az), and elevation (El). For example, for a given measured (*x, y, z*) point, the range is calculated as the Euclidean distance from the origin to this point. Azimuth is the counterclockwise angle in the *x*-*y* plane measured in radians from the positive *x*-axis. The value of the azimuth angle is in the range [-pi pi]. Finally, elevation is the angle in radians from the *x*-*y* plane. The value of the elevation angle is in the range [-pi/2, pi/2]. This provides a total of 35 (5 statistics x 7 variables) potentially independent variables, also known as metrics. The word metric or variable will be used interchangeably in this report.

The next series of analysis steps identified the main metrics of interest. This was an interactive process that used a combination of tools. Principal component analysis is a dimensionality-reduction method that is often used to reduce the dimensionality of large data sets. PCA identifies a smaller number of uncorrelated variables, called “principal components” or

"components" for short, from a large set of data. PCA analysis creates new variables (components) that are linear combinations of the observed variables. The goal of PCA is to explain the maximum amount of variance with the fewest number of components. A step-by-step explanation of PCA can be found in Jaadi (2021). PCA was used to identify metrics that have a strong correlation to the targets presented, which were cone, vehicle, pedestrian, and speed sign (i.e., inputs). PCA showed similar variables clustered together (Figure 26). The *x* and *y* axes in Figure 26 show the first and second components determined by PCA. A component is a linear combination of the 35 independent variables in consideration. The variables in consideration were explained at the beginning of this section and include statistics on *x, y, z*, elevation, azimuth, etc. Orange circles were overlayed in Figure 26 to indicate grouping of the variables. Dependent variables are in a circle. For example, the point cloud data measuring *z* and elevation are grouped closely together as indicated by the overlayed orange circle. This is logical because the measured height of an object by the sensor will correlate to its corresponding measured elevation angle. Therefore, PCA was used to cluster similar variables together into groups.

The clear distinction of the groups provides an indication of unique type of response. Groups that are close to each other indicate similar effects (Figure 26). For example, statistics for azimuth and lateral distance (*y*) are in the same group. Removing the highly correlated metrics (i.e., independent variables) and rerunning the PCA gave the main metrics of interest. Eigenvalues (a.k.a. characteristic values) are determined computing the variability in the data during PCA. There is an eigenvalue per component. The number of metrics to be removed and be kept was provided by the left portion of eigenvalues on Figure 27. There is an exponential drop in the eigenvalue plot that ends around five components, which suggests keeping five metrics. A vertical line to show the threshold of the components kept has been drawn in Figure 27. The *x*-axis in Figure 27 shows the "component number," which is the numerical identifier or label assigned to each component obtained during PCA. A component is a linear combination of the 35 independent variables in consideration. According to PCA, the most valuable variables to be kept from the first five components are: std_n, std_x, std_z, std_i, and mean_i, which correspond to standard deviation on the number of points returned, standard deviation on *x*, standard deviation on *z*, standard deviation on intensity, *y*, and mean intensity. These five variables (i.e., metrics) were kept for lidar.

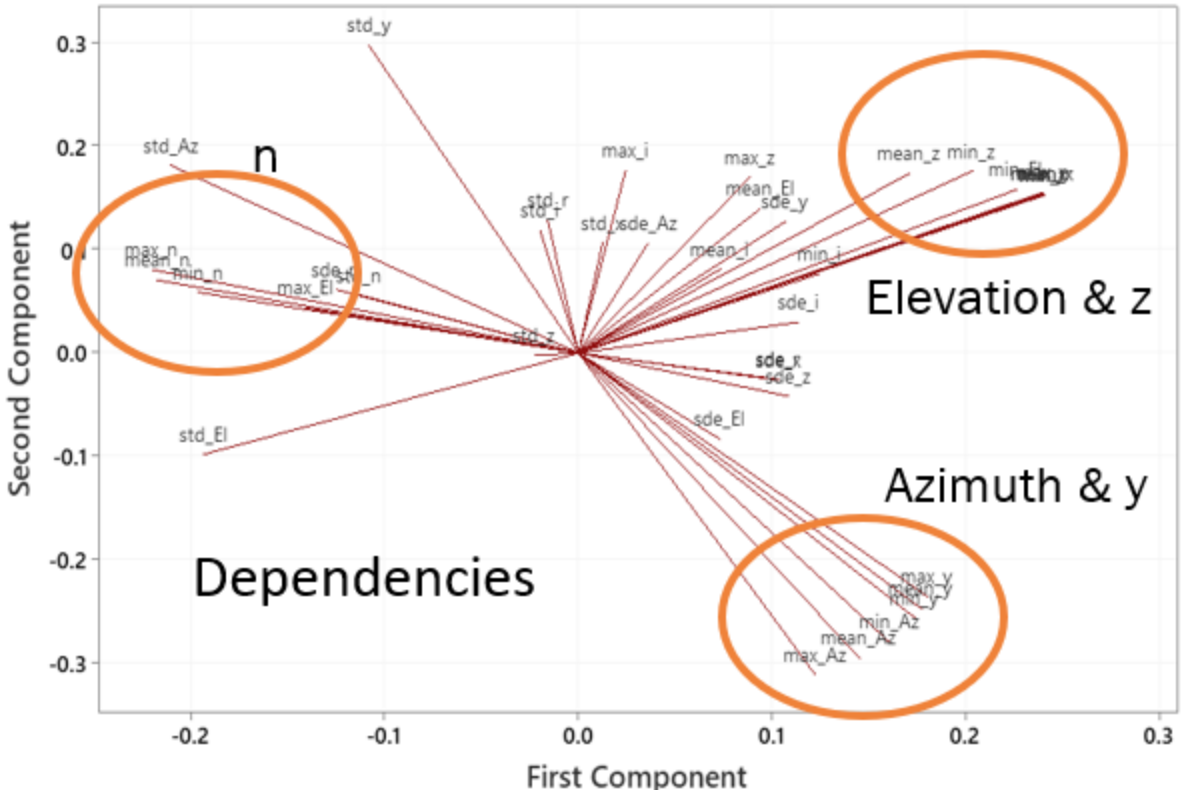

Figure 26. PCA plot

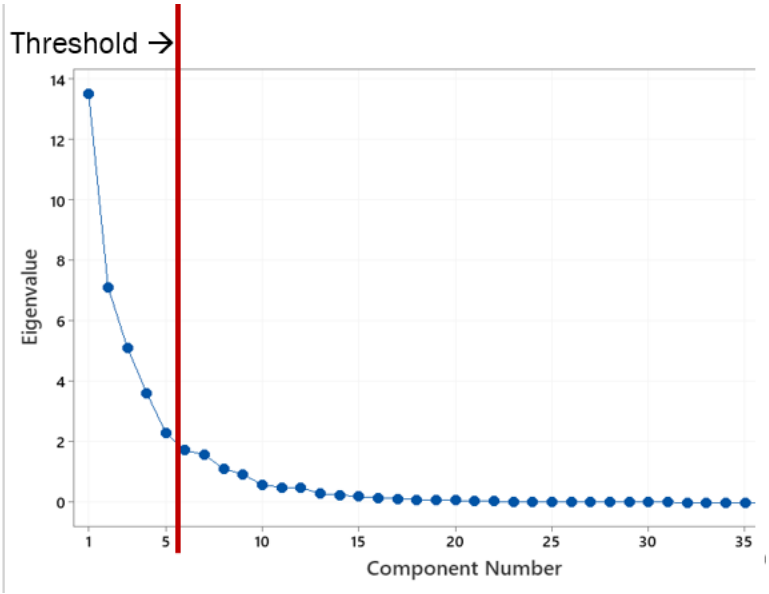

Figure 27. Plot of eigenvalues for principal components

The selected metrics should not be correlated or have as little correlation as possible. To check correlation between metrics, correlation plots for the five metrics selected (std_n, std_x, std_z, std_i, and mean_i) are shown in Figure 28. The metrics appear in the *x* and *y* axes to indicate the two metrics being compared. As an example, the two metrics being compared in the orange

rounded rectangle are std_z and std_i. Scatter data indicates that there is no correlation (or little correlation) between this two metrics. The Pearson correlation value for this example is r = 0.288. Pearson values can fall between -1 and +1. A positive sign indicates a proportional correlation, and a negative sign indicates an inverse correlation. A value close to zero indicates low correlation. The 95 percent confidence interval for the rounded rectangle is (0.185,0.385), which indicates that 95 percent of the data falls within this correlation values. Data corresponding to each target is marked as shown by the figure key as follows: blue circles are for the cone, red squares for the vehicle, green rhomboids for the pedestrian, and purple triangles for the speed sign. The low correlation values, as indicated by the r values in Figure 28, confirm that the selected metrics are the best to pursue further analysis of the data.

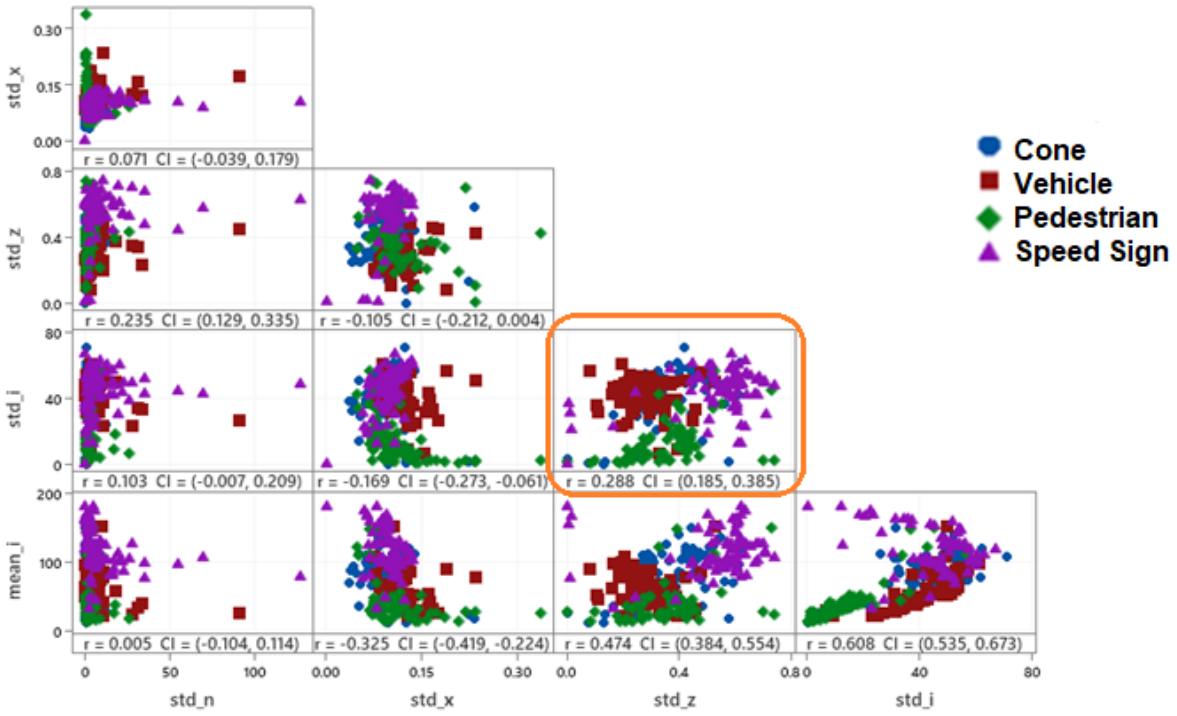

Figure 28. Correlation plots between metrics and targets

Identify Important Factors: The next step in the analysis identifies factors that affect the sensor performance based on the metrics identified during the PCA. Factors are the variables that experimenters can control during an experiment to determine their effect on the response being measured. The factors for the lidar case are the degradations applied (e.g., shellac, scratches), the base material used to apply the degradation (e.g., acrylic, borosilicate), the target presented to the sensor (e.g., cone, vehicle), and the distance at which the target is located (e.g., 20 m, 40 m, 60 m). These important factors and the selected metrics were then used to identify which degradation had the greatest impact on performance. The analysis uses three tools as part of this step: the main effects plot, the interaction plot, and variability chart.

1. Main Effects Plot. The main effects plot, Figure 29, provides an indication of the strength of a factor's ability to affect the sensors. The example shown is for the standard deviation of lidar intensity. The mean of the given signal in each test category is used so that interaction or

individual responses are averaged out. Large values, compared to the typical values measured by the sensor, could be reported occasionally by the sensor; one way to filter them out is by collecting data over time and then taking the mean. The occasionally reported values by the sensor could be considered individual responses due to interactions between sensor and object. The values occasionally reported by a sensor do not represent the average behavior of the sensor, and therefore the mean value is a better representation of its behavior. A large deviation from the rest of the factors can indicate something to investigate further, but the context of the sensor and metrics being shown needs to be considered. For example, the data in *Figure **29*** highlights a few things. The high peak shown by the salt suggests that further exploration of this degradation must be considered. The reflectivity properties of the salt together with its granular shape could be the cause of the high peak. The pedestrian target had a significantly lower standard deviation of intensity in lidar returns. This indicates it was more uniform. The pedestrian's low mean intensity shows the target intensity was consistently low across its entire profile. This is logical as there are no retroreflectors on the pedestrian, as with the other targets, and the clothing is absorptive to the lidar beam.

This leads to considerations of either including the pedestrian target in the rest of the project because it is unique and might provide strong variability in responses or excluding it as it will be a confounding variable that must be accounted for in future test matrices and expand the scope of the project. Because the pedestrian target is difficult to detect given its low strength on the return, the pedestrian target was excluded for the rest of the project.

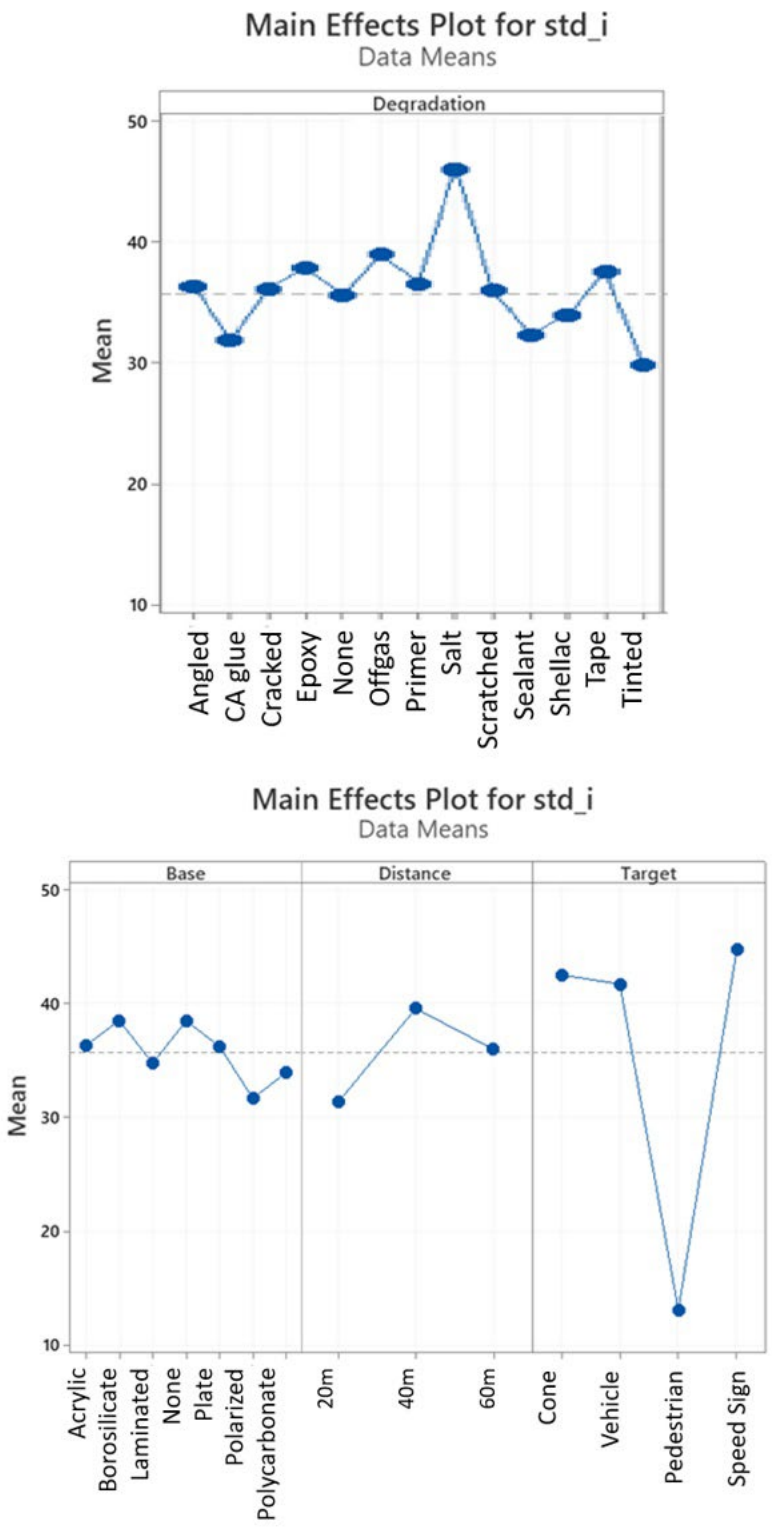

Figure 29. Main effects plots for standard deviation in lidar intensity

2. Interaction Plot. Like the main effects plot, the interaction plot (Figure 30) uses the metrics selected during PCA for the standard deviation in lidar intensity; however, interaction plots also

show how each of the factors affects the response. This provides an additional insight into the effects due to specific factors. The interaction plot breaks the data into different views by plotting it with different overlays and *x*-inputs. This makes subtleties more evident that would not be obvious just looking at the data in one way. The *y*-value for each subplot is the same variable, in this case standard deviation of intensity. The *x*-value changes by column of subplot, and the overlay changes by each row of subplot.

The shape of the plots, tightness of the overlays, and the outliers give an indication of how the sensor responds to the different input factors. The right column (Target) shows a consistent dip across all the other inputs for the pedestrian target showing a fundamental difference in its response, not just a sensitivity to the input factors. The shape of the middle subplot (Distance, marked by the orange rounded rectangle) plots response versus distance and shows an approximate linear correlation to distance. As the target moves away (at 60 m), its range of standard deviation of intensity returns increases. Some of the factors (e.g., sealant) show a non-linear relation as illustrated by a drop in intensity after rising initially, indicating the standard deviation of intensity of returns expands and then collapses as more and more points of data are lost with increasing distance for those factors. Certain outliers and missing data points highlight factors that need to be explored further and either expanded or removed. For example, the salt degradation in the top left subplot only has one case that lidar returns were present, and in that one case, the standard deviation was high, indicating the distribution of the few data points returned had their intensity highly distorted. This means that factor should be removed or adjusted in severity. The indication that salt is a degradation of particular interest was shown also by the high peak that the salt produced in the interaction plots.

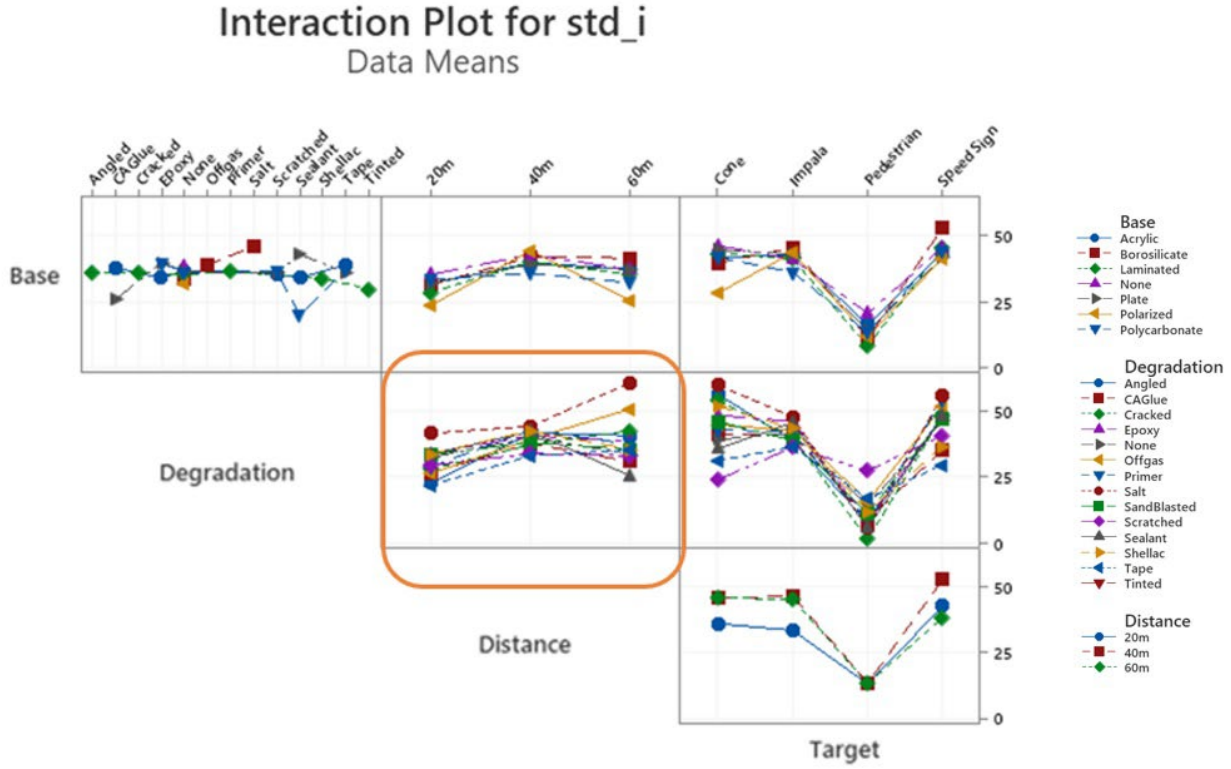

Figure 30. Interaction plot for standard deviation in lidar intensity

3. Variability Chart. Lastly, a variability chart for the standard deviation in lidar intensity (Figure 31) allows a single variable to plot against all categorical variables and factors. The y-axis in Figure 31 provides the mean intensity value from lidar data. The variability chart also provides insight into standout cases and general trends. If there are repeating patterns of rising/falling line segments in one of the grouped factors along the *x*-axis, it can be interpreted as persistent proportional relationships to that factor. Likewise, if there are blocks of unchanging response, this can indicate insensitivity to that factor. For example, the sealant factor on polycarbonate has a relatively low response across the other factors.

As mentioned in the beginning of the section Identifying Important Factors, the three charts (main effects plot, interaction plot, and variability chart) were taken together to understand the responses to input factors and corroborate each other to find the root cause of the different responses. It highlights what is seen as a fundamental response in the sensors and what is driven by the factors applied. The factors that produced high peaks (e.g., degradation by salt) and non-linear relationships (e.g., degradation by sealant) suggested further testing that was carried out later during component and system testing and are reported in this report.

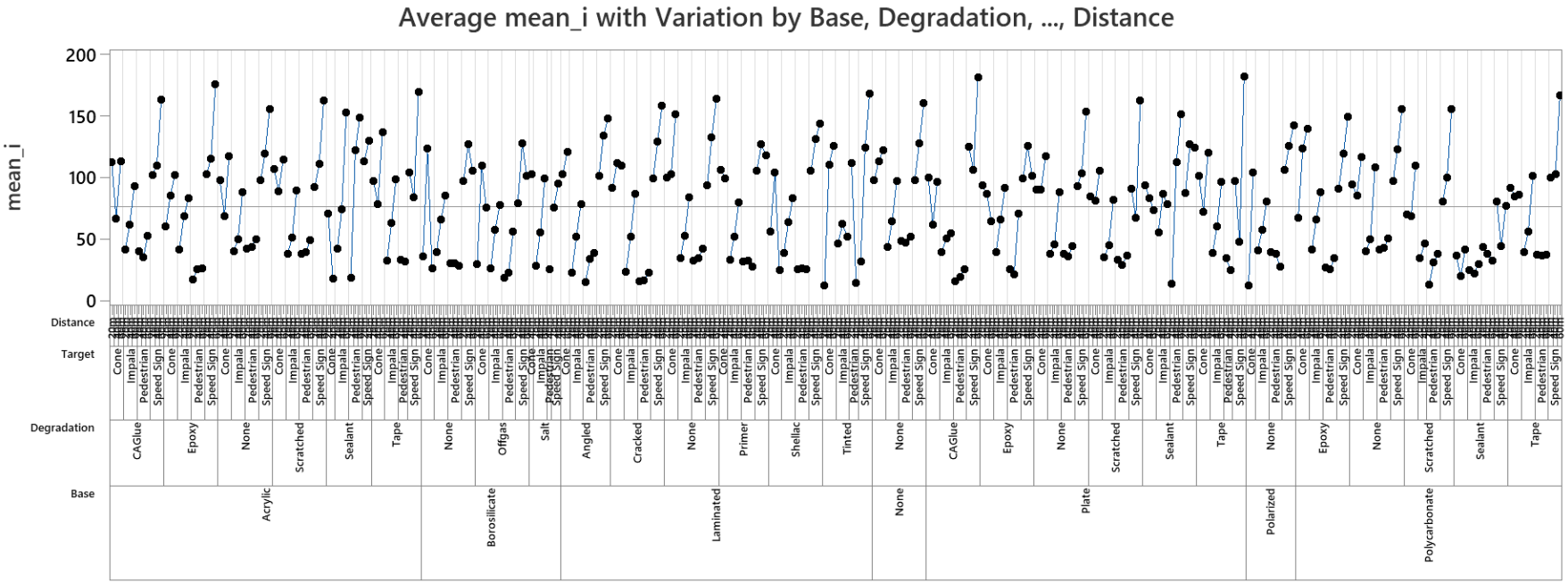

Figure 31. Variability chart for mean intensity of lidar

Identification of Primary Degradations: The final step identified the primary degradations as follows. Data collected using the selected metrics and the factors previously mentioned went under the following transformation: (1) Each data point was written by delta values. A delta value is the amount of change compared to the baseline response. (2) The absolute value of each delta value was taken. (3) The absolute values of the deltas were normalized. Normalization is a process that transforms any value to the interval 0 and 1. Normalized values are obtained by dividing a numerator by a denominator. Assume D represents all calculated absolute delta values, max(D) represents the maximum within D, and min(D) represents the minimum within D. The numerator equals the value being normalized minus min(D) (i.e., absolute delta – min(D)). The denominator equals max(D) minus min(D). For the lidar case, each selected metric (i.e., std_n, std_x, std_z, std_i, and mean_i) produced normalized values. The transformation of the data produced by a metric will be represented by T( ). For example, the transformation of std_x will be represented by T(std_x). Since there are five metrics, five weights are required (w1 to w5), and the following linear equation is used to calculate the weighted scores: y = w1 * T(std_n) + w2 * T(std_x) + w3 * T(std_z) + w4 * T(std_i) + w5 * T(mean_i). The variable y represents the weighted scores, referred to from this point as scores. The selection of the weights is chosen by the designer, but each weight should be greater and/or equal to zero (i.e., $w \geq 0$) and the sum of all weights should add up to 1 (i.e., w1 + w2 + w3 + w4 + w5 = 1). It is good practice to assign the same weight to each metric. For example, for five weights (i.e., w1 to w5), the value of 0.2 for each was given. Scores are calculated per degradation. In order to compare degradations, a degradation is picked (i.e., degradation i) and compared to the rest (i.e., degradations j = 1,…,n). Every degradation is picked and compared to the rest. This produces what is called a relation matrix, as shown in Table 18 for the SR 77GHz radar case. The matrix is square with degradations across the rows and columns and symmetric across the diagonal. The elements are pairwise scores of relation with 0 being completely similar and 1 being maximally opposite across the observed input metric ranges.

Table 18. Relation Matrix for SR 77GHz Radar

	3M Safety Walk	**Blacktop**	**Bondo**	**Bondo Mesh**	**Dirt Scratches**	**Duct Tape**	**Epoxy**	**SRE**	**Leaves**	**None**	**Pine Needles**	**Scratches**
3M Safety Walk	0	0.33	0.44	0.26	0.10	0.23	0.19	0.33	0.26	0.14	0.38	0.14
Blacktop	0.33	0	0.39	0.37	0.28	0.51	0.42	0.10	0.58	0.37	0.30	0.39
Bondo	0.44	0.39	0	0.53	0.44	0.36	0.38	0.46	0.62	0.46	0.26	0.32
Bondo Mesh	0.26	0.37	0.53	0	0.17	0.40	0.21	0.40	0.43	0.23	0.48	0.36
Dirt Scratches	0.10	0.28	0.44	0.17	0	0.29	0.19	0.29	0.31	0.14	0.38	0.24
Duct Tape	0.23	0.51	0.36	0.40	0.29	0	0.19	0.50	0.37	0.20	0.30	0.18
Epoxy	0.19	0.42	0.38	0.21	0.19	0.19	0	0.41	0.35	0.13	0.32	0.16
SRE	0.33	0.10	0.46	0.40	0.29	0.50	0.41	0	0.59	0.36	0.29	0.37
Leaves	0.26	0.58	0.62	0.43	0.31	0.37	0.35	0.59	0	0.30	0.61	0.33
None	0.14	0.37	0.46	0.23	0.14	0.20	0.13	0.36	0.30	0	0.39	0.14

	3M Safety Walk	Blacktop	Bondo	Bondo Mesh	Dirt Scratches	Duct Tape	Epoxy	SRE	Leaves	None	Pine Needles	Scratches
Pine Needles	0.38	0.30	0.26	0.48	0.38	0.30	0.32	0.29	0.61	0.39	0	0.27
Scratches	0.14	0.39	0.32	0.36	0.24	0.18	0.16	0.37	0.33	0.14	0.27	0

In addition to the scores and the relation matrix, a uniqueness score is calculated. The uniqueness score is the minimum value found on each row of the relation matrix without the diagonal elements. For example, the uniqueness score for the degradation "3M safety walk" (i.e., first row of the relation matrix) is 0.1, with 0.1 for Blacktop, 0.26 for Bondo, and so on. With the goal of reducing the number of degradations to carry for further testing in this project, degradations are grouped as follows. Degradations with similar scores are combined into a group. Their similarity is mathematically represented by the difference between scores, but it is worth noticing that the maximum number of groups is when no degradations are grouped, which will leave each degradation in its own group. The final number of groups depends on how big of a difference among the scores is set by the designer. The difference among scores is called the threshold. If the threshold on the scores did not produce the desired number of groups, uniqueness scores can be used to split groups. To reduce the number of tests carried for the rest of the project, five groups for each sensor were considered a good number of degradations to be carried forward.

For the radar example, each of the tested radars produced scores (a.k.a. weighted normalized average) and uniqueness scores as shown on Table 30 and Table 33. The researchers then combined this information to identify the final degradations (shown in bold) in Figure 32. Visually, the columns are color coded from low (red) to high (green) to make the important scores stand out.

Since these scores were averaged across bases and sensors, the min and max score across these subsets are shown so that the range of variation is considered to ensure the final selection was not driven by one test case that drove up the mean. Likewise, the final selections are not just the top five scoring responses, as many of the top degradations were not unique. For example, the Bondo degradation ranked 4 but was skipped as it had a relation to the Bondo+mesh degradation already chosen at rank 2.

Given the similarity in the frequency of the signal of the camera and lidar, the degradations for these light-based sensors overlapped in scoring and grouping. The separated lidar and camera tables can be found in Table 28 and Table 29, respectively. Given the similarity of the results for lidar and camera, and to simplify subsequent testing, the study combined the results. The final degradations for the camera + lidar sensors were: offgas, sealant, tinted, sandblasted, and shellac. The final degradations for the radar were: steel reinforced epoxy, Bondo+mesh, pine needles, epoxy, and blacktop.

		Radar Scores		
Deg	Rank	Min	Mean	Max
3MSafetyWalk	8	28.3%	33.1%	41.3%
Blacktop	7	12.0%	35.7%	71.1%
Bondo	4	11.2%	39.2%	70.0%
BondoMesh	2	34.1%	50.3%	70.0%
DirtScratches	12	14.4%	27.7%	46.5%
DuctTape	11	19.6%	28.1%	40.0%
Epoxy	5	17.0%	37.4%	56.1%
SRE	1	45.4%	56.9%	69.3%
Leaves	9	11.0%	28.8%	47.5%
None	10	18.2%	28.2%	40.9%
PineNeedles	3	12.7%	41.0%	65.8%
Scratches	6	32.5%	37.1%	44.2%

		Camera + LiDAR Scores		
Deg	Rank	Min	Mean	Max
Angled	14	2.4%	8.8%	13.6%
CAGlue	6	21.1%	35.4%	72.5%
Cracked	10	2.4%	23.7%	66.6%
Epoxy	8	7.0%	33.0%	56.0%
None	12	4.6%	17.1%	41.2%
Offgas	1	35.3%	56.9%	77.5%
Primer	11	2.6%	18.6%	47.4%
Salt	7	20.2%	33.7%	48.1%
SandBlasted	4	21.6%	44.4%	65.1%
Scratched	13	5.5%	15.1%	42.7%
Sealant	2	21.3%	52.7%	74.9%
Shellac	5	9.2%	36.6%	57.7%
Tape	9	8.8%	24.6%	45.9%
Tinted	3	30.8%	47.7%	63.0%

Figure 32. Final degradation ranking

Discussion

According to *Understanding How We Repair Your Plastic Bumper the Quickest* by Badell (2017), car manufacturers use a variety of plastics to make bumpers. The most common include polycarbonates, polypropylene, polyamides, polyesters, polyurethanes, and thermoplastics olefins, or TPOs. Front and rear bumpers use a combination of these materials. Since the same materials are being used to build front and rear bumpers, either a front or a rear bumper can be chosen to test the material properties of it. Even though the same materials are used, the aesthetic appeal is designed for each specific mounting location in a vehicle. The two rear bumpers tested were both designed for a specific vehicle from a specific manufacturer. The OEM bumper was acquired from the dealer parts shop. The aftermarket bumper was purchased from an online retailer not associated with the manufacturer. However, the aftermarket bumper resulted in slightly different results in the component analysis. The aftermarket bumper resulted in 1 dB less SNR, and 0.8 dB more standard deviation of SNR.

The difference could be from the difference in thickness of the materials. Thickness measurements distributed in a line horizontally from the center in the flattest face of the bumper show 0.1 to 0.2 mm more thickness in the aftermarket bumper (Table 19).

Table 19. Aftermarket and OEM Bumper Thickness Sample Measurements

Horizontal Distance From Center, mm	**Thickness, mm**					
	-381	**-229**	**-76**	**76**	**229**	**381**
Aftermarket	3.0	3.0	3.0	2.9	2.9	2.9
OEM	2.8	2.8	2.8	2.8	2.8	2.8

To simulate degradations, degradations (dirt, scratches, etc.) must be applied to a base (e.g., bumper), and therefore, a base must be selected. A comparison of two specific bases that were considered for degradations are shown in Table 19. The aftermarket bumper and OEM bumper were identified as being made from the same base material. The OEM bumper is identified as

PET, which stands for polyethylene terephthalate, while the aftermarket bumper was marked with recycle symbol 1, which is also PET. However, PET is not known to have significant radio wave losses in the 77-GHz range.

Alternatively, PET quality determines how many micro voids there are in the material that could have accumulated water from the atmosphere. It is possible that the lower quality aftermarket bumper absorbed more water, which resulted in the differences in quality of the radar data returned.

In terms of the optical degradations, the sealant had a more significant effect than expected considering the clarity of the sealant as visible to the naked eye. The main effect for the sealant is believed to be the lensing of the FOV near the edges of the treatment where the meniscus created curvature in the cross-section. There were also some undulations in the surface that caused some distortion.

The main degradation mechanisms can be broadly identified as refraction and attenuation. Radar, cameras, and lidar all rely on electromagnetic radiation of differing wavelengths, and thus all are sensitive to both attenuation and refraction.

Refraction can be from scatter caused by surface erosion (sandblasted) or from liquid coatings that then solidify into surfaces with lensing or distortion effects observed in the sealant and shellac degradations.

Color filters (tint) attenuate the optical signal by absorbing the light in a specific wavelength. Water can also attenuate the signal of radars significantly, as observed in the component testing, and is well known to absorb lighting in the mid infra-red range.

The body filler/mesh degradation for radar in particular has several attenuation mechanics. The talc in body filler absorbs water when left unpainted. The mesh is made from aluminum, which can act as an antenna and either refract or absorb radio waves, turning the energy into current that is then dissipated as heat. The most complex is destruction interference. Through complex interactions, radio waves typically cannot pass through holes that are smaller than the wavelength of the radio wave. In the case of this experiment, the mesh had holes on the order of 3 to 4 mm. The 77-GHz radars were less affected by the body filler/mesh than the 24-GHz radars because the wavelength for 77 GHz is 3.89 mm versus 12.5 mm for 24 GHz.

This page is intentionally left blank.

Chapter 5. Component Testing

We carefully considered the collection of precise bench test data versus more practical testing completed in environments such as the test track. The interviews with sensor suppliers and OEMs gave information about available test methods, especially the test methods that are widely accepted by the industry.

The degradations identified gave an initial point for component testing. For component testing, VTTI attached the sensors onto the test fixture mounted to a vehicle. The study executed range sweeps in the SV (instrumented vehicle) in conjunction with a TV and a lane slalom with a stationary TV (see Appendix E). The design of the test procedures exercised the longitudinal range and lateral range of the sensors.

Methodology

Development of Component Testing

To perform component testing in a more realistic environment, the sensors under test were installed on a custom frame on a VTTI test vehicle. A differential GPS was installed on both the SV and TV to serve as ground truth measurement independent of the sensing technologies. Note that the term TV has the same meaning as the term POV mentioned earlier, in the literature review. A DAS was installed in the SV to interface with the sensors under test. The DAS comprised a high-performance laptop personal computer, ethernet networking switches, USB hubs, multiple power supplies, a miniature high-performance computer for collecting data from the machine vision cameras, and a second laptop to interface with the camera computer and the low-cost lidar (Figure 33). A 2.4 GHz wireless serial link was used to link the TV DGPS to the DAS in the SV. GPS time was used to time synchronize the data collected with the two laptops. It was important to collect data from all the sensors at the same time due to repeatability concerns and to reduce data collection time. Since several automotive sensors were added to a commercially available vehicle (the SV), there was a need to add a high current (250 A) alternator that increased the idle speeds in the SV and to allow all the sensors to run simultaneously along with the data collection computers.

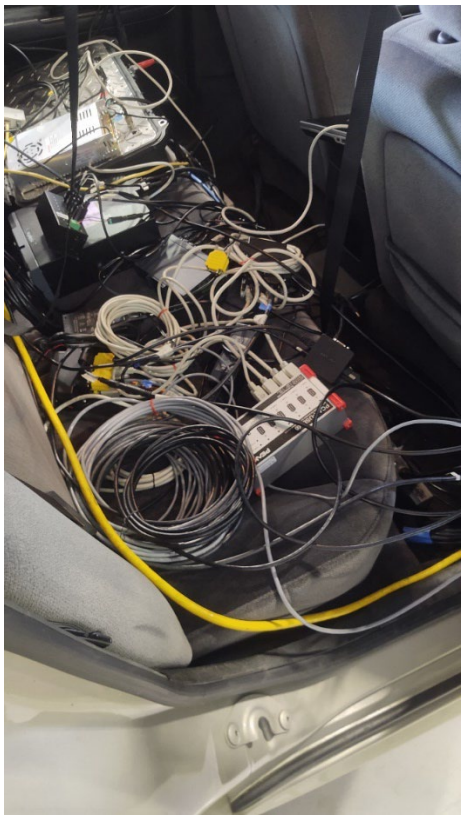

Figure 33. Sensor network to DAS

Analysis of the sensors required all sensor outputs be in a similar format. Given that two of the radars and one of the cameras only output object data from a built-in perception algorithm, the point cloud data from the other sensors had to be converted into some form of object tracking to compare. However, the methods had to be relatively simple to prevent the analysis from becoming a perception algorithm test. This also involved coordinate transforms to convert the ground truth into the reference frame of the sensors on the SV.

To compare across sensors, an absolute ground truth had to be captured as well. Because both the SV and TV were moving in most of the experimental designs, the absolute ground truth location and heading were needed for each. The researchers considered using a lidar sensor to locate the vehicle. However, this approach would have involved developing a complex perception algorithm that would entail significant effort. Given the limitations of other sensor technologies as shown in Table 20, we decided that DGPS would provide sufficiently accurate data to locate the two vehicles.

Table 20. Comparison of Ground Truth Technologies

Technology	Pros	Cons
Radar	Some of the sensors incorporate algorithms to identify and locate objects.	Object position is at the largest reflection, which can move around on the target vehicle as the vehicle pitches and yaws. No insight into algorithm assumptions; uncertainties.
Lidar	Very accurate range, typically +/-2 cm but less accurate vertical and horizontal.	Involves algorithm development, human-in-the-loop and/or hybrid approach with video to identify consistent point on the object of interest in the point cloud. Accuracy in object position is better than lidar accuracy due to the error introduced by the additional processing.
Camera	Algorithm available to locate obstacles (target vehicle) and report x, y, z centroid.	Range error is 10% or 2 m, whichever is larger.
DGPS	Accurately locates position of the target and SV at antenna location. No additional algorithm needed. Independent of the sensor technologies and inherent performance.	+/-10 cm (4 in) accuracy

For data processing, the approach used was based on fusion of the ground truth method with some simple bounding box selection. The DGPS data was used to locate the two vehicles in world coordinates at each sample point. DGPS data collected by the TV was communicated via wireless transmission to the SV. The wireless transmission worked when there was line-of-sight between SV and TV. If LOS was not maintained, data incoming from the TV into SV was lost. Data loss occurred when there was an obstacle in between the SV and TV such as a physical obstacle (e.g., metallic containers) or climate effects (e.g., fog). The experiment was re-run, assuring LOS, in the cases when data from the TV was lost. The TV location data was interpolated to the timestamps of the SV. A gradient calculation was used to calculate the heading of each of the vehicles using the time history data. The location and heading of the TV were transformed into the SV coordinate system with the origin at the GPS antenna near the center of the vehicle on the roof.

The location of the sensors relative to the GPS antenna was carefully measured and used to transform the object coordinate's output from the sensor into the SV coordinates. The locations

of the GPS antennas on each vehicle were also carefully measured. This allowed the calculation of relative position of the reflective surfaces of the TV relative to the SV.

Prior to down-selection of the data representing the TV from the lidar point clouds, the ground plane data was removed using a script from MATLAB called *pcfitplane*. The function *pcfitplane* fits a mathematical plane to three-dimensional point cloud data. Within the *pcfitplane* function, the M-estimator SAmple Consensus algorithm is used to find the plane. The M-estimator SAmple Consensus algorithm is a variant of the RANdom SAmple Consensus algorithm. For the plane fit, limits of 5° and 0.05 meters from the reference vector of [0,0,1] were used.

The relative position of the TV was used to create a bounding box for data down-selection and pseudo fusion of the DGPS data with each sensor's data. The bounding box was a virtual three-dimensional box in the coordinate frame centered on the DGPS location of the TV. The bounding box is created with the goal of collecting only data points that belong to the TV. This was selected as a multiplication factor of the TV size. For example, a factor of 2 would indicate that data points in a bounding box with twice the vehicle size will be analyzed. A large factor (e.g., 3) would include data points surrounding the TV (rails on the side road, vegetation, etc.), and the exact factor of 1, in principle, will contain only data points that belong to the TV. A factor bigger than 1, but not too large, was required to capture data points that belong to the TV in the presence of noise. A factor of 1.8 was determined to provide the required TV data. Any data point from a sensor's cloud that fell in this box was selected.

The object centroid (*x, y, z*) was then calculated from the selected points within the bounding box. In addition to (*x, y, z*) positional data coming out of the sensors, all other sensor outputs were averaged for data points within the bounding box. Additional sensor outputs from the sensors tested in this project included reflectivity from lidar, RCS, and SNR from radar. It is logical that the outputs provided by the sensor are used by perception algorithms. The object centroid (*x, y, z*) is calculated each time (*t*) the sensor provided output data. The *x, y, z, t* parameters were then compared to the *x, y, z, t* of the relative position of the TV (DGPS) for analysis.

Data captured by the DAS was analyzed using MATLAB. In addition to the positional error, the standard deviation and standard errors were calculated on the time history of the positional data from each sensor. Additionally, the time history positional and signal quality (reflectivity, SNR, RCS) data from the baseline runs (no degradation) were compared to the data from the runs with degradations.

Sensors Under Test

Four radars, four lidars, and two cameras were tested. The details of those sensors are shown in Table 21. The same set of sensors as those used during the degradation development were used. In the table, SR stands for short range and LR stands for long range. One of the 77 GHz radars produced two data sets: (1) short range with a wide FOV without any vertical information, and (2) long range with a narrow FOV and vertical location information.

Table 21. Sensors Under Test

Sensor Type	Anonymized Name	Brief description	Sensor Output
Camera	Object Camera	Mono camera, widely used automotive camera capable of lane marker recognition, object identification and classification	Objects
Camera	Machine vision	Mono camera, used in automotive applications and capable of lane marker recognition, object identification and classification	Objects
Radar	SR 24 GHz	Short range radar operating at 24 GHz.	Objects
Radar	LR 24 GHz	Long range radar operating at 24 GHz.	Objects
Radar	SR 77 GHz	Short range radar operating at 77 GHz.	Point Cloud
Radar	LR 77 GHz Near	Near field of the long-range radar operating at 77 GHz	Point Cloud
Radar	LR 77 GHz Far	Far field of the long-range radar operating at 77 GHz	Point Cloud
Lidar	32	Mechanical lidar scanning 360 degrees at 10 Hz using 32 laser beams	Point Cloud
Lidar	128	Mechanical lidar scanning 360 degrees at 10 Hz using 128 laser beams	Point Cloud
Lidar	Solid State	Solid state lidar scanning forward at 10 Hz using multiple laser beams	Point Cloud
Lidar	Budget	Mechanical lidar scanning forward at 10 Hz using single beam scanning	Point Cloud

Final Degradations

The initial set of degradations produced for simulations aimed at severe (high) intensity of degradations. During component testing, the severity of degradation intensity was expanded as shown in Table 22 and Table 23. For an example using Table 22, for the shellac degradation, 3 intensity levels of degradation were produced with 3, 6, and 12 coats of shellac applied to a surface with no previous treatment corresponding to low, medium, and high intensity of degradation for shellac. Low, medium, and high intensity levels are marked in bold in Table 22 and Table 23. The final list of degradations appears in Table 22 and Table 23. These degradations were developed based on the results from the original component testing and the statistical analysis of the correlations between the degradations tested. Figure 34 and Figure 35 show some of the final degradations. The procedures used to prepare the samples with the degradation intensity details from Table 22 and Table 23 are provided in Appendix D.

Table 22. Optical Degradations (Camera, Lidar)

Degradation Type	Base	Number of Intensity Levels	Intensity Level Details
Sealant	0.086” Acrylic	6	**0.02**, 0.04, 0.08” thick, no surface treatment 0.04” thick, **1/8**, 3/16, **1/4**” notches surface treatment
Shellac	0.086” Acrylic	3	**3**, **6**, **12** coats no surface treatment
Sandblasted	0.086” Acrylic	3	**1**, **5**, **10** passes
Offgas	0.086” Acrylic	3	**1**, **4.5**, **25** in^2 sacrificial material
Tinted	0.086” Acrylic	6	35%, 20%, 5% Transmission Grey window tint, **1**, **2**, **3** layers of green optical material (red and blue filter)

Table 23. Radar Degradations

Degradation Type	Base	Number of Intensity Levels	Intensity Level Details
Blacktop	0.25” corrugated PE	3	**1/8**, **3/16**, **1/4**” notches/thickness
Bondo/Mesh	0.25” corrugated PE	3	Slightly **less than mesh thick**, **mesh thick**, **1/8 notch over mesh**
JB-Weld Steel reinforced epoxy	0.25” corrugated PE	3	**1/16**, **1/8**, **3/16** notches/thickness
Epoxy	0.25” corrugated PE	3	**1/16**, **1/8**, **3/16** notches/thickness
Biological	0.25” corrugated PE	4	8 pieces/5”, ~**16/5**”, ~**32/5**”, ~**64/5**”

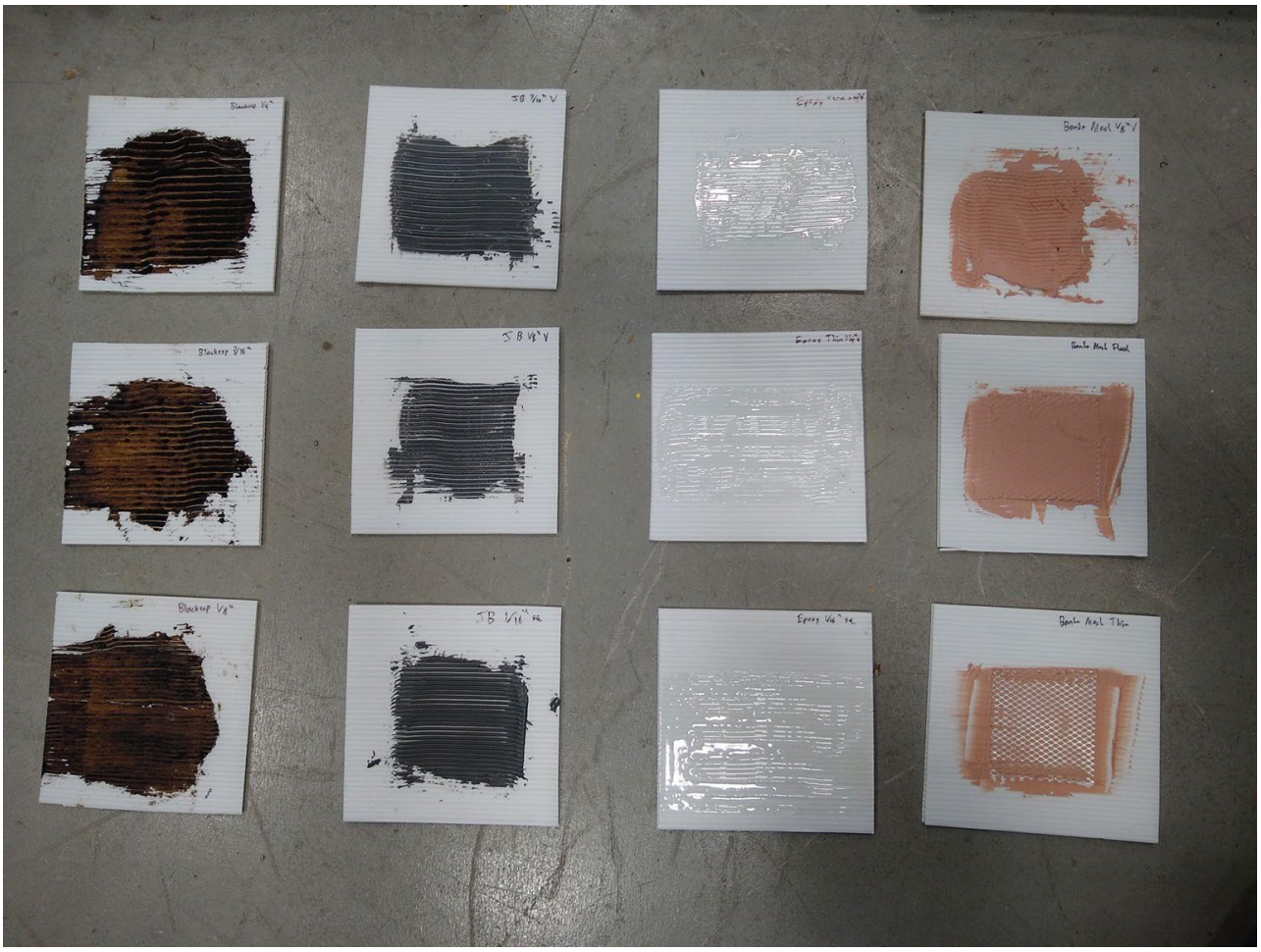

Figure 34. Polyethylene specimens prepared for radar testing

Figure 35. Biological material degradations from lightest to heaviest (left to right)

The test vehicles were two identical 2010 Chevrolet Impalas. Both vehicles were equipped with DGPS. A frame was constructed from 1-in (2.54 cm) square T-slot aluminum extrusions, also sometimes referred to as “8020” or “8020 aluminum sensor frame” (Figure 36). The frame was designed to be temporarily attached to the data collection vehicle. The sensor stand was completed before all the sensors for testing were acquired. The T-slot design enabled rapid deployment of the sensors on the SV and minimized the amount of time needed to adapt additional sensors to the vehicle after the frame was installed on the vehicle. The frame included

self-leveling feet to conform to the curved surface of the roof of the SV and was held to the SV with ratchet straps.

Figure 36. SV with sensor frame and sensors

The sensors were mounted to the sensor frame with cantilevered extrusions, except in the case of the 128 beam lidar. The 128 beam lidar was attached to an extrusion supported on both ends to keep the vehicle-induced vibrations to a minimum. The cantilevered mounts were setup with rotating mounts that can be adjusted in yaw and pitch to enable alignment of the sensors. The sensors were all aligned to be parallel to the gravity vector and perpendicular to the vehicle center line.

Testing Setup

Two different dynamic test types for component testing were identified: range sweeps and lane slaloms. Each test type had a low-speed and high-speed variation. The low-speed lane slaloms and range sweeps were conducted on a surface street at VTTI, while the high-speed tests were performed on the highway section of the test track.

Range Sweeps

Range sweep tests were designed to test longitudinal accuracy of the sensor across a large variation in range (Figure 37). Each sensor has a slightly different maximum range that the range sweep tests can show. The low-speed range test starts with the TV 40 meters ahead of the SV, stationary. The TV accelerates to a constant target speed of 15 mph while the SV accelerates to 10 mph greater than the target speed (25 mph), closing the gap. The DAS starts recording data when the SV reaches the target speed; once the SV is less than one car length behind the TV, the

SV reduces speed to 10 mph lower than the target speed (5 mph) and lets the following distance to the TV gradually increase. For high-speed lane slaloms, the same procedure was done on the highway section (not including the bridge in Figure 38) of the track at a greater target speed, 45 mph in this case. The SV will gradually approach the TV at 55 mph and then reduce to 35 mph as the following distance increases to over 180 meters. Repeated trials for the different degradations were conducted by placing them into the slots of the 8020 aluminum sensor frame on the roof of the SV.

Lane Slaloms

Lane slalom tests were designed to vary the lateral position of the TV across a sensor's FOV. Unlike the range sweeps, the TV is static for the lane slalom tests and is parked in the middle of the surface street at VTTI. For the low-speed lane slaloms, the SV accelerates to the target speed, 15 mph, and performs small "s-turns" on a repeated time interval with a fixed amplitude until past the TV (Figure 39). The driver of the SV reaches the apex of an s-turn every 2 seconds (0.5 Hz) and traveling laterally across 50 percent of the lane width. The rate and amplitude were kept constant for all lane slalom tests. High-speed lane slalom tests were conducted at a greater target speed, 35 mph, and performed on the highway section of the test track. Repeated trials for the different degradations were conducted by placing them into the slots of the 8020 aluminum sensor frame on the roof of the SV.

Figure 37. SV and TV positions for lane slalom and low-speed range sweep

Figure 38. Highway section: lane slaloms (not including the bridge) and range sweeps

Figure 39. SV maneuvers and TV position for the low-speed lane slalom

Test Matrices

A test matrix of all trials completed for the low-speed range sweeps, high-speed range sweeps, low-speed lane slaloms, and high-speed range slaloms is available in Appendix F. The run log code, test type, location, degradation variant, target speed, amplitude (for lane-slaloms), frequency (for lane slaloms), and vehicle rate (for range sweeps) are all specified for each trial run. Additionally, Appendix G indicates which degradation was applied to the individual sensors for each trial run based on the run log code.

Results

Lidar

Lidar data was captured running several dynamic vehicle scenarios such as range sweeps and lane slaloms (see Appendix E). The objective of the data collection was to capture sensor performance with and without degradations applied. Several lidar sensors were used (Table 21). Data was captured and then analyzed to extract points belonging to the TV as described next.

Data Analysis for TV Extraction

Lidar captures data in the form of point clouds. To easily locate the TV (an unmodified 2010 Chevrolet Impala) within the point cloud, DGPS antennas were mounted on the roof. The SV (also a 2010 Chevrolet Impala) was also equipped with DGPS antennas.

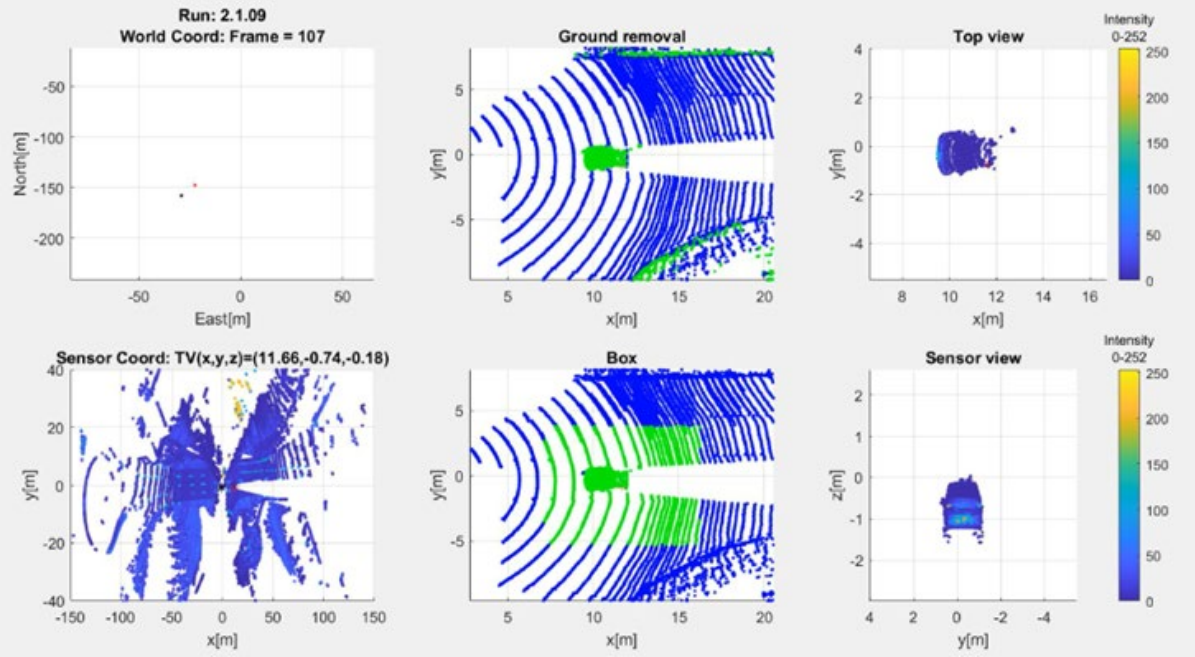

Figure 40. Lidar data analysis

Based on the run label shown on the top left in Figure 40, "(Run: 2.1.09)," a snapshot of a range sweep at low speeds is shown. The top left figure shows two points: the red point is the DGPS position of the TV in world coordinates. Similarly, the black point is the SV. World coordinates are then transformed into sensor coordinates. The bottom left figure shows what the lidar 128 "sees" as represented by the point cloud. In sensor coordinates, the lidar sensor is found at (x, y, z) = (0, 0, 0) and the TV is found at (x, y, z) = (11.66, -0.74, -0.18), all in meters. Two independent data processes are shown simultaneously operating on the point cloud: ground removal and bounding box. The purpose of the ground removal is to remove the points from the point cloud belonging to the ground. The top middle figure in Figure 40 is zooming into the TV to show the detail of the ground removal. The blue colored points are identified as belonging to the ground, and the green colored points are not part of the ground. The bottom middle figure shows the detail of the bounding box. A bounding box is created using the (*x, y, z*) TV coordinates and a proportional box determined using the size of the TV. As discussed earlier, the proportional factor was 1.8. The green colored points are identified as being within the bounding

box, and the blue colored points are not part of the box. Finally, the identified object (TV) within the point cloud is obtained using the points that are green in color from the ground removal and the bounding box. The top right and bottom right figures show the top view and the sensor view of the TV identified via this data analysis.

Lidar Degraded Versus Non-Degraded

Data was obtained with no degradations applied for the purpose of having a baseline comparison before and after degradations. A snapshot of range sweeps at low speed using the lidars is shown in Figure 41 through Figure 43. In Figures 41 and 43, the two figures on the left present a run for the non-degraded case, and the two figures on the right present the degraded case. Figure 43 only shows the degraded state. To make the comparison time independent, the same range from the degraded and non-degraded runs, as reported by the DGPS, was selected. Comparisons of lidar points and intensities are shown next.

Lidar 128 Beams

A snapshot of range sweeps at low speed using the lidar 128 is shown in Figure 41. The optical degradation applied was the highest level of sandblast. From Figure 41, DGPS reported the TV to be at a similar longitudinal range: 13.12 meters and 13.15 meters away from the sensor mounted on the SV on the left and right figures, respectively. At this range, the number of points returned by the TV and read by the lidar went from 2,050 for the non-degraded case to 62 for the degraded case. The mean intensity went from 24.1 to 4.9. The number of points and the intensity levels drop with the degradations.

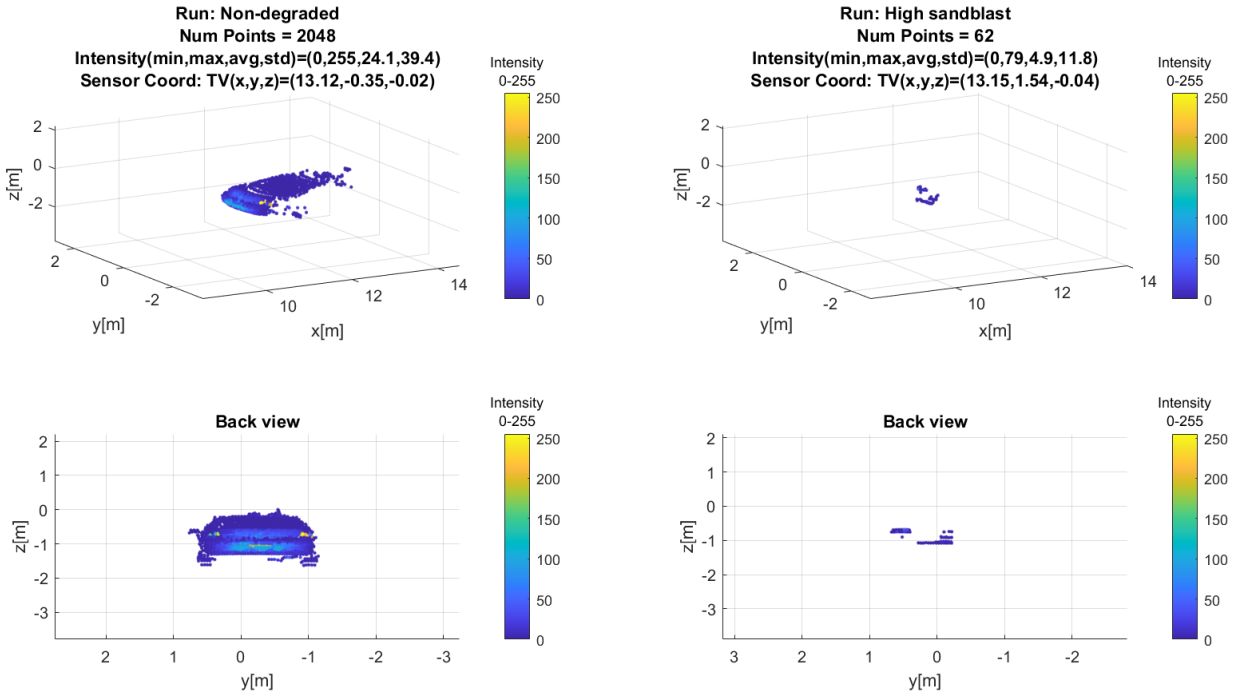

Figure 41. Lidar 128: Non-degraded versus degraded (high sandblast)

Solid-State Lidar

A snapshot of range sweeps at low speed using the solid-state lidar is shown in Figure 42. The optical degradation applied was the highest level of sealant. From Figure 42, DGPS reported the

TV to be at an identical longitudinal range: 13.05 meters away from the sensor mounted on the SV on the left and right figures, respectively. At this range, the number of points returned by the TV and read by the lidar went from 666 for the non-degraded case to 425 for the degraded case. The mean intensity went from 29.6 to 25.6. As with the 128 beam lidar, the number of points and the intensity levels drop with the degradations.

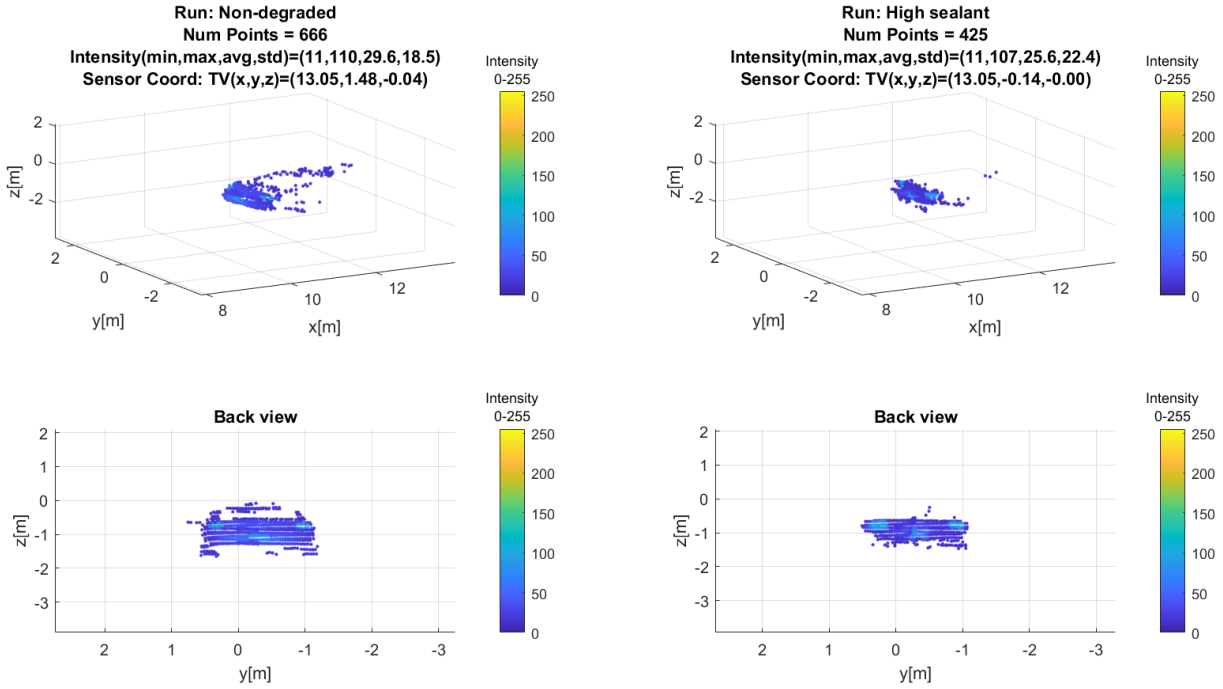

Figure 42. Solid-state lidar: Non-degraded versus degraded (high sealant)

Lidar 32 Beam

A snapshot of range sweeps at low speed using the lidar 32 is shown in Figure 43. DGPS reported the TV to be at a longitudinal range of 13.03 meters away from the sensor mounted on the SV. At this range, the number of points returned by the TV and read by the lidar is 143 for the non-degraded case. The mean intensity is 4.7. Comparing the non-degraded cases across the lidars shown, the number of points and the intensity corresponding to lidar 128, solid-state lidar, and lidar 32 are (n = 2050, i = 24.1), (n = 666, i = 29.6), and (n = 14, i = 4.7). lidar 128 is the most expensive lidar, but it gave the greatest number of points returned on the TV. The solid-state lidar aims at penetrating the automotive market with a performance that is in between the most expensive sensor (lidar 128) and one of the first lidar prototypes (lidar 32). lidar intensity is the return strength of a laser beam. The strength of the return depends on several factors including the target's location and orientation and the sensor technology transmitting and receiving the laser beam. Comparing the intensity for the non-degraded cases from Figure 41 and Figure 42, the back view shows that the lidar 128 returned low intensity points from the windshield and the solid-state did not returned any points from the windshield. The collection of low intensity points in the lidar 128 skewed the average intensity and resulted in a lower intensity value (i = 24.1) as compared to intensity (i = 29.6) from the solid-state lidar.

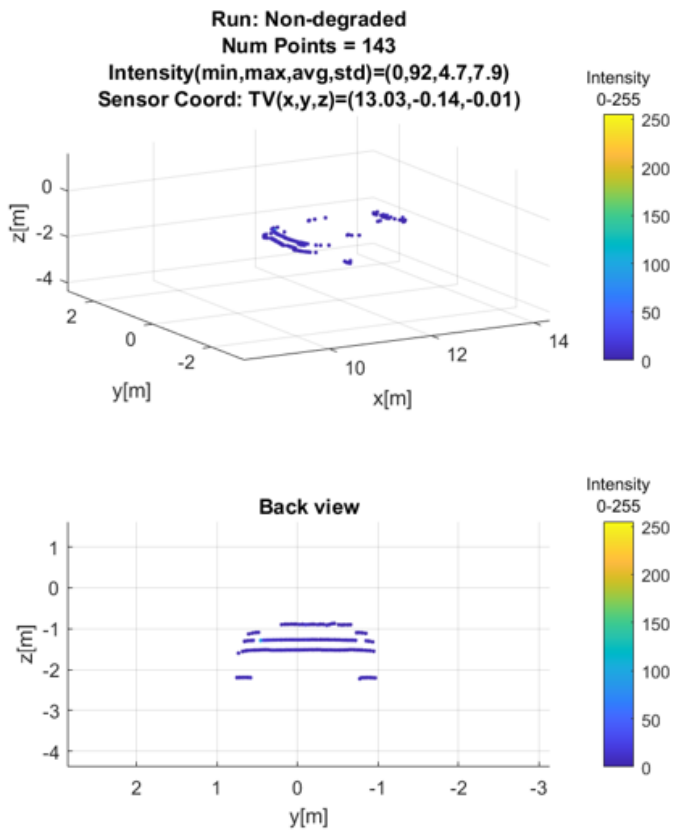

Figure 43. Lidar 32: Non-degraded

Solid-State Lidar Versus Five Degradations

Following the previous analysis, range, as reported by the ground truth DGPS, is being used to compare lidars. Figure 44 shows the number of points returned by a solid-state lidar under five different degradations. The non-degraded case, or baseline, is plotted in blue across the figures. Degradations 1, 2, 3, 4, and 5 correspond to low levels of: sealant, sandblasted, offgas, tint, and shellac. In all cases, the number of points returned to the lidar (*y*-axis) seem to drop exponentially with mean range (*x*-axis). Sandblasted (degradation 2) has the most effect on the number of points returned as shown by the red line under the blue line (baseline). As an example, at a mean distance of 20 meters, the non-degraded case returns around 270 points and the degraded case returns around 150 points.

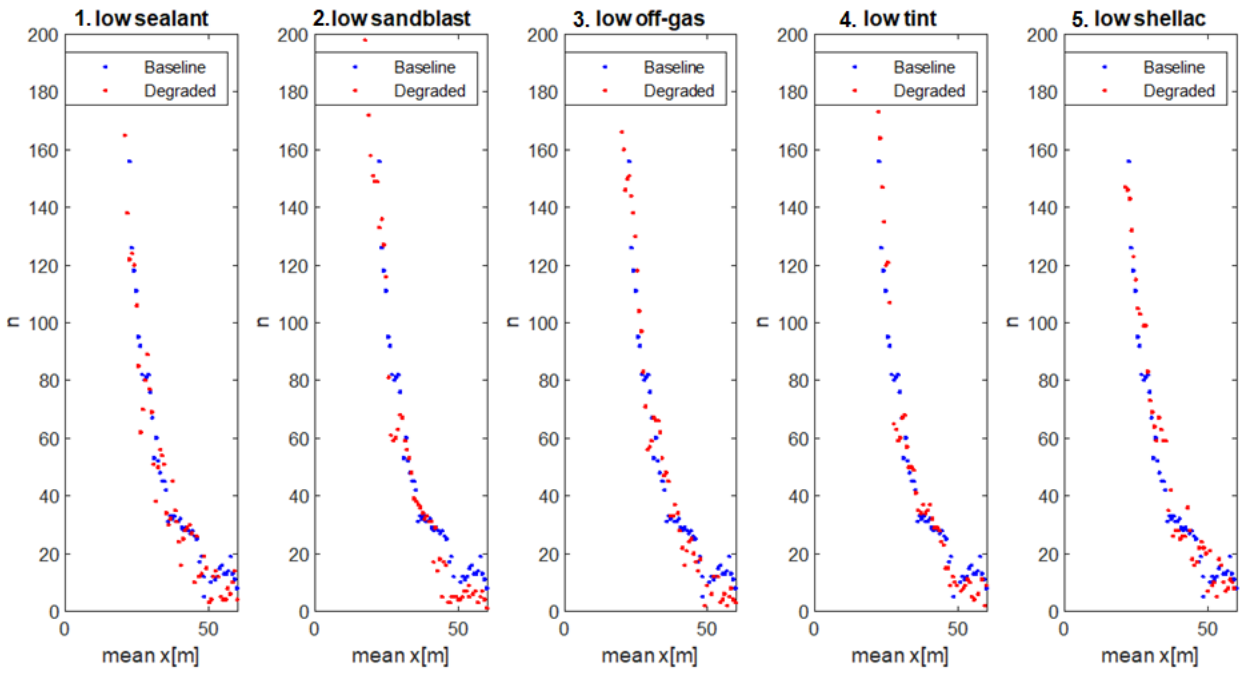

Figure 44. Solid-state lidar: Non-degraded versus five degradations

A snapshot of range sweeps at low speed using the solid-state lidar is shown in Figure 45 to Figure 47. To be consistent with the previous plots, DGPS reported the TV to be at a range of approximately 13 meters away from the sensor mounted on the SV. At this range, the number of points returned by the TV and read by the lidar is 495 for the non-degraded case, and the mean intensity is 29.6. At this specific range, the low level of tint (degradation 4) retuned the least number of points (n = 172). The low sandblasted (degradation 2) reported the lowest mean intensity (mean i = 24.9).

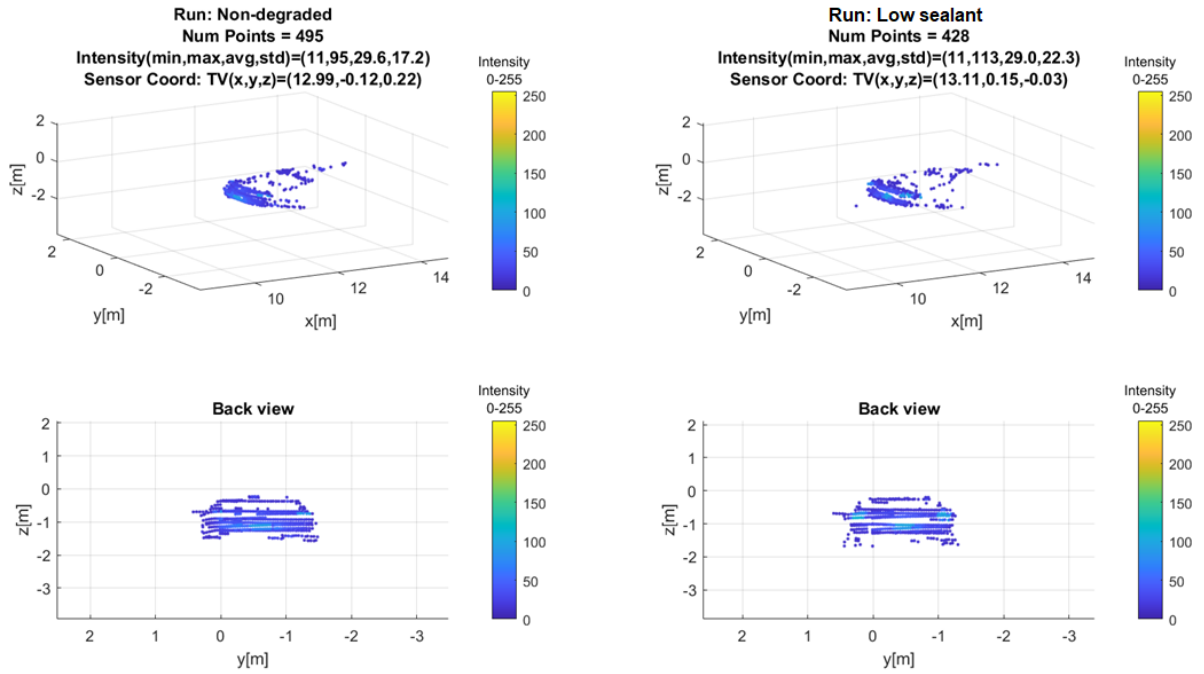

Figure 45. Solid-state lidar: Non-degraded and low sealant degradation

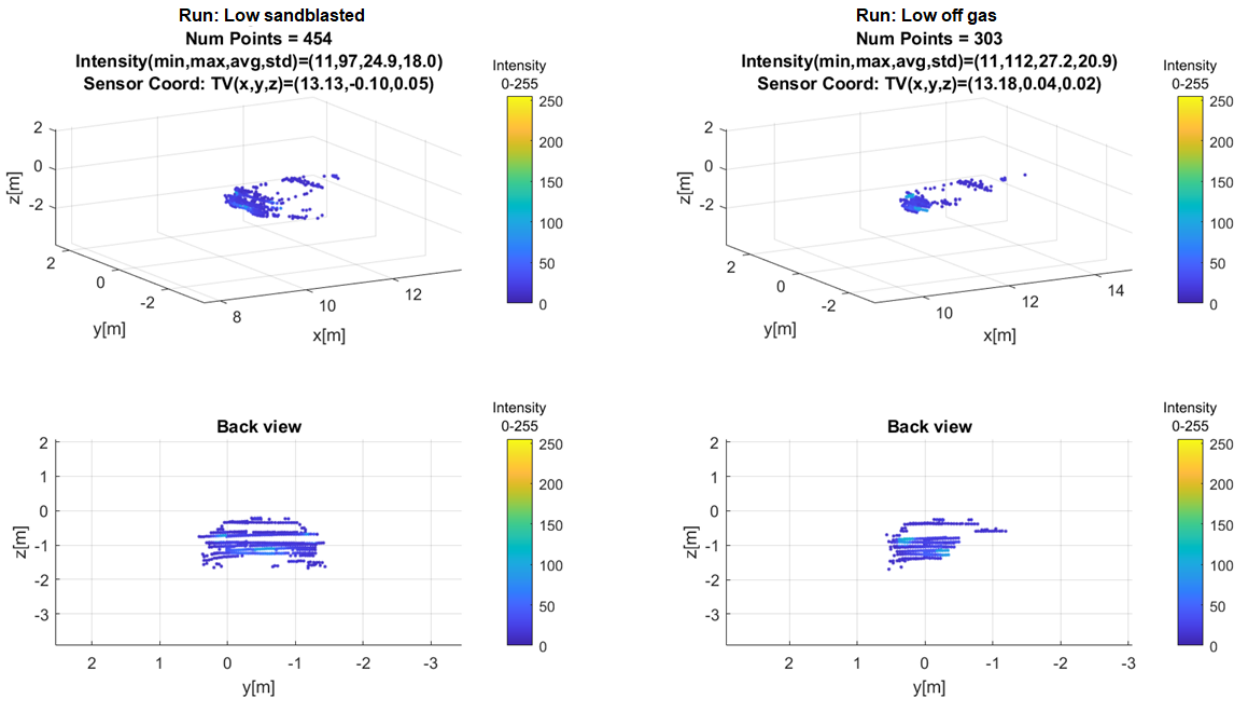

Figure 46. Solid-state lidar: Low sandblasted and low offgas

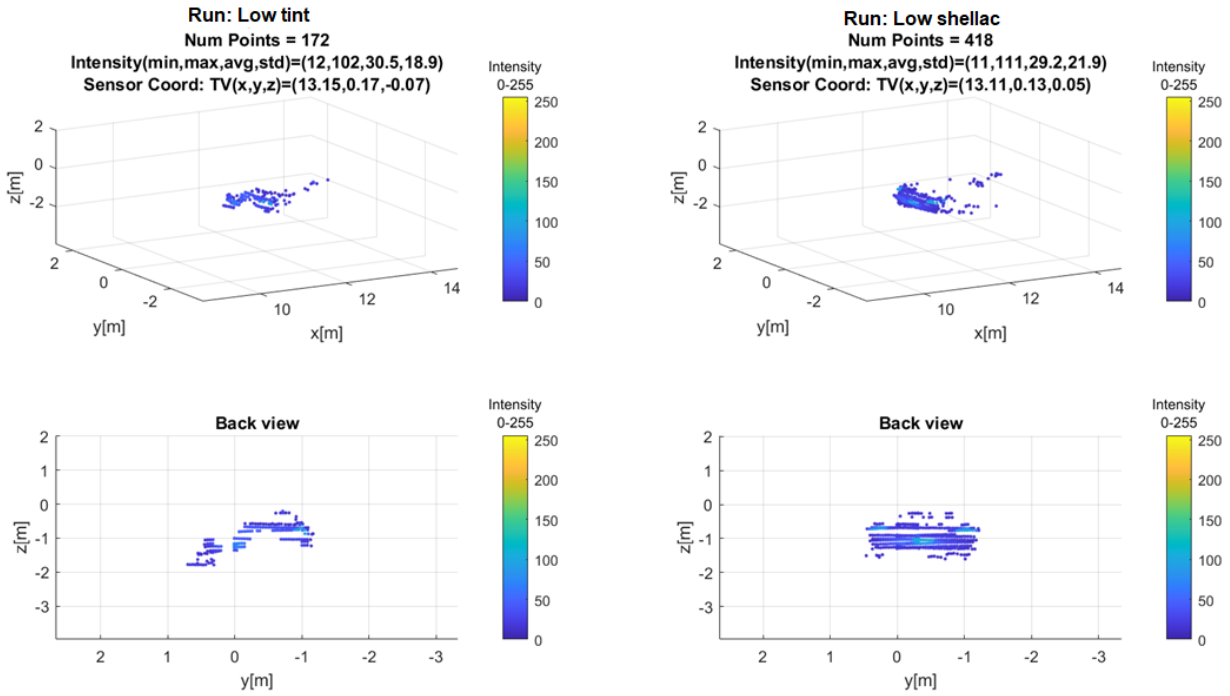

Figure 47. Solid-state lidar: Low tint and low shellac

Solid-State Lidar Versus Levels of Degradation

Following the previous analysis, range, as reported by the ground truth DGPS, is being used to compare lidars. Figure 48 shows the number of points returned by a solid-state lidar with three different levels for the sealant degradation: low, medium, and high. As before, the plot shows the non-degraded case, or baseline, in blue. In all cases, the number of points returned to the lidar drops with range.

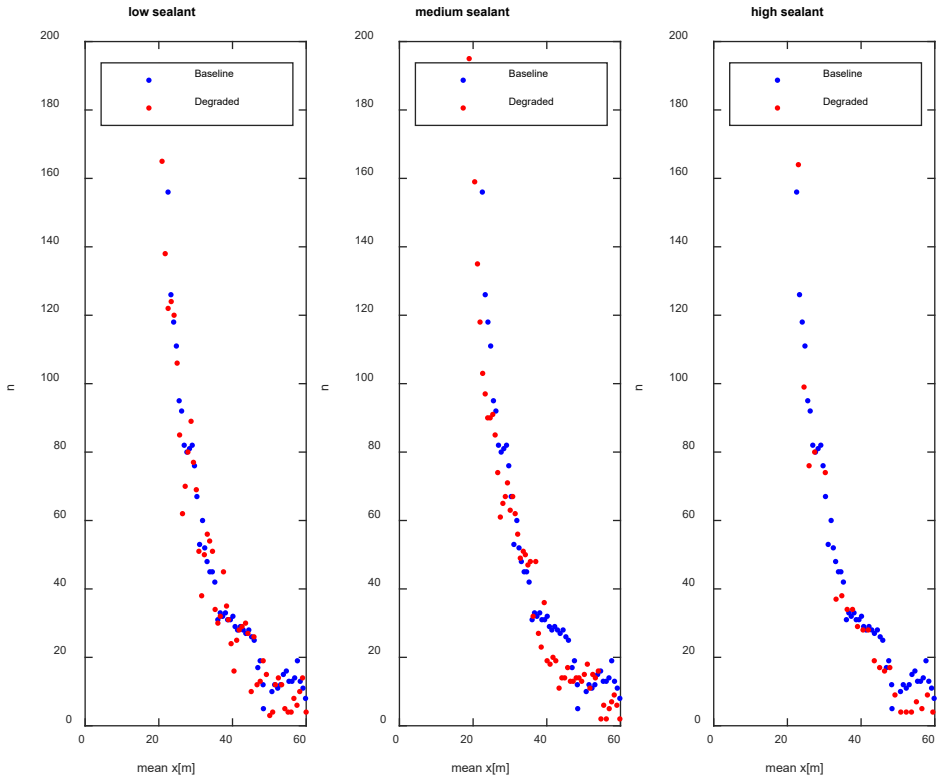

Figure 48. Solid-state lidar: Non-degraded versus degradation levels

A snapshot of range sweeps at low speed using the solid-state lidar is shown in Figure 49 to Figure 50. To be consistent with the previous analysis plots, DGPS reported the TV to be at a range of approximately 13 meters away from the sensor mounted on the SV. The number of points returned by the lidar is a function of the target location within its FOV. The further away the target is, the fewer points are returned, and the harder it becomes to identify the target. It is easier to identify the target when it is located within the FOV of the sensor such that the number of points returned are easier to process for target identification. Several distances showed the target located within the FOV of the sensor. One of those distances (i.e., 13 meters) was chosen arbitrarily for this study. At this range, the number of points returned by the TV and read by the lidar is 495 for the non-degraded case, and the mean intensity is 29.6. At this specific range, the number of points returned in the order from non-degraded, to low sealant, to medium sealant, to high sealant are: 495, 428, 454, and 303. Similarly, at this specific range, the mean intensities returned in the order from non-degraded, to low sealant, to medium sealant, to high sealant are: 29.6, 29.0, 24.9 and 27.2. The overall trend seems to be that the number of points returned decreases as the level of degradation increases. Similarly, the target intensity decreases as the level of degradation increases.

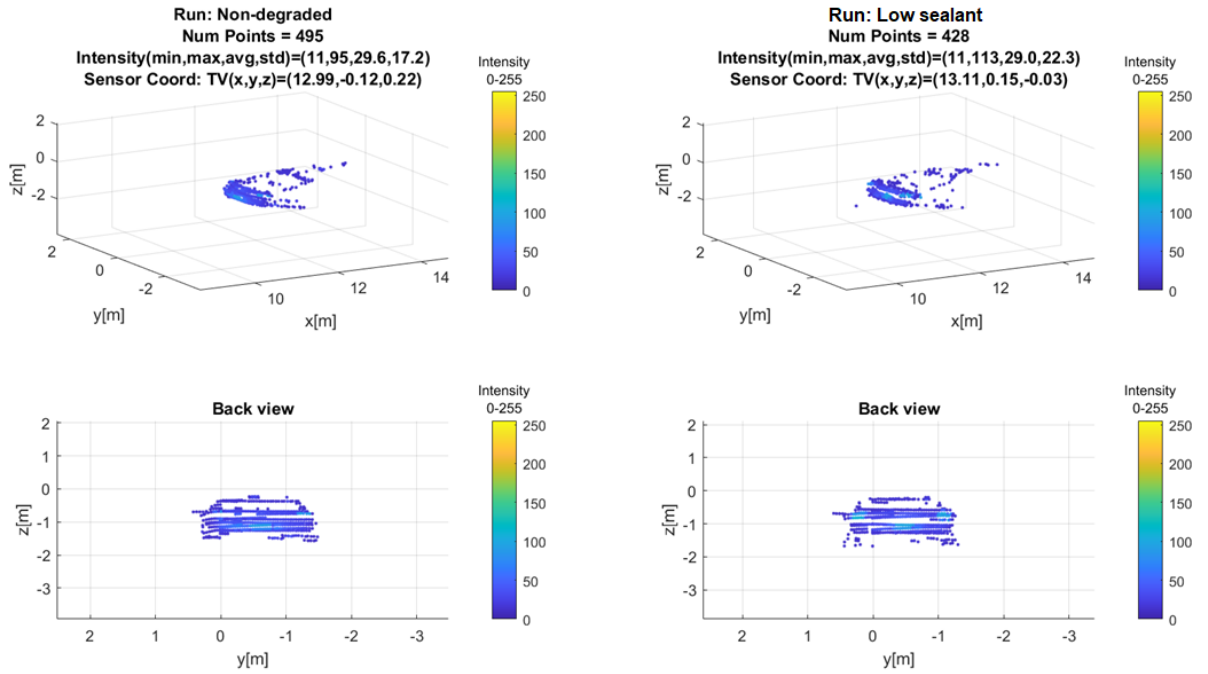

Figure 49. Solid-state lidar: Non-degraded and low sealant degradation

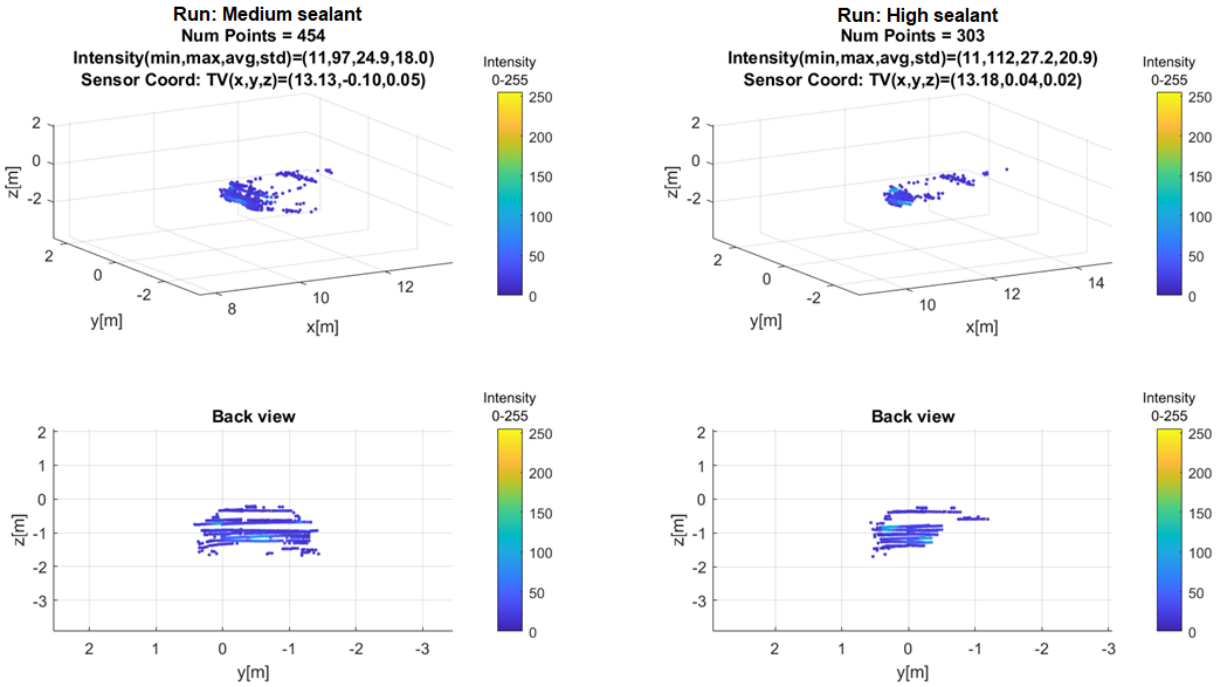

Figure 50. Solid-state lidar: Medium sealant degradation and high sealant degradation

Radar

Radar data was captured running several dynamic vehicle scenarios such as range sweeps and lane slaloms concurrently with the lidar sensors (see Appendix H). The objective of the data collection was to capture sensor performance with and without degradations applied. Five radar sensors were used (Table 21) for these component tests.

Radar Data Analysis for TV Extraction

The radars do not inherently output data in the same format. Two radars, the SR 24 GHz and LR 24 GHz, output object data while all others return point clouds for each timestep. Further, all radars except the LR 24GHz reported returns with an RCS value, while only the LR 77GHz radar reported SNR values. To compare object data with point cloud data, the point cloud data was transformed into an object as follows. Point cloud data was bounded by a box created using the DGPS position of the TV. Data contained within the bounding box is treated as belonging to the TV. The average values of the data within the box provide several quantities that describe the object. The average position of the data points contained within the bounding box is known as centroid. In addtion, the object's average velocity, RCS, and SNR were calculated (see Chapter 4 Methodology). As an example, Figure 51 shows the position and heading direction of the SV as reported by DGPS (in green), the position and heading of the TV as reported by DGPS (in red), the bounding box created around the TV (in blue), and the point cloud data as reported by the LR 77GHz radar (two black points). The bounding box created using the DGPS antennas contained the returns originating from the object of interest, i.e., TV. Point cloud data within the bounding box is known as gated return. The total number of gated returns for each timestep was also recorded for additional information.

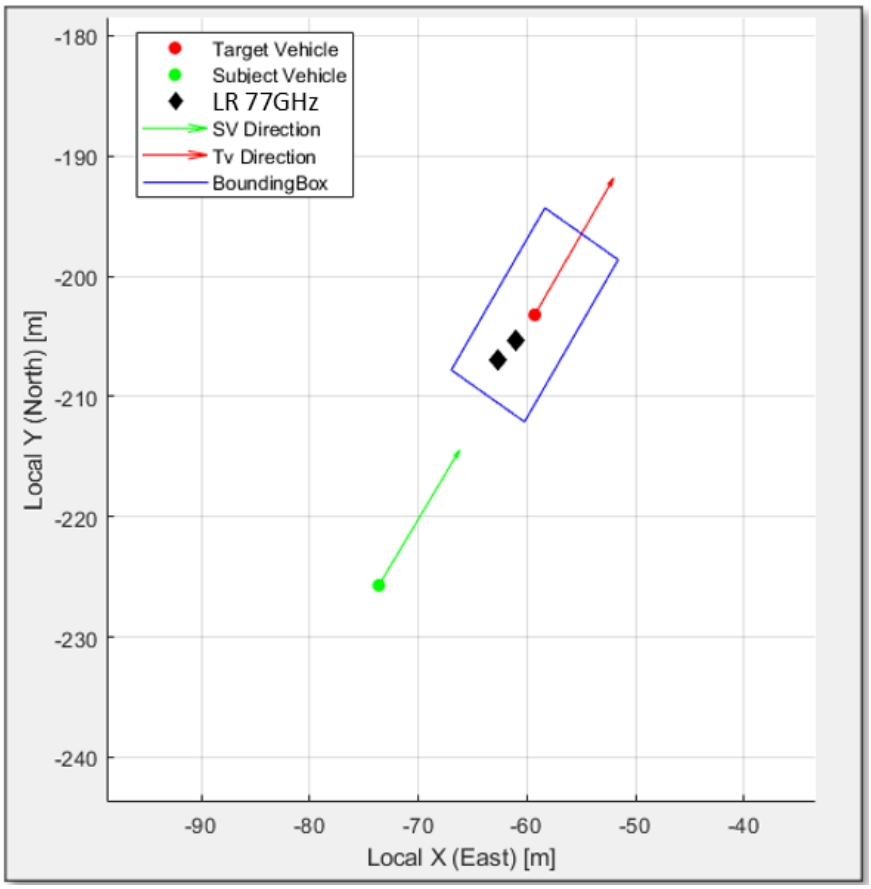

Figure 51. Snapshot showing data for TV extraction using the LR 77GHz radar. Two points detected within a TV bounding box for this timestep for the LR 77GHz radar.

Analysis and Results

Table 21 shows that the sensor output for the radars can be object data or point cloud data. Table 21 also shows that two object radars and three point cloud radars were tested. As described under Data Analysis for TV Extraction, point cloud data was transformed into object data. Therefore, comparison across all radar sensors was done using object data. Since each radar sensor has its own sampling rate, every object from each radar was interpolated to the SV DGPS's sampling rate. This allowed comparison of object data at the same time. Recall that the average position of the data points contained within the bounding box is known as centroid. In other words, the centroid provides the (*x, y*) location of the object, and the object is the TV. In the radar sensors themselves, centroid (i.e., location) data was compared over time and by distance to analyze degradation effects. Several tests using lane-slaloms and range sweeps were conducted to collect radar data. The results are reported next.

Non-Degraded Versus Degraded Radar Trials

The researchersnoticed the "lane slalom" trial type had a large impact on some tracking performance for the LR 24GHz and SR 24GHz object radars. When plots of the TV DGPS versus the object radar from the LR and SR 24GHz are compared for the low speed lane slalom (15 mph) in both the longitudinal (*x*) and lateral (*y*) directions relative to the SV, it is obvious that the two object radars have considerable trouble tracking the static TV through the slalom maneuver (Figure 52). Figure 52 shows time in the *x*-axis as reported by the SV DGPS. The *y*-

axis shows longitudinal (x) and lateral (y) positions of the stationary TV. The y-axis was labeled "Position" to represent either the lateral or longitudinal positions as determined by the legend or key in Figure 52. For example, for the SR 24 GHz case (Figure 52, right), the longitudinal position of the TV (i.e., SR 24 GHz – x in the figure key) during the slalom test took values larger than 0 m and less than 40 m. Similarly, the lateral position of the TV (i.e., SR 24 GHz – y in the figure key) during the slalom test took values between 0 and -10 m (red cross data points in Figure 52). In other words, red points and crosses in Figure 52 are shown when the TV is detected by the radar sensor longitudinally, and laterally, respectively. According to the specifications for the radar sensors, the radars are capable of detecting objects that are longitudinally located beyond 75 m. Tracking is defined as maintenance of a constant detection. During slalom tests, the static TV was not tracked by the radars until the TV's position was longitudinally located within 40 m (red data points in Figure 52), suggesting that sufficient SV yaw rates can affect tracking ability for those two radars. Similar results are seen for the higher speed lane slaloms (35 mph) in Figure 53. The LR 24GHz did not successfully track the static vehicle under any non-degraded or degraded cases for the lane slalom trials during the entire run (see Figure 53, left). The SR 24GHz radar tracked the static vehicle at low ranges only during one of the lane slalom maneuvers with no degradations (see Figure 53, right).

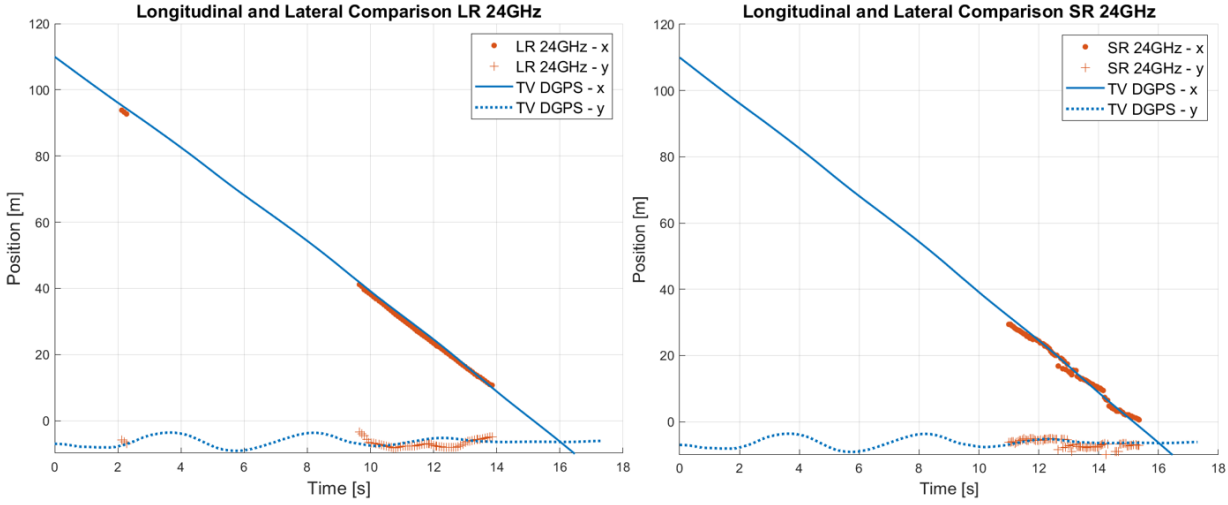

Figure 52. Non-degraded ground truth comparison plots for the low-speed lane slalom trials: LR 24GHz (left) and SR 24GHz (right)

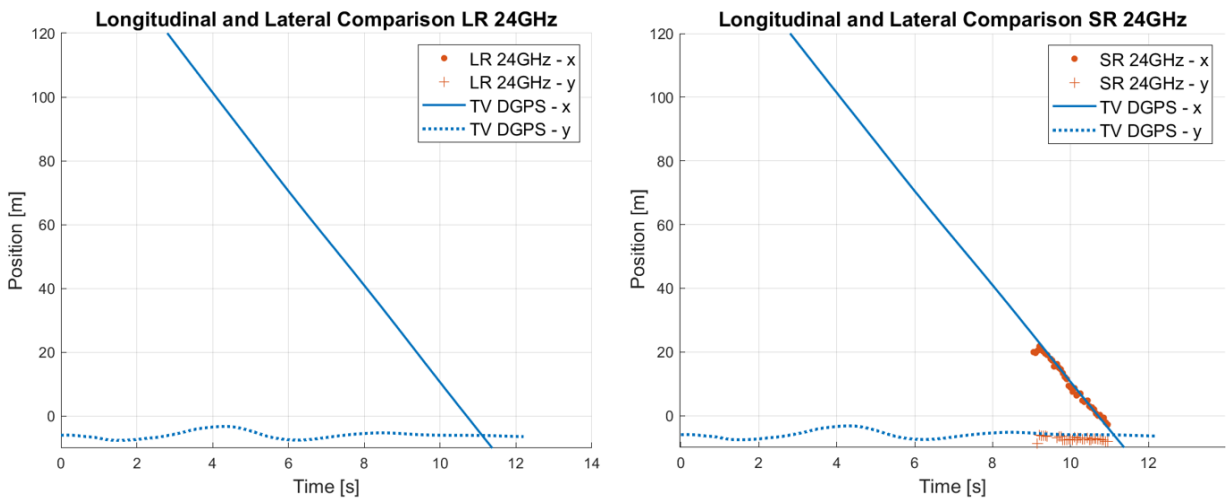

Figure 53. Non-degraded ground truth comparison plots for the higher-speed lane slalom trials, LR (left) and SR 24GHz (right) trials

Additionally, some degradations were found to affect the number of sensor returns during the trials. For example, this was shown in DGPS ground truth plots versus radar outputs in the following trial runs: SRE (medium) degradation for the low speed lane slalom trial with the LR 24GHz radar (Figure 54); the Bondo mesh (low and medium) degradation for the higher speed range sweeps with the SR 24GHz radar (Figure 55); and the Bondo mesh (low) degradation for the low speed range sweep with the SR 77GHz radar (Figure 56). In each of the figures, most of the degradation effects were seen as reducing the number of returns over the trial duration when compared to the non-degraded case. The results suggest that some degradations may affect the performance for some sensors during certain test types.

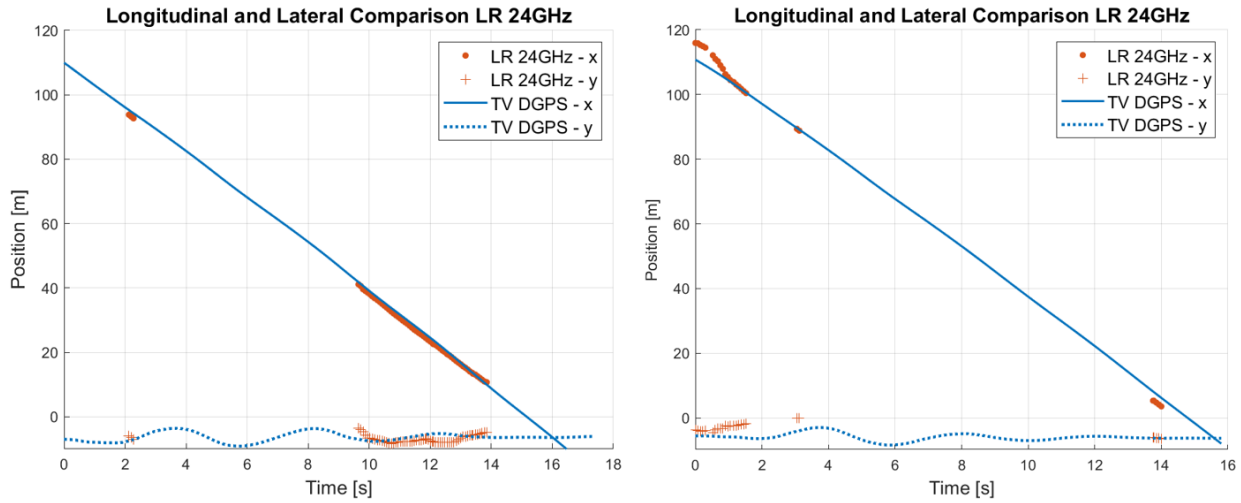

Figure 54. Non-degraded (left) versus degraded (SRE, medium [right]) ground truth comparison plots for the low-speed lane slalom trial, LR 24GHz

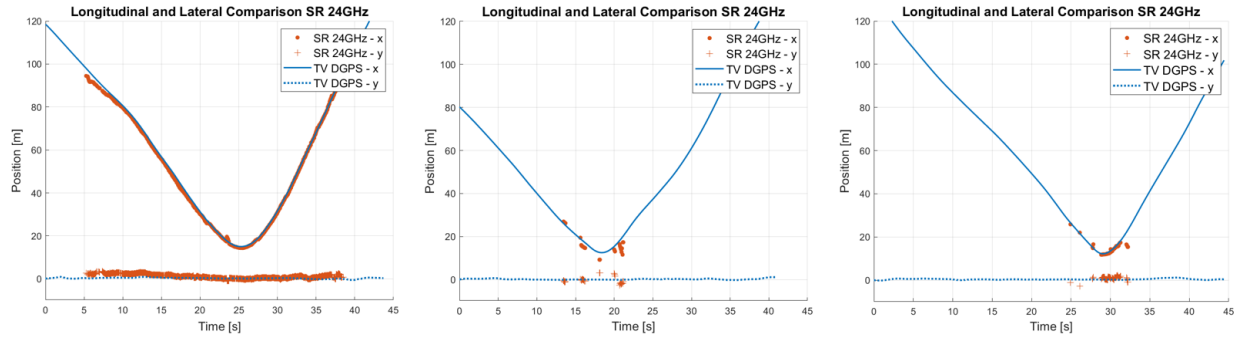

Figure 55. Non-degraded (left) versus degraded (Bondo, low [middle] and medium [right]) ground truth comparison plots for the low range sweep trial, SR 24GHz

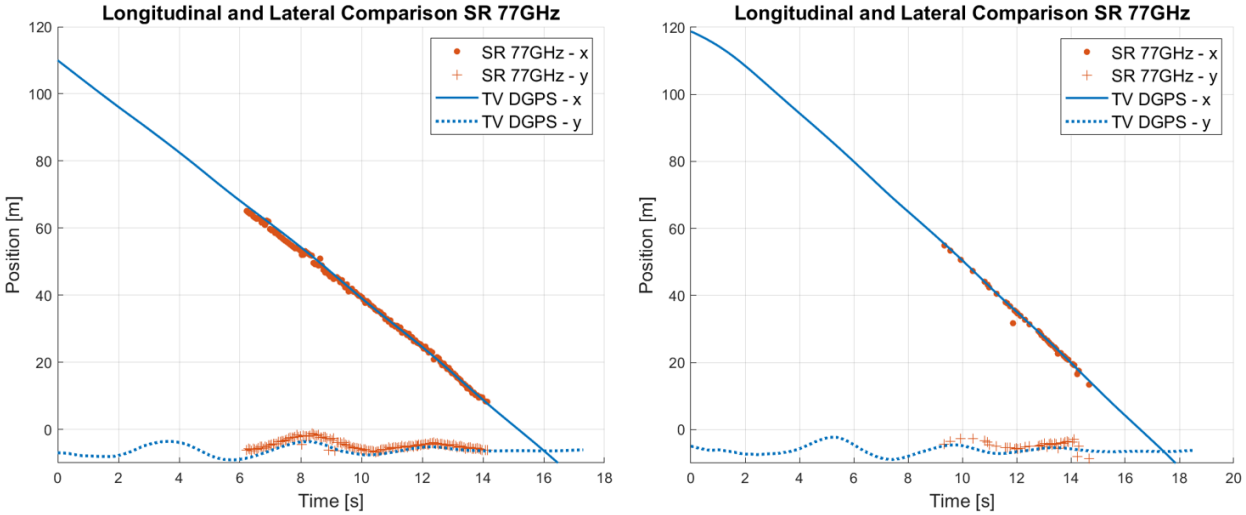

Figure 56. Non-degraded (left) versus degraded (Bondo, low [right]) ground truth comparison plots for the low-speed range sweep trial, SR 77 GHz

Moreover, the three different levels (low, medium, and high) of degradation were plotted for comparison for two degradation types: blacktop for the low speed lane slalom trials with the LR 77GHz near scan (Figure 57), and Bondo mesh for the higher speed range sweep trials with the SR 24GHz radar (Figure 58). The blacktop levels do not show a large difference in accuracy performance of number of returns between the low, medium, and high levels for that test type and radar. Alternatively, the Bondo mesh degradation levels for the SR 24GHz do show significant difference between low, medium, and high cases, though, counterintuitively, the high degradation level trial produced the most tracks from the TV during this trial of the higher speed range sweep.

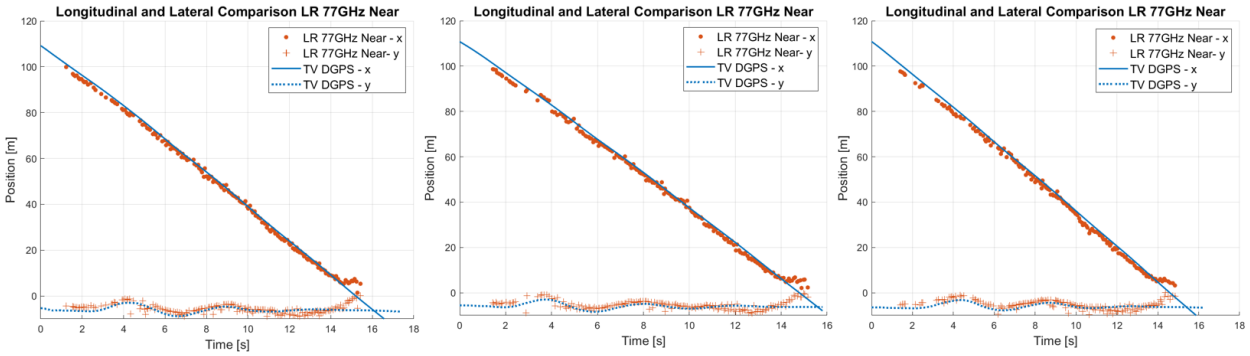

Figure 57. Ground truth comparison plots for the low (left), medium (middle), and high (right) blacktop degradation levels during low-speed lane slalom trials, LR 77GHz near scan

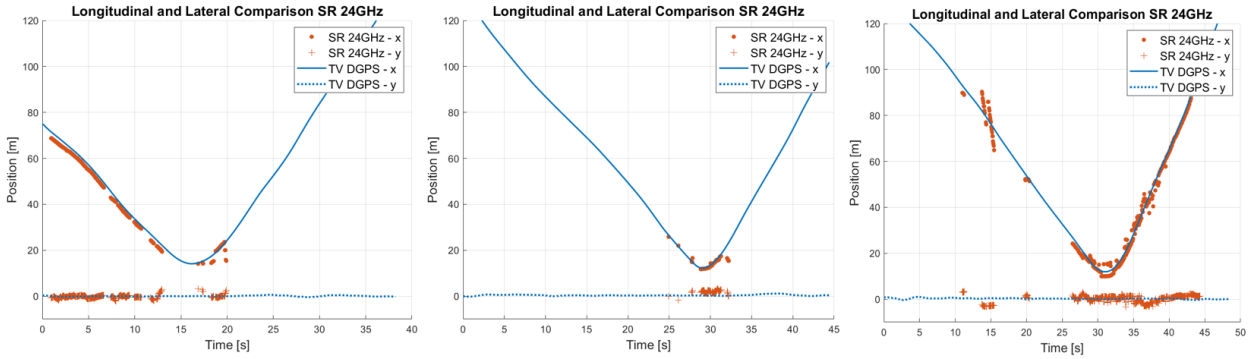

Figure 58. Ground truth comparison plots for the low (left), medium (middle), and high (right) Bondo mesh degradation levels during higher speed range sweep trials, SR 24GHz near scan

It is unclear exactly why the high level Bondo mesh degradation produces more points during the range sweep for the object-oriented SR 24GHz radar than those of the medium and low level, but clearly the degradation level can produce variable effects within test types. One possibility could be that higher degradation limits the number of returns from the radar to only the strongest returns that most likely originated from the vehicle. This could, at specific times, aid the radar's perception algorithm. A full test matrix was not done to show the medium and high level Bondo mesh degradations for other radars during the high-speed range sweep. The initial exploration of the degradation effects was done testing low levels.

The calculated difference between the lateral and longitudinal ground truth DGPS reading and the radar centroid outputs provide the ability to compare average accuracy metrics across different sensor modalities, the degradations, and the non-degraded cases.

Number of Gated Returns Versus Distance

As described under Data Analysis for TV Extraction, point cloud data within the bounding box is known as gated return. The number of gated returns were plotted by distance to determine if there was an effect between the degraded and non-degraded cases. For the radar, three distance ranges, 0 to 45 meters, 45 to 100 meters, and 100 to 180 meters, were chosen to compare average number of returns between degradations. Assuming typical urban vehicle driving speeds of 35 mph, these range gates correspond to positions on the roadway that are approximately 0 to 3, 3 to 6, and 6 to 12 seconds ahead of the vehicle. The number of returns for each sensor in each range

gate were averaged, and the effects of the average number of returns for each range gate and degradation were compared against the baseline.

Within the closest range gate, 0 to 45 meters, there were several degradations that significantly reduced the average number of points when compared to the non-degraded case for all degradation component trials, particularly for the SR 77GHz radar and the near scan of the LR 77GHz radar (Figure 59). These include the Bondo mesh, epoxy, SRE, and Spruce degradations for the SR 77GHz radar, as well as the Bondo mesh, epoxy, and SRE degradations for the near scan of the LR 77GHz radar. For the next two range gates, 45 to 100 meters and 100 to 180 meters, only the SRE degradation for the near scan of the LR 77GHz showed significant decrease in the average number of returns. The fact that some degradations resulted in fewer average returns than the non-degraded case aligns with individual findings from Figure 54 to Figure 56. Additionally, based on the data collected, only the Bondo mesh degradation shows a significant increase in returns when moving from any lower level degradation to a higher one. Namely, this is seen for the medium and high levels of Bondo mesh with the SR 24GHz radar for both the 0 to 45 m and 45 to 100 m range gates. This reinforces the variable Bondo mesh results for the high speed range sweep shown in Figure 58. Where applicable, the remaining degradations did not produce significantly different average number of returns for any of the radars in the range gates when comparing in the low, medium, or high levels of severity. See Appendix I for additional range gated data.

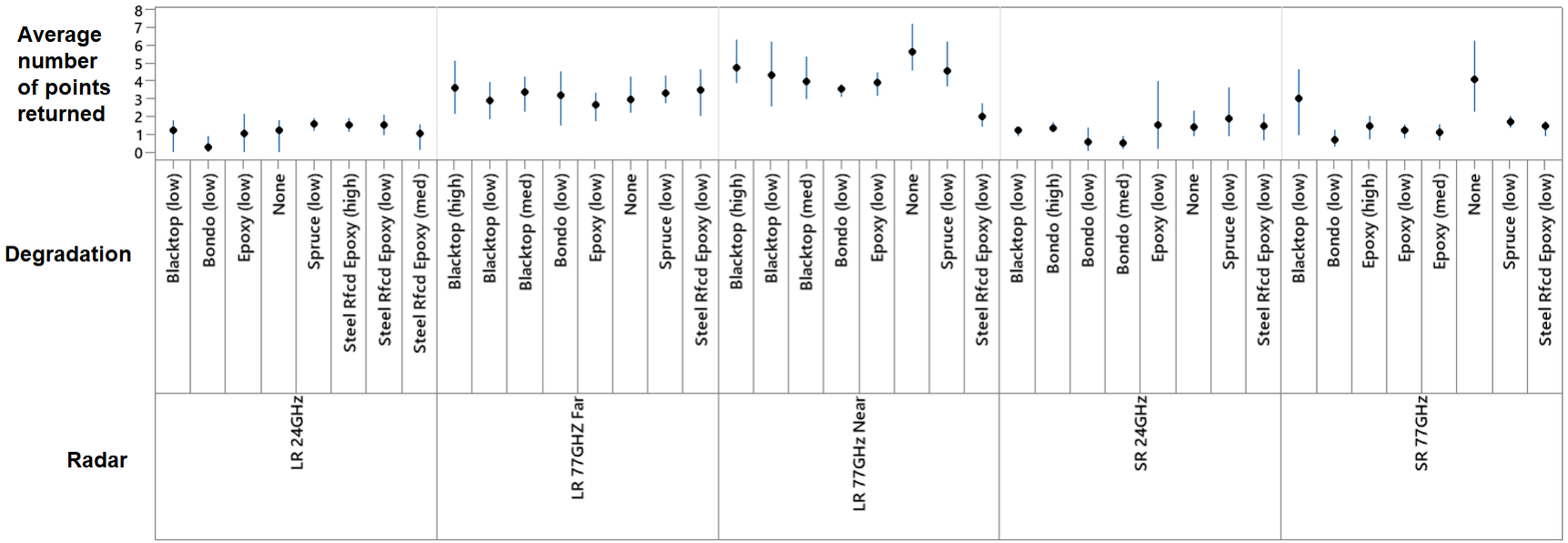

Figure 59. Average number of points returned for the range 0-45 m plotted with respect to radar type and degradation and averaged over the component testing degradation trials

The majority of degradations for the LR 24GHz radar, the SR 24GHz radar, and the far scan of the LR 77GHz radar did not significantly differ from the baseline cases when comparing number of returns for the closest range gate when averaged over the different degradation trials. Only the Bondo mesh for the SR 24GHz and LR 24GHz radars showed a significant reduction in average number of returns for this range gate. Though some degradations largely affected the LR 24GHz and the SR 24GHz radar for individual trials, when averaged over the repeated degradation trials, the effect is not significantly different than the non-degraded trials, except for the Bondo mesh degradation, as previously mentioned.

A lack of overall difference between the baseline and degraded cases for this range gate for the SR 24GHz radar and the LR 24GHz radar could be attributed by the extra data processing and filtering conducted by those sensors to output tracks and objects instead of the point cloud data from the LR 77GHz radar and the SR 77GHz radar.

RCS Analysis

The complete set of plots showing the effects degradations had on radars can be found in Appendix I. All the figures in the appendix have the same format. The high-speed lane slalom (Figure 60) was arbitrarily chosen to explain the contents of the figures.

Figure 60 shows the impact of the degradations applied on RCS. The x-axis shows the degradation applied to the radars, such as none, blacktop, Bondo/mesh, epoxy, SRE, and spruce (i.e., pine needles). Degradation tested match those listed in Table 23. The y-axis shows the mean intensity of the RCS in decibel square meters (dBsm), and 1 standard deviation displayed by the whiskers. Whiskers are the vertical bars originating from the mean value. The legend in Figure 60 shows the intensity of the degradation applied, such as none, low, medium, and high. The title shows the dynamic vehicle maneuver executed, in the case of Figure 60, a lane slalom at high speed. The subtitle shows the radar under test, such as LR 24GHz (object radar), SR 77Hz (point cloud radar), SR 24GHz (object radar), LR 77GHz Near (point cloud radar), and LR 77GHz Far (point cloud radar). Radars under tests were listed in *Table **21***. An empty plot, such as the top figure in *Figure **60***, indicates that no output was reported by the sensor. In other words, the degradation applied during the dynamic vehicle maneuver prevented the radar from providing RCS values. In specific, the first graph shows the object oriented LR 24GHz radar was not able to track the TV during this testing due to the maneuvering of the SV, even for the baseline trials. The remaining four radars in this graph show various impacts of the degradations. The units of RCS are square meters. However, the RCS is typically reported in dBsm which is the decibels related to $1m^2$ of RCS. To convert between RCS in square meters and RCS in dBsm, the following formula is used: dBsm = 10 x log10 (RCSsm). The fundamental log10 function produces negative values for arguments between 0 and 1. When the degradation affects the RCSsm to values between 0 and 1, the reported dBsm is negative.

Effects that degradations had on radars are demonstrated comparing the baseline with a specific degradation applied. The baseline is the case when no base is used, and no degradation is applied. The baseline in Figure 60 corresponds to “None” to indicate no base for the x-axis, and “None” in the legend to indicate no degradation applied. For the mean RCS in the high-speed lane slalom trials (Figure 60), and for the SR 24 GHz radar sensor (middle figure), the medium intensity level Bondo mesh and low intensity level spruce degradations show the most deviation from the baseline. The mean intensity RCS value for the baseline for the SR 24 GHz radar is obtained from the middle Figure 60. It is shown by the edge of the blue square, which is around -6 dBsm. Similarly, the mean intensity RCS value for the Bondo (shown by the edge of the

yellow square) is around -18 dBsm. This is an 82 percent decrease. The mean intensity RCS value for the spruce (shown by the edge of the orange square) is around 8 dBsm. This is a 172 percent increase. Figure 60 also shows that the high level of the blacktop and low level of the SRE degradations had the largest effect for the LR 77GHz near radar (41% and 45% increase, respectively, from the baseline). For the LR 77GHz far radar, the low level of the spruce degradation had the largest impact, resulting in a 109 percent decrease in mean intensity RCS when compared to the baseline. In many cases, the degradations increased the mean intensity RCS, which could be again due to the loss of the low RCS reflections in the sampled data points. Overall, Figure 60 shows the impact of the degradations applied on RCS. An empty figure indicates that no RCS output was reported by the sensor. In other words, the degradation applied during the dynamic vehicle maneuver prevented the radar from providing RCS. Therefore, the emptier the figure is, the more the sensor was affected by the degradation applied and could not provide RCS.

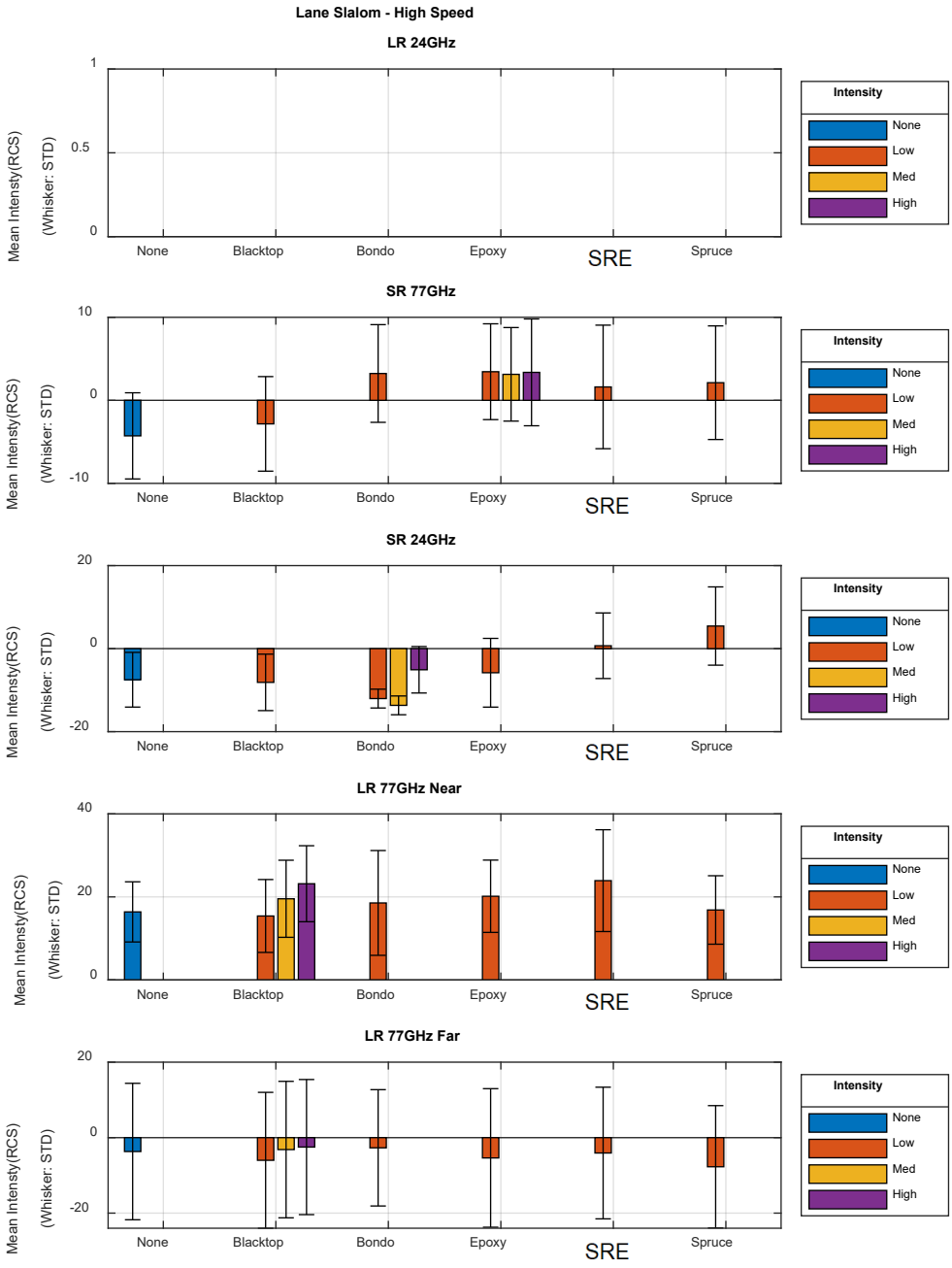

Figure 60. Mean Intensity RCS analysis across degradations and radars for high-speed lane slalom trials

Camera

The object camera from Table 21 was the only camera evaluated for the component-level data. This camera has internal processing for object detection. This reduces the post processing burden compared to the sensors that output point cloud data such as some radars and lidar. The machine vision camera outputs large files of raw data at every single sampling time. Finding ways to process large raw data files to produce objects in a reasonable amount of time is outside the

scope of this project. Therefore, the machine vision camera was not evaluated at the component level. The TV position (Figure 61) and velocity (Figure 62) as reported by the object camera during a range sweep maneuver with no degradations applied is shown in Figure 61 and Figure 62 below. The no degradations applied case is known as baseline and it is used to compare the effects degradations have on the sensor. In specific, Figure 61 shows the longitudinal (x) and lateral (y) positions of the TV. The blue points are measurements as reported by the DGPS, the small orange circles are measurements as reported by the object camera. The x-axis shows time in seconds, and the y-axis show position in meters. Similarly, Figure 62 shows the longitudinal velocity (v) of the TV as reported by the DGPS (blue points) and the object camera (small orange circles).

The accuracy of the object camera is determined by the overlap of the object camera measurements (small orange circles) and DGPS measurements (blue points). The least amount of overlap corresponds to the least amount of accuracy. The accuracy of the TV longitudinal velocity, longitudinal position, and lateral position is consistent across the range sweep maneuver (Figure 61 and Figure 62). The range sweep maneuver consists of two parts, SV approaching TV, and SV distancing from TV. The largest deviation, or overshoot (i.e., the least measurement overlap), occurred when the SV changed from getting closer to the TV to moving away. The distancing portion of the range sweep, as reported by the object camera (small orange circles) starts with a lower longitudinal distance (as compared to the DGPS, blue points) that slowly returned (a.k.a. hysteresis) to overlap with the longitudinal position as reported by the DGPS. This hysteresis and overshoot are likely a result of the camera's internal processing such as a filter. Similarly, the longitudinal velocity response (Figure 62) has a periodic offset of about 1 m/s every 1.25 seconds. This may be an artifact of the internal processing. The lateral position response shows some similar hysteresis and overshoot; however, the scale is considerably smaller in this test, given the range sweep is a longitudinal maneuver.

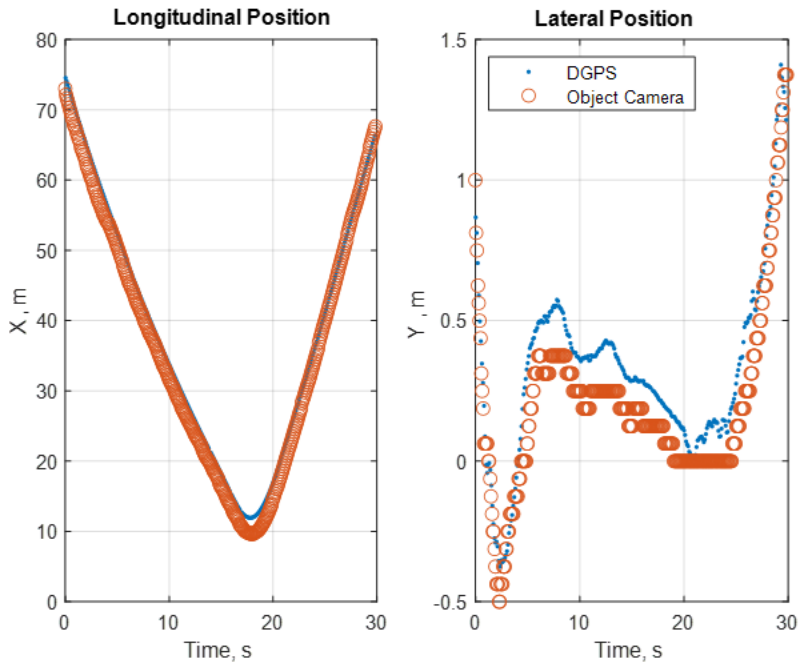

Figure 61. TV position during range sweep with no degradations applied

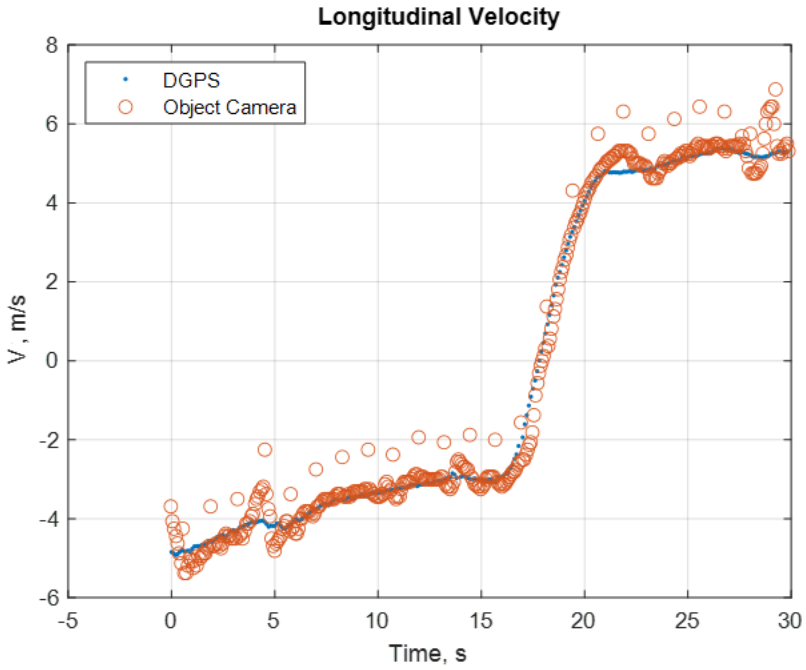

Figure 62. TV longitudinal velocity during range sweep with no degradations applied

Another downside to not having access to the post processing layer is missing some of the more qualitative metrics of the signal, such as evaluating the relationship of the number of returned points in the range, as shown for the radar and lidar data. The object camera sensor performance was only evaluated using the available sensor outputs.

Figure 63 shows the impact of the degradations applied on maximum range. The x-axis shows the degradation applied to the optical sensors, such as none, offgas, sandblast, sealant, shellac, and tint. Degradations tested matched those listed in Table 23. The y-axis shows the maximum range. The legend in Figure 63 shows the intensity of the degradation applied, such as none, low, medium, and high. The title shows the dynamic vehicle maneuver executed. The subtitle shows the sensor under test, i.e., object camera. An empty plot, such as the shellac case at the top figure in Figure 63, indicates that no output was reported by the sensor when low, medium, and high intensity levels of shellac were applied. In other words, the degradation applied during the dynamic vehicle maneuver prevented the camera from providing maximum range values.

Comparing the four results in Figure 63, the maximum range at which the camera could detect an object did not change for the majority of degradations. However, the low, medium, and high intensity shellac degradation had a large effect for the low-speed lane slalom, high-speed lane slalom, and high-speed range sweep, ultimately causing the object camera to not engage to identify the TV during these nine trials. Additionally, the low intensity sealant degradation had a sizable effect on the high-speed lane slalom and, to a lesser extent, the high-speed range sweep where the maximum range of the TV identified was significantly lower than the baseline. The low intensity offgas degradation had a similar effect for the high-speed range sweep, though the camera was still able to identify the TV at a distance greater than 100 meters. In these trials, all degradation intensities (low, medium, and high) for both the shellac and sealant degradations

caused higher optical distortion when compared to the other degradations, which could lead to lower maximum object detection ranges or no detection at all for some of the trials.

However, for the remaining degradations during these trials, this does not mean the interpreted position from the camera was not affected by the degradations. An evaluation was done in the following section covering the error analysis relative to the DGPS ground truth.

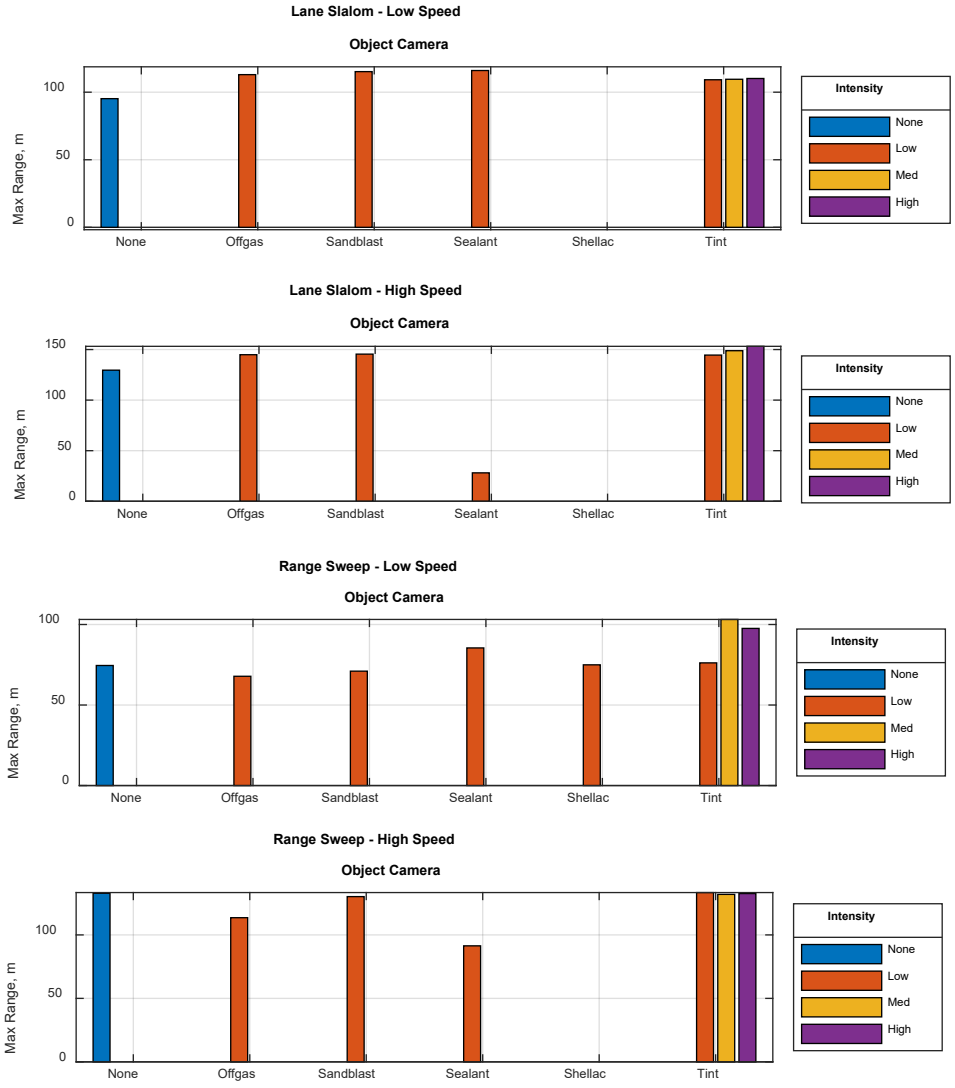

Figure 63. Object camera detection maximum range for all four scenarios and degradation types and intensities

Error Analysis Relative to Ground Truth

Once all the data is at the object level, comparisons can be made to the ground truth from the DGPS to calculate the error of the sensors. This section will highlight some examples of the observed types of error response. Data from all the sensors and degradations is shown in Appendix I.

Figure 64 through Figure 67 have the same format. The x-axis shows the degradations applied, or the lack thereof (i.e., none case). The y-axis shows the mean error of the position in meters and 1 standard deviation (STD) displayed by the whiskers. Whiskers are the vertical bars originating from the mean value. The legend shows the intensity of the degradation applied, such as none, low, medium, and high. An empty plot, such as the lack of medium and intensity bars in the figures, indicates that no output was reported by the sensor. In other words, the degradation applied during the dynamic vehicle maneuver prevented the object camera radar from providing position.

In specific, the x-axis in Figure 64 shows the degradations applied such as none, sandblast, offgas, sealant, shellac, and tint. The baseline is when no degradation is applied (i.e., none in the x-axis), and no intensity is applied (i.e., none in intensity legend). The baseline is used to compare the effects degradations have on sensor performance. The baseline in Figure 64 shows that the budget lidar reports an average of around 3 meters error in TV position when the SV performs a high-speed lane slalom maneuver. Similarly, Figure 65 shows that the SR 77GHz radar reports an average of around 0.8 meters error, Figure 66 shows that the SR 24 GHz radar reports an average of around 1.7 meters error, and Figure 67 shows that the object camera reports an average of around 3 meters error. All these sensors (i.e., budget lidar, SR 77GHz, SR 24GHz, and object camera) are being tested under a high-speed slalom maneuver to test maneuvers not within the scope of the sensor's operational range.

The error in Figure 64 through Figure 67 is calculated by interpolating all sensor data to DGPS time intervals and taking the difference between the position data returned by the sensor and the ground truth. The difference between two points is computed as the Euclidean distance between them. The difference between the x and y positions is the error. The calculated time history error data is then reduced to the mean and STD of error across the run.

There is a wide variety of mean error responses to the degradations in the data collected. Some degraded responses are no different than the baseline (e.g., Budget lidar with low intensity tint in Figure 64) while some degraded responses vary based on the type of sensor (e.g., SR 77GHz versus SR 24GHz radar with blacktop degradation in Figure 65 and Figure 66, respectively). Some conditions such as the SR 77GHz with the epoxy (Figure 65) and camera with tint (Figure 67) show a nonlinear response between low, medium, and high intensities, though the mean error for all three intensities of degradation could fall within one standard deviation of each other. Another observed response is the reduction in mean error with higher intensity degradations as seen for the SR 24GHz radar with Bondo degradation (Figure 66).

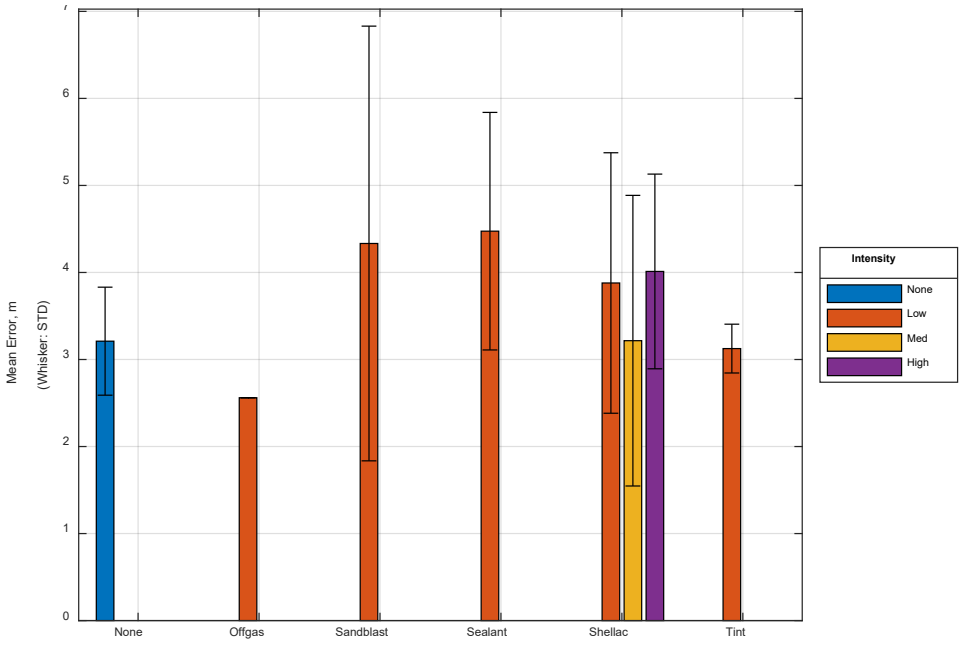

Figure 64. Mean error and STD for high-speed lane slalom (Budget lidar)

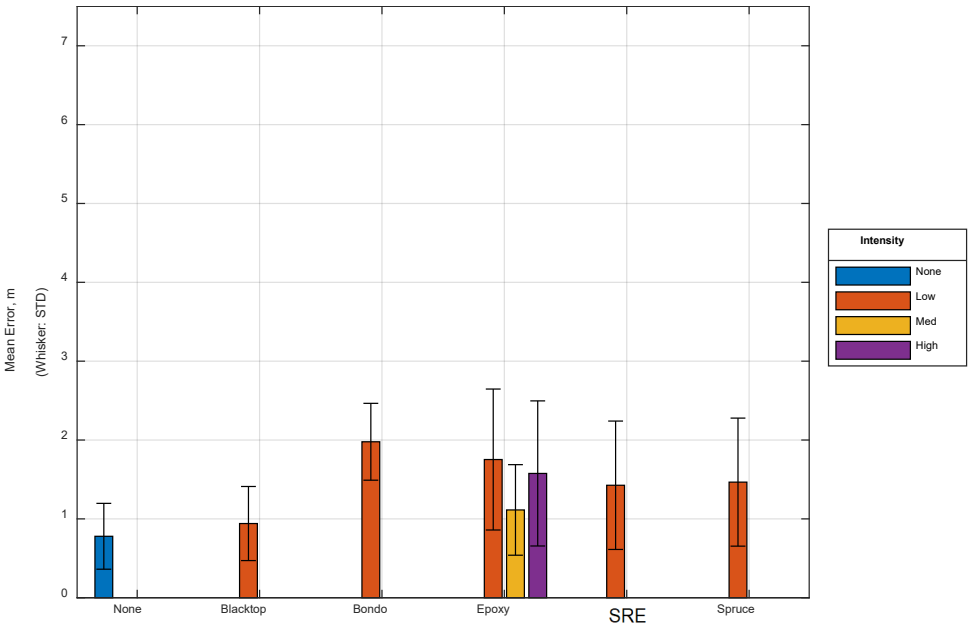

Figure 65. Mean error and STD for high-speed lane slalom (SR 77GHz radar)

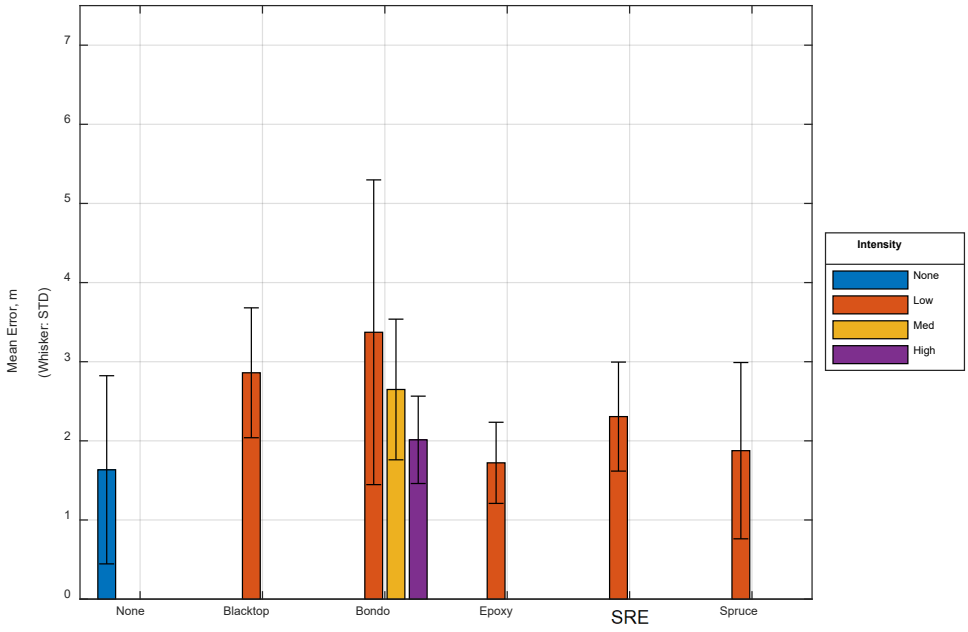

Figure 66. Mean error and STD for high-speed lane slalom (SR 24GHz radar)

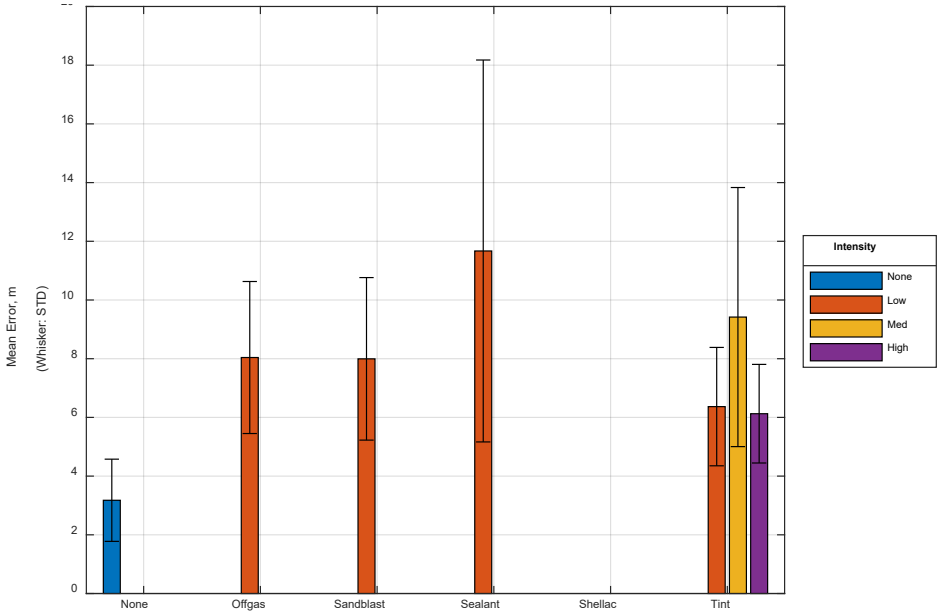

Figure 67. Mean error and STD for low-speed lane slalom (object camera)

Discussion of Degradation Impacts on Component Tests

The component level testing of the sensors illustrated the degradation impact on the sensing of the TV location in front of the SV during dynamic scenarios (e.g., lane-slaloms at high and low speeds). The results are not that different compared to the results obtained during degradation development where everything was stationary, including the target. For the sensors that have objects as output (i.e., object camera, object radars from Table 21), built-in perception algorithms can be taken at face value. However, there are two factors to consider for the analysis.

First, the sensors were operating in a relatively uncluttered environment (few objects) with only one TV. The clean environment was intentional to minimize the noise in the sensor return and simplify the object identification algorithms to isolate the sensor effects and to further limit the scope of the project to a manageable size.

The second factor is more important and applies to those sensors that do not have built-in perception algorithms (i.e., sensors that do not output object information such as lidar and some radars [Table 21] that output point cloud data). The analysis of the data uses the position of the TV from the mounted DGPS antenna. The TV DGPS position served as a method to infer that the point cloud data within the bounding box belonged to the TV. In other words, the presented analysis of the point cloud data is limited to the use of a DGPS mounted on the target, or any other technology able to provide ground truth position of the target. Knowing the a priori location of the TV to 10 cm RMS from the ground truth measurements for the initial condition for the perception algorithm used in the component testing could have masked the impacts on the sensor outputs by greatly reducing the difficulty of selection of data points corresponding to the TV. The DGPS data is not available for perception algorithms in typical automated systems. Therefore, the perception algorithm used here could lead to higher performance than those relying only on their own data to detect objects. Given the degradation impact, as shown by dynamic and static tests, on perception across the inputs, it would be hard to compare these sensor methods with this dataset. Furthermore, this difference in perception method performance is beyond the original scope of this project.

Finally, there was more of an impact from the degradations on the RCS signal intensity of the radars than the positional error. This could indicate that the degradations on average do not change the position of the reflections coming to the sensors or change the doppler frequency shift. However, it does indicate a change in signal strength and a potential delay in object detection.

This page is intentionally left blank.

Chapter 6. System Testing

Building from the previous component testing work, system testing incorporated the identified degradations (Table 22 and Table 23) onto production vehicles with longitudinal and lateral ADAS features equipped. The goal of these tests was to determine the effect of perception systems downstream of the raw sensor data inputs when degradations were applied. To do so, we conducted crash avoidance and driver assistance tests for FCW, AEB, ACC, LKA, and LDW for degraded and non-degraded tests. The limited availability of vehicles with LCA prevented testing LCA within this study. Longitudinal functions (i.e., FCW, AEB and ACC) mainly rely on radar due to their native ability to measure range to targets. On the other hand, lateral functions (i.e., LKA and LDW) mainly rely on camera due to their ability to detect lane markers on the road. Therefore, degradations were applied to radar for longitudinal tests, and camera for lateral tests.

Methodology

Sensors Under Test

Two main perception sensors are targeted by these system level tests: camera and radar. These sensors can provide functionality for longitudinal and lateral ADAS. Lack of widely available production vehicles with lidar perception excludes lidar sensors from these tests.

Longitudinal

FCW, AEB, and ACC were identified as possible longitudinal ADAS functions to test. All three functions monitor time-to-collision between the SV and other vehicles on the roadway. It was found during testing that the SVs used sensor fusion to execute FCW, ACC, and AEB. Sensor fusion specifically for the vehicles tested meant that camera and radar were both used.

Lateral

LDW and LKA were the lateral ADAS system-level functions tested under degradations. Both LDW and LKA use the windshield-mounted camera to monitor lane line position, to either issue visible or audio warnings to the driver, and/or physically steer the vehicle back into the lane when an imminent lane departure is detected.

Equipment

System testing involved four main equipment components: an SV with adequate longitudinal and lateral ADAS features, the DAS, a “soft target” vehicle used to perform and repeat FCW and AEB tests safely, and a moving TV used for the ACC tests.

SV

The study targeted acquisition of vehicles with the most ADAS functions from the following list: FCW, AEB, ACC, LDW, LKA and LCA. As mentioned earlier, the limited availability of vehicles with LCA prevented testing LCA in this study. The vehicles tested came with camera and radar. No radar-only vehicles were tested. Three different vehicles had both the forward-facing radar sensor and a windshield-mounted camera needed to test the acquired ADAS features (FCW, AEB, ACC, LDW, and LKA). The three vehicles acquired for testing came with multiple settings for FCW and ACC, and settings that allowed the maximum distance and the earliest

warnings were selected. The three vehicles were capable of issuing an FCW to the driver on the instrument cluster and engaging the AEB at speeds greater than 20 mph. For lane line detection, LKA and LDW were features available on the vehicles at speeds higher than 30 mph. Left and right lane line detection information as well as LDW were conveyed to the driver through the instrument cluster when engaged. Vehicles with these minimum ADAS activation speeds were selected based on the advice of the VTTI safety committee.

DAS

The DAS previously described in Chapter 4, Methodology, was used to collect video data for video reduction for the ADAS features under test. Figure 68 shows two cameras mounted to capture the dashboard and the roadway simultaneously.

Figure 68. Camera placement for the instrument cluster

GVT

To perform consecutive FCW and AEB tests safely without damaging the SV, a GVT from DRI Advanced Test Systems (Figure 69) was used. The GVT replicated the look (i.e., the camera sensor signature) and radar signature of a small passenger vehicle. If struck, the GVT would not damage the SV and could be reconstructed quickly.

Figure 69. Deployed GVT for FCW and AEB testing

TV

The same TV described in Chapter 4 and used for the Component Testing was used for the ACC tests.

Testing Setup

Longitudinal ADAS Tests

The FCW, AEB, and ACC tests were conducted based on Appendix J, Longitudinal Test Procedures. The FCW and AEB tests were modified from U.S. NCAP to be performed at 25 mph with the stationary GVT, and the ACC test procedures were conducted using the lowest speed settings available for each vehicle above 25 mph. AEB testing standards with lead vehicle stopped scenarios include SV speeds up to 50 mph (80 FR 68604, 2015), but the tests were run at lower speeds based on the recommendations from the VTTI safety committee, which recommended running the test at the minimal possible speed the feature activated. Additionally, the ACC tests were only conducted on non-curved roadway segments. The identified degradations (Table 22 and Table 23) during component testing were applied on production vehicles. Degradation tests were completed by securing the radar degradations levels in front of the forward-facing radar (left side, Figure 70).

Lateral ADAS Tests

The LKA and LDW tests were conducted based on Appendix J, Lateral Test Procedures, though modified to be performed at 35 mph. A straight section of the VTTI highway test track with even lighting conditions was selected for the testing. During this section of road, the left lane was always a discontinuous (dashed) yellow, while the right lane was always continuous (solid) white. Degradation tests were completed by securing the optical degradation levels in front of the windshield mounted camera (right side, Figure 70).

Figure 70. Radar and optical degradation placement

Results

Longitudinal ADAS Features

Stationary TV tests were conducted to determine the effect of degradations on the FCW and AEB systems. The vehicles under test had a forward mounted radar and camera that could be used to issue pre-collision warnings, and ultimately, AEB crash prevention if necessary. Because the native function of a radar is to measure ranges, all degradation data collection trials for the FCW and AEB features were conducted with the camera unobstructed and the radar degraded.

Several degradations on the radar prevented the FCW and AEB systems from engaging during the stationary soft TV tests and contrasted with the non-degraded performance for Vehicle 1 (Table 24). These include the SRE degradations, the medium and high-level Blacktop degradations, the high level Bondo/mesh degradations, and the high-level Spruce degradation. The SRE (high) degradation trial was not run for Vehicle 1, as the previous two lower levels of the degradation caused the two FCW and AEB ADAS features to not engage. Based on previous component testing, only the Bondo mesh degradation saw an increased number of average returns when comparing lower-level degradations to higher levels. Therefore, for the SRE degradation, it was assumed the high level would produce a similar result. FCW and AEB were not affected by any of the three levels of epoxy degradations for Vehicle 1, and no degradations had an effect on either Vehicle 2 or Vehicle 3 for the FCW and AEB tests. Additionally, no degradation had a difference in performance between the FCW and AEB systems, indicating that the degradation's effects were binary for these systems. Either the ADAS feature detected the stopped vehicle to issue an FCW and apply emergency braking, or it was completely unable to detect the vehicle and issue FCW alerts or intervene with AEB due to the degradation.

During the tests with the stationary TV, Vehicle 2 did not give any FCW or AEB errors during the degradation trials. Vehicle 1 and Vehicle 3 did issue system errors during these tests. More details are provided in the ADAS Sensor Self-Diagnostics discussion.

Table 24. Stationary Vehicle Longitudinal ADAS Testing Results for FCW and AEB

Radar Degradation	Vehicle 1		Vehicle 2		Vehicle 3	
	FCW	**AEB**	**FCW**	**AEB**	**FCW**	**AEB**
None	Yes	Yes	Yes	Yes	Yes	Yes
Epoxy (low)	Yes	Yes	Yes	Yes	Yes	Yes
Epoxy (med)	Yes	Yes	Yes	Yes	Yes	Yes
Epoxy (high)	Yes	Yes	Yes	Yes	Yes	Yes
Blacktop (low)	Yes	Yes	Yes	Yes	Yes	Yes
Blacktop (med)	No	No	Yes	Yes	Yes	Yes
Blacktop (high)	No	No	Yes	Yes	Yes	Yes
Steel Reinforced Epoxy (low)	No	No	Yes	Yes	Yes	Yes
Steel Reinforced Epoxy (med)	No	No	Yes	Yes	Yes	Yes
Steel Reinforced Epoxy (high)	N/A*	N/A*	Yes	Yes	Yes	Yes
Bondo Mesh (low)	Yes	Yes	Yes	Yes	Yes	Yes
Bondo Mesh (med)	Yes	Yes	Yes	Yes	Yes	Yes
Bondo Mesh (high)	No	No	Yes	Yes	Yes	Yes
Spruce (low)	Yes	Yes	Yes	Yes	Yes	Yes
Spruce (med)	Yes	Yes	Yes	Yes	Yes	Yes
Spruce (high)	No	No	Yes	Yes	Yes	Yes

Note: *Yes* indicates system functioned as intended; *No* means the system failed to function at all.
* The Steel Reinforced Epoxy (high) degradation trial was not run for Vehicle 1, as the previous two lower levels of the degradation caused the two FCW and AEB ADAS features to not engage.

The researchers also tested the ACC features of each vehicle by applying the degradations to the forward-facing radar and leaving the camera sensor uncovered. Because the native function of a radar is to measure ranges, they are used in ACC features to measure distance to targets. However, none of the degradation trials for any of the three vehicles caused the ACC system to not engage. Vehicles were able to maintain adequate headway during the tests.

Lateral ADAS Features

The researchers installed cameras in the test Vehicles 1 and 3 to identify when the lateral ADAS features (LKA and LDW) activated and where the vehicle was relative to the lane line. The test driver executed the test described in Appendix J, performing one trial per degradation type and level of severity. Each run was performed on the non-curved section of the highway test track at VTTI that has a solid white lane line on the right of the vehicle to mark the edge of the SV's lane, and a discontinuous (dashed) yellow lane line always on the left of the SV's lane (Figure

71). To assess system performance, the forward FOV video was analyzed and compared with the dashboard displayed by the vehicle as described below. The forward FOV video can see the dashboard displayed by the vehicle (i.e., yellow circles in Figure 71 and Figure 72), and it can also see the lane markers on the road. Comparing the lane markers on the road with what the dashboard displayed by the vehicle allows assessment of the number of errors made by the vehicle with and without degradations applied.

Video Reduction

Video reduction began by first watching the forward FOV video to assess the quality, determine if the road and/or instrument cluster was visible within the forward FOV video, and record the length of the forward FOV video. Then the video was watched a second time to mark the times and length of time whenever the state of the vehicle changed. The following list denotes the abbreviations of the possible system states:

- NaN – no lane marker detected
- LD – left lane marker detected
- LW – left lane marker warning
- RD – right lane marker detected
- RW – right lane marker warning

The forward FOV video was then watched a third time to mark the times and length of time whenever the vehicle changed states. To simplify the process, the vehicle states were denoted by the same abbreviations as above (i.e., the vehicle state is what the vehicle should have shown).

For each lane marker (left and right), another column denoted how incorrect the vehicle was.

- A value of 0 meant that the vehicle was correct (zero errors). In other words, the vehicle detected markers and issued warnings correctly.
    1. Ex: The vehicle correctly detected a lane marker (e.g., left and right lanes in Figure 71, both detected by the vehicle as shown inside the yellow circle).
    2. Ex: The vehicle correctly warned the driver when the vehicle traveled over that lane marker (e.g., right marker colored red inside yellow circle in Figure 71).
- A value of 1 meant that the vehicle had one error. In other words, the vehicle detected markers but did not issue warnings correctly.
    1. Ex: The vehicle only detected a left lane marker and did not issue a left LDW when it traveled over the lane marker.
- A value of 2 meant that the vehicle had two errors. In other words, the vehicle did not detect markers and did not issue warnings correctly.
    1. Ex: The vehicle did not detect the left lane marker (see how lane markers were not bolded or colored within the yellow circle in Figure 72) and did not issue a left LDW when it traveled over the lane marker

After all the timestamps were recorded, the data for each event was compiled for comparison and later data visualization. For each lane marker, the time and percentage of the event were summed for when the vehicle was correct (two scenarios), incorrect by one error (two scenarios), and incorrect by two errors (one scenario). Additionally, some of those scenarios were combined to

show the time and percentage in which the vehicle was totally correct per lane line and when the vehicle did not detect any lane lines *for each event*.

Figure 71. An example of the system correctly detecting the left lane line (see bold left lane line in yellow circle) and issuing a right LDW (see red lane line)

Figure 72. Example of the system not detecting any lane lines and did not issue a left LDW (two errors) and did not detect the right lane line (one error)

Reduction Analysis

To determine how the sensor degradation affects the LKA and LDW accuracy of the systems onboard the vehicles tested, the study first looked at the percentage of time that each event (degradation state) was correct and incorrect during the trial in which it was applied to the camera sensor. The identified optical degradations (Table 22) during component testing were applied on production vehicles. Low, medium, and high intensities (bolded in Table 22) were applied. In summary, the degradation types analyzed are:

- Tint,
- Sealant,
- Shellac,
- Offgas, and
- Sandblasted (limited data available based on poor camera quality, so this degradation was not included for Vehicle 1)

For this report, one test run was performed for the non-degraded case and one test run for each of the degradations. Vehicle availability determined the number of tests conducted. LKA and LDW were tested on Vehicles 1 and 3, for a total of 21 runs, with no data collected from Vehicle 2. For Vehicle 1, the study excluded more severe levels of degradations from the LKA and LDW testing if a lower level of that same degradation prevented the vehicle from detecting any lane markers during a test. The availability of Vehicle 3 permitted more testing as compared to Vehicle 1, and for Vehicle 3, all levels of degradations were run no matter the lower level's performance. As seen in Figure 73 for Vehicle 1, the degradation type significantly affected how the system detected the lanes. In general, the system detected the right lane line with higher accuracy than the left lane line for all degradation types, including the baseline trials. The same pattern was seen in Vehicle 3 (Figure 74), but with considerably less severity than Vehicle 1. The discrepancy between left and right lane line detection could be attributed to the difference in lane lines (i.e., dashed [left in Figure 71] versus continuous [right in Figure 71] lane markers). The right lane, always solid white, could provide better contrast between the lane and the pavement than the dashed yellow could. Increased contrast and the fact that the right lane line is always continuous could lead to easier detection by the lane line identification system on the vehicle in these cases. The condition of the left lane marker is also a factor that played a role when the vehicle attempted its detection as demonstrated by the baseline test as described next.

The percentage of times Vehicle 1 did not detect the left lane marker when no degradations were applied (a.k.a. baseline) is shown by the none-none case in the x-axis in Figure 73, which was approximately 60 percent of the time. This indicates that the condition of the left lane marker played a role when the vehicle attempted its detection. For Vehicle 1, the tint, sealant, and shellac degradations greatly affected the detection ability of the vehicle for both lane markers, while the offgas degradation mostly only affected detection of the left lane marker. Similar data reduction was done for Vehicle 3 (Figure 74) and showed that the high-sandblasted and low- and medium-shellac degradations negatively affected the lane line marker detection the most. All levels of the shellac degradation (low, medium, and high) caused decreased vehicle accuracy (including the cases of no lane detection and no lane detection nor warning) when detecting both the left and right lane line markers, while only the medium and high levels of the sandblasted degradations saw performance decreases for both lane line markers. Additionally, the low-level

sealant degradation and the high-level offgas degradation did negatively affect system performance as well. All other degradations for Vehicle 3 did not cause problems as significant for the lane marker identification vehicle's system.

Interesting to note for Vehicle 3, the medium level sealant degradation caused minimal vehicle error (as shown by the green bars in Figure 74), while the low and high level did cause vehicle errors such as no lane detection and no lane detection nor warning issued; the high level shellac degradation caused fewer vehicle errors than the low or medium levels. The other degradation types did not exhibit this trend for Vehicle 3. One explanation for the variance in performance for the shellac degradations is formation of small air bubbles in the material. The shellac degradation levels were classified by the number of application levels, though we noticed that the high-level shellac degradation exhibited less air bubble formation than the medium or low-level shellac degradations. More air bubbles may have resulted in more light distortion and less accuracy for those levels. Another factor to note is that, for Vehicle 1, we excluded more severe levels of degradations from the LKA and LDW testing if a lower level of that same degradation prevented the system from detecting any lane lines during a test. Also, the availability of Vehicle 3 permitted more testing as compared to Vehicle 1. For Vehicle 3, all levels of degradations were run no matter the lower level's performance. Based on doing this, it was observed that some non-linear responses in higher level degradations may have been lost for Vehicle 1, though the results from Vehicle 3 suggest that, outside of the sealant and shellac degradations, higher level degradations do not perform any better than its associated lower levels at the system level.

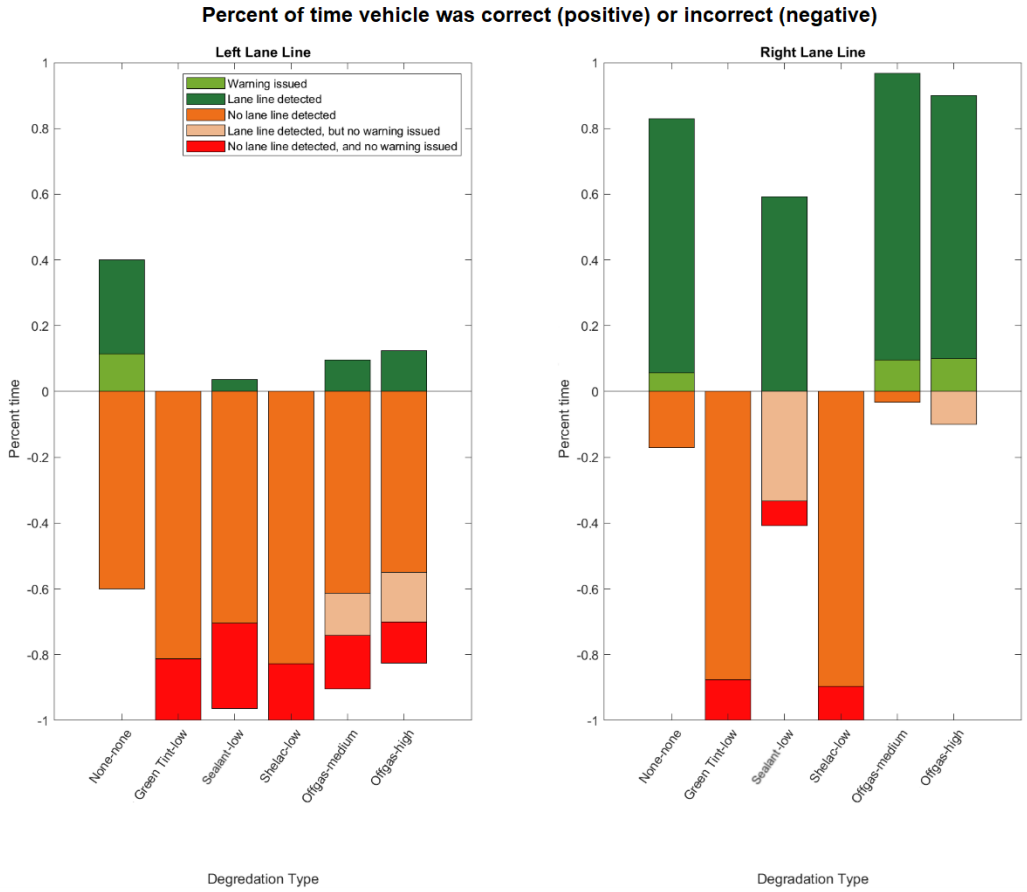

Figure 73. Percent of time for each degradation for Vehicle 1 that the system was correct (positive) and incorrect (negative)

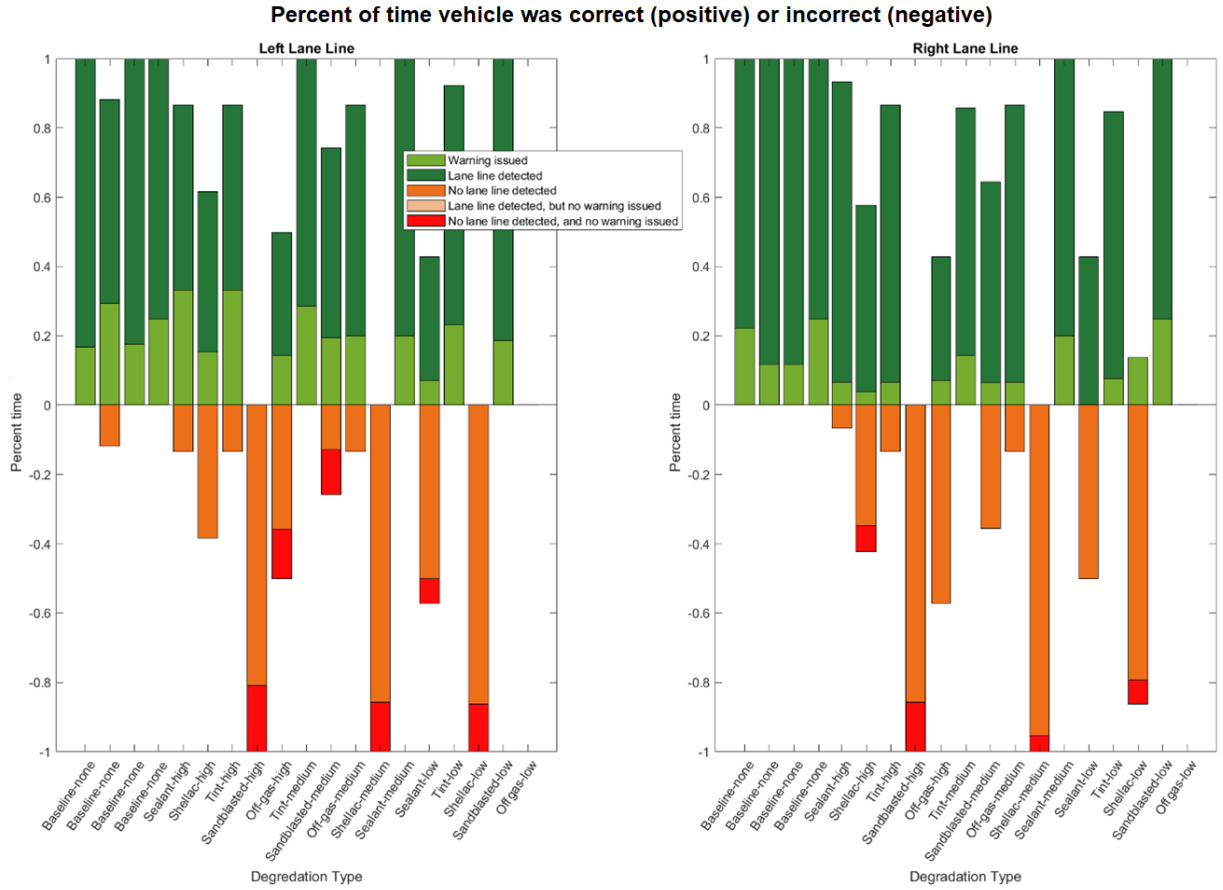

Figure 74. Percent of time for each degradation for Vehicle 3 that the system was correct (positive) and incorrect (negative)

ADAS Sensor Self-Diagnostics

The previous results from the longitudinal ADAS feature tests with degradations applied (Table 24) showed that the three levels of SRE degradations affected FCW and AEB for Vehicle 1. To assess whether Vehicle 1 had self-diagnostics, the highest degradation level of SRE was applied to one of the radar sensors and the test for FCW/AEB was re-run.

After re-running approximately three tests (approximately 15 minutes in duration), the vehicle reported an error at the system level as shown in Figure 75. Because of the degraded radar, Vehicle 1 reported radar functions unavailable, such as cruise control and ACC. At the top of the circle on the dashboard, a triangular LED-warning turned on, which (according to the vehicle owner's manual) indicates to bring the vehicle in for service. In addition, at the bottom left (behind the needle), the LED was ON, indicating that FCW/AEB was OFF. Therefore, there are sensor self-diagnostics running in this particular production vehicle with FCW, AEB, and ACC. To bring the vehicle back to full ADAS functionality, degradations were removed, and the vehicle was turned off and on. This allowed the ADAS system to reset and the previously not available functions (i.e., FCW, AEB, and ACC) returned to normal. Like Vehicle 1, Vehicle 3 (Figure 76) also issued system warnings. This time, however, they were issued during the longitudinal system tests. Vehicle 2 never issued a system warning during testing.

Figure 75. ADAS sensor self-diagnostics reporting a system error for Vehicle 1

Figure 76. ADAS sensor self-diagnostics of Vehicle 3

Discussion

The degradations used in the ADAS testing were the same ones used in the component level testing. For the FCW and AEB features in Vehicle 1, those degradations had a bigger impact on ADAS performance than the position data collected during component testing would suggest. However, for Vehicles 2 and 3, the degradation effects seen in component testing were not pronounced enough for system level malfunctions to occur for the FCW and AEB features. Differences between the performance of Vehicle 1 and Vehicles 2 and 3 could come from how each radar identifies objects from the raw data. The component testing showed larger variability and mean changes in the RCS of road targets than that of position. If, for example, Vehicle 1 used a radar perception system that relied on accurate readings of RCS, its performance could suffer when compared to another perception system that did not rely on RCS as much.

No radar degradations caused the ACC system to not engage on any of the vehicles. Sensor fusion between the camera and radar and the fact that perception systems usually have longer periods of time to detect and track vehicles during an ACC scenario are the most likely reasons each vehicle was unaffected by the radar degradations. More testing that isolates the individual camera and radar inputs during ACC scenarios would be needed to determine the effect of degradations for this ADAS feature, especially for those vehicles that use sensor fusion to perform ACC.

Lane line detection was affected by camera degradations on the vehicles tested, particularly the green tint, shellac, and sandblasted degradations. The green tint may disrupt the lane line detection process the ADAS feature uses, such as contrast identification, causing malfunction and inability to detect lane lines even at low level degradations. The other two degradations, shellac and sandblasted, can obscure or refract light reaching the camera sensor, making lane line detection challenging. Additionally, the lane line type can play a significant part in the system's ability to detect lane lines. In these trials, the yellow, discontinuous lane line on the left was detected less often by the two vehicles than the solid white lane line on the right.

This page is intentionally left blank.

Chapter 7. Conclusions

The research focused on three primary types of sensors that represent those technologies most prevalent for more dynamic driving conditions (camera and radar) or that are emerging (lidar). Within these sensor types, the study selected different sensor models that had varying price points, technology, or, in the case of radar, operated at different frequencies. Testing during the degradation development employed static tests that used a variety of targets to allow for repeatable evaluation of the multitude of combinations of base materials and degradations to be used throughout the project. The results of this effort identified the degradations that most affected sensor performance and narrowed the degradation samples to carry forward into component testing.

Based on the results from the degradation development, three levels (high, medium, and low) of each degradation of interest were developed. While all the degradations alter the signal between the sensor and the object of interest, the way the degradations affect the sensor signal can vary. Degradations that occluded the signal path (e.g., sandblasting, which simulates heavy pitting and scratching) reduced the response of the sensor (i.e., camera and lidar). In addition, degradations such as pitting and scratching in front of a light-based sensor scattered or deflected the light, which can result in a weak or distorted signal. This may reduce the strength of the signal, but in some cases, it may also reduce the number of spurious signals, effectively increasing the SNR. An occlusion of the signal, regardless of the sensor, blocks a portion of the signal and therefore reduces the information returned regarding an object of interest.

For optical sensors, degradations that create a lensing affect (e.g., sealant), had a greater impact on sensor performance than expected. Degradation due to road grime accumulation behind a bumper or improper repair for a radar, simulated using Bondo, resulted in a significant reduction in sensor range and number of returned points. Since these types of degradations tend to be hidden from sight, any impact to performance may be unexpected. It should be noted that the impact these had on performance varied across the different radars tested which included ones with different operating frequencies and different levels of on board processing. This highlights the challenge associated with quantifying generalized sensor performance in different conditions.

When these sensors are integrated into a vehicle's ADAS, the effect of degradations becomes more varied. Some of the degradations that had a relatively low impact on the sensor output caused the ADAS to perform poorly or not at all. The SRE and blacktop had a significant impact on the operation of the ADAS for one of the vehicles. The different response of the vehicles with the same degradation could be due to sensors used, the processing of the signals, or the way that the manufacturer has designed the system to operate in degraded conditions. During the stakeholder interviews, manufacturers confirmed that sensor health is monitored, however the way the vehicle responds to this information varies between manufacturers, vehicles, and system configuration. The research identified long-term degradations that may be important to consider for system level performance.

The results of this research provide a foundation for understanding sensor degradation. The project successfully developed and demonstrated methods for identifying and creating surrogate degradation treatments. These were used in a structured approach to assess the impact the degradations have on a variety of sensors and sensor types during on-vehicle testing. This knowledge was then used to select degradations of interest to demonstrate how the approach could be used to assess system level performance of an ADAS equipped vehicle.

This page is intentionally left blank.

Bibliography

Abou-Jaoude, R. (2003). ACC radar sensor technology, test requirements, and test solutions. *IEEE Transactions on Intelligent Transportation Systems, 4*(3), 115-122. doi:10.1109/TITS.2003.821286

American Automobile Association. (2018). Advanced driver assistance systems (ADAS) repair costs*, AAA NewsRoom*.

Asano, Y., Ohshima, S., Harada, T., Ogawa, M., & Nishikawa, K. (2001, May 19-26). Proposal of millimeter-wave holographic radar with antenna switching. *2001 IEEE MTT-S International Microwave Symposium, Phoenix, AZ.*

ASTM International. (2015). *E2938-15 standard test method for evaluating the relative-range measurement performance of 3D imaging systems in the medium range*.

ASTM International. (2017a). *E2566-17a standard test method for evaluating response robot sensing: Visual acuity.*

ASTM International. (2017b). *E3125-17 standard test method for evaluating the point-to-point distance measurement performance of spherical coordinate 3D imaging systems in the medium range*.

Basantis, A., Doerzaph, Z., Harwood, L., & Neurauter, L. (2019). Developing a standardized performance evaluation of vehicles with automated driving features. *SAE International Journal of Connected and Automated Vehicles*, *2*(12-02-03-0011).

Belohoubek, E. (1982). Radar control for automotive collision mitigation and headway spacing. *IEEE Transactions on Vehicular Technology*, *31*(2), 89–99. https://doi.org/10.1109/t-vt.1982.23918

Bergmiller, P., Maurer, M., & Lichte, B. (2011, September 28-30). Probabilistic fault detection and handling algorithm for testing stability control systems with a drive-by-wire vehicle. 2011 IEEE International Symposium on Intelligent Control, Denver, CO. https://doi.org/10.1109/isic.2011.6045395

Bertozzi, M., Bombini, L., Broggi, A., Buzzoni, M., Cardarelli, E., Cattani, S., Cerri, P., Coati, A., Debattisti, S., Falzoni, A., Fedriga, R. I., Felisa, M., Gatti, L., Giacomazzo, A., Grisleri, P., Laghi, M. C., Mazzei, L., Medici, P., Panciroli, M., Versari, P. (2011, June 5-9). VIAC: An out of ordinary experiment. 2011 IEEE Intelligent Vehicles Symposium, Baden-Baden, Germany. https://doi.org/10.1109/ivs.2011.5940531

Blackmore Sensors and Analytics, Inc. (2018, June 26-28). *Frequency modulated automotive lidar*. Autonomous Vehicle Sensors Conference, San Jose California.

Börner, M., & Isermann, R. (2003). Supervision, fault detection, and sensor fault tolerance of passenger cars. *IFAC Proceedings Volumes*, *36*(5), 319–326. https://doi.org/10.1016/s1474-6670(17)36511-4

Brus, E. (1987, September). *Vehicular radar: The ultimate aid for defensive driving*? Microwaves & RF, pp. 53–58.

Camiade, M., Domnesque, D., Alleaume, P., Mallet, A., Pons, D., & Dambkes, H. (1999, June 13-19). *Full MMIC millimeter-wave front end for a 76.5 GHz adaptive cruise control car radar.* 1999 IEEE MTT-S International Microwave Symposium, Anaheim, CA. https://doi.org/10.1109/mwsym.1999.780234

Carlin, J., Birdsong, C., Schuster, P., Thompson, W., & Kawano, D. (2005, November 15-17). *Evaluation of cost effective sensor combinations for a vehicle precrash detection system* (SAE Technical Paper 2005-01-3578). 2005 SAE Commercial Vehicle Engineering Conference, Detroit, MI. https://doi.org/10.4271/2005-01-3578

Catalá-Prat A., R., J., Reulke, R. (2006, September 25-27). *Self-calibration system for the orientation of a vehicle camera*. ISPRS Commission V Symposium: Image Engineering and Vision Metrology, Dresden, Germany, www.isprs.org/proceedings/xxxvi/part5/paper/cata_650.pdf

Crowe, S. (2019, April 25). *Researchers back Tesla's non-LIDAR approach to self-driving cars.* [Web page]. The Robot Report. www.therobotreport.com/researchers-back-teslas-non-lidar-approach-to-self-driving-cars/

Dickey, M. R. (2018, April 26). *BMW is working with LIDAR company Innoviz to make self-driving cars*. [Web page]. TechCrunch. https://techcrunch.com/2018/04/26/bmw-is-working-with-lidar-company-innoviz-to-make-self-driving-cars/?guccounter=1

Dixit, R., & Rafaelli, L. (1997, June 8-13). *Radar requirements and architecture trades for automotive applications.* 1997 IEEE MTT-S International Microwave Symposium, Denver, CO. https://doi.org/10.1109/mwsym.1997.596554

Elgharbawy, M., Schwarzhaupt, A., Scheike, G., Frey, M., & Gauterin, F., (2016, November 29 – December 2). *A generic architecture of ADAS sensor fault injection for virtual test*. IEEE/ACS 13th International Conference of Computer Systems and Applications, Agadir, Morocco. https://doi.org/10.1109/AICCSA.2016.7945680

Feilhauer, M., Haering, J., & Wyatt, S. (2016, October 4-6). *Current approaches in HiL-based ADAS testing* (SAE Report No. 2016-01-8013). SAE 2016 Commercial Vehicle Engineering Congress, Rosemont, IL. https://doi.org/10.4271/2016-01-8013

Ferreira, J. C., & Martins, A.L. (2018, November 21-23). *Intelligent transport systems, from research and development to the market uptake.* Second EAI International Conference, Guimarães, Portugal. https://link.springer.com/content/pdf/10.1007%2F978-3-030-14757-0.pdf

Fujimura, K., Hitotsuya, M., Yamano, S., & Higashida, H., (1999, November 8-12) *76 GHz automotive radar for ACC*. 6th World Congress on Intelligent Transport Systems, Toronto, Canada.

Galko, C., Rossi, R., & Savatier, X. (2014, July 14-17). Vehicle-hardware-in-the-loop system for ADAS prototyping and validation. *2014 International Conference on Embedded Computer Systems: Architectures, Modeling, and Simulation, New Delhi, India*. https://doi.org/10.1109/samos.2014.6893229

Gao, X., Xing, G., Roy, S., & Liu, H. (2019, November 3-6). *Experiments with mmWave automotive radar test-bed.* 2019 53rd Asilomar Conference on Signals, Systems, and Computers, Pacific Grove, CA. doi:10.48550/arXiv.1912.12566

Ghosh, D., Sharman, R., Rao, H. R., & Upadhyaya, S. (2007). Self-healing systems — Survey and synthesis. *Decision Support Systems*, *42*(4), 2164–2185. https://doi.org/10.1016/j.dss.2006.06.011

Gietelink, O., Ploeg, J., Schutter, B. D., & Verhaegen, M. (2004). VEHIL: A test facility for validation of fault management systems for Advanced Driver Assistance Systems. *IFAC Proceedings Volumes*, *37*(22), 397–402. https://doi.org/10.1016/s1474-6670(17)30376-2

Gong, R., Wang, Q., Shao, X, & Liu, J. (2016, January 12). A color calibration method between different digital cameras. *Optik*, *27*(6), 3281-3285. https://doi.org/10.1016/j.ijleo.2015.12.003

Goodin, C., Carruth, D., Doude, M., & Hudson, C. (2019). Predicting the influence of rain on LIDAR in ADAS. *Electronics*, *8*(1), 89. https://doi.org/10.3390/electronics8010089

Grimaldi, C. N., & Mariani, F. (2001, March 5-8). *OBD Engine fault detection using a neural approach* (SAE Technical Paper No. 2001-01-0559). SAE World Congress, Detroit, MI. https://doi.org/10.4271/2001-01-0559

Grove, K., Atwood, J., Blanco, M., Krum, A., & Hanowski, R. (2016, October 4-6). *Field study of heavy vehicle crash avoidance system performance*. SAE 2016 Commercial Vehicle Engineering Congress, Rosemont, IL. https://doi.org/10.4271/2016-01-8011

Grzechca, D., Ziębiński, A., & Rybka, P. (2017). Enhanced reliability of ADAS sensors based on the observation of the power supply current and neural network application. In N. Nguyen, G. Papadopoulos, P. Jędrzejowicz, B. Trawiński, & G. Vossen, eds., *Computational Collective Intelligence. ICCCI 2017. Lecture Notes in Computer Science*, 215–226. Springer. https://doi.org/10.1007/978-3-319-67077-5_21

Gustafsson, F., Ahlqvist, S., Forssell, U., & Persson, N. (2001, March 5-8). *Sensor fusion for accurate computation of yaw rate and absolute velocity* (SAE Technical Paper 2001-01-1064). SAE World Congress, Detroit, MI. https://doi.org/10.4271/2001-01-1064

Helmer, T., Kühbeck, T., Gruber, C., & Kates, R. (2012). Development of an integrated test bed and virtual laboratory for safety performance prediction in active safety systems. In Society of Automotive Engineers of China & International Federation of Automotive Engineering Societies, eds., *Proceedings of the FISITA 2012 World Automotive Congress*, 417–431. https://doi.org/10.1007/978-3-642-33805-2_34

Hernandez, C. A., & Adams, A. J. (2001). *Application of mathematical models to detect and diagnose reciprocating compressor valve leakage* (SAE Technical Paper No. 2001-01-1724). Vehicle Thermal Management Systems Conference & Exposition, Nashville, TN. https://doi.org/10.4271/2001-01-1724

Howard, D. (2018, February 5-8). *Enhanced driver safety with advanced vision systems*. 2018 Pan Pacific Microelectronics Symposium, Kohala Coast, HI. https://doi.org/10.23919/panpacific.2018.8318992

Isermann, R., Schwarz, R., & Stolzl, S. (2002). Fault-tolerant drive-by-wire systems. *IEEE Control Systems Magazine*, *22*(5), pp. 64-81, Oct. https://doi.org/10.1109/MCS.2002.1035218

Johansson, G., & Rumar, K. (1971). Drivers brake reaction times. *Human Factors: The Journal of the Human Factors and Ergonomics Society, 13*(1), 23–27. https://doi.org/10.1177/001872087101300104

Jones, R. C., & Ziegahan, K., (2002, December 2-4). *Technologies for static air bag suppression systems*. 6th International Symposium on Sophisticated Car Occupant Safety Systems, Karlsruhe, Germany.

Kim, Y. W. (1999). *A methodology for integration of control and fault diagnostics*. PhD Dissertation, Ohio State University.

Knoll, P. M., Schaefer, B.-J., Guettler, H., Bunse, M., & Kallenbach, R. (2004, March 7-11). *Predictive safety systems - Steps towards collision mitigation*. SAE Technical Paper. SAE 2004 World Congress & Exhibition, Detroit, MI. https://doi.org/10.4271/2004-01-1111

Levinson, J., Askeland, J., Becker, J., Dolson, J., Held, D., Kammel, S., Kolter, J. Z., Langer, D., Pink, O., Pratt, V., Sokolsky, M., Stanek, G., Stavens, D., Teichman, A., Werling, M., & Thrun, S. (2011, June 5-9). *Towards fully autonomous driving: Systems and algorithms*. 2011 IEEE Intelligent Vehicles Symposium, Baden-Baden, Germany. https://doi.org/10.1109/ivs.2011.5940562

Lindgren, A., & Chen, F. (2006, April 5-7). State of the art analysis: An overview of Advanced Driver Assistance Systems (ADAS) and possible human factors issues. Swedish Human Factors Network Conference, Linköping, Sweden.

Lindner, P., Richter, E., Wanielik, G., Takagi, K., & Isogai, A. (2009, October 4-7). *Multi-channel lidar processing for lane detection and estimation*. 2009 12th International IEEE Conference on Intelligent Transportation Systems, St. Louis, MO. https://doi.org/10.1109/itsc.2009.5309704

Liu, J., Sun, Q., Fan, Z. &Jia, Y. (2018, September 4-7). *TOF lidar development in autonomous vehicle* [sic] (Trans.). 2018 IEEE 3rd Optoelectronics Global Conference, Shenzhen, China. https://doi.org/10.1109/OGC.2018.8529992

Lyons, C., & Taskin, I. (2000, October 3-5). *A low-cost MMIC based radar sensor for frontal, side or rear automotive anticipatory precrash sensing applications*. IEEE Intelligent Vehicles Symposium, Dearborn, MI. https://doi.org/10.1109/ivs.2000.898428

Mahlisch, M., Schweiger, R., Ritter, W., & Dietmayer, K., (2006, June 13-15). *Sensorfusion using spatio-temporal aligned video and lidar for improved vehicle detection*. 2006 IEEE Intelligent Vehicles Symposium, Tokyo, Japan. https://doi.org/10.1109/IVS.2006.1689665

Matsumura T., Hirao, M., Sato, T., Saryo, T., Ohmuro, M., Mizutani, H., & Sida, N. (1999, November 8-12). *76 GHz FM-CW radar with electrically scanned seven beams for automotive applications*. 6th World Congress on Intelligent Transport Systems, Toronto, Canada. November 8-12.

Menzel, W., Pilz, D., & Leberer, R. (1999, June 13-19). *A 77 GHz FM/CW radar frontend with a low-profile, low-loss printed antenna*. 1999 IEEE MTT-S International Microwave Symposium, Anaheim, CA. https://doi.org/10.1109/mwsym.1999.780233

Nothdurft, T., Hecker, P., Frankiewicz, T., Gacnik, J., & Koster, F. (2011). *Reliable information aggregation and exchange for autonomous vehicles*. 2011 IEEE Vehicular Technology Conference (VTC Fall). https://doi.org/10.1109/vetecf.2011.6092937

Nothdurft, T., Hecker, P., Ohl, S., Saust, F., Maurer, M., Reschka, A., & Bohmer, J. R. (2011). *Stadtpilot: First fully autonomous test drives in urban traffic*. 14th International IEEE Conference on Intelligent Transportation Systems, Washington, D.C. https://doi.org/10.1109/itsc.2011.6082883

Ocular Robotics. (2015a). RobotEye RE08 3D LIDAR 3D Laser Scanning System. [Product Datasheet]. www.ocularrobotics.com/wp-content/uploads/2018/08/RobotEye-RE08-3D-LIDAR-Datasheet.pdf

Ocular Robotics. (2015b). RobotEye REHS25 Hyperspectral Ultrafast Broadband Spectral Scanner. [Product Datasheet]. www.ocularrobotics.com/wp-content/uploads/2015/12/RobotEye-REHS25-Hyperspectral-Datasheet.pdf

Ocular Robotics. (2015c). RobotEye REN25 NAKED Two-Axis Optical Pointing System. [Product Datasheet]. www.ocularrobotics.com/wp-content/uploads/2015/12/RobotEye-REN25-NAKED-Datasheet.pdf

Ohl, S., & Maurer, M. (2011, October 5-7). *A contour classifying Kalman filter based on evidence theory*. 14th International IEEE Conference on Intelligent Transportation Systems, Washington, D.C. https://doi.org/10.1109/itsc.2011.6082816

Olbrich, H., Beez, T., Lucas, B., Mayer, H., & Winter, K. (1998, February 23-26). *A small, light radar sensor and control unit for adaptive cruise control* (SAE Technical Paper 980607). SAE International Congress & Exposition, Detroit, Michigan. https://doi.org/10.4271/980607

Panasonic. (2020). Ultrasonic Sensors. [Web page]. https://eu.automotive.panasonic.com/solutions/components/sensors

Prabhu, S. M. (1999, April 14-15). *An overview of neural network and fuzzy logic applications to earthmoving machine systems control* (SAE Technical Paper 1999-01-1880). 1999 SAE Earthmoving Industry Conference & Exposition, Peoria, Illinois. https://doi.org/10.4271/1999-01-1880

Reschka, A., Böhmer, J. R., Nothdurft, T., Hecker, P., Lichte, B., & Maurer, M., (2012, June 15-29). *A surveillance and safety system based on performance criteria and functional degradation for an autonomous vehicle* (pp. 237-242). 15th International IEEE Conference on Intelligent Transportation Systems, Anchorage, AK. https://doi.org/10.1109/ITSC.2012.6338682

Reschka, A., Böhmer, J. R., Saust, F., Lichte, B., & Maurer, M. (2012, June 3-7). *Safe, dynamic and comfortable longitudinal control for an autonomous vehicle*. 2012 IEEE Intelligent Vehicles Symposium, Alcala de Henares, Spain. https://doi.org/10.1109/ivs.2012.6232159

Roy, R., & Kailath, T. (1989). ESPRIT-estimation of signal parameters via rotational invariance techniques. *IEEE Transactions on Acoustics, Speech, and Signal Processing, 37*(7), 984–995. https://doi.org/10.1109/29.32276

Russell, M., Crain, A., Curran, A., Campbell, R., Drubin, C., & Miccioli, W. (1997, June 8-13). *Millimeter wave radar sensor for automotive intelligent cruise control* (ICC). 1997 IEEE MTT-S International Microwave Symposium, Denver, CO. https://doi.org/10.1109/mwsym.1997.596555

Schmidt, R. (1986). Multiple emitter location and signal parameter estimation. *IEEE Transactions on Antennas and Propagation, 34*(3), 276–280. https://doi.org/10.1109/tap.1986.1143830

Sparks, D., Noll, T., Agrotis, D., Betzner, T., & Gschwend, K. (1999, February 28). *Multi-sensor modules with data bus communication capability* (SAE Technical Paper 1999-01-1277). 1999 SAE International Congress & Exposition, Detroit, MI. https://doi.org/10.4271/1999-01-1277

Spies, H. D. (2002, December 24). *What is achievable today and in the near future? - Overview on technologies: Radar, video, IR*. 6th International Symposium on Sophisticated Car Occupant Safety Systems, Karlsruhe, Germany.

Subaru. (2012, March 15). *Subaru debuts new EyeSight system*. [Web page press release]. PR Newswire. www.prnewswire.com/news-releases/subaru-debuts-new-eyesight-system-142811985.html

Teledyne FLIR. (2020). Thermal vision automotive development kit. [Product Datasheet]. https://flir.netx.net/file/asset/5648/original/attachment

Teledyne Vision Solutions. (2019). *How to evaluate camera sensitivity*. [Web page]. www.flir.com/discover/iis/machine-vision/how-to-evaluate-camera-sensitivity/

Vinci, G., Koelpin, A., & Weigel, R. (2009, December 7-10). *Employing six-port technology for phase-measurement-based calibration of automotive radar*. 2009 Asia Pacific Microwave Conference, New Delhi, India. https://doi.org/10.1109/apmc.2009.5385312

Vining, W., & Husman, E. (2008, October). *Standard testing protocols for high speed imagers* (Document 463-08). Secretariat, Range Commanders Council. www.trmc.osd.mil/wiki/download/attachments/113019939/463-08%20Standard%20Testing%20Protocols%20for%20Hi%20Speed%20Digital%20Imagers.pdf?version=1&modificationDate=1623181169489&api=v2

Wang, Y., Chao, W.-L., Garg, D., Hariharan, B., Campbell, M., & Weinberger, K. Q. (2019, June 15-19). *Pseudo-lidar from visual depth estimation: Bridging the gap in 3D object detection for autonomous driving*. 2019 IEEE/CVF Conference on Computer Vision and Pattern Recognition, Long Beach, CA. https://doi.org/10.1109/cvpr.2019.00864

Wenger, J. (1998, February 9). *Automotive mm-wave radar: status and trends in system design and technology*. IEE Colloquium on Automotive Radar and Navigation Techniques, London, UK. https://doi.org/10.1049/ic:19980188

Wille, J. M., Saust, F., & Maurer, M. (2010, June 21–24). *Stadtpilot: Driving autonomously on Braunschweigs inner ring road*. 2010 IEEE Intelligent Vehicles Symposium, La Jolla, CA. https://doi.org/10.1109/ivs.2010.5548034

Woll, J. (1995). *VORAD collision warning radar*. Proceedings International Radar Conference. https://doi.org/10.1109/radar.1995.522574

Zelubowski, S. A. (1994, July). Low cost antenna alternatives for automotive radars. *Microwave Journal, 37*(7), 54+. https://link-gale-com.ezproxy.lib.vt.edu/apps/doc/A15697703/AONE?u=viva_vpi&sid=AONE&xid=2de71d02

Ziebinski, A., Cupek, R., Grzechca, D., & Chruszczyk, L. (2017). *Review of advanced driver assistance systems (ADAS)*. AIP Conference Proceedings, 1906(1), 120002. https://doi.org/10.1063/1.5012394

Ziebinski, A., Cupek, R., Erdogan, H., & Waechter, S. (2016). *A survey of ADAS technologies for the future perspective of sensor fusion*. Computational Collective Intelligence Lecture Notes in Computer Science, 135–146. https://doi.org/10.1007/978-3-319-45246-3_13

This page is intentionally left blank.

References

80 FR 68604, New Car Assessment (NCAP), November 5, 2015. [Docket No. NHTSA–2015–0006]. [Final decision announcing NHTSA's decision to include AEB technologies as part of NCAP Recommended Advanced Technology Features, if the technologies meet NCAP performance criteria. The specific technologies included are crash imminent braking (CIB) and dynamic brake support (DBS). www.govinfo.gov/content/pkg/FR-2015-11-05/pdf/2015-28052.pdf

87 FR 13452, 2022-04894, 13452-13521 [{Docket No. NHTSA-2021-0002], March 9, 2022. [Request for comments on proposing to add four more ADAS technologies, blind spot detection, blind spot intervention, lane keeping support, and pedestrian automatic emergency braking.] www.regulations.gov/document/NHTSA-2021-0002-0001

AAA Automotive. (2018). *ADAS sensor calibration increases repair costs*. [Web page]. American Automobile Association. www.aaa.com/autorepair/articles/adas-sensor-calibration-increases-repair-costs

Abuelsamid, S. (2019, September 4). *Ford launches bugs at sensors because keeping them clean is crucial for self-driving cars*. Forbes. www.forbes.com/sites/samabuelsamid/2019/09/04/ford-launches-bugs-at-sensors-keeping-it-clean-will-be-crucial-for-automated-vehicles/

Adarsh, S., Kaleemuddin, S., Bose, D., & Ramachandran, K. (2016, July 14-16). *Performance comparison of infrared and ultrasonic sensors for obstacles of different materials in vehicle/robot navigation applications*. International Conference on Advances in Materials and Manufacturing Applications (IConAMMA-2016), Bangalore, India. Also published in *IOP Conference Series: Material Science Engineering, 149*. https://doi.org/10.1088/1757-899X/149/1/012141

Allied Market Research. (2020). Automotive camera market outlook -- 2025. [Web page]. www.alliedmarketresearch.com/automotive-camera-market

Arage Hassen, A. (2006). Indicators for the signal degradation and optimization of automotive radar sensors under adverse weather conditions (Trans.) [PhD thesis, Technischen Universitat Darmstadt]. https://tuprints.ulb.tu-darmstadt.de/epda/000765/

Badell, B. (2017, March 14). *Understanding how we repair your plastic bumper the quickest*. [Web page]. Badell's Collision. www.badellscollision.com/blog/quick-repair-plastic-bumper/

Becker, C., Yount, L., Rosen-Levy, S., & Brewer, J. (2018, August). *Functional safety assessment of an automated lane centering system* (Report No. DOT HS 812 573). National Highway Traffic Safety Administration. https://rosap.ntl.bts.gov/view/dot/37211

Birdsong, C., Schuster, P., Carlin, J., Kanawo, D., & Thompson, W. (2005, March). *Test methods and results for sensors in a pre-crash detection system* (Paper No. 06AE-19). SAE World Congress, Detroit, MI. https://digitalcommons.calpoly.edu/cgi/viewcontent.cgi?article=1025&context=meng_fac

Blanco, M., Atwood, J. Vasquez, H., Trimble, T.E., Fitchett, V., Radlbeck, J., Fitch, G. M., Russell, S. M., Green, C. A., Cullinane, B., & Morgan, J. F. (2015, August). *Human factors evaluation of level 2 and level 3 automated driving concepts* (Report No. DOT HS 812 182). National Highway Traffic Safety Administration. www.nhtsa.gov/sites/nhtsa.gov/files/812182_humanfactorseval-l2l3-automdrivingconcepts.pdf

Blanco, M., Chaka, M., Stowe, L., Gabler, H. C., Weinstein, K., Gibbons, R. B., Neurauter, L., McNeil, J., Fitzgerald, K. E., Tatem, W., & Fitchett, V. L. (2020, April). *FMVSS considerations for vehicles with automated driving systems: Volume 1* (Report No. DOT HS 812 796). National Highway Traffic Safety Administration. www.nhtsa.gov/sites/nhtsa.dot.gov/files/documents/ads-dv_fmvss_vol1-042320-v8-tag.pdf

Buller, W., Wilson, B., Garbarino, J., Kelly, J., Subotic, N., Thelen, B., & Belzowski, B. (2018, September). *Radar congestion study* (Report No. DOT HS 812 632). National Highway Traffic Safety Administration. https://rosap.ntl.bts.gov/view/dot/38820

Cartelligent. (2018). *Should your next car have rear cross traffic alert?* [Web page]. https://cartelligent.com/blog/should-you-next-car-have-rear-cross-traffic-alert/

Chappell, L. (2019, June 24). *The biggest suppliers beef up for change*. [Web page]. In Supplement to Automotive News [North America, Europe and the world top suppliers]. [Includes *Top 100 global OEM parts suppliers – Ranked by sales of original equipment parts in 2018*.] https://s3-prod.autonews.com/data-protected/062419-2019TopSuppliers-062419.pdf?djoDirectDownload=true

Continental Engineering Services. (2018). *ARS 404-21 Long Range Radar Sensor 77 GHz*. https://conti-engineering.com/wp-content/uploads/2020/02/ARS_404_21_EN_HS.pdf

European New Car Assessment Programme. (2015). *Test protocol – AEB systems, Version 1.1.* https://cdn.euroncap.com/media/1569/aeb-test-protocol-v-10.pdf

European New Car Assessment Programme. (2017). *Test protocol – Speed assist systems Version 2.0.* https://cdn.euroncap.com/media/17721/euro-ncap-sas-test-protocol-v11.pdf

European New Car Assessment Programme. (2018). *Test protocol– Lane support systems Version 2.0.2* https://cdn.euroncap.com/media/41770/euro-ncap-lss-test-protocol-v202.201811091311328900.pdf

European New Car Assessment Programme. (2021). *Test protocol – AEB systems, Version 1.1*. https://cdn.euroncap.com/media/1569/aeb-test-protocol-v-10.pdf

European Machine Vision Association. (2010, November 29). *Standard for characterization of image sensors and Cameras, EMVA Standard 1288*. www.emva.org/wp-content/uploads/EMVA1288-3.0.pdf

Fritsch, J., Kuhl, T.& Geiger, G.. (2013, October 6-9). *A new performance measure and evaluation benchmark for road detection algorithms*. 16th International IEEE Annual Conference on Intelligent Transportation Systems, The Hague, Netherlands.

Gamarra-Diezma, J. L., Miranda-Fuentes, A., Llorens, J., Cuenca, A., Blanco-Roldán, G. L., & Rodríguez-Lizana, A. (2015). Testing accuracy of long-range ultrasonic sensors for olive tree canopy measurements. *Sensors*, *15*(2), 2902–2919. https://doi.org/10.3390/s150202902

Gold, A. (2016, August 9). 10 Cars with active park assist. www.autobytel.com/car-buying-guides/features/10-cars-with-active-park-assist-131248/

Granig, W., Fallerb, L.-M., & Zangl, H. (2018, June 15). Sensor system optimization to meet reliability targets. *Microelectronics Reliability, 87*, pp.13-124. https://doi.org/10.1016/j.microrel.2018.06.005

IEEE P2020 Working Group. (2018, August). IEEE P2020 automotive imaging white paper. [White paper]. Institute of Electrical and Electronics Engineers, Inc. www.image-engineering.de/content/library/white_paper/P2020_white_paper.pdf

Institute of Electrical and Electronics Engineers, Inc. (2017, September). *IEEE standard for radar definitions*, IEEE Std 686-2017. https://ieeexplore.ieee.org/document/8048479/definitions#definitions

IHS Markit. (2016, November). *Vehicles getting older: Average age of light cars and trucks in U.S. rises again in 2016 to 11.6 years, IHS Markit says*. [Press release].

IHS Markit. (2021, June 14). *Average age of cars and light trucks in the U.S. rises to 12.1 years* [Press release].

Insurance Institute for Highway Safety. (2013, October). Autonomous emergency braking test protocol (Version I). https://www.iihs.org/media/a582abfb-7691-4805-81aa-16bbdf622992/REo1sA/Ratings/Protocols/current/test_protocol_aeb.pdf

IIHS. (2019a). *About our tests.* www.iihs.org/ratings/about-our-tests

IIHS. (2019b, January*). Pedestrian autonomous emergency braking test protocol (Version II).* www.iihs.org/media/f6a24355-fe4b-4d71-bd19-0aab8b39aa7e/TfEBAA/Ratings/Protocols/current/test_protocol_pedestrian_aeb.pdf

International Organization for Standardization. (2010). *ISO 15622, first edition, Intelligent transport systems — Adaptive cruise control systems — Performance requirements and test procedures*.

ISO. (2011). *ISO 26262, Compliance & tools*

ISO. (2015a). *ISO 17850, Photography — Digital cameras — Geometric distortion (GD) measurements.*

ISO. (2015b). *ISO 19084, Photography — Digital cameras — Chromatic displacement measurements*.

ISO. (2017a). *ISO 12233, Photography — Electronic still picture imaging — Resolution and spatial frequency responses*.

ISO. (2017b). *ISO 15739, Photography — Electronic still-picture imaging — Noise measurements*.

ISO. (2018). *ISO 15622, third edition, Intelligent transport systems — Adaptive cruise control systems — Performance requirements and test procedures*.

ISO. (2020). *ISO 11270, Intelligent transport systems — Lane keeping assistance systems (LKAS) — Performance requirements and test procedures*.

Jaadi, Z. (2021). *A step-by-step explanation of principal component analysis*. [Web page currently titled *Principal component analysis (PCA): A step-by-step explanat*ion and updated on February 23, 2024, by Whitfield, B., at https://builtin.com/data-science/step-step-explanation-principal-component-analysis]

Jiang, L., Djurdjanovic, D., & Ni, J. (2007). A new method for sensor degradation detection, isolation and compensation in linear systems. *American Society of Mechanical Engineers*. 1089-1101. https://doi.org/10.1115/IMECE2007-43819

Jokela, M., Kutila, M., & Pyykönen, P. (2019). Testing and validation of automotive point-cloud sensors in adverse weather conditions. *Applied Sciences, 9*(11), 2341. MDPI AG. http://dx.doi.org/10.3390/app9112341

Koopman, P., & Wagner, M. (2016). Challenges in autonomous vehicle testing and validation. *SAE International Journal of Transportation Safety, 4*(1), 15–24. https://doi.org/10.4271/2016-01-0128

Krome, C. (2016, March 9). *10 Cars with forward collision warning and affordable pricing*. [Web page]. Autobytel. www.autobytel.com/car-buying-guides/features/10-cars-with-forward-collision-warning-and-affordable-pricing-130798/

LeddarTech. (2020). SoC and software for the auto and mobility lidar platform. [Current web page: www.readkong.com/page/leddarengine-soc-and-software-for-the-auto-and-mobility-2801853]

Li, Y., Duthon, P., Colomb, M., & Ibanez-Guthman, J. (2021, November). *What happens to a ToF lidar in fog? IEEE Transactions on Intelligent Transportation Systems*, 22(11).

Linkov, J. (2018, August 10). *The race to protect car sensors from their biggest foes: Dirt and weather*. [Web page]. Consumer Reports. www.consumerreports.org/car-maintenance/protect-car-sensors-from-dirt-and-weather/

MarketsandMarkets Research. (2019). *Automotive RADAR market*. www.marketsandmarkets.com/Market-Reports/automotive-radar-market-75536718.html

Marshall, C., & Rossman, G. B. (1999). *Designing qualitative research* (3rd ed.). Sage Publications.

Mathew, V., Sengupta, S., Chatterjee, M., & Kamath, S. (2016, January 4-6). Sensor health monitoring using simple data driven approaches. 2016 Indian Control Conference, Hyderabad, India. https://doi.org/10.1109/indiancc.2016.7441102

MathWorks. (2020). *Image processing tool box*. [Web page]. www.mathworks.com/products/image.html

MATLAB Help Center. (2020a). [Imatest edge spatial frequency response] eSFRchart [sic]. [Web page]. MathWorks. www.mathworks.com/help/images/ref/esfrchart.html

MATLAB Help Center. (2020b). [Measure chromatic aberration at slanted edges] measureChromaticAberration [sic]. [Web page]. Mathworks. www.mathworks.com/help/images/ref/esfrchart.measurechromaticaberration.html

MATLAB Help Center. (2020c). vision.ChromaResampler [sic]. [Web page]. MathWorks. www.mathworks.com/help/vision/ref/vision.chromaresampler-system-object.html

Mays, K. (2019, May 22). Which cars have self-driving features for 2019? [Web page]. Cars.com. www.cars.com/articles/which-cars-have-self-driving-features-for-2019-402645/

McManamon, P. (2019). *LiDAR technologies and systems*. SPIE [Society of Photo-Optical Instrumentation Engineers].

McManamon, P. (2020). *Lidar benchmarking development.* SPIE.

National Center for Statistics and Analysis. (2019, April [Updated 2019, July]) *Police-reported motor vehicle traffic crashes in 2017* (Traffic Safety Facts Research Note. Report No. DOT HS 812 696). National Highway Traffic Safety Administration. https://crashstats.nhtsa.dot.gov/Api/Public/ViewPublication/812696

National Highway Traffic Safety Administration. (2005). *A compilation of motor vehicle crash data from the Fatality Analysis Reporting System and the General Estimates System* (Traffic Safety Facts 2003. Report No. DOT HS 809 775). https://crashstats.nhtsa.dot.gov/Api/Public/ViewPublication/809775

NHTSA. (2013a, February). *Forward collision warning system confirmation test.* [Docket submission. Docket ID NHTSA-2006-26555-0134 in Regulations.gov.] https://downloads.regulations.gov/NHTSA-2006-26555-0134/attachment_2.pdf

NHTSA. (2013b). *Lane departure warning system confirmation test and lane keeping support performance documentation*. [Docket submission. Docket ID NHTSA-2015-0119-0033 in Regulations.gov.] www.regulations.gov/document/NHTSA-2015-0119-0033

NHTSA. (2013c, February). *Lane departure warning system confirmation test and lane keeping support performance documentation*. [Docket submission. Docket ID NHTSA-2006-26555-0135 in Regulations.gov.] https://downloads.regulations.gov/NHTSA-2006-26555-0135/attachment_2.pdf

NHTSA. (2015). *Blind spot detection system confirmation testing for NCAP* (Working Draft). National Highway Traffic Safety Administration. https://lindseyresearch.com/wp-content/uploads/2019/12/NHTSA-2019-0102-0010-Blind_Spot_Detection_052019.pdf

NHTSA. (2020, December 17). *NHTSA announces 2020 update on AEB installation by 20 automakers* [Press release]. www.nhtsa.gov/press-releases/nhtsa-announces-2020-update-aeb-installation-20-automakers

National Instruments. (2019). Vehicle radar test system. Product Flyer. www.ni.com/pdf/product-flyers/vrts.pdf

National Instruments. (2020). Sensor Fusion. www.ni.com/en-us/innovations/white-papers/17/altran-and-ni-demonstrate-adas-hil-with-sensor-fusion.html

NewsRoom.AAA.com. (2019, January). *Advanced driver assistance technology names*. [Web page]. American Automobile Association. www.aaa.com/AAA/common/AAR/files/ADAS-Technology-Names-Research-Report.pdf

Nill, N., (2006). *Test procedures for verifying image quality requirements for personal identity verification (PIV) single finger capture devices*. The MITRE Corporation. www.appliedimage.com/wp-content/uploads/pdf/k362nB.pdf

Nill, N., Lepley, M., & Bas, C. (2016). *Test procedures for verifying IAFIS image quality requirements for fingerprint scanners and printers, v1.5*. MITRE Technical Report MTR05 B0 01 6R9. The MITRE Corporation.

Rasshofer, R. H., Spies, M., & Spies, H. (2011). Influences of weather phenomena on automotive laser radar systems, *Advances in Radio Science., 9*, 49–60, https://doi.org/10.5194/ars-9-49-2011

Reway, F., Huber, W., & Ribeiro, E. P., (2018, September 12-14). *Test methodology for vision-based ADAS algorithms with an automotive camera-in-the-loop.* IEEE International Conference on Vehicular Electronics and Safety, Madrid, Spain.

Ritchie, J., Spencer, L., & O'Conner, W. (2003). Carrying out qualitative analysis: A guide for social science students and researchers. In J. Ritchie & J. Lewis (eds.), *Qualitative research practice* (pp. 219-262). Sage Publishing.

SAE International. (2014). *J2399_201409, Adaptive cruise control*. www.sae.org/standards/content/j2399_201409/

SAE International. (2015a). *J3029, Forward collision warning and mitigation vehicle test procedure - truck and bus.*

SAE International. (2015b). *J3063, Active safety systems terms & definitions.*

SAE International. (2017). *J3087, Automatic emergency eraking (AEB) eystem performance testing.*

SAE International. (2018). *J3045, Truck and bus lane departure warning systems test procedure and minimum performance requirements*.

SAE International. (2019). *Safety-relevant guidance for on-road testing of SAE Level 3, 4, and 5 prototype automated driving system (ADS)-operated vehicles*.

SAE International. (2020). *J3122, Test target correlation - Radar characteristics.*

Seppelt, B. D., Lees, M. N., & Lee, J. D. (2005). Driver distraction and reliance: Adaptive cruise control in the context of sensor reliability and algorithm limits, Driving Assessment 2005, (pp. 254-261). *Proceedings of the 3rd International Driving Symposium on Human Factors in Driver Assessment, Training, and Vehicle Design*. https://doi.org/10.17077/drivingassessment.1168

Shin, H. (2013). *The Development of the ACC System Performance Evaluation Using VRS*. (p. 8). SAE International.

Siddiqui, O. F. (2020). *Empirical study of the braking performance of pedestrian autonomous emergency braking (P-AEB).* SAE International.

Sinclair, S. (2019, August 20). *Cars with advanced safety systems*. [Web page]. Consumer Reports. www.consumerreports.org/car-safety/cars-with-advanced-safety-systems/

Stove, A. G. & Hurd, D.L. (2003). Performance evaluation for modern radars. *Proceedings of the International Conference on Radar*. https://doi.org/10.1109/RADAR.2003.1278800

Taie, M. A., Moawad, E. M., Diab, M., & ElHelw, M. (2016). Remote diagnosis, maintenance and prognosis for Advanced Driver Assistance. SAE International, 114-122.

Threewitt, C. (2020, December 1). *10 Affordable cars with blind spot warning systems*. [Web page]. Autobytel. www.autobytel.com/car-buying-guides/features/10-affordable-cars-with-blind-spot-warning-systems-130434/

Tracxn. (2020). *Top autonomous vehicles LIDAR startups*.

Tzafestas, S. G. (2014). Mobile robot localization and mapping. Introduction to Mobile Control, Chapter 12. pp 479-531

Vehicle Research and Test Center. (2019, August). *Active park assist system confirmation test (Working draft)* (Report No. DOT HS 812 714). National Highway Traffic Safety Administration. https://downloads.regulations.gov/NHTSA-2019-0102-0007/attachment_1.pdf

Wang, S., Al-Atat, H., Ghaffari, M., Lee, J., & Xi, L. (2008, April 6-8). *Prognostics of automotive sensors: tools and case study*. 62nd Meeting of the Society for Machinery Failure Prevention Technology, Virginia Beach, VA. www.researchgate.net/publication/271270955_Prognostics_of_Automotive_Sensors_Tools_and_Case_Study

Wasserzier, C., Stove A. G., & Lukin, K. A., (2019). Verification of a continuous wave noise radar. *2019 20th International Radar Symposium (IRS).*

Watts, S., Griffiths, H. D., Holloway, J. R., Kinghorn, A. M., Money, D. G., Price, D. J., Whitehead, A. M., Moore, A. R., Wood, M. A., & Bannister, D. J. (2002). The specification and measurement of radar performance. *RADAR 2002*, pp. 542-546.

Xique, I. J., Buller, W., Fard, Z. B., Dennis, E., & Hart, B. (2018, August 27-30). *Evaluating complementary strengths and weaknesses of ADAS sensors*. 2018 IEEE 88th Vehicular Technology Conference (VTC-Fall), Chicago, IL. https://doi.org/10.1109/vtcfall.2018.8690901

This page is intentionally left blank.

Appendix A: Stakeholder Outreach Discussion Guide

This appendix contains the list of questions used during interviews to gather information related to this project.

VTTI Sensor Degradation Discussion Guide

**Note: Researchers only asked for organization approaches/information. Researchers did not collect or document personal opinions or information.*

Background

- What ADAS and/or sensors does your organization produce or use?

Degradation

- What forms of degradation are considered by your organization during design and development activities?
- Where are the degradations that are of particular interest for each type of sensor identified previously?
    - What makes these degradations your organization's focus (challenging to identify, have particularly negative impact or unpredictable impact on performance, etc.)
    - What levels of degradation does your organization consider during design and development?
        - Permanent (degradation does not resolve and will generally worsen over time)
        - Temporary (degradation does not persist)
- For each degradation identified previously, describe how these levels are adjusted by your organization during the testing.

ADAS Perception Sensors

- What are the primary sensors that your organization uses and/or develops?
- In general, does your organization set the performance requirements and specifications or are these provided to your organization?
    - When provided, what type of organization provides them?
    - When set by your organization, what processes is used to identify and set the requirements/ specifications?

Sensor-Level Testing

- What are the processes and tests used to validate sensor performance?
    - Standardized testing (IEEE, ASTM, etc.)
    - Specialized testing
- Does your organization perform sensor testing under degraded states?
    - What metrics are used to quantify performance under degraded state?
    - During testing, how does your organization simulate the degraded states identified previously?

    - Considering the tests identified in the Sensors section above, are there any additional tests that your organization performs specifically to evaluate sensors in degraded states?
    - Does the sensor perform self-diagnostics?

System-Level Considerations

- What tests does your organization perform while validating ADAS systems?
    - Standardized testing (e.g. NCAP)
    - Specialized testing
- System operation under degraded state
    - What metrics are used to quantify performance under degraded state?
    - Are there specific tests run to evaluate system performance in degraded states?
    - Does the system perform self-diagnostics?
    - What is the desired system response to degraded states and are there different levels of action?
    - What communication is provided to driver?
- Does your organization use interaction/fusion between sensors to help address degradation?

This page is intentionally left blank.

Appendix B: Sensor Metric Testing Procedures

The procedures provided the bases for the evaluation of the degradation samples and an initial evaluation of baseline sensor performance.

Camera Test Procedures

The study used the following standards.

- ISO 12233. (2017a). *Photography — Electronic still picture imaging — Resolution and spatial frequency responses*.
- ISO 15739. (2017b). *Photography — Electronic still-picture imaging — Noise measurements.*
- ISO 17850. (2015a). *Photography — Digital cameras — Geometric distortion (GD) measurements.*
- ISO 19084. (2015b). *Photography — Digital cameras — Chromatic displacement measurements.*

The method of evaluation uses the MATLAB Image Processing (MathWorks, 2020). There are many parameters of a camera that can be evaluated, but the selection was made based on their relation to the sensing application of an ADAS and to limit scope. For stereo cameras, this procedure would only be applied to one camera at a time.

1) Parameters
    a) Color Accuracy
    b) MTF
        i) Resolution
        ii) Contrast
    c) Dynamic Range
    d) Geometric and Chromatic Distortion
2) Equipment

a) CIPA Resolution Test Chart. CIPA stands for Camera & Imaging Products Association.

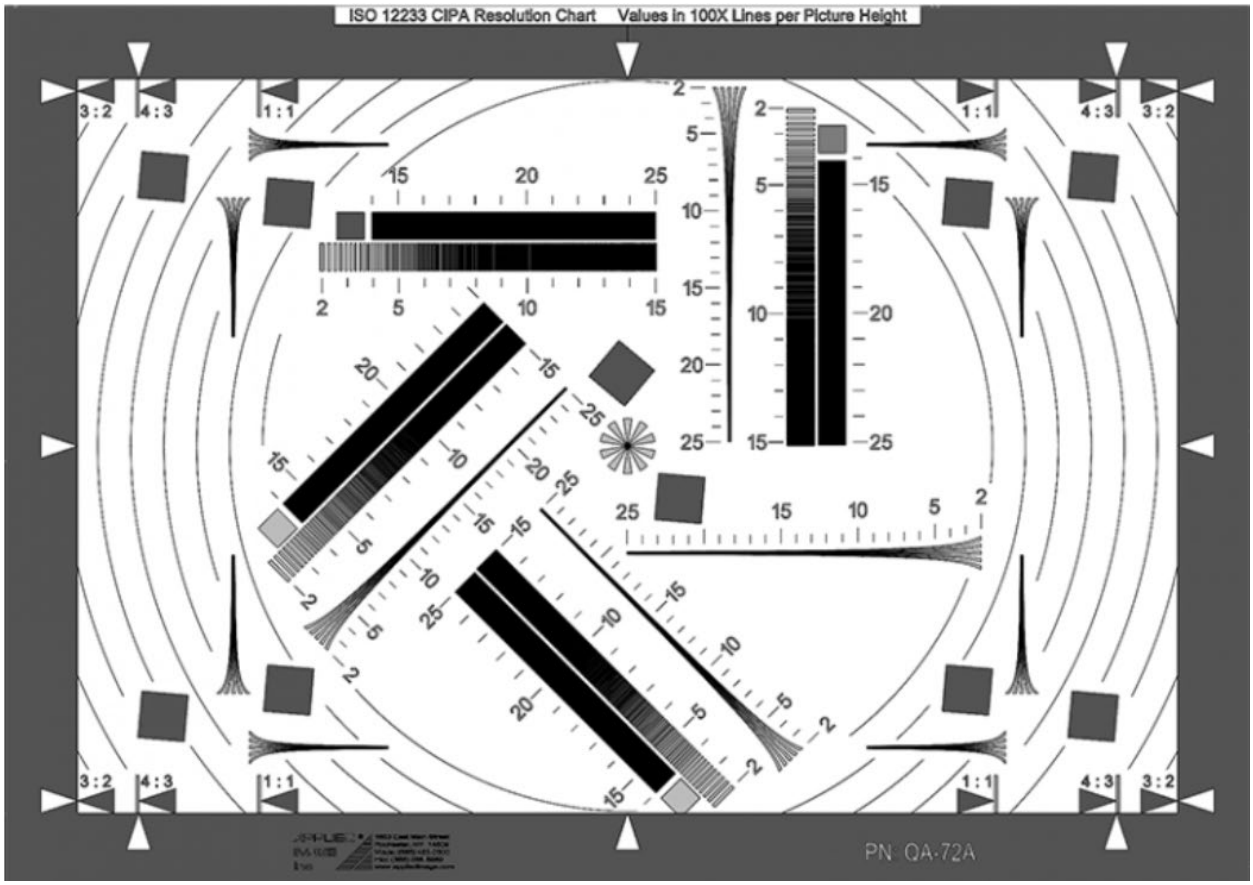

b) x-rite standard

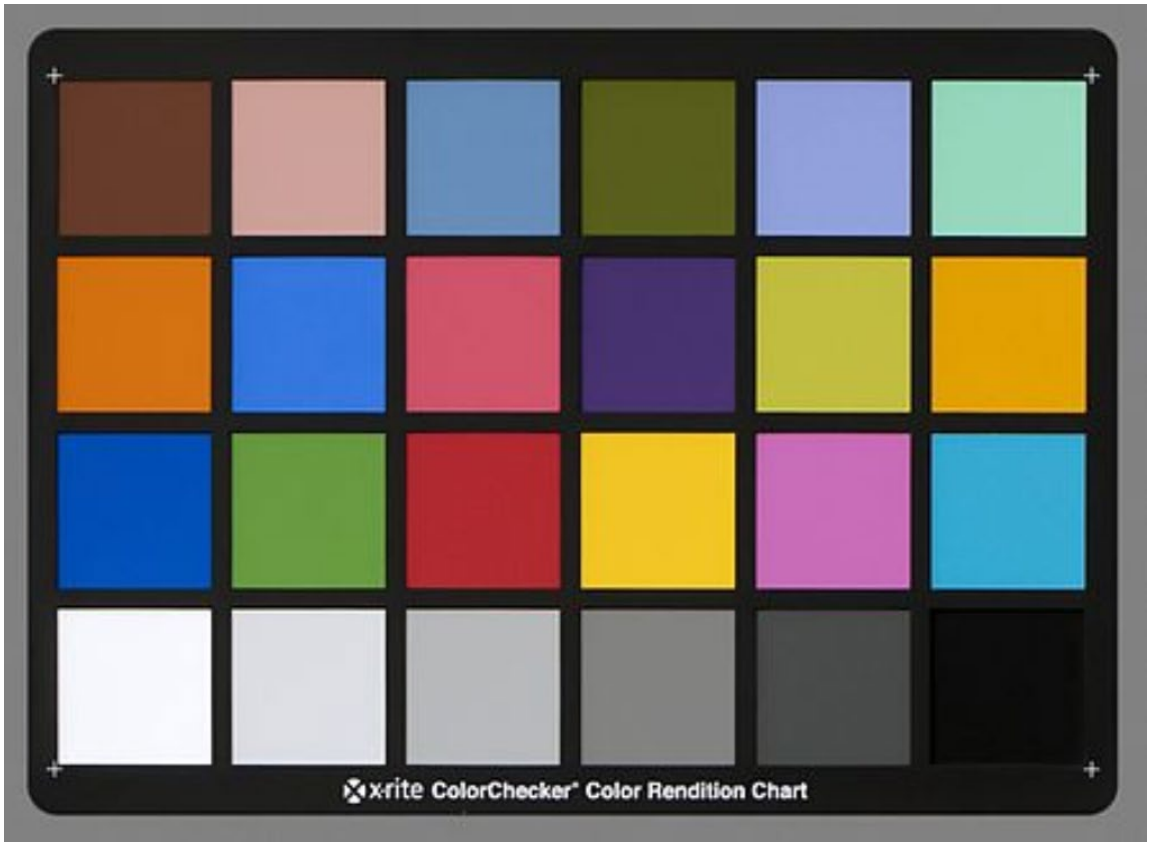

X-Rite, Inc.,[1] is a manufacturer of color measurement and management products

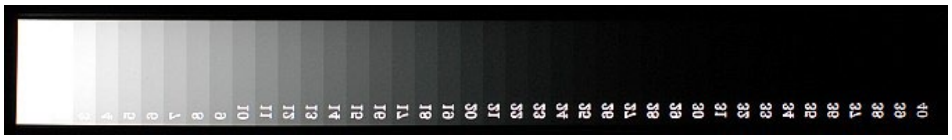

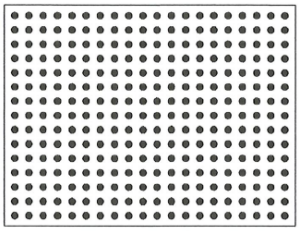

c) Step Chart
d) Dot Chart
e) Camera Stand
f) Target Stand
g) Black felt curtains
h) Two full-spectrum lamps.[2] Full spectrum refers to electromagnetic radiation from ultraviolet to infrared wavebands.

[1] X-Rite, Inc., Grand Rapids, MI, was rebranded as Calibrite ColorChecker
[2] Lumigrow light from Greenfall AS, Trondheim, Norway.

i) Small mirror
j) Lux and spectrum meter

3) Setup

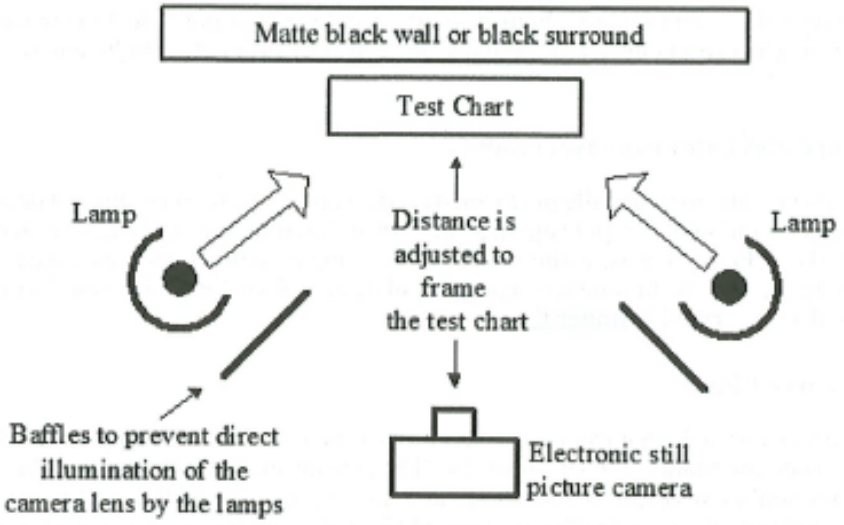

Figure 1 — Test chart illumination method

a) Setup the camera testing area as shown in the figure.
b) Using a mirror, align the camera lens to the center of the test chart area
c) Record and verify the luminance and spectrum from the test lamps or environmental lighting conditions
    i) Track every minute if testing outdoor or adjust under other variable lighting scenario
d) For each test procedure, check and record the following variables of the camera, if possible, for constancy and comparison.
    i) Focus
    ii) White balance
    iii) Gamma correction (Linearization)
    iv) RAW output format
    v) ISO

4) Procedures
    a) For each test chart in 4) b):
        i) Center the test chart on the target stand.
        ii) Adjust the camera distance to fill the frame (or suggested manufacturer distance).
        iii) Check alignment with mirror.
        iv) Capture Image.
        v) Verify image quality and retake if necessary.
    b) Test Charts:
        i) Color Accuracy: Use the X-Rite ColorChecker standard chart
        ii) MTF: CIPA Resolution Test Chart

iii) Dynamic Range: Step Chart
iv) Geometric and Chromatic Distortion: Dot Chart

5) Evaluation
    a) Use existing image evaluation tools (i.e., Imatest edge spatial frequency response test chart, MathWorks (2020).) to generate the output metrics and plots
        i) Gong (2016). *A color calibration method between different digital cameras – Method. Evaluation of color error*
        ii) ISO 12233. (2017a). *Photography – Electronic still picture imaging – Resolution and spatial frequency responses. Evaluation of modular transfer function (MTF) in grayscale and color*
        iii) ISO 15739. (2017b). *Photography – Electronic still picture imaging – Noise measurements. Evaluation of dynamic range, including density, f#, and contrast ratio*
        iv) *Geometric and Chromatic Distortion*
    b) (ISO 19084, 2015b) and (ISO 17850, 2015a)

Radar Test Procedures

The radar procedure outlined below adapted procedures from Gao (2020) with some testing considerations taken from SAE J3122 (2020). The evaluation relied on analysis of the IF (intermediate frequency) signal in the frequency domain without relying on the manufacturer object detection. This removed manufacturer data processing from the comparisons and evaluated the native output of the radar.

1) Parameters:
   a) Azimuth Resolution (using Fast Fourier Transform)
   b) Range Resolution (using FFT)
   c) Range (using FFT)
   d) Field of view (FOV)
2) Equipment
   a) DAS
   b) Calibrated Radar Cross Section (RCS) Target (Sphere, Corner Reflector, Reference Target)
   c) Target stand (Minimal radar cross-section)
   d) Sensor stand
   e) Anechoic Radar Panels
   f) Tape measure
   g) Wheel odometer
   h) Calibrated high-accuracy distance measurement device
   i) Virtual Reference Standard (VRS) or Instrumented Track
3) Setup
   a) Use existing anechoic chamber or large enough area with no interference
      i) Use anechoic radar panels to block objects and surfaces that cannot be moved in test area.
   b) VRS
      i) Depending on sensor under test, it may be easier to use a VRS system to ease the measurement of true value for longer distances.
      ii) Ensure VRS reading is within test space.
      iii) Validate stationary VRS accuracy using a different distance measuring device.
      iv) Accuracy of this procedure will be limited to the accuracy of the VRS.
4) Procedures
   a) Azimuth Resolution (FFT)
      i) Set two targets at the desired test distance.
         (1) Radially equidistant from sensor.
         (2) Use low-RCS stands.
         (3) Start with the targets adjacent (or appearing as a single peak in the FFT).
         (4) Suggested ranges: 10, 50, 100 percent Max range of sensor.
      ii) Record the true value of the distance from the sensor to the target and the distance between the targets.
      iii) Manual Collection
         (1) Capture data.

(2) Move one of the targets away from the other (tangentially from the sensor).
(3) Repeat until the signal shows two peaks in azimuth.

iv) Automated Collection
(1) Set the moving target on an instrumented track or VRS.
(2) Start continuous recording.
(3) Move the target on the slide at a constant, slow rate. According to test target correlation from "surface vehicle recommended practice" (SAE J3122, 2020), the slow rate should facilitate measurement data resolution of at least 0.2 meters.
(4) Stop recording.

v) Optional variants:
(1) Use two different sized targets.

b) Range Resolution (FFT)

i) Set two targets at the desired test distance.
(1) Radially equidistant from sensor.
(2) Use low-RCS stands.
(3) No gap between targets (adjacent, but not overlapping in FOV).
(4) Suggested range: 10, 50, 100 percent Max range of sensor.

ii) Record the true value of the distance from the sensor to the target.

iii) Manual Collection
(1) Capture data.
(2) Move one of the targets away from the other by X m (radially from the sensor, increasing distance).
(3) Repeat until the signal shows two peaks in range.

iv) Automated Collection
(1) Set the moving target on an instrumented track or VRS.
(2) Start continuous recording.
(3) Move the target on the slide at a constant slow rate.
(4) Stop recording.

v) Optional variants:
(1) Use two different sized targets.

c) Max Range

i) Max Range will be defined by a minimum SNR and target cross section.
(1) SNR can be system dependent, but 2 dB is a common measure.
(2) Use a standard target with $1m^2$ radar cross section (Gao, 2020).

ii) Set the target just beyond max sensor range.

iii) Record the true value of the distance between the sensor and target.

iv) Move the target toward the sensor in intervals of X m or desired increment.
(1) Alternatively, measure continuously if using instrumented system for measuring true value.

v) Repeat until the returned power reaches 2 dB or desired threshold.

d) Field of View

i) Use the same targets and thresholds in (c) to measure FOV.

ii) For symmetric sensors, measurements can be done on one side of the target range.

iii) FOV can be a function of range. Test at multiple ranges.
   (1) Suggested ranges: 10, 50, 100 percent Max Range.
iv) Set the target beyond the max azimuth for the sensor.
v) Record the true value of the distance and angle between the sensor and target.
vi) Move the target toward the center of the sensor FOV in intervals of X m or desired increment.
   (1) Alternatively, measure continuously if using instrumented system for measuring true value.
vii) Repeat until the returned power reaches 2 dB or desired threshold.

5) Evaluation
   a) Resolution
      i) Use FFT, or Multiple signal classification algorithm (a.k.a. MUSIC) analysis on the IF signal from the radar to calculate azimuth and range response. More details in "Experiments with mmWave automotive radar test-bed" by Gao (2020)

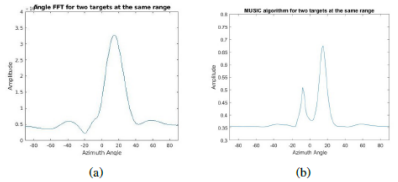

(a) (b)

Fig. 7: (a) FFT-based DoA estimation result for two corner reflectors with 20° azimuth difference (b) MUSIC-based DoA estimation result for the same scenario as (a)

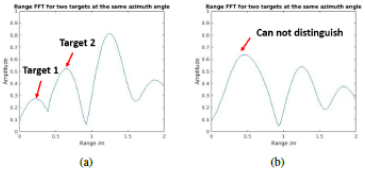

(a) (b)

Fig. 6: (a) FFT-based range estimation for two static targets with 0.3m range difference (b) FFT-based range estimation for two static targets with 0.23m range difference

      (1) Figures obtained from *Experiments With mmWave Automotive Radar Test-Bed* by Gao (2020)
      ii) Use a peak-trough-peak threshold of X to identify the Azimuth and Range Resolution.
   b) FOV and Max Range
      i) Use a threshold of 2 dB, or desired, on returned signal to determine the Max Range of the radar.

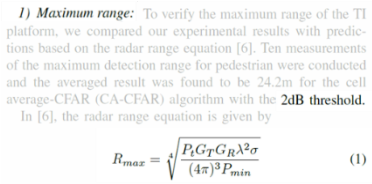

1) Maximum range: To verify the maximum range of the TI platform, we compared our experimental results with predictions based on the radar range equation [6]. Ten measurements of the maximum detection range for pedestrian were conducted and the averaged result was found to be 24.2m for the cell average-CFAR (CA-CFAR) algorithm with the 2dB threshold. In [6], the radar range equation is given by

$$R_{max} = \sqrt[4]{\frac{P_t G_T G_R \lambda^2 \sigma}{(4\pi)^3 P_{min}}} \quad (1)$$

      (1) Snip from "Experiments with mmWave automotive radar test-bed" by Gao (2020)
      ii) The use the same threshold to determine FOV
         (1) Alternatively, define the 2D region of detection that shows the interaction of FOV and Range.

LiDAR Test Procedures

Automotive lidar is a relatively new and growing technology. As such, it has fewer existing standards and procedures for evaluation. Procedures were adapted from those in the radar test procedures with considerations for the similarities and differences in operation. The following references were considered: Jokela et al., 2019; Li et al., 2021; and McManamon, 2020.

1) Parameters:
   a) Spatial Accuracy
   b) Resolution
   c) Range
2) Equipment
   a) Lidar test targets (10, 50, 80 reflectance)
   b) Bar Target
   c) Target stand
   d) Sensor stand
   e) Tape measure
   f) Wheel odometer
   g) Lux and spectrum meter
3) Setup
   a) Set the target and sensor stands in the desired testing environment.
   b) Record the lighting conditions.
      i) Track every minute, if testing outdoor or adjust under other variable lighting scenario.
4) Procedures
   a) Spatial Accuracy
      i) Set the target and sensor stand at the desired distances and angles.
         (1) 10, 50, 100 percent max range
         (2) 0°, +/- 100 percent FOV
      ii) Measure true value of distance and angle between sensor center and target surface.
      iii) If possible, use several stands and targets to capture the data at the same time.
   b) Resolution
      i) Set the bar target and sensor stand at the desired distances.
         (1) 50 percent max range (Target dependent)
      ii) Measure true value of distance between sensor center and target surface.
      iii) Capture data
      iv) Use time series data to also capture beam diffraction effects.
         (1) Start recording data.
         (2) Slowly move the bar target tangentially from the sensor by a distance of at least the width of the largest bar.
         (3) Stop recording. Amount of data collected depends on sensor outputs.
   c) Max Range
      i) Set the target. One sensor stands at a distance beyond the max range of the sensor and record the precise location.
      ii) Set three other reference targets around the sensor stand and record their precise locations relative to the sensor.

(1) Depending on FOV, the triangulation targets may need to be forward of the sensor.

iii) While continuously recording, move the sensor until the evaluation target is within sensor range.

5) Evaluation
   a) Spatial Accuracy
   b) Resolution
      i) Find the first bar within the target that contains two data points returned.
      ii) Beam diffraction evaluation (angular accuracy)
         (1) Search the time series data for a bar.
   c) Range
      i) Find the point in the time history data when the evaluation target becomes visible.
      ii) Take the reference targets at this point in the data to triangulate the distance moved and subtract that from the original evaluation target distance to get the max range.
      iii) Note:
         (1) Max range will be defined by minimum power returned.
         (2) Depending on model or test mode this may be done by the device or need to be applied to the data stream during evaluation.
         (3) Use a value of X dB returned power.

This page is intentionally left blank.

Appendix C: Degradation Development Tables

This appendix contains the table data for degradation development. The first set of three tables (Table 25, Table 26, and Table 27) contain all the radar, lidar, and camera sensor metric channels used in signal selection. The items in bold were the selected channels to carry forward with the scoring.

The degradation score and grouping are shown in Table 28, Table 29, and Table 30 for lidar, camera, and radar, respectively. These tables show the weighted score for each degraded sensor and show the group assignment for low scoring degradations. The degradation rank and uniqueness scores are shown in Table 31, Table 32, and Table 33 for lidar, camera, and radar, respectively. These tables show the degradation rank, with 1 being the degradation with the highest impact on the corresponding sensor. The uniqueness columns in the tables are similar, but the score is a measure of how unique the combined signal response is to each degradation applied to a sensor. Finally, summary tables for radar degradations (Table 34) and corresponding uniqueness scores (Table 37) and for optical degradations (Table 35) and corresponding uniqueness scores (Table 36) are made by combining all the optical sensors into one group and all the radars into another. The final selection of degradations carried to component and system testing are indicated in bold.

The full detail of how metrics were normalized to become weighted normalized average, percentages, and groups is given in Chapter 4, Degradation Development.

Sensor Metric Tables

Table 25. Radar Metrics Used for Degradation Development (Selected Channels in Bold)

LR 77GHz		SR 24GHz	SR 77GHz	LR 24GHz
SNR mean	Azimuth STD	numPts	avg_points_per_scan	***numPts***
SNR STD	Azimuth STDerr	ymean	x_mean	ymean
SNR STDerr	Elevation Mean	ystd	***x_std_dev***	ystd
X mean	Elevation STD	ystderr	x_std_err	***ystderr***
X STD	Elevation STDerr	vxmeam	y_mean	vymean
X STDerr	Radial Rel Vel Mean	vxstd	y_std_dev	***vystd***
Y mean	Radial Rel Vel STD	***vxstderr***	***y_std_err***	vystderr
Y STD	Radial Rel Vel STDerr	***vymean***	z_mean	***vxmean***
Y STDerr	***RCS Mean***	vystd	***z_std_dev***	vxstd
Z mean	***RCS STD***	vystderr	z_std_err	***vxstderr***
Z STD	RCS STDerr	rcsmean	rr_mean	xmean
Z STDerr	Num Points	***rcsstd***	rr_std_dev	xstd
Range Mean	xDet	***rcsstderr***	rr_std_err	xstderr
Range STD	yDet	xmean	***rcs_mean***	
Range STDerr	zDet	xstd	***rcs_std_dev***	
Azimuth Mean		xstderr	rcs_std_err	

Radars have varying output depending on the sensor type. Some radars, such as the LR 77GHz and the SR 77GHz radars, produce point cloud-like data that includes position (*x, y, z*), radial velocity, and RCS, among other channels. Other radars, like the LR 24GHz and SR 24GHz radars, are more object oriented and return position, velocity, and RCS data based on tracked

objects. Additionally, both the LR 24GHz radar and the SR 24GHz radar break down the velocity into *x* and *y* components that are not available from either of the 77GHz radars. For each trial, the mean, the standard deviation (STD), and the standard error (STDerr) can be calculated and treated as an independent variable (also referred to as metrics) for analysis.

Based on the methods outlined in Chapter 3, the study used a combination of principal component analysis and correlation values to identify the metrics that were most impactful and unique for each radar for the static radar tests. Many metrics were inter-related, such as average number of points and range, or highly correlated, such as the standard deviation and standard error values for a certain variable, and, thus, could not be selected together. The metrics identified are shown in bold for each radar.

Table 26. Lidar Metrics Used for Degradation Development (Selected Channels in Bold)

Solid State LiDAR			**Budget LiDAR**	**32-Beam LiDAR**			
min_n	cov_y	sde_r	***z***	min_n	cov_y	sde_r	std_ring
max_n	min_z	cov_r	***Reflectivity***	max_n	min_z	cov_r	sde_ring
mean_n	max_z	min_Az	***yStdDev***	mean_n	max_z	min_Az	cov_ring
std_n	mean_z	max_Az	***zStdDev***	***std_n***	mean_z	max_Az	min_delay
sde_n	std_z	mean_Az	***RefStdDev***	sde_n	std_z	mean_Az	max_delay
cov_n	***sde_z***	std_Az	***yStdErr***	cov_n	***sde_z***	std_Az	mean_delay
min_x	cov_z	sde_Az	***zStdErr***	min_x	cov_z	sde_Az	std_delay
max_x	min_i	cov_Az	***xCoefVar***	max_x	min_i	cov_Az	sde_delay
mean_x	max_i	min_El	***yCoefVar***	mean_x	max_i	min_El	cov_delay
std_x	***mean_i***	max_El	***zCoefVar***	std_x	***mean_i***	max_El	
sde_x	***std_i***	mean_El	***xSize***	sde_x	***std_i***	mean_El	
cov_x	sde_i	std_El	***refSize***	cov_x	sde_i	std_El	
min_y	***cov_i***	sde_El	***FnumAvgPointsFrame***	min_y	***cov_i***	sde_El	
max_y	min_r	cov_El	***FnumFrames***	max_y	min_r	cov_El	
mean_y	max_r		***FnumCoefVar***	mean_y	max_r	min_ring	
std_y	mean_r			***std_y***	mean_r	max_ring	
sde_y	std_r			sde_y	std_r	mean_ring	

Lidar outputs (*x, y, z*) location and intensity from a number of points (*n*) that correspond to objects encountered in its surroundings. In addition, every (*x, y, z*) point was used to compute their equivalent in spherical coordinates, which corresponds to range (*r*), azimuth (Az), and elevation (El). In some cases, lidars also output the "ring" index of their scanning. Typically, the lidars that scan 360 degrees all around them do so in circular fashion in the form of rings. Also, some lidars gave information related to the time "delay" of each individual point (within the point cloud) when preforming a full scan. The following statistics can be calculated for each of the outputs: minimum (min), maximum (max), mean, standard deviation (std), standard error (sde), and coefficient of variation (cov, i.e., standard deviation divided by the mean). lidar points are grouped into objects, and then their statistics can be calculated for each of the following quantities: *x, y, z, r*, Az, El, and intensity; and in some cases, ring and delay. Each of the statistics on each of the variables is treated as an independent variable, also known as metrics.

Table 27. Camera Metrics Used for Degradation Development (Selected Channels in Bold)

Cellphone Camera	Machine Vision Camera	OEM Camera
ESFR_Hor (Nyquist) AUC_norm	ESFR_Hor (Nyquist) AUC_norm	ESFR_Hor (Nyquist) AUC_norm
ESFR_Ver (Nyquist) AUC_norm	ESFR_Ver (Nyquist) AUC_norm	ESFR_Ver (Nyquist) AUC_norm
ESFR Mean	***ESFR Mean***	***ESFR Mean***
Gray (Red) SSE	Gray (Red) SSE	Gray (Red) SSE
Gray (Green) SSE	Gray (Green) SSE	Gray (Green) SSE
Gray (Blue) SSE	Gray (Blue) SSE	Gray (Blue) SSE
Gray SSE Mean	***Gray SSE Mean***	***Gray SSE Mean***
Gray Illuminant (Red)	Gray Illuminant (Red)	Gray Illuminant (Red)
Gray Illuminant (Green)	Gray Illuminant (Green)	Gray Illuminant (Green)
Gray Illuminant (Blue)	Gray Illuminant (Blue)	Gray Illuminant (Blue)
Mean Euclidian Distance	Mean Euclidian Distance	Mean Euclidian Distance
Min Euclidian Distance	Min Euclidian Distance	Min Euclidian Distance
Max Euclidian Distance	Max Euclidian Distance	Max Euclidian Distance
Y RMS Noise AUC	***Y RMS Noise AUC***	***Y RMS Noise AUC***
Cb RMS Noise AUC	Cb RMS Noise AUC	Cb RMS Noise AUC
CR RMS Noise AUC	CR RMS Noise AUC	CR RMS Noise AUC
CbCR AUC Mean	***CbCR AUC Mean***	***CbCR AUC Mean***
Aberration	***Aberration***	***Aberration***

The Edge Spatial Frequency Response is a performance metric for cameras that quantifies how well a camera can balance detecting high contrast and fine resolution features. The ESFR is evaluated both horizontally and vertically, then combined as a mean. To make the response a single value for each test, the area under curve was calculated and then normalized to be compared across sensors. The Gray response is a metric that evaluates how much error is in the red, green, and blue channels given a perfectly gray input. The values are converted to a sum of squares error (SSE) to convert the response to a single value and highlight the nonlinearity in color response. The Gray illuminant metric was not used; however, it is a measure of identifying the color of light used to illuminate the target. This is required for automated white balancing of the image (e.g., sunlight versus incandescent). The Euclidian Distance is measuring the error distance of the camera color response on a colormap. This metric was not used. The YCbCR Noise is a measure of noise in the color signal using the YCbCr color space (Y is Luminance and CbCr are the two chroma values, essentially, the brightness and color). The area under curve was taken from the responses and used in the evaluation. Finally, the aberration is a measure of how the color and intensity of pixel response changes along a high contrast edge.

Degradation Score and Grouping Tables

Table 28. Lidar Degradation Development Score and Grouping

	32-beam LiDAR		Solid State Lidar		Budget LiDAR	
Degradation	**Weighted, Normalized Average**	**Group**	**Weighted, Normalized Average**	**Group**	**Weighted, Normalized Average**	**Group**
Angled	13.0%	1	13.6%	1	3.5%	12
CAGlue	31.0%	2	30.0%	2	34.3%	2
Cracked	66.6%	3	28.6%	2	29.3%	14
Epoxy	28.8%	4	27.1%	2	48.2%	4
None	41.2%	5	4.6%	5	8.4%	12
Offgas	68.8%	6	60.9%	6	77.5%	6
Primer	47.4%	7	26.5%	2	2.6%	12
Salt	48.1%	8	39.4%	8	37.3%	8
SandBlasted	21.6%	11	-	-	57.5%	9
Scratched	42.7%	7	19.9%	13	5.5%	12
Sealant	21.3%	11	73.0%	11	74.9%	11
Shellac	50.5%	14	49.7%	12	14.6%	12
Tape	45.9%	13	27.3%	13	8.8%	12
Tinted	56.5%	14	63.0%	14	30.8%	14

Table 29. Camera Degradation Development Score and Grouping

	Cellphone Camera		Machine Vision Camera		OEM Camera	
Degradation	**Weighted, Normalized Average**	**Group**	**Weighted, Normalized Average**	**Group**	**Weighted, Normalized Average**	**Group**
Angled	8.6%	7	2.4%	5	11.8%	13
CA Glue	21.1%	2	72.5%	2	23.7%	2
Cracked	2.4%	7	2.8%	5	12.3%	13
Epoxy	56.0%	4	30.9%	4	7.0%	13
None	8.0%	7	8.7%	5	31.5%	5
Off-gas	35.3%	6	53.2%	6	45.9%	6
Primer	9.3%	7	7.1%	5	-	-
Salt	35.7%	8	21.2%	8	20.2%	8
Sandblasted	65.1%	9	50.0%	9	27.6%	9
Scratched	7.5%	7	5.7%	5	9.2%	13
Sealant	73.7%	11	48.7%	11	24.8%	11
Shellac	57.7%	12	37.9%	12	9.2%	12
Tape	31.0%	13	22.7%	13	12.1%	13
Tinted	45.2%	14	40.4%	14	50.7%	14

Table 30. Radar Degradation Development Score and Grouping

	LR 77GHz		SR 77GHz		LR 24GHz		SR 24GHz	
Degradation	**Weighted, Normalized Average**	**Group**	**Weighted, Normalized Average**	**Group**	**Weighted, Normalized Average**	**Group**	**Weighted, Normalized Average**	**Group**
3MSafetyWalk	29.7%	1	41.3%	5	28.3%	11	-	-
Blacktop	42.0%	2	71.1%	2	17.8%	2	12.0%	9
Bondo	70.0%	3	50.4%	3	25.2%	3	11.2%	3
BondoMesh	34.1%	12	48.4%	4	48.7%	4	70.0%	4
DirtScratches	24.5%	5	46.5%	5	25.6%	5	14.4%	9
DuctTape	40.0%	6	19.6%	6	24.7%	6	-	-
Epoxy	48.0%	7	28.7%	7	17.0%	5	56.1%	7
SRE	45.4%	8	69.3%	8	67.2%	8	45.9%	8
Leaves	47.5%	9	22.7%	9	34.0%	11	11.0%	10
None	18.2%	10	33.6%	10	40.9%	10	20.4%	10
PineNeedles	65.8%	11	48.5%	11	37.0%	11	12.7%	10
Scratches	36.4%	12	32.5%	12	44.2%	12	35.3%	12
Corner	53.2%	13	-	-	-	-	-	-
Front	46.7%	14	-	-	-	-	-	-
Side	40.8%	15	-	-	-	-	-	-
Zone1	37.9%	16	-	-	-	-	-	-
Zone2	25.7%	17	-	-	-	-	-	-
Zone3	36.5%	18	-	-	-	-	-	-
Zone4	44.9%	19	-	-	-	-	-	-
ZoneA	52.1%	20	-	-	24.8%	20	9.8%	3
ZoneB	46.7%	21	-	-	19.5%	5	10.3%	10
ZoneC	37.9%	22	-	-	-	-	-	-
ZoneD	16.7%	23	-	-	-	-	-	-
ZoneE	42.9%	24	-	-	-	-	-	-

Degradation Uniqueness Tables

Table 31. Lidar Degradation Uniqueness Score and Rank

	32-beam LiDAR		Solid State Lidar		Budget LiDAR	
	Uniqueness	**Rank**	**Uniqueness**	**Rank**	**Uniqueness**	**Rank**
Angled	25.0%	2	14.0%	7	4.7%	11
CAGlue	12.0%	5	6.0%	10	18.0%	5
Cracked	19.0%	4	4.0%	12	8.4%	7
Epoxy	12.0%	5	6.0%	10	22.2%	4
None	11.0%	7	16.0%	6	4.2%	12
Offgas	38.0%	1	22.0%	1	28.1%	2
Primer	10.0%	8	4.0%	12	3.8%	13
Salt	22.0%	3	19.0%	5	16.6%	6
SandBlasted	9.0%	11	-	-	28.1%	2
Scratched	10.0%	8	9.0%	8	3.8%	13
Sealant	9.0%	11	21.0%	3	31.8%	1
Shellac	9.0%	11	22.0%	1	8.1%	9
Tape	10.0%	8	9.0%	8	6.6%	10
Tinted	9.0%	11	21.0%	3	8.4%	7

Table 32. Camera Degradation Uniqueness Score and Rank

	Cellphone Camera		Machine Vision Camera		OEM Camera	
Degradation	**Uniqueness**	**Rank**	**Uniqueness**	**Rank**	**Uniqueness**	**Rank**
Angled	5.0%	11	4.0%	10	8.0%	9
CA Glue	15.0%	7	15.0%	7	11.0%	7
Cracked	7.0%	10	4.0%	10	8.0%	9
Epoxy	19.0%	5	15.0%	7	6.0%	12
None	3.0%	12	4.0%	10	18.0%	4
Off-gas	22.0%	4	19.0%	3	19.0%	3
Primer	3.0%	12	4.0%	10	-	-
Salt	14.0%	8	17.0%	5	11.0%	7
Sandblasted	23.0%	2	22.0%	1	16.0%	5
Scratched	3.0%	12	4.0%	10	3.0%	13
Sealant	23.0%	2	22.0%	1	13.0%	6
Shellac	19.0%	5	17.0%	5	7.0%	11
Tape	14.0%	8	15.0%	7	3.0%	13
Tinted	32.0%	1	19.0%	3	29.0%	2

Table 33. Radar Degradation Uniqueness Score and Rank

	LR 77GHz		SR 77GHz		LR 24GHz		SR 24GHz	
Degradation	**Uniqueness**	**Rank**	**Uniqueness**	**Rank**	**Uniqueness**	**Rank**	**Uniqueness**	**Rank**
3MSafetyWalk	14.0%	13	9.7%	11	8.0%	10	-	-
Blacktop	14.0%	13	10.4%	9	15.9%	5	6.4%	10
Bondo	23.0%	2	26.1%	1	19.3%	3	8.4%	5
BondoMesh	8.0%	23	17.1%	5	30.9%	2	55.6%	1
DirtScratches	14.0%	13	9.7%	11	7.2%	12	4.8%	11
DuctTape	14.0%	13	17.6%	4	17.5%	4	-	-
Epoxy	12.0%	22	13.4%	7	5.5%	13	21.0%	2
SRE	16.0%	7	10.4%	9	44.0%	1	21.0%	2
Leaves	17.0%	6	25.6%	3	8.0%	10	4.8%	11
None	16.0%	7	13.4%	7	14.6%	6	8.2%	8
PineNeedles	13.0%	19	26.1%	1	8.7%	9	7.1%	9
Scratches	16.0%	7	13.9%	6	14.6%	6	15.0%	4
Corner	23.0%	2	-	-	-	-	-	-
Front	8.0%	23	-	-	-	-	-	-
Side	14.0%	13	-	-	-	-	-	-
Zone1	16.0%	7	-	-	-	-	-	-
Zone2	13.0%	19	-	-	-	-	-	-
Zone3	24.0%	1	-	-	-	-	-	-
Zone4	20.0%	4	-	-	-	-	-	-
ZoneA	13.0%	19	-	-	11.1%	8	8.4%	5
ZoneB	16.0%	7	-	-	5.5%	13	8.3%	7
ZoneC	15.0%	12	-	-	-	-	-	-
ZoneD	18.0%	5	-	-	-	-	-	-
ZoneE	14.0%	13	-	-	-	-	-	-

Note: Degradations were applied to bumper areas (or zones) by automotive shops. Degradation treatments applied to each zone are defined in Table 17.

Degradation Development Summary Tables

Table 34. Radar Degradation Score Summary (Final Selection in Bold)

(Weighted, Normalized Average)		Radar Scores		
Deg	**Rank**	**Min**	**Mean**	**Max**
3MSafetyWalk	8	28.3%	33.1%	41.3%
Blacktop	7	12.0%	35.7%	71.1%
Bondo	4	11.2%	39.2%	70.0%
BondoMesh	2	34.1%	50.3%	70.0%
DirtScratches	12	14.4%	27.7%	46.5%
DuctTape	11	19.6%	28.1%	40.0%
Epoxy	5	17.0%	37.4%	56.1%
SRE	1	45.4%	56.9%	69.3%
Leaves	9	11.0%	28.8%	47.5%
None	10	18.2%	28.2%	40.9%
PineNeedles	3	12.7%	41.0%	65.8%
Scratches	6	32.5%	37.1%	44.2%

Table 35. Optical Degradation Score Summary (Final Selection in Bold)

(Weighted, Normalized Average)		Camera + LiDAR Scores		
Deg	**Rank**	**Min**	**Mean**	**Max**
Angled	14	2.4%	8.8%	13.6%
CAGlue	6	21.1%	35.4%	72.5%
Cracked	10	2.4%	23.7%	66.6%
Epoxy	8	7.0%	33.0%	56.0%
None	12	4.6%	17.1%	41.2%
Offgas	1	35.3%	56.9%	77.5%
Primer	11	2.6%	18.6%	47.4%
Salt	7	20.2%	33.7%	48.1%
SandBlasted	4	21.6%	44.4%	65.1%
Scratched	13	5.5%	15.1%	42.7%
Sealant	2	21.3%	52.7%	74.9%
Shellac	5	9.2%	36.6%	57.7%
Tape	9	8.8%	24.6%	45.9%
Tinted	3	30.8%	47.7%	63.0%

Table 36. Optical Uniqueness Score Summary (Final Selection in Bold)

	(Uniqueness)	Camera + LiDAR Scores		
Deg	**Rank**	**Min**	**Mean**	**Max**
Angled	9	4.0%	10.1%	25.0%
CAGlue	8	6.0%	12.8%	18.0%
Cracked	12	4.0%	8.4%	19.0%
Epoxy	7	6.0%	13.4%	22.2%
None	11	3.0%	9.4%	18.0%
Offgas	1	19.0%	24.7%	38.0%
Primer	14	3.0%	5.0%	10.0%
Salt	5	11.0%	16.6%	22.0%
SandBlasted	4	9.0%	19.6%	28.1%
Scratched	13	3.0%	5.5%	10.0%
Sealant	2	9.0%	20.0%	31.8%
Shellac	6	7.0%	13.7%	22.0%
Tape	10	3.0%	9.6%	15.0%
Tinted	3	8.4%	19.7%	32.0%

Table 37. Radar Uniqueness Score Summary (Final Selection in Bold)

	(Uniqueness)	Radar Scores		
Deg	**Rank**	**Min**	**Mean**	**Max**
3MSafetyWalk	11	8.0%	10.6%	14.0%
Blacktop	10	6.4%	11.7%	15.9%
Bondo	3	8.4%	19.2%	26.1%
BondoMesh	1	8.0%	27.9%	55.6%
DirtScratches	12	4.8%	8.9%	14.0%
DuctTape	4	14.0%	16.4%	17.6%
Epoxy	9	5.5%	13.0%	21.0%
JBWeld	2	10.4%	22.9%	44.0%
Leaves	6	4.8%	13.9%	25.6%
None	8	8.2%	13.1%	16.0%
PineNeedles	7	7.1%	13.7%	26.1%
Scratches	5	13.9%	14.9%	16.0%

Appendix D: Degradation Sample Preparation

The following describes the preparation of the degradation samples.

Light Sensing: Acrylic

For this series, 0.086-inch-thick acrylic material was cut into 6-inch by 6-inch squares. The material was purchased with a protective film on both sides, and that film was removed from one side only just before application as described below.

The notched trowels used were the following Marshalltown 5-in V-Notch Ceramic Floor Trowel (Lowes Item # 845141, Model # 6286). These trowels are described as "ground steel" on the Lowe's website but were plastic instead. However, they worked well for this application.

Offgas

Three acrylic samples were prepared by heating Type 1 plastic from a 2-liter bottle to its smoke point and exposing the samples as follows. The samples were cleaned with acetone and then taped to the inside bottom of a bucket which was inverted over the heated samples so that the smoke was captured and directed up over the samples.

The first sample was exposed to approximately 1 square inch of plastic which was heated to the smoke point until the smoke dissipated. The second and third samples were created similarly using approximately 29.03 square centimeters and 161.29 square centimeters of plastic, respectively.

Sandblasted Acrylic

Ten 6-inch square acrylic specimens were created and numbered. After sandblasting, each specimen was rinsed and patted dry with a paper towel and protected from additional abrasion. The number on each specimen corresponds to the number of passes across one entire face only of that specimen.

Each pass covered the entire face and involved eight complete swipes from one side to the other with the sandblaster gun held at a constant distance of 38.1 centimeters from the specimen. The pattern used for each pass is shown in Figure 77. Travel speed for each swipe was controlled by hand and was held as constant as possible.

The air pressure on the sandblaster was set at 95 psi, and the sandblasting media used was *10X Blasting Media* (grit: MP 70/100). The Technical Data sheet for this media is located at https://www.columbiacoatings.com/shared/images/TDS/10x-Blasting-Media-TDS.pdf.

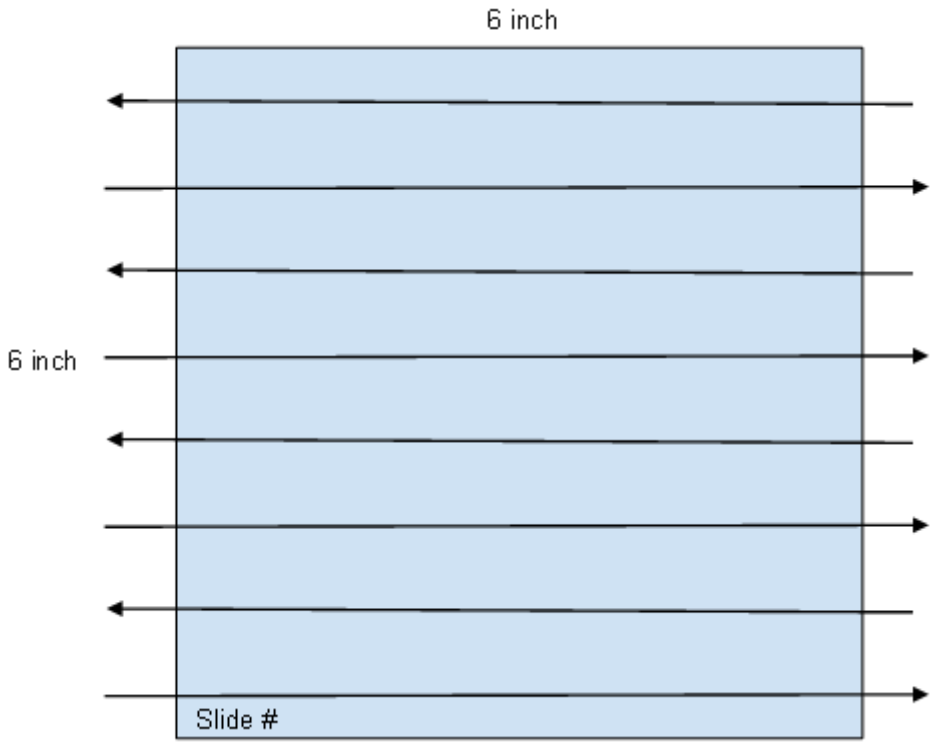

Figure 77. Sandblasting pattern

Sealant

Six acrylic specimens were coated on one side with a clear sealant. Three were then given a surface texture and the other three were left with the natural texture that resulted from the application. The sealant used is Ultra Clear DAP Flexible All Purpose Waterproof Sealant (070798183872).

The three textured specimens were applied at 0.04-inch thickness using a 3D printed PLA mold to maintain thickness. This 0.04-inch-thick mold was superglued to the acrylic (see Figure 78). One sample was textured with a 1/8-inch V-notch plastic trowel, and the other two specimens were textured with 3/16-inch and 1/4-inch V-notch trowels, respectively.

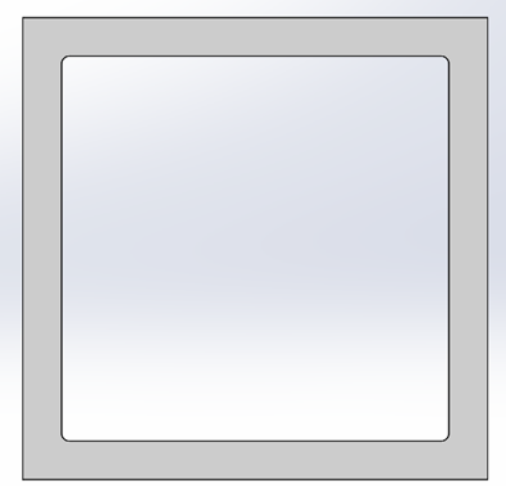

Figure 78. PLA mold

The other three samples were not given a texture, but were created using 0.02-inch-thick, 0.04-inch-thick, and 0.08-inch-thick 3D printed PLA molds.

In all cases, the sealant was spread using a new polyethylene board (plastic cardboard). The sealant was spread in alternating directions until the sealant was smooth and until the air bubbles were worked out.

Shellac

Three acrylic specimens were coated on one side with shellac by following the manufacturer's instructions. The entire surface was "painted" with a series of light coats and waiting between coats for the shellac to get tacky. The sample was rotated 90 degrees between each successive coat. The first specimen received three coats, the second specimen received six coats, and the third specimen received 12 coats total. Each specimen was marked accordingly.

A fourth acrylic specimen was also made with a different technique in case it is found to be useful. This specimen was given six coats of shellac following the same procedure described above. Then, with the topcoat still tacky, a 3/16-inch V-notch plastic trowel was used to create texture. Finally, with the topcoat still tacky, a seventh coat of shellac was applied.

The shellac used is clear Zinsser Bulls Eye Shellac (product number 00408) in an aerosol can. The degradations samples prepared were measured and their properties were documented on Table 22 and Table 23.

Tinted

Six acrylic samples were made using two different types of tints. The first set of three samples was made with green film similar to sunshade found in windshields. This film was cleaned and then taped onto the acrylic slides. One sample was made with a single layer of film, and the second and third samples were made with two and three layers of film, respectively.

To replicate the tinted windshield sun shield, the spectral transmission of the windshield sample and three potential color filters were measured, and the results plotted (Figure 79). All have been smoothed by an 11-point centered box car moving average. The 11-point moving average

computes the mean using a window of 11 points to smooth data. As can be seen, the windshield tint (MovingAvgWindBlue) still transmits 20 percent of red, 10 percent of orange, and 55 percent of green. The blue and blue-green sheets allow 5 percent of red, 0 percent yellow, and thus several levels of red degradations would not be feasible. Green sheet allows 30 percent red, 10 percent yellow, and 75 percent green light through. It was decided to use stacked green sheets to get several levels of filtering. Since stacking multiplies the loss mechanism, the levels achieved are shown in Table 38.

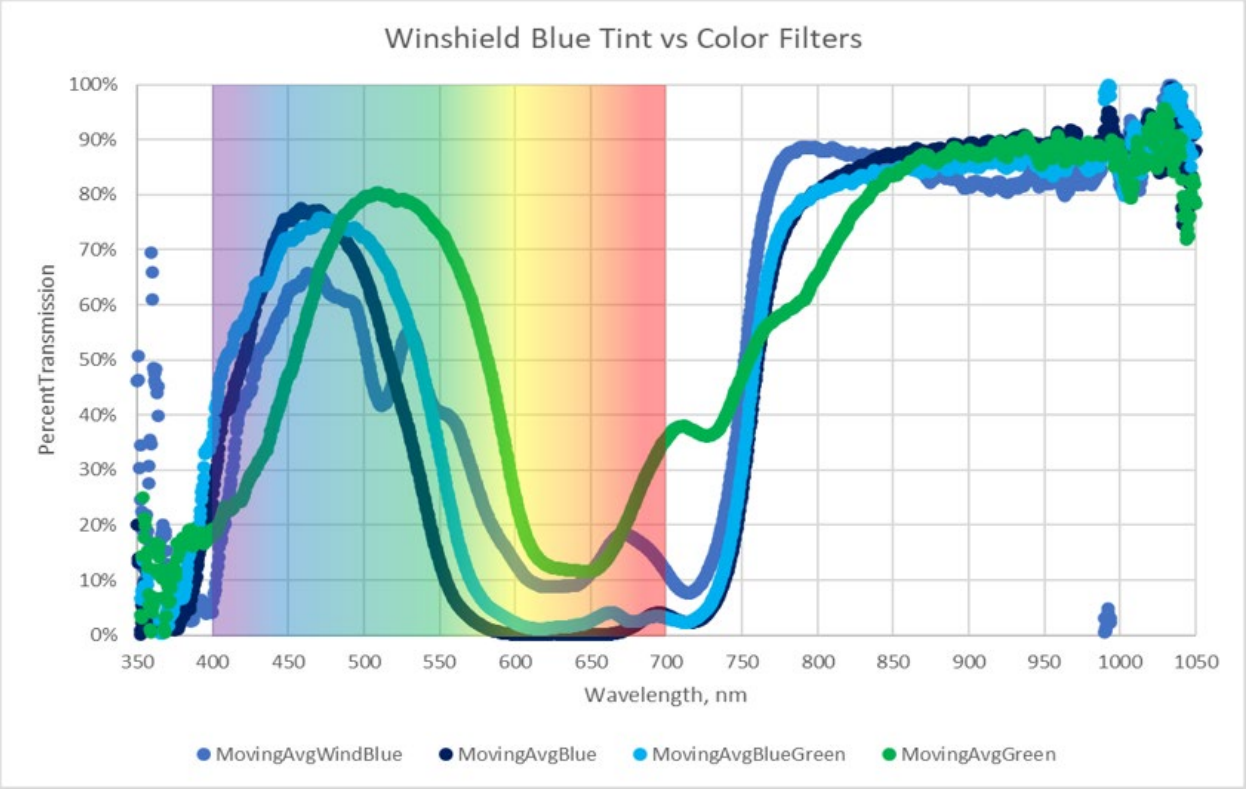

Figure 79. Transmission spectra of windshield tint and color filter samples

Table 38. Color Degradation Transmission Levels in Percentages

Transmission	Red	Yellow	Green
Windshield Blue	20	10	55
1 Green	30	10	75
2 Green	9	1	56
3 Green	3	0.1	42

The second set of samples were made using standard automotive window tint purchased from Advance Auto Parts. In this case, all three samples were made with a single layer of film, but each sample was given film with a different level of darkness.

First, the slides were sprayed with the solution provided with the Gila Window Film Complete Application Kit (Part # FS600/18003), and the film was applied following the manufacturer's instructions. The different samples were made with the following window tinting film.

- Gila Basic 35 percent VLT Automotive Window Tint DIY Glare Control UV Blocking (Part # NRS46),
- Gila Basic 20 percent VLT Automotive Window Tint DIY Glare Control UV Blocking (Part # NRS44)
- Gila Basic 5 percent VLT Automotive Window Tint DIY Glare Control UV Blocking (Part # NRS42).

Radar Specimens: Polyethylene Panels

For this series, 1/4-inch-thick white polyethylene panels were cut into 6-inch by 6-inch squares and prepared as described below (see Figure 80).

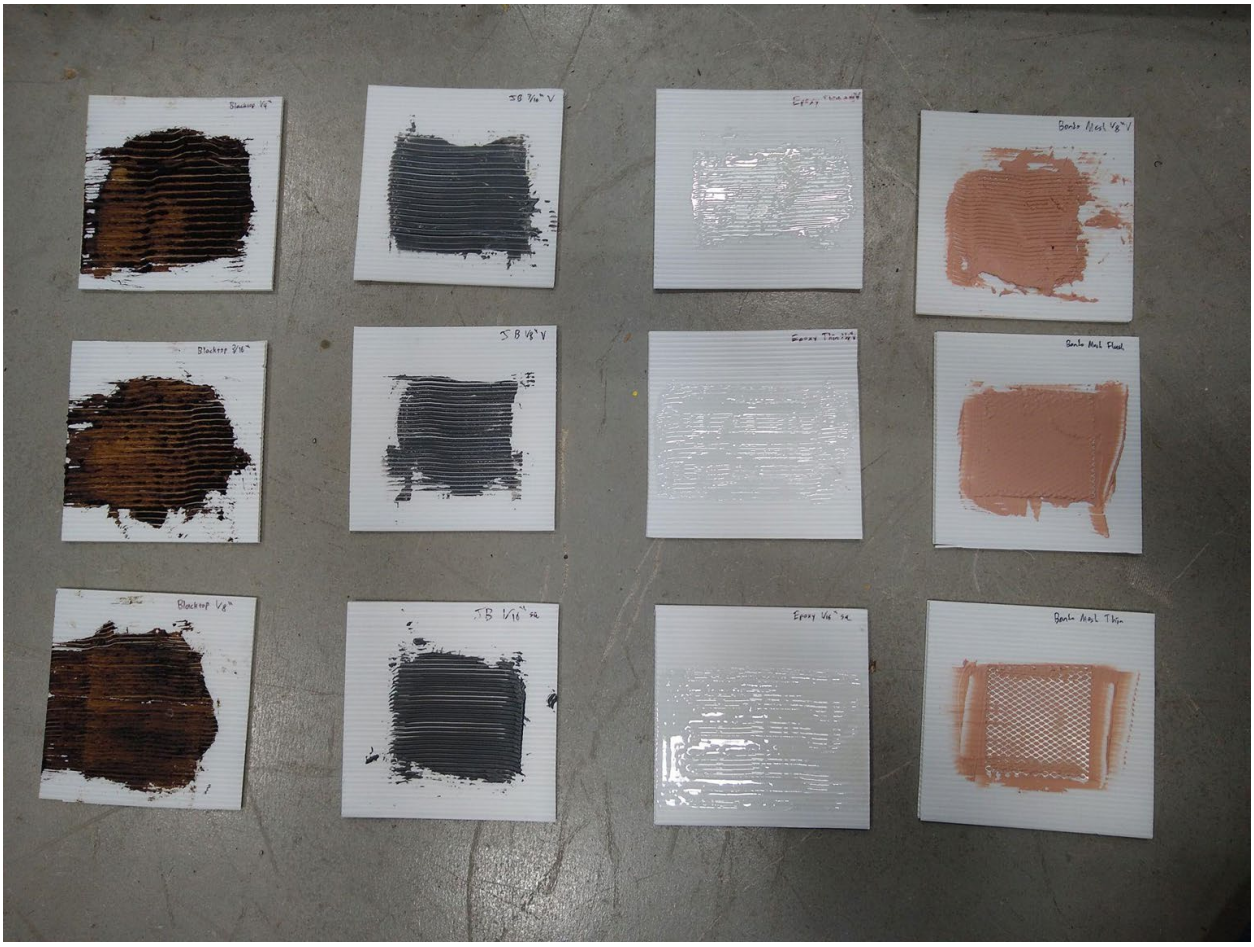

Figure 80. Polyethylene specimens prepared for radar testing

The notched trowels used were the Marshalltown 5-in V-Notch Ceramic Floor Trowel (Lowes Item # 845141, Model # 6286), and Marshalltown 5-in Square Notch Ceramic Floor Trowel

(Lowe's Item # 45142, Model # 6287). These trowels are described as "ground steel" on the Lowe's website but were plastic instead. However, they worked well for this application.

Blacktop

Three polyethylene specimens were prepared with a layer of Gardner Blacktop Drive Patch (Item # 8071-GA). This material was applied at approximately constant thickness and about the same thickness on all specimens. Once the blacktop began to set so that it would hold a shape, V-notch plastic trowels were used to create texture. The trowels used were 1/8-inch, 3/16-inch, and 1/4-inch.

Bondo/Mesh

Three polyethylene specimens were prepared using Bondo body filler and a self-adhesive body mesh. The body filler was Bondo (Item # 262, https://www.3m.com/3M/en_US/p/d/b40067483/) and was mixed and applied according to manufacturer's instructions. The mesh was 0.014-inch thick Bondo (Item # 932, https://www.3m.com/3M/en_US/p/d/b40069646). The mesh was cut into approximately 3-inch squares and applied to the center of each specimen, and body filler was applied over top and spread according to three different methods.

One specimen was covered with a smooth layer of body filler that was just deep enough to completely cover the mesh. The second specimen was covered with body filler which was spread thin enough to just make the top of the mesh visible, and on the third specimen, the body filler was spread with enough pressure to wipe some of the filler out of the holes of the mesh, creating small recesses.

No additional texture was applied, and the notched trowels were not used on these specimens.

Epoxy

Three polyethylene specimens were prepared with a layer of epoxy following the manufacturer's instructions. The epoxy used for these specimens was manufactured by J-B Weld (Clear Weld Professional Grade Epoxy, Product # 50240H).

One specimen was made with a smooth, thin layer of epoxy without creating any texture. The second and third specimens were given progressively thicker layers of epoxy. This was allowed to begin to cure to the point where it would hold a shape and then was shaped with a 1/8-inch V-notch plastic trowel.

SRE Made by JB-Weld

Three polyethylene specimens were prepared with a layer of traditional J-B Weld following the manufacturer's instructions. The epoxy used for these specimens was manufactured by J-B Weld (Original Cold-Weld Formula Steel Reinforced Epoxy, Product # 8265S).

One specimen was made with a smooth, thin layer of epoxy without creating any texture. The second and third specimens were given progressively thicker layers of epoxy. This was allowed to begin to cure to the point where it would hold a shape and then was shaped with a 1/8-inch V-notch plastic trowel.

Spruce Needles

The biological material degradation was created using dead needles and branches from the same spruce tree in Blacksburg, VA. The needles were collected and taped to corrugated polyethylene holders to place in front of the radars. The amount of degradation was varied by varying the density of the needles versus the clear space between the needles as shown in Figure 81.

Figure 81. Biological material degradations from lightest to heaviest (left to right)

Appendix E: Functional Tests

Object Detection Test Procedures

The researchers adapted object detection functional test procedures from *The Development of the ACC System Performance Evaluation Using VRS* (Shin, 2013) and expanded them to work for generalized object detection. The study performed a subset of the parameters that best satisfied the needs to test under degradations, as discussed in the main body, and as defined below (e.g., single TV, two speeds). Other entities performing similar tests can reduce or expand the parameters as necessary. Similarly, the metrics are not intended to be all inclusive, but were left concise to retain scope and focus on factors related to sensor degradation. Other parameters may be of interest for different research applications. "X" is used to designate numbers to be defined by the executor of the testing.

1) Parameters:
   a) Resolution
   b) Spatial error
   c) Max range
   d) Time lag
   e) Object classification
2) Equipment
   a) VRS (Virtual Reference Station) or RTK (Real Time Kinematic)
   b) DAS
   c) Targets (TV, Pedestrian Target, other vehicles?)
   d) Tape measure
   e) Wheel odometer
3) Setup
   a) Prepare vehicles and VRS
      i) Check vehicle fluids and pressures.
      ii) Warm up vehicles, if dynamic test.
      iii) Ensure VRS reading within test space.
      iv) Validate stationary VRS accuracy using a different distance measuring device.
   b) Capture environmental and lighting conditions
      i) Track every X minutes and/or record before each test segment.
      ii) Avoid unwanted glare conditions.
   c) Capture test track
      i) Use a VRS receiver to capture reference points of the test track.
         (1) Static signs/objects
         (2) Reference points of lane lines
            (a) Straight line: minimum of once every X m.
            (b) Curved line: minimum of once every X m.
            (c) Broken line: include line breaks if required for evaluation.

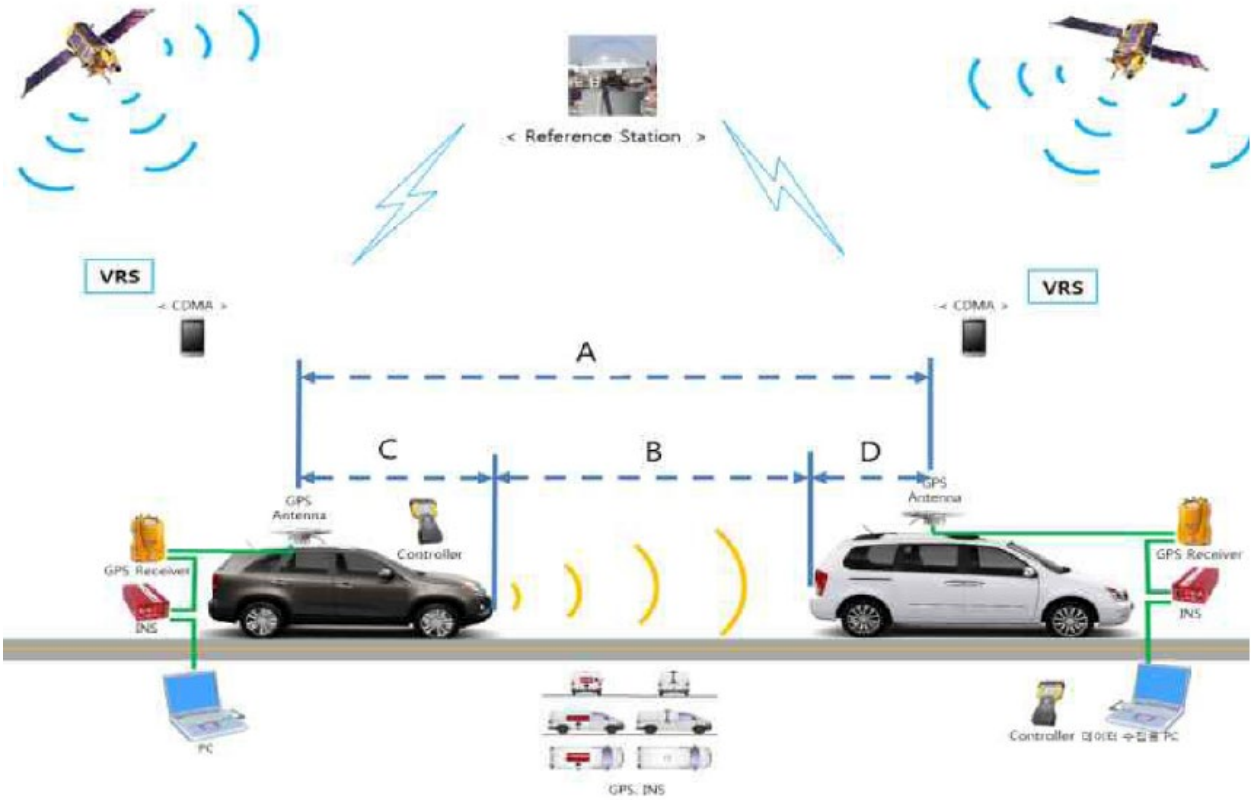

Figure from Shin (2013)

4) Procedures
   a) Steady-State Test
      i) Record the data in the following configurations.
         (1) 0, 40, 100 kph (TV and SV)
         (2) 10, 50, 100 percent max sensor range gap distance.
         (3) TV one lane left, TV same lane, TV one lane right
      ii) Repeat with other TVs (0 kph only)
      iii) Repeat with pedestrian target (0 kph only)
   b) Sustained Test
      i) With the TV travelling at a constant speed and the SV following it at a distance just beyond its max sensor range, close the gap to the TV to X percent max sensor range at the following speed differentials:
         (1) 5, 10, 20 kph
      ii) Once the gap has been closed, return to initial gap distance at the same speed differential to record negative rates.
   c) Object Differentiation
      i) Place two objects of the same type beyond the max sensor range of the SV with a gap between them of X percent their total width.
      ii) Drive the SV towards the objects at a rate of X kph recording data.

5) Evaluation
    a) Steady State Test
        i) Evaluate spatial error versus the VRS.
        ii) Evaluate object classification accuracy.
    b) Sustained Test
        i) Evaluate effects of range rate, max range, and time lag.
    c) Object Differentiation
        i) Evaluate effects of resolution.

Lane Detection Test Procedures

The lane detection test procedures used in this study were based on *A New Performance Measure and Evaluation Benchmark for Road Detection Algorithms* (Fritsch et al., 2013). This test procedure was picked because it tests the boundaries of unmarked or weakly marked roads and lanes. However, the format and evaluation methods described below were adjusted to match the test procedures for object detection previously presented in this Appendix, with the aim of achieving a similar flow of procedures and scope. The evaluation methods may be dependent on the available output of lane detection sensors as described in the body of this test plan.

1) Parameters
    a) Error (SV relative position, line spacing, line curvature, line type)
    b) Sight distance (lateral, longitudinal)
    c) Latency
2) Equipment
    a) VRS
    b) DAS
    c) Tape measure
    d) Wheel odometer
    e) Line identification test track requirements
        i) Two or more line types
        ii) Two or more lanes
        iii) Curved section
3) Setup
    a) Prepare vehicles and VRS
        i) Check vehicle fluids and pressures
        ii) Warm up vehicles if dynamic test
        iii) Ensure VRS reading within test space
        iv) Validate stationary VRS accuracy using a different distance measuring device
    b) Capture environmental and lighting conditions
        i) Track every minute and/or record before each test segment
        ii) Avoid unwanted glare conditions
    c) Capture test track
        i) Use a VRS receiver to capture reference points of the test track
            (1) Static signs/objects
            (2) Reference points of lane lines
                (a) Straight line: minimum of once every X m
                (b) Curved line: minimum of once every X m
                (c) Broken line: include line breaks, if required for evaluation
4) Procedures
    a) Steady State tests
        i) Drive the SV through the test track at 40 kph or desired speed
        ii) Capture the following scenarios:
            (1) Drive on multi-lane straight in a far right or left lane
            (2) Drive on curved lane

(3) Approach curved lane
(4) Approach line type transition
(5) Drive in a lane of each line type available on track
(6) Lane Change Maneuver, taking >5 s

iii) Use an integrated track marker in the DAS if available or make separate runs for each scenario to ease data processing

b) Slalom Test

i) Drive the SV through the test track at 40 kph or desired speed
ii) Capture on a straight and curved section of track
iii) Slalom within the lane
(1) On center
(2) 50 percent lane width in amplitude (or desired)
(3) 0.5 Hz rate (or desired)

5) Evaluation

a) Line Error

i) Use the drive on multilane straight and curved data to calculate line spacing error.
ii) Use the drive on curved data to calculate curvature error.
iii) Use the line type test to verify the system correctly identifies all available line types.
iv) Use the lane change maneuver to evaluate the SV relative position error.

b) Sight distance

i) Use the approach data to find the distance from a change in line type and line curvature when the system first identifies that change.
ii) Use the multilane straight data to evaluate the max lateral distance a line is perceived.
(1) Limited by the number of lanes on the test track.

c) Latency

i) Use the slalom test to calculate the time lag in the SV relative position.
ii) Verify the system functions for both straight and curved lanes.
iii) Report both latency values if there is a difference between straight and curved lanes.

Appendix F: Component Test – Run Log

File Code	Test	Location	Variant	Speed, mph	Amplitude, percent	Freq, Hz	Offset, %	Rate
1.1.01	Lane Slalom	Surface Street	Baseline	15	50	0.5	0	-
1.1.02	Lane Slalom	Surface Street	Degradation Set (Low Intensity) 1	15	50	0.5	0	-
1.1.03	Lane Slalom	Surface Street	Degradation Set (Low Intensity) 2	15	50	0.5	0	-
1.1.04	Lane Slalom	Surface Street	Degradation Set (Low Intensity) 3	15	50	0.5	0	-
1.1.05	Lane Slalom	Surface Street	Degradation Set (Low Intensity) 4	15	50	0.5	0	-
1.1.06	Lane Slalom	Surface Street	Degradation Set (Low Intensity) 5	15	50	0.5	0	-
1.1.07	Lane Slalom	Surface Street	Degradation Set (Low Intensity) 6	15	50	0.5	0	-
1.1.08	Lane Slalom	Surface Street	Baseline	15	50	0.5	0	-
1.1.09	Lane Slalom	Surface Street	Degradation Set (Med Intensity) 1	15	50	0.5	0	-
1.1.10	Lane Slalom	Surface Street	Degradation Set (High Intensity) 1	15	50	0.5	0	-
1.2.01	Lane Slalom	Highway	Baseline	35	50	0.5	0	-
1.2.02	Lane Slalom	Highway	Degradation Set (Low Intensity) 1	35	50	0.5	0	-
1.2.03	Lane Slalom	Highway	Degradation Set (Low Intensity) 2	35	50	0.5	0	-
1.2.04	Lane Slalom	Highway	Degradation Set (Low Intensity) 3	35	50	0.5	0	-
1.2.05	Lane Slalom	Highway	Degradation Set (Low Intensity) 4	35	50	0.5	0	-
1.2.06	Lane Slalom	Highway	Degradation Set (Low Intensity) 5	35	50	0.5	0	-
1.2.07	Lane Slalom	Highway	Degradation Set (Low Intensity) 6	35	50	0.5	0	-
1.2.08	Lane Slalom	Highway	Baseline	35	50	0.5	0	-
1.2.09	Lane Slalom	Highway	Degradation Set (Med Intensity) 1	35	50	0.5	0	-
1.2.10	Lane Slalom	Highway	Degradation Set (High Intensity) 1	35	50	0.5	0	-
2.1.01	Ranging Sweep	Surface Street	Baseline	15	-	-	0	10
2.1.02	Ranging Sweep	Surface Street	Degradation Set (Low Intensity) 1	15	-	-	0	10
2.1.03	Ranging Sweep	Surface Street	Degradation Set (Low Intensity) 2	15	-	-	0	10
2.1.04	Ranging Sweep	Surface Street	Degradation Set (Low Intensity) 3	15	-	-	0	10
2.1.05	Ranging Sweep	Surface Street	Degradation Set (Low Intensity) 4	15	-	-	0	10
2.1.06	Ranging Sweep	Surface Street	Degradation Set (Low Intensity) 5	15	-	-	0	10
2.1.07	Ranging Sweep	Surface Street	Degradation Set (Low Intensity) 6	15	-	-	0	10
2.1.08	Ranging Sweep	Surface Street	Baseline	15	-	-	0	10
2.1.09	Ranging Sweep	Surface Street	Degradation Set (Med Intensity) 1	15	-	-	0	10
2.1.10	Ranging Sweep	Surface Street	Degradation Set (High Intensity) 1	15	-	-	0	10
2.2.01	Ranging Sweep	Highway	Baseline	45	-	-	0	10
2.2.02	Ranging Sweep	Highway	Degradation Set (Low Intensity) 1	45	-	-	0	10
2.2.03	Ranging Sweep	Highway	Degradation Set (Low Intensity) 2	45	-	-	0	10
2.2.04	Ranging Sweep	Highway	Degradation Set (Low Intensity) 3	45	-	-	0	10
2.2.05	Ranging Sweep	Highway	Degradation Set (Low Intensity) 4	45	-	-	0	10
2.2.06	Ranging Sweep	Highway	Degradation Set (Low Intensity) 5	45	-	-	0	10
2.2.07	Ranging Sweep	Highway	Degradation Set (Low Intensity) 6	45	-	-	0	10
2.2.08	Ranging Sweep	Highway	Baseline	45	-	-	0	10
2.2.09	Ranging Sweep	Highway	Degradation Set (Med Intensity) 1	45	-	-	0	10
2.2.10	Ranging Sweep	Highway	Degradation Set (High Intensity) 1	45	-	-	0	10

Appendix G: Component Testing – Degradation Matrix

File Code	LR(Far) & SR(Near) 77 GHz	SR 24 GHz	SR 77 GHz	LR 24 GHz	32 beams	128 beams	Solid-State	Budget	Object Camera	Machine Vision
1.1.01										
1.1.02	Blacktop	Bondo	Epoxy	SRE	Offgas	Sandblast	Sealant	Shellac	Tint	
1.1.03	Spruce	Blacktop	Bondo	Epoxy		Offgas	Sandblast	Sealant	Shellac	Tint
1.1.04	SRE	Spruce	Blacktop	Bondo	Tint		Offgas	Sandblast	Sealant	Shellac
1.1.05	Epoxy	SRE	Spruce	Blacktop	Shellac	Tint		Offgas	Sandblast	Sealant
1.1.06	Bondo	Epoxy	SRE	Spruce	Sealant	Shellac	Tint		Offgas	Sandblast
1.1.07	Blacktop	Bondo	Epoxy	SRE	Sandblast	Sealant	Shellac	Tint		Offgas
1.1.08										
1.1.09	Blacktop	Bondo	Epoxy	JSRE	Offgas	Sandblast	Sealant	Shellac	Tint	
1.1.10	Blacktop	Bondo	Epoxy	SRE	Offgas	Sandblast	Sealant	Shellac	Tint	
1.2.01										
1.2.02	Blacktop	Bondo	Epoxy	SRE	Offgas	Sandblast	Sealant	Shellac	Tint	
1.2.03	Spruce	Blacktop	Bondo	Epoxy		Offgas	Sandblast	Sealant	Shellac	Tint
1.2.04	SRE	Spruce	Blacktop	Bondo	Tint		Offgas	Sandblast	Sealant	Shellac
1.2.05	Epoxy	SRE	Spruce	Blacktop	Shellac	Tint		Offgas	Sandblast	Sealant
1.2.06	Bondo	Epoxy	SRE	Spruce	Sealant	Shellac	Tint		Offgas	Sandblast
1.2.07	Blacktop	Bondo	Epoxy	SRE	Sandblast	Sealant	Shellac	Tint		Offgas
1.2.08										
1.2.09	Blacktop	Bondo	Epoxy	SRE	Offgas	Sandblast	Sealant	Shellac	Tint	
1.2.10	Blacktop	Bondo	Epoxy	SRE	Offgas	Sandblast	Sealant	Shellac	Tint	
2.1.01										
2.1.02	Blacktop	Bondo	Epoxy	SRE	Offgas	Sandblast	Sealant	Shellac	Tint	
2.1.03	Spruce	Blacktop	Bondo	Epoxy		Offgas	Sandblast	Sealant	Shellac	Tint
2.1.04	SRE	Spruce	Blacktop	Bondo	Tint		Offgas	Sandblast	Sealant	Shellac
2.1.05	Epoxy	SRE	Spruce	Blacktop	Shellac	Tint		Offgas	Sandblast	Sealant
2.1.06	Bondo	Epoxy	SRE	Spruce	Sealant	Shellac	Tint		Offgas	Sandblast
2.1.07	Blacktop	Bondo	Epoxy	SRE	Sandblast	Sealant	Shellac	Tint		Offgas
2.1.08										
2.1.09	Blacktop	Bondo	Epoxy	SRE	Offgas	Sandblast	Sealant	Shellac	Tint	
2.1.10	Blacktop	Bondo	Epoxy	SRE	Offgas	Sandblast	Sealant	Shellac	Tint	
2.2.01										
2.2.02	Blacktop	Bondo	Epoxy	SRE	Offgas	Sandblast	Sealant	Shellac	Tint	
2.2.03	Spruce	Blacktop	Bondo	Epoxy		Offgas	Sandblast	Sealant	Shellac	Tint
2.2.04	SRE	Spruce	Blacktop	Bondo	Tint		Offgas	Sandblast	Sealant	Shellac
2.2.05	Epoxy	SRE	Spruce	Blacktop	Shellac	Tint		Offgas	Sandblast	Sealant
2.2.06	Bondo	Epoxy	SRE	Spruce	Sealant	Shellac	Tint		Offgas	Sandblast
2.2.07	Blacktop	Bondo	Epoxy	SRE	Sandblast	Sealant	Shellac	Tint		Offgas
2.2.08										
2.2.09	Blacktop	Bondo	Epoxy	SRE	Offgas	Sandblast	Sealant	Shellac	Tint	
2.2.10	Blacktop	Bondo	Epoxy	SRE	Offgas	Sandblast	Sealant	Shellac	Tint	

Appendix H: Average Number of Gated Returns by Range

As described under Radar Data Analysis for TV Extraction, point cloud data within the bounding box is known as gated return, and it was a post-processing of the data needed for the radars that output point cloud data. The number of gated returns were plotted by distance to determine if there was an effect between the degraded and non-degraded cases. Figure 59 shows the closest range gate, 0 to 45 meters. The next two range gates, 45 to 100 meters and 100 to 180 meters, are shown in Figure 82 and Figure 83, respectively. Figure 82 shows that the SRE (low) degradation for the LR 77GHz Near showed significant decrease in the average number of returns. Figure 83 shows that the following radars have a low average number of returns: SR 77GHz, SR 24GHz, and LR 24GHz.

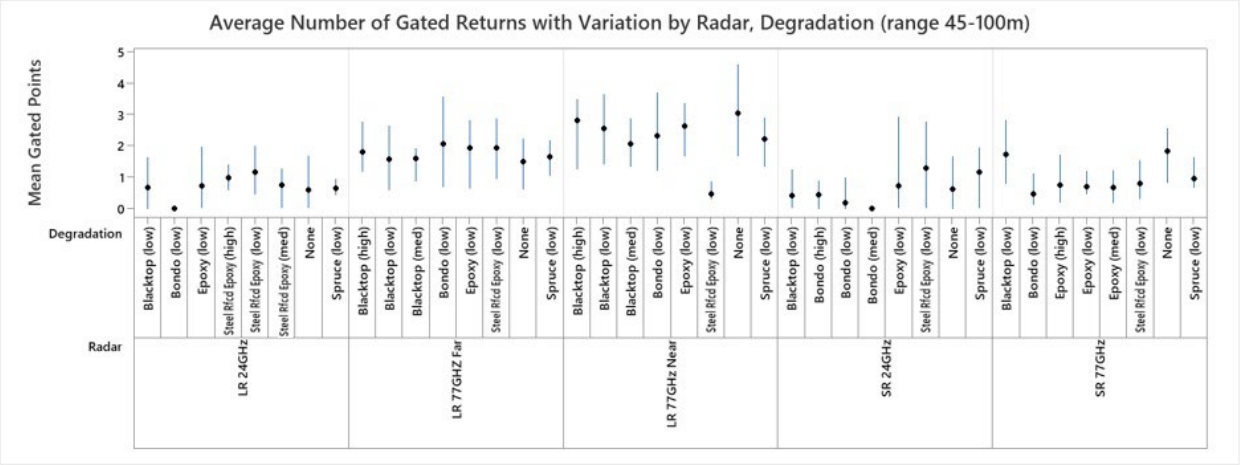

Figure 82. Average number of gated returns, range 45-100m

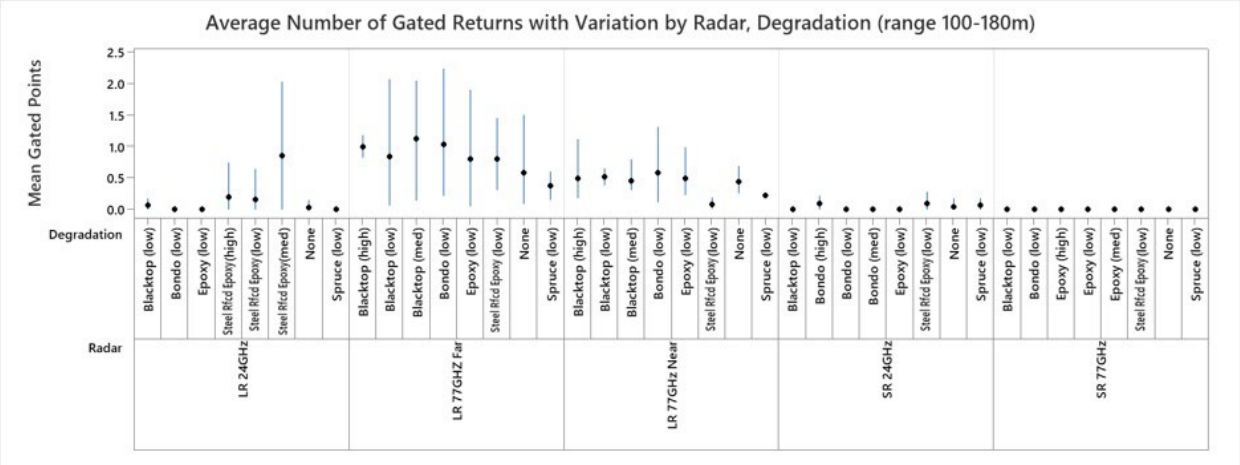

Figure 83. Average number of gated returns, range 100-180m

Appendix I: Detailed Analysis Results

There is a wide variety of responses to the degradations in the data. Some degraded responses are no different than baseline (e.g., Budget lidar with tint). Some degraded responses vary across sensors (e.g., SR 24GHz versus SR 77GHz with Blacktop). Some degraded responses are not linear with intensity (e.g., Object Camera with tint). Some degraded responses nonintuitively increase in accuracy with increased degradation intensity (e.g., SR 24GHz with Bondo). This could be due to the elimination of low power returns, leaving only the most reflective features of the TV in the returned sensor data. This is borne out in the reduced STD of error across the SR 24GHz Bondo data.

Note: The following sensors were not always physically available for data collection: 128-beam, budget, and object camera. Therefore, an empty plot related to these sensors is because "sensor was not available for data collection." On the other hand, empty plots for other sensors, such as the ones belonging to radar, are empty because the degradation applied was so severe that the sensor did not provide any output data.

All the figures in this appendix have the same format. Figure 84 was arbitrarily chosen as an example to explain the figure contents.

The x-axis shows the type of degradation applied. In the case of Figure 84: none, blacktop, Bondo/mesh, epoxy, SRE, and spruce (i.e., pine needles). Degradation tested match those listed in Table 23. The y-axis shows the mean and 1 standard deviation (STD) of the sensor output being tested. The standard deviation is displayed by the whiskers. Whiskers are the vertical bars originating from the mean value. The legend in each figure shows the intensity of the degradation applied, such as none, low, medium, and high. The title shows the dynamic vehicle maneuver executed, in the case of Figure 84, a lane slalom at low speed. The subtitle shows the sensor under test. In the case of Figure 84: LR 24GHz (object radar), SR 77Hz (point cloud radar), SR 24GHz (object radar), LR 77GHz Near (point cloud radar), and LR 77GHz Far (point cloud radar). Radars under tests are listed in Table 21.

Mean Error Figures

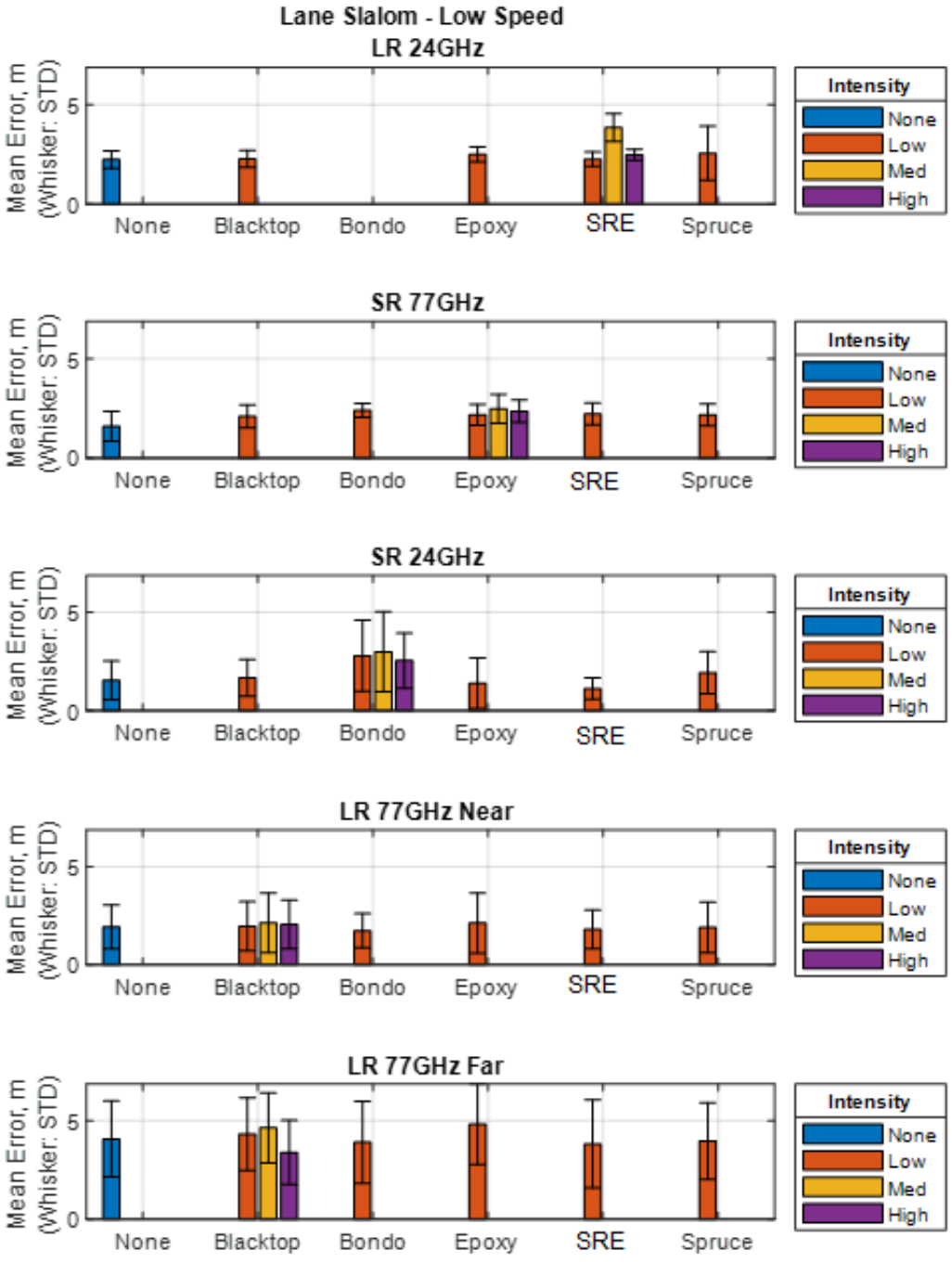

Figure 84. Mean error for lane slalom at low speed: Radars

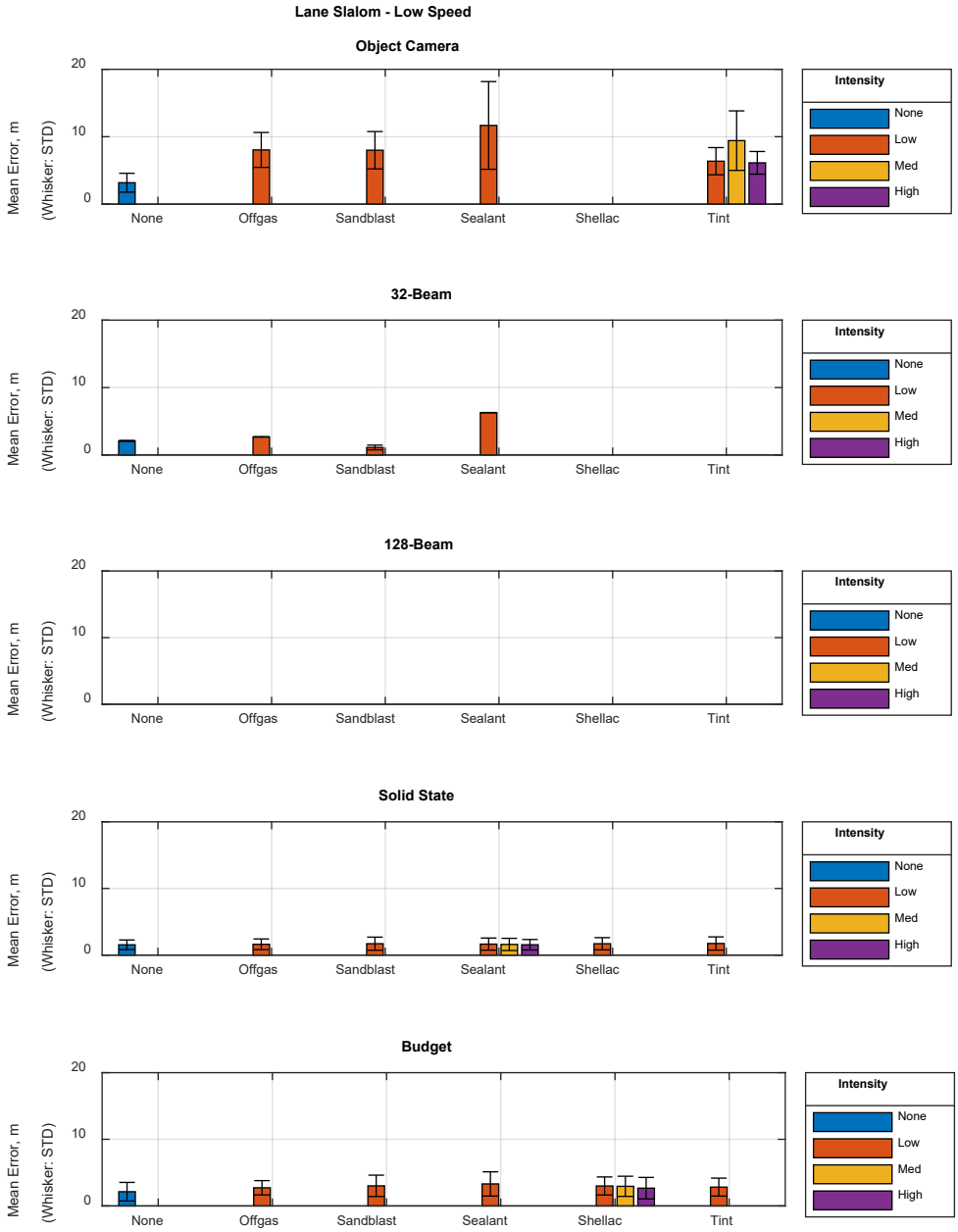

Figure 85. Mean error for lane slalom at low speed: Camera and lidars

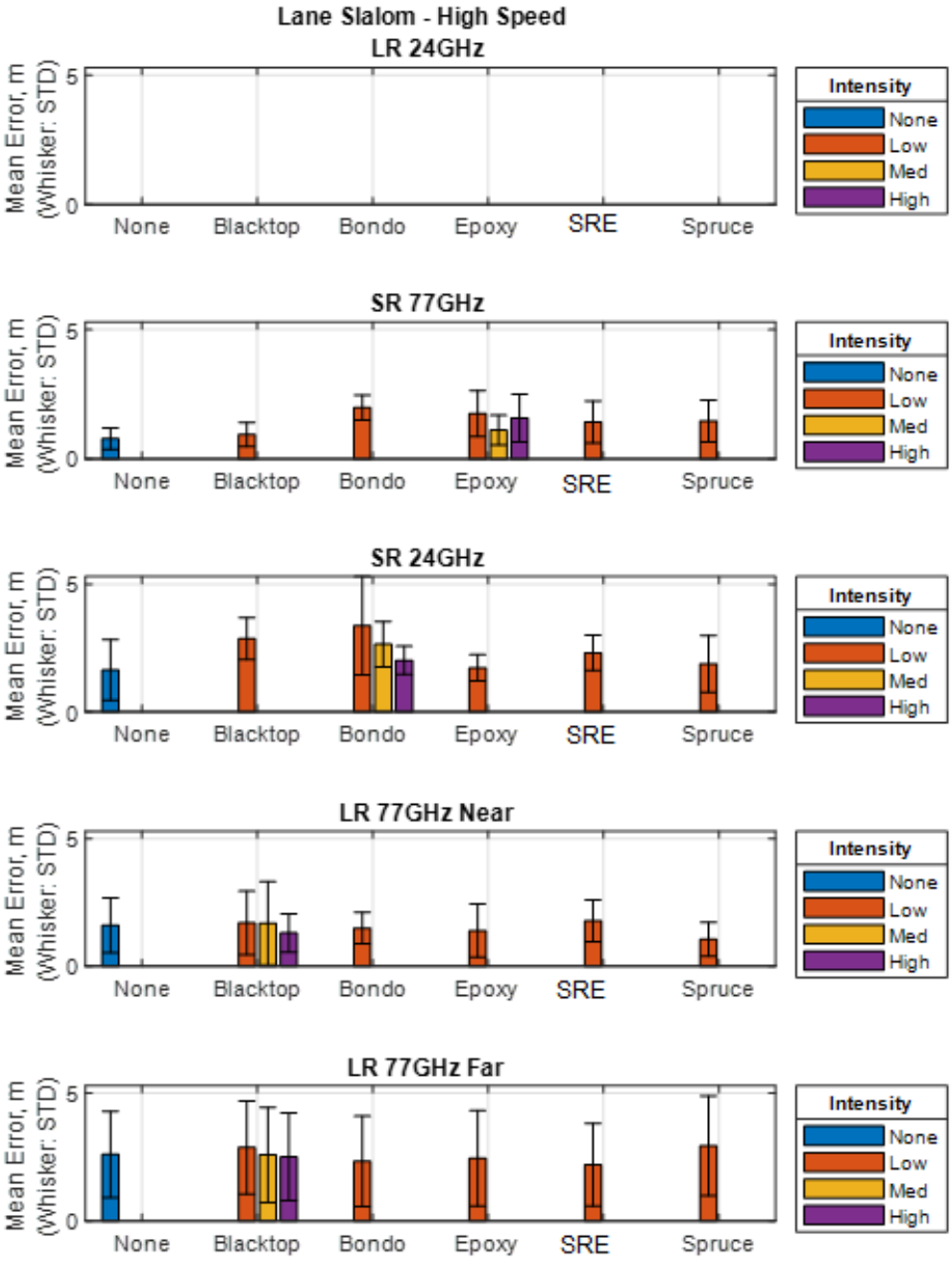

Figure 86. Mean error for lane slalom at high speed: Radars

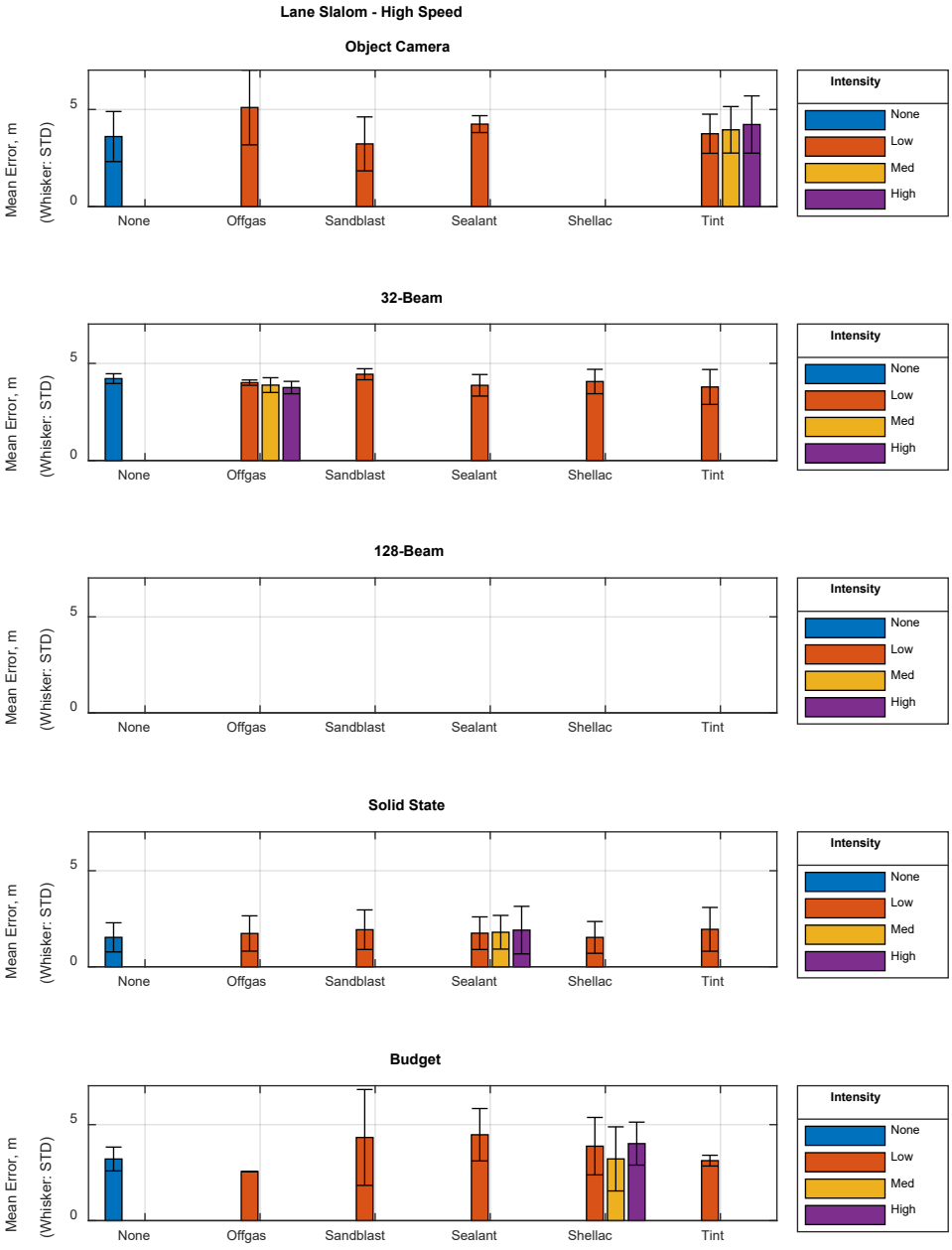

Figure 87. Mean error for lane slalom at high speed: Camera and lidars

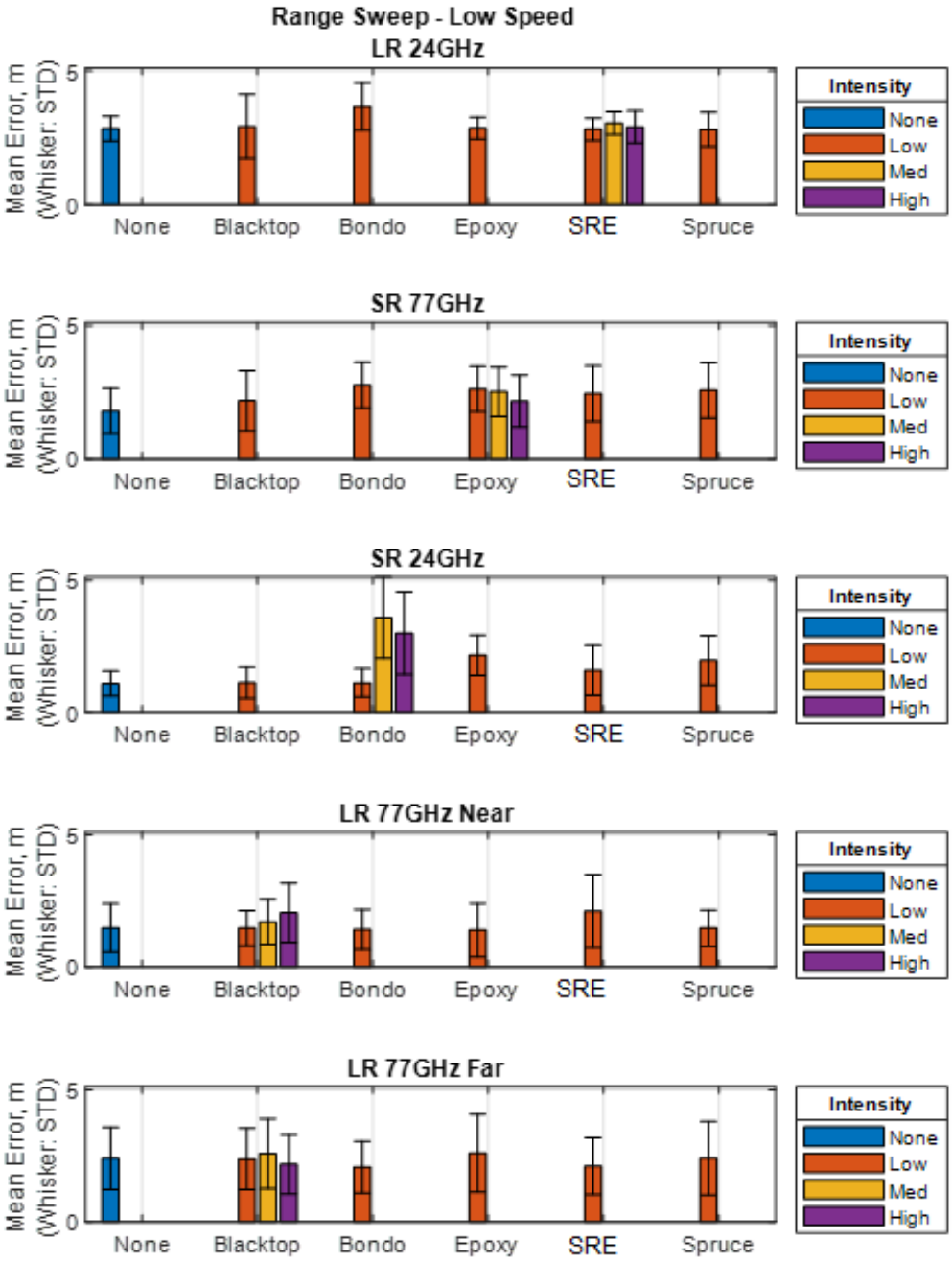

Figure 88. Mean error for range sweep at low speed: Radars

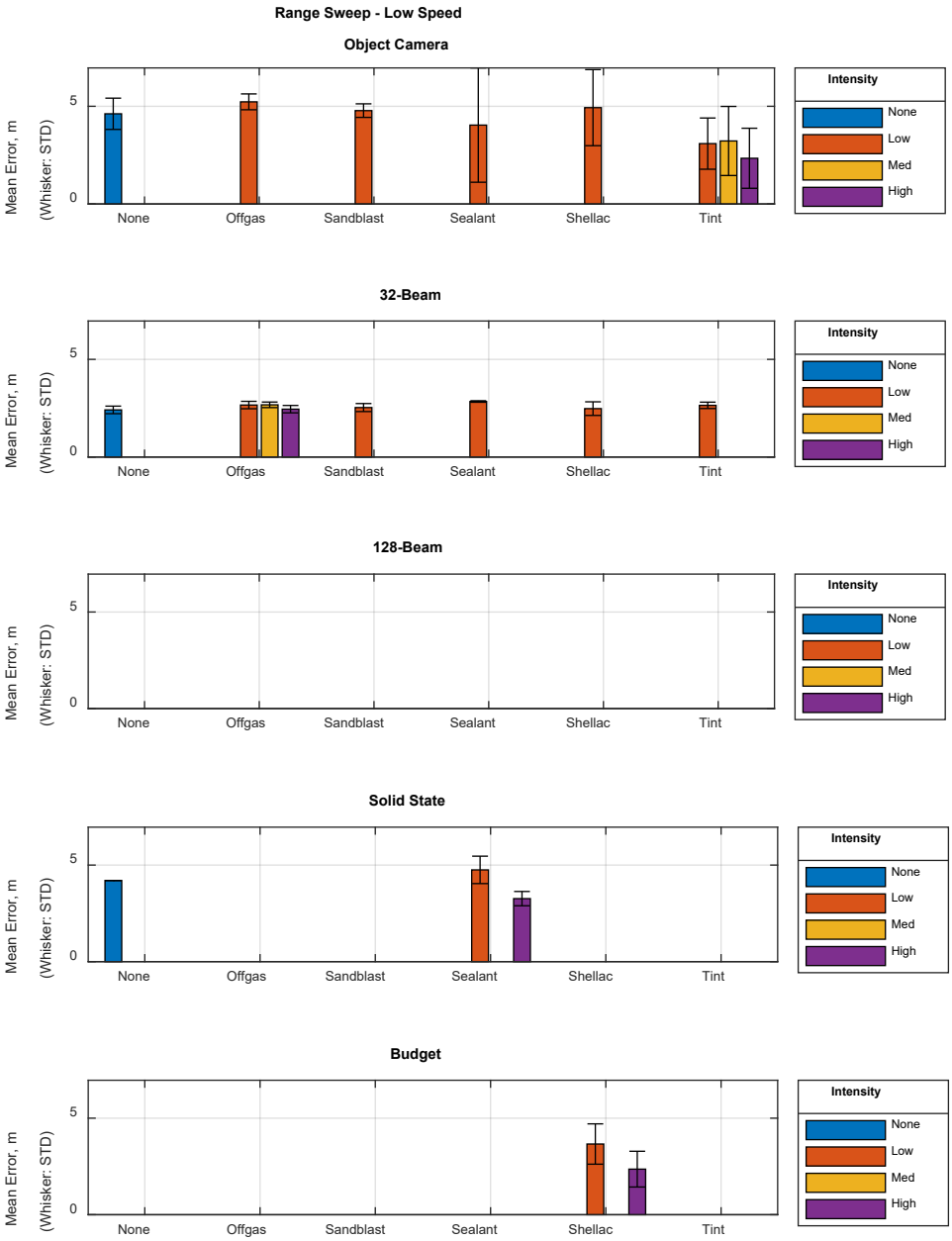

Figure 89. Mean error for range sweep at low speed: Camera and lidars

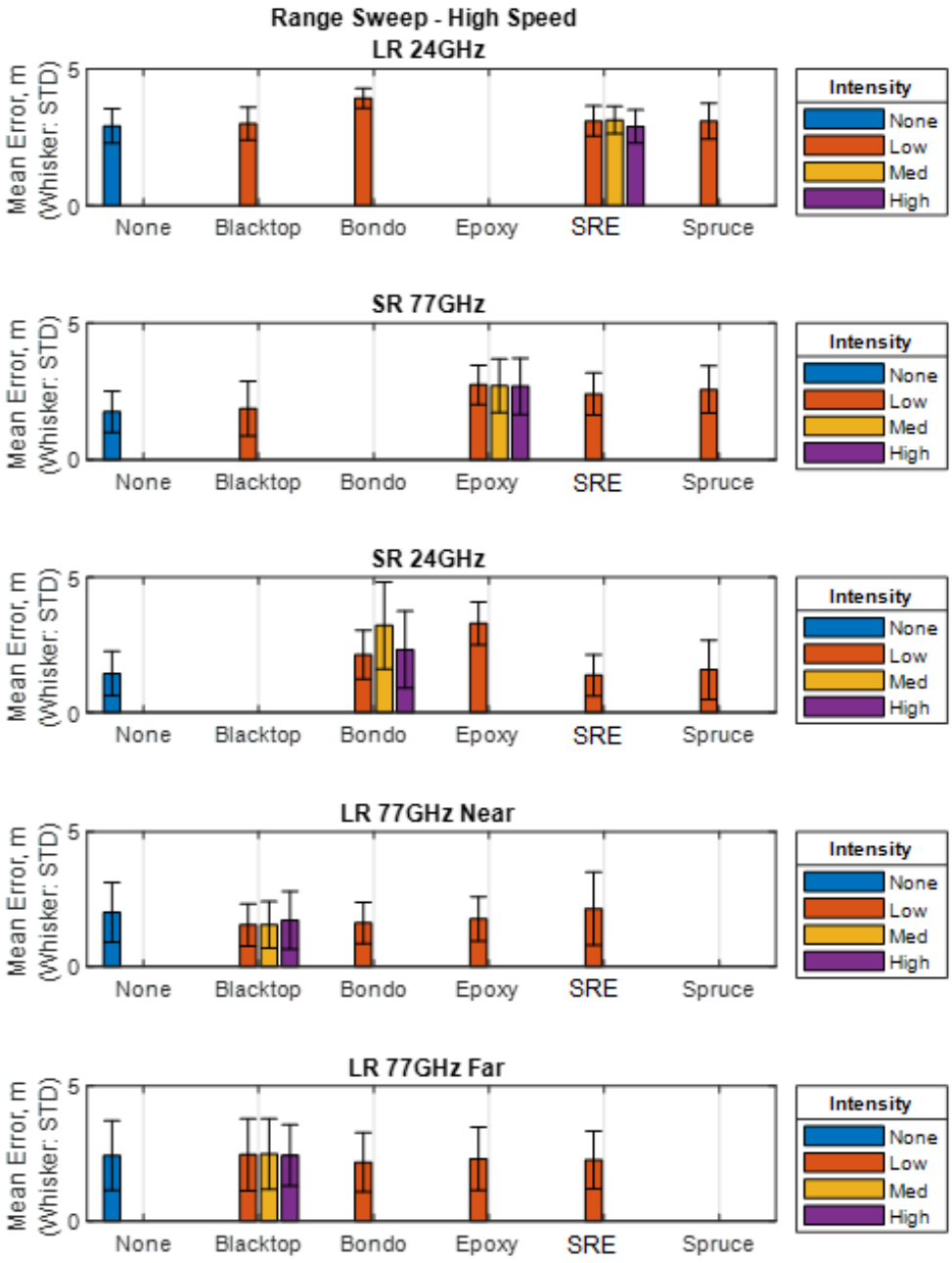

Figure 90. Mean error for range sweep at high speed: Radars

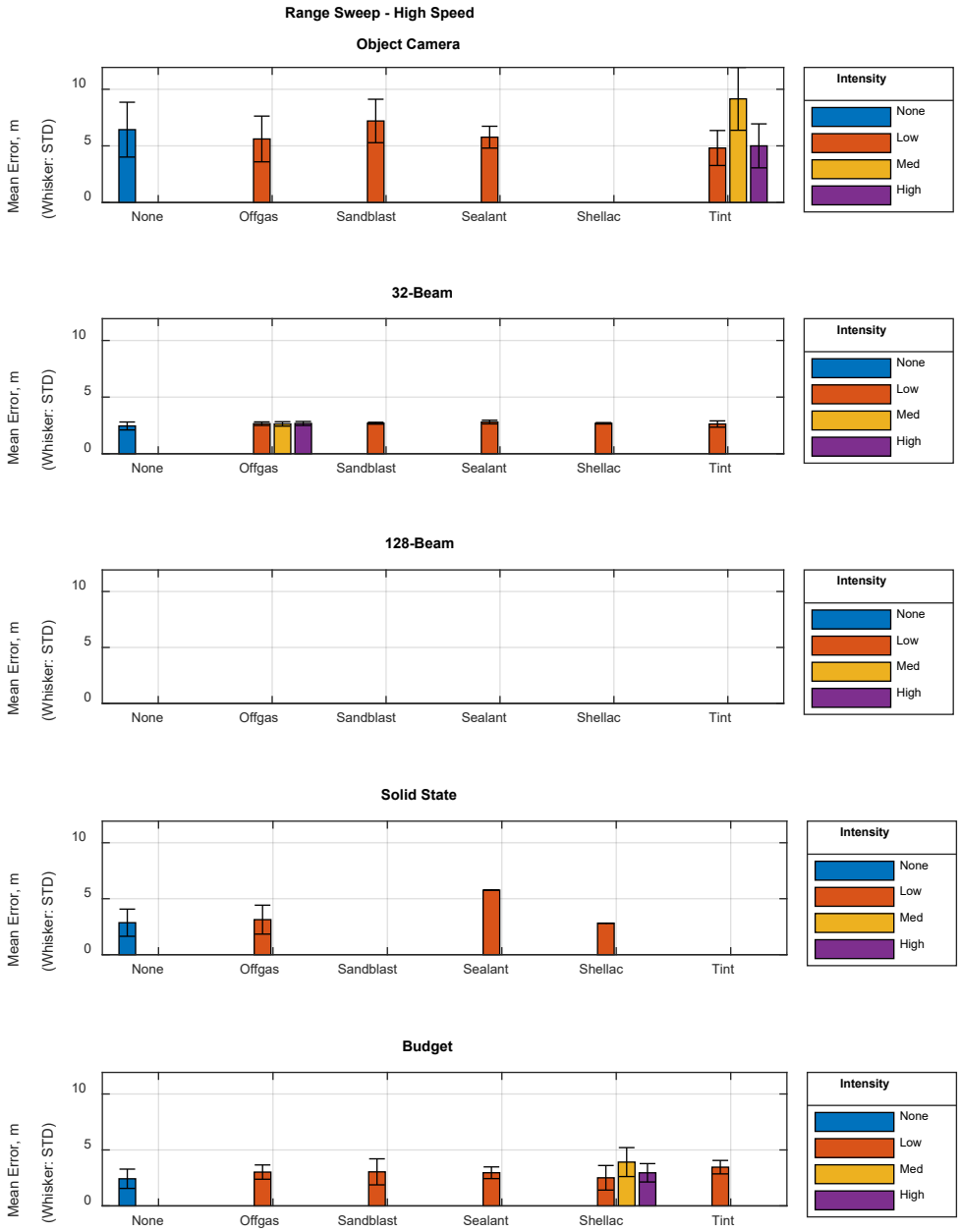

Figure 91. Mean error for range sweep at high speed: Camera and lidars

Mean Number of Points Returned

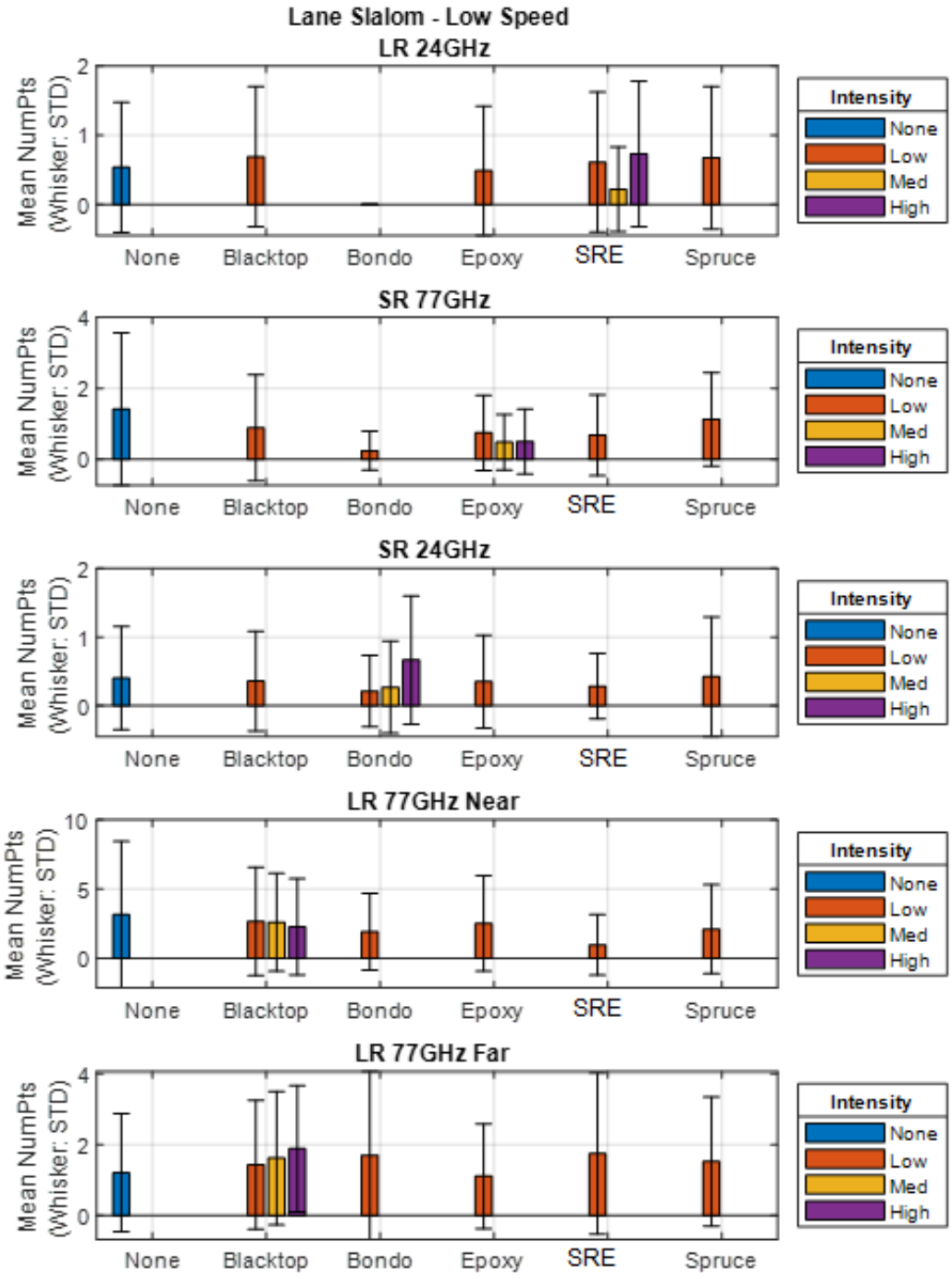

Figure 92. Mean number of points returned for lane slalom at low speed: Radars

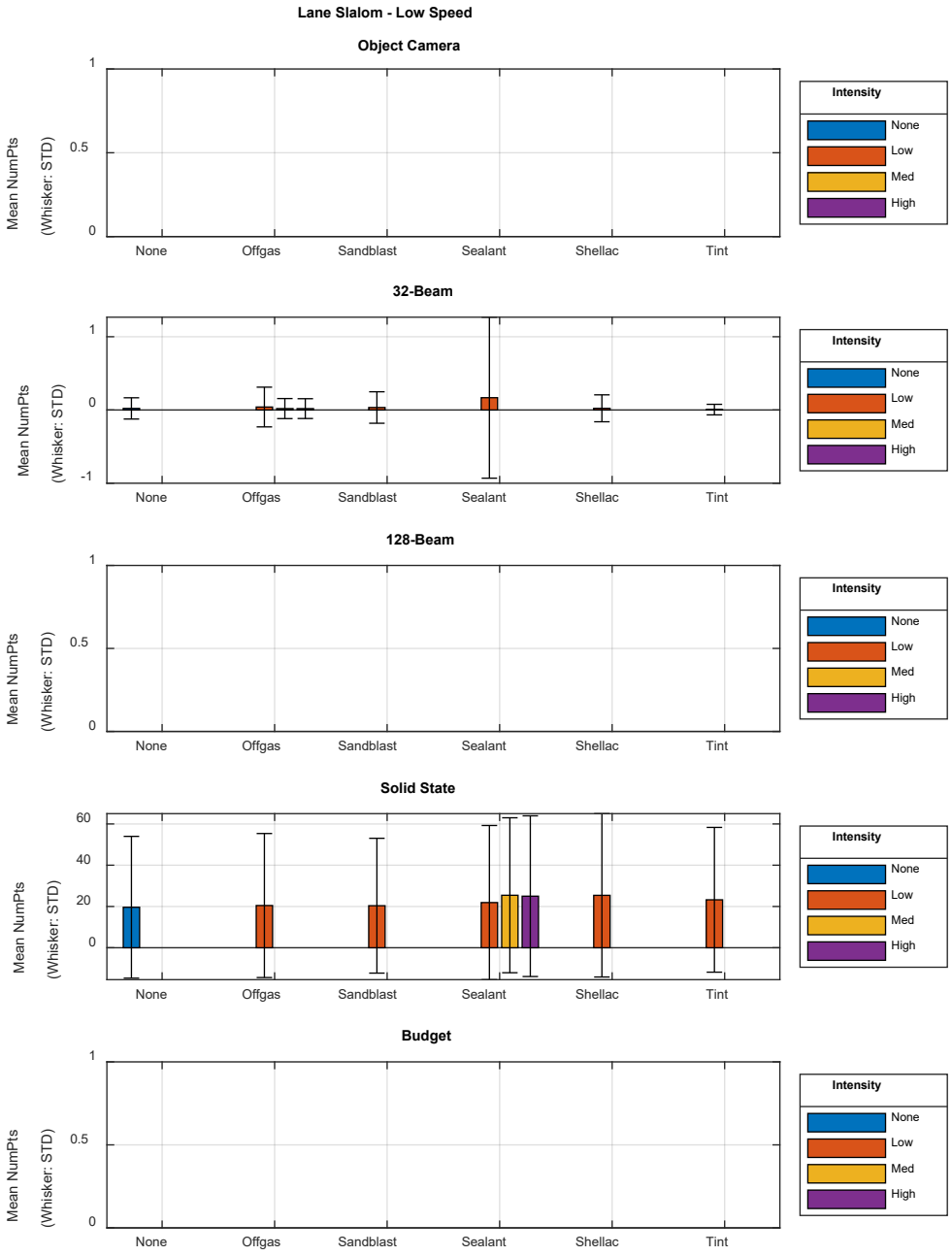

Figure 93. Mean number of points returned for lane slalom at low speed: Camera and lidars

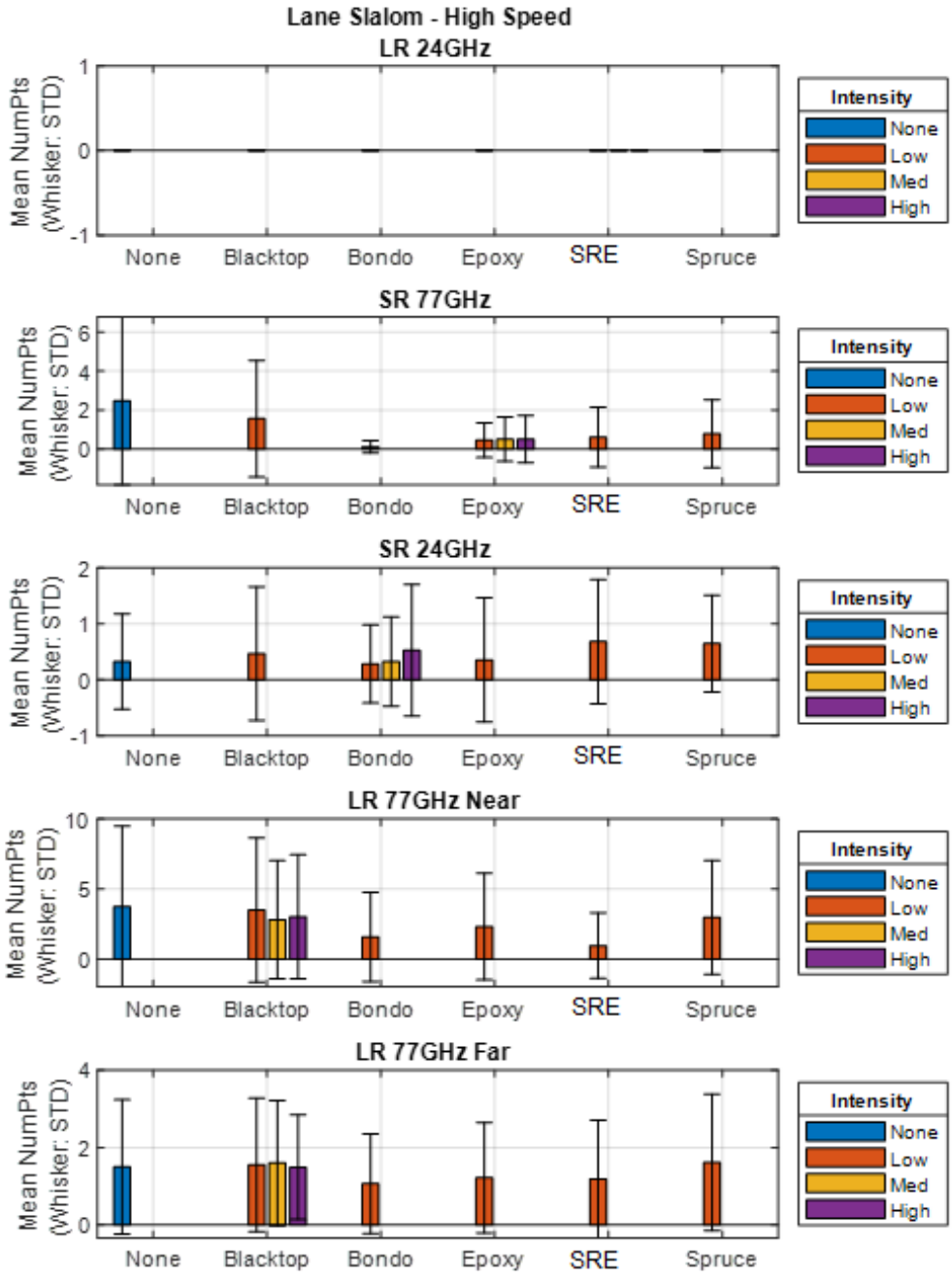

Figure 94. Mean number of points returned for lane slalom at high speed: Radars

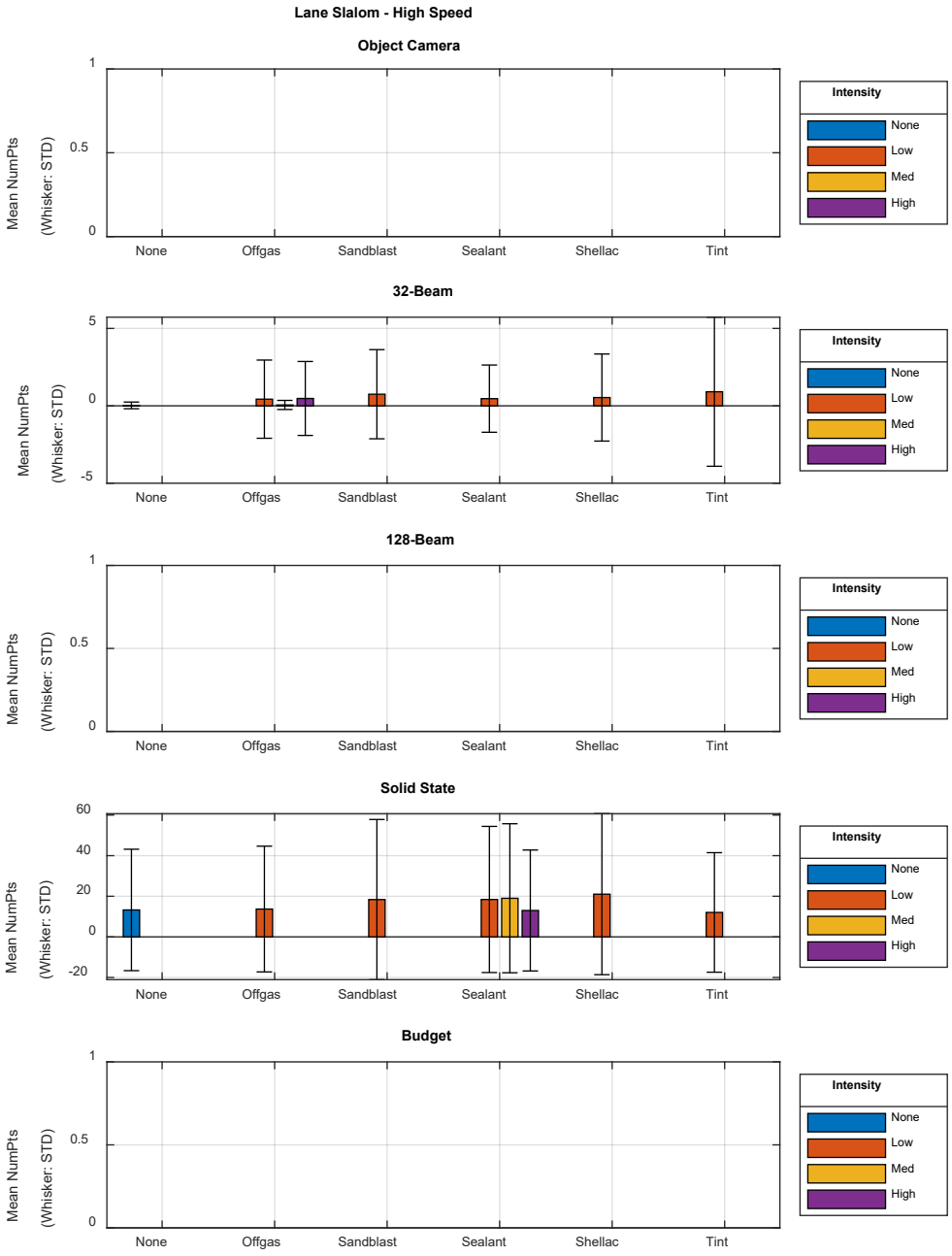

Figure 95. Mean number of points returned for lane slalom at high speed: Camera and lidars

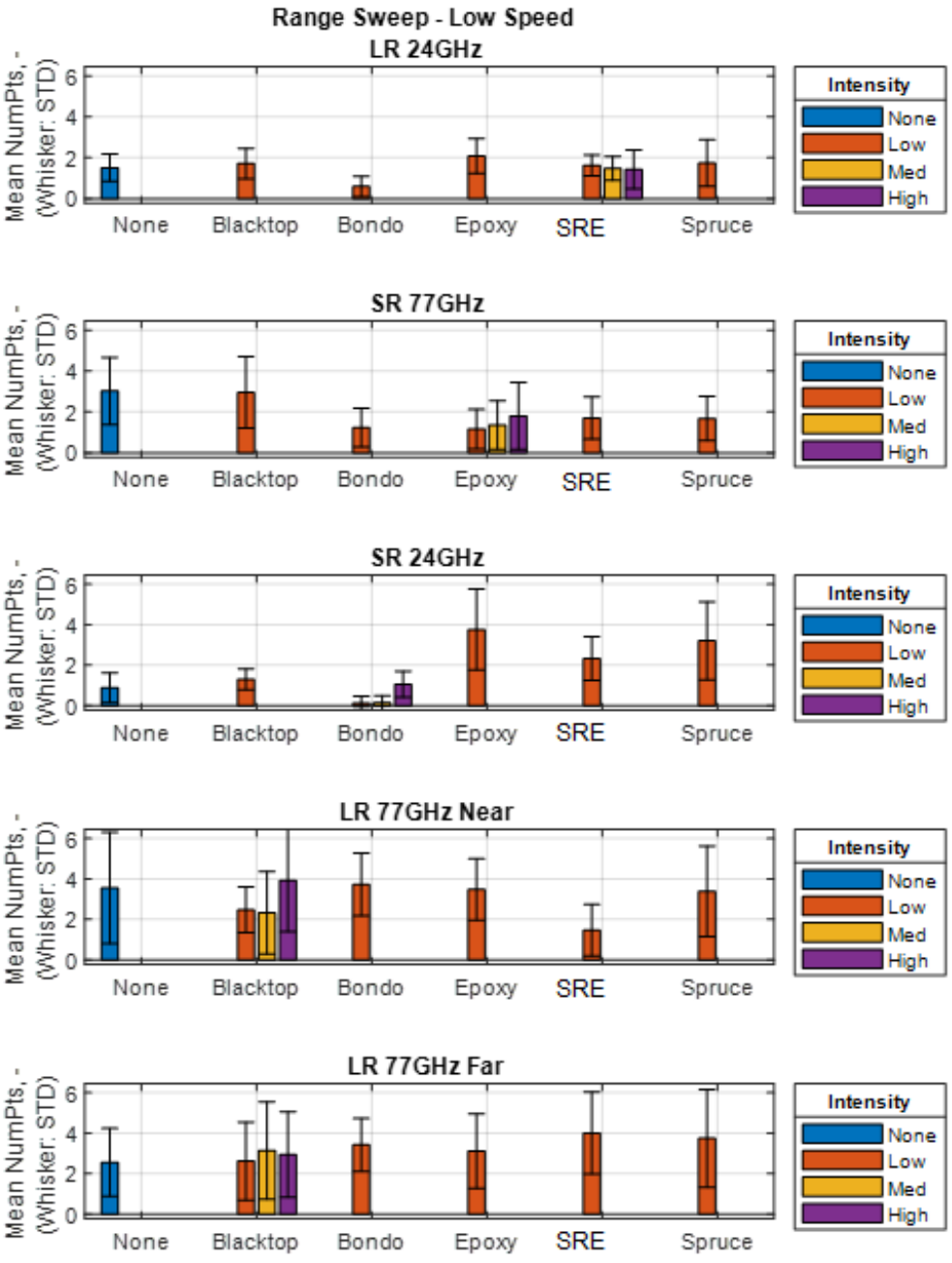

Figure 96. Mean number of points returned for range sweep at low speed: Radars

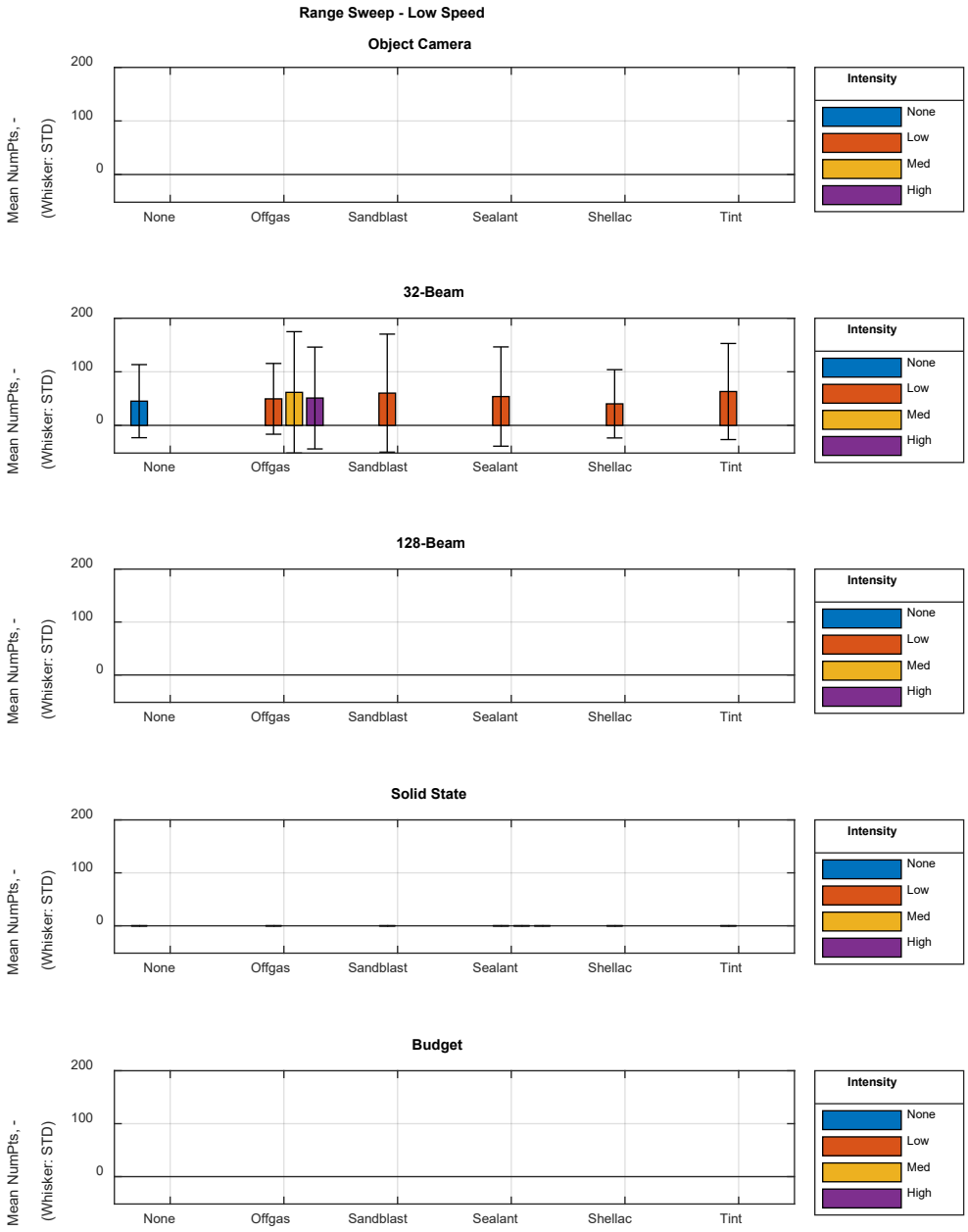

Figure 97. Mean number of points returned for range sweep at low speed: Camera and lidars

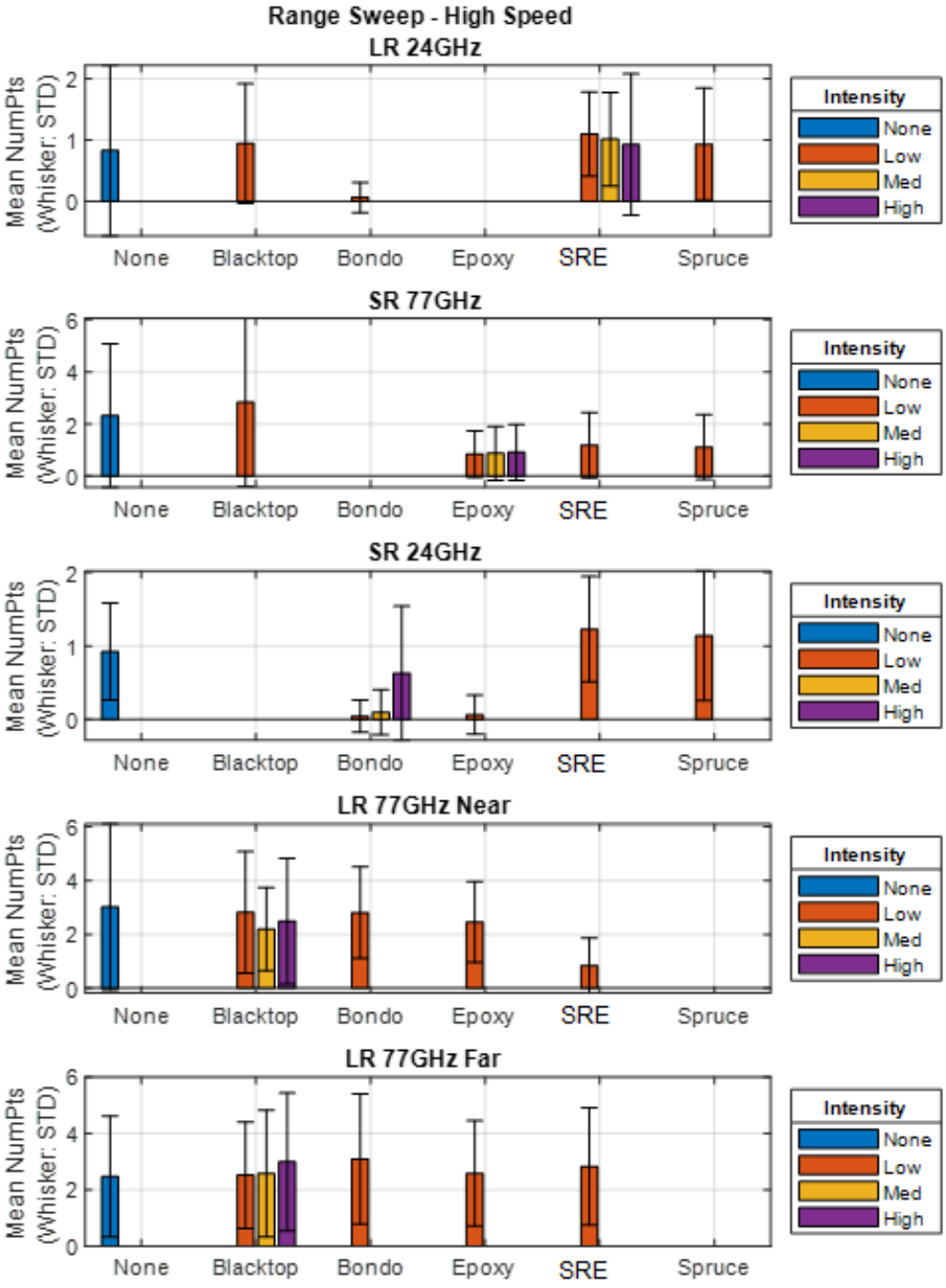

Figure 98. Mean number of points returned for range sweep at high speed: Radars

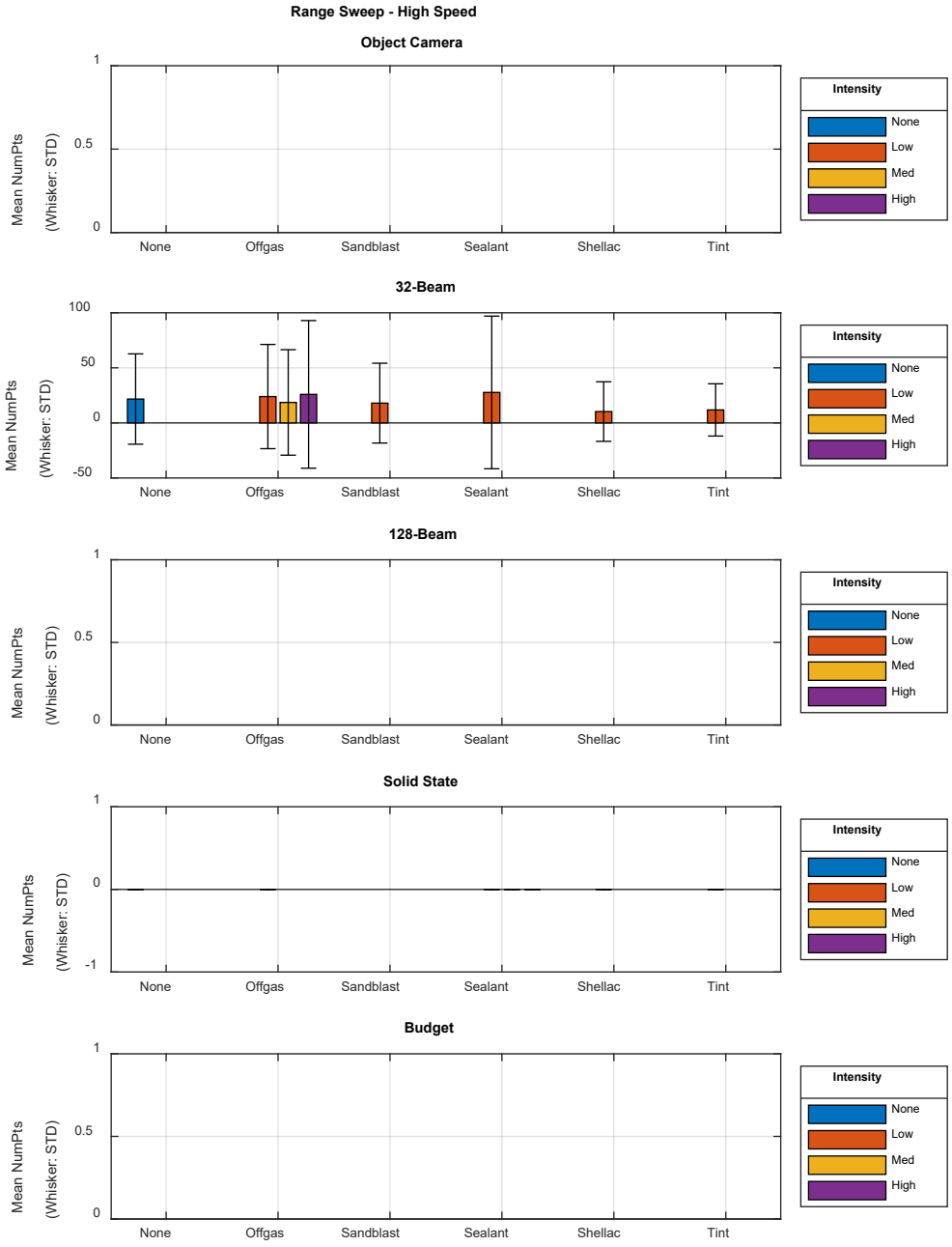

Figure 99. Mean number of points returned for range sweep at high speed: Camera and lidars

Mean Intensity Plots

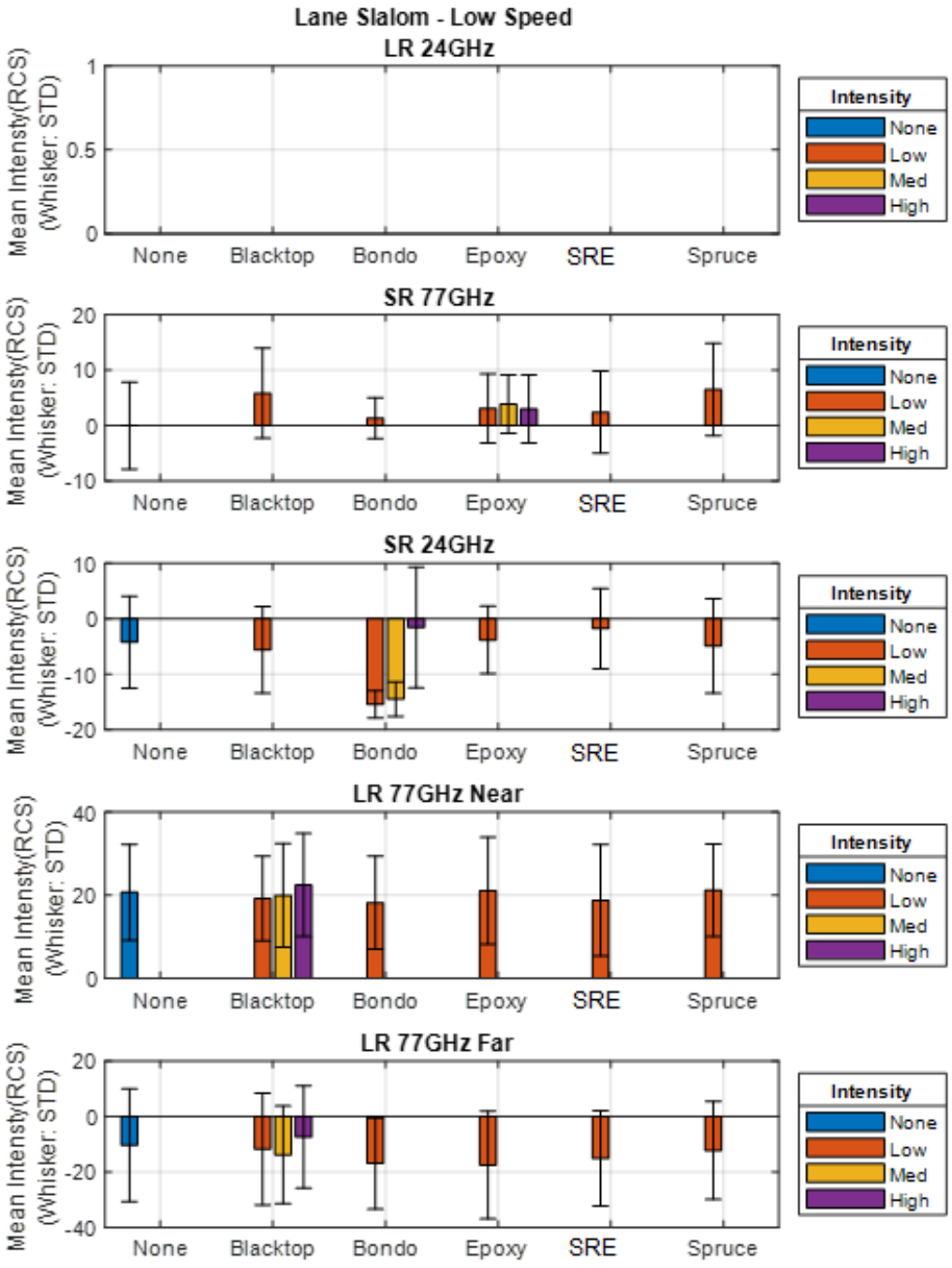

Figure 100. Mean intensity for lane slalom at low speed: Radars

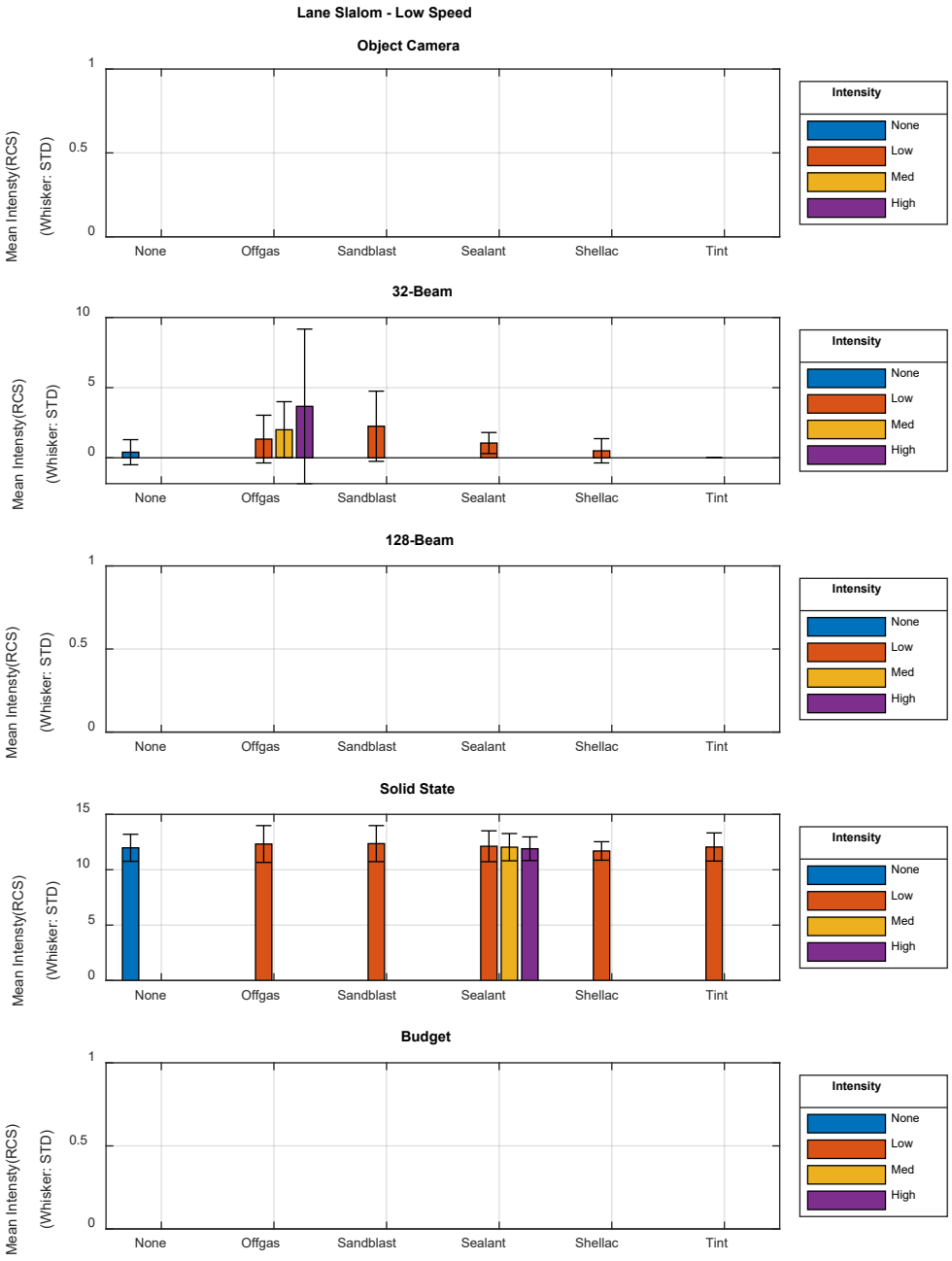

Figure 101. Mean intensity for lane slalom at low speed: Camera and lidars

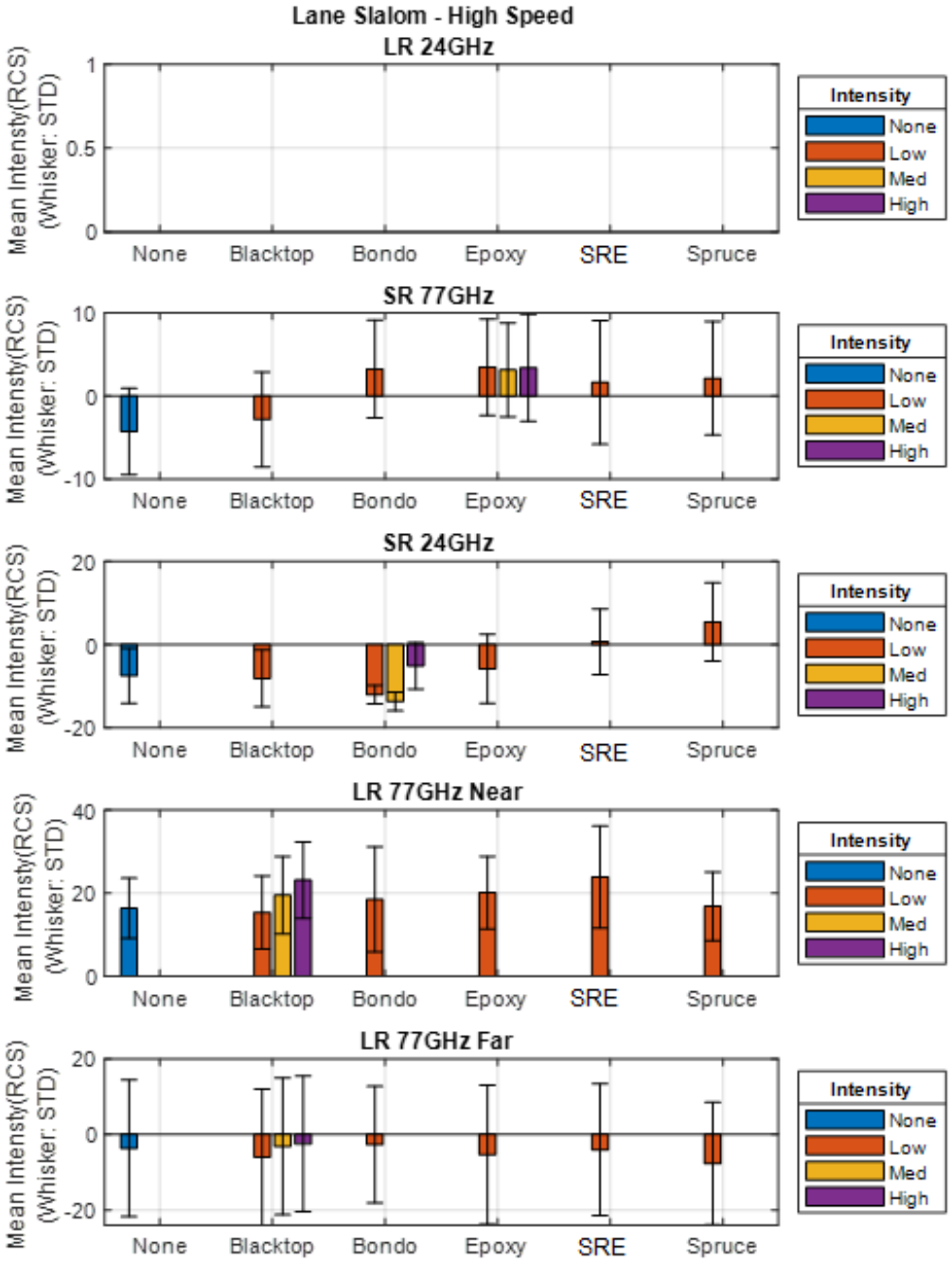

Figure 102. Mean intensity for lane slalom at high speed: Radars

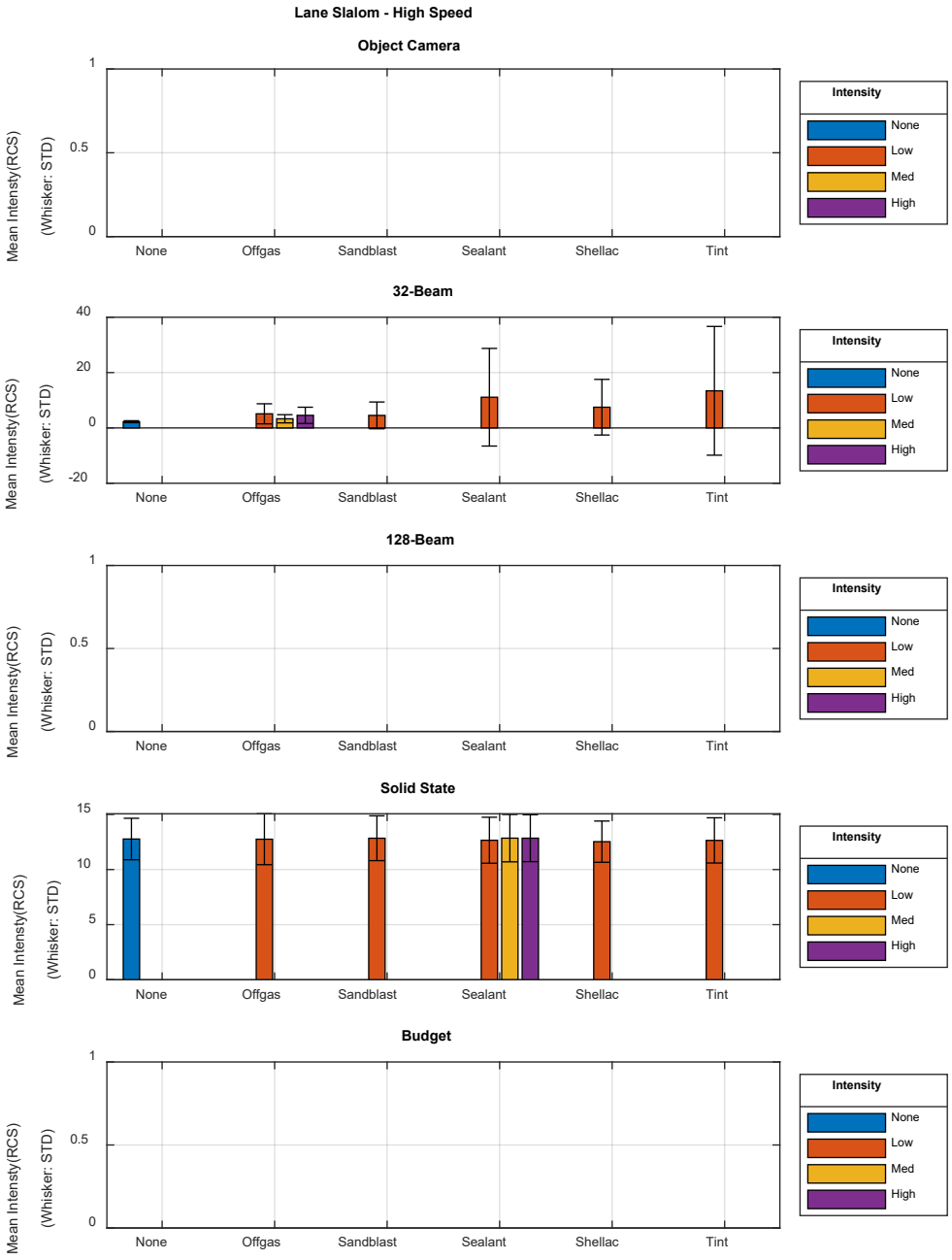

Figure 103. Mean intensity for lane slalom at high speed: Camera and lidars

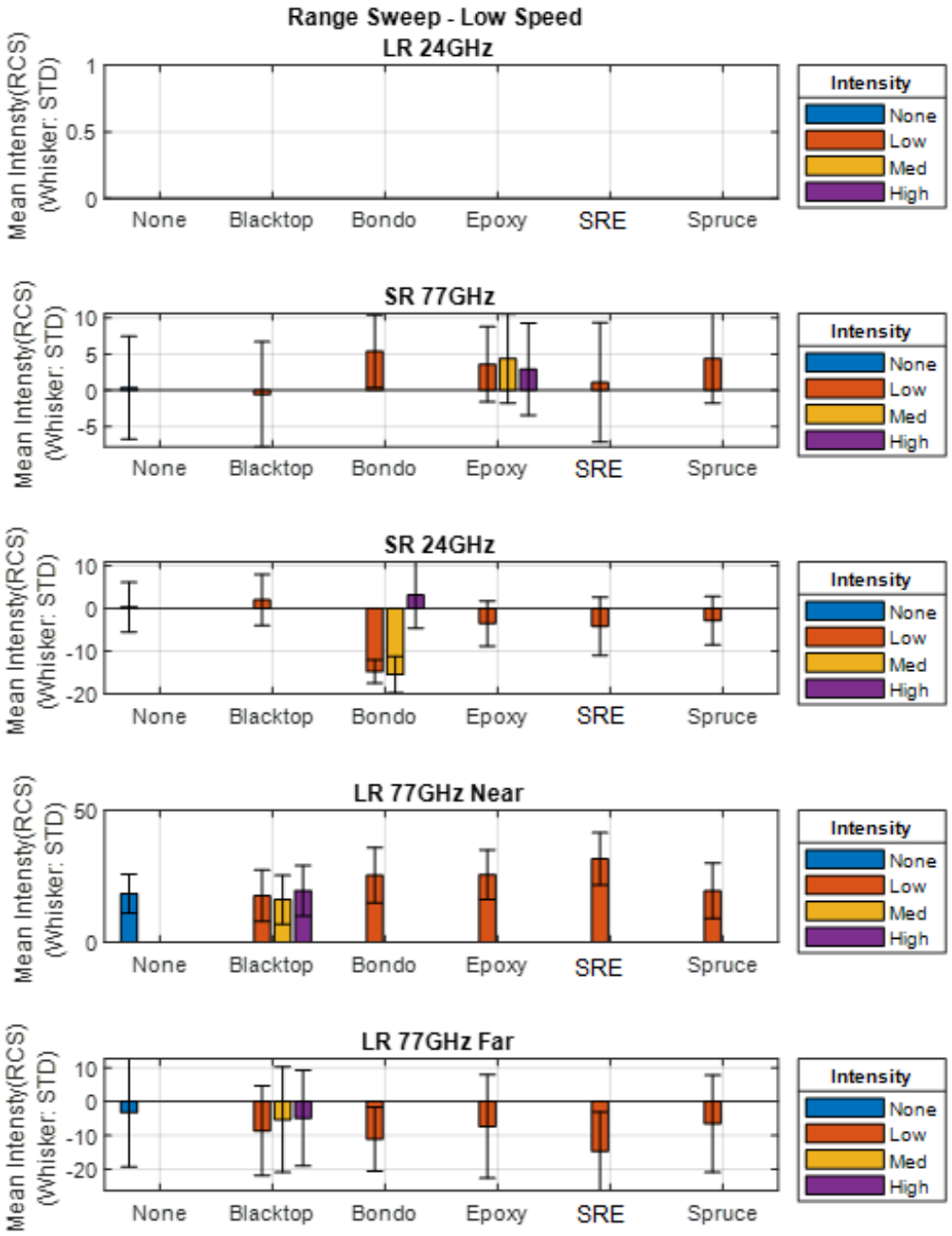

Figure 104. Mean intensity for range sweep at low speed: Radars

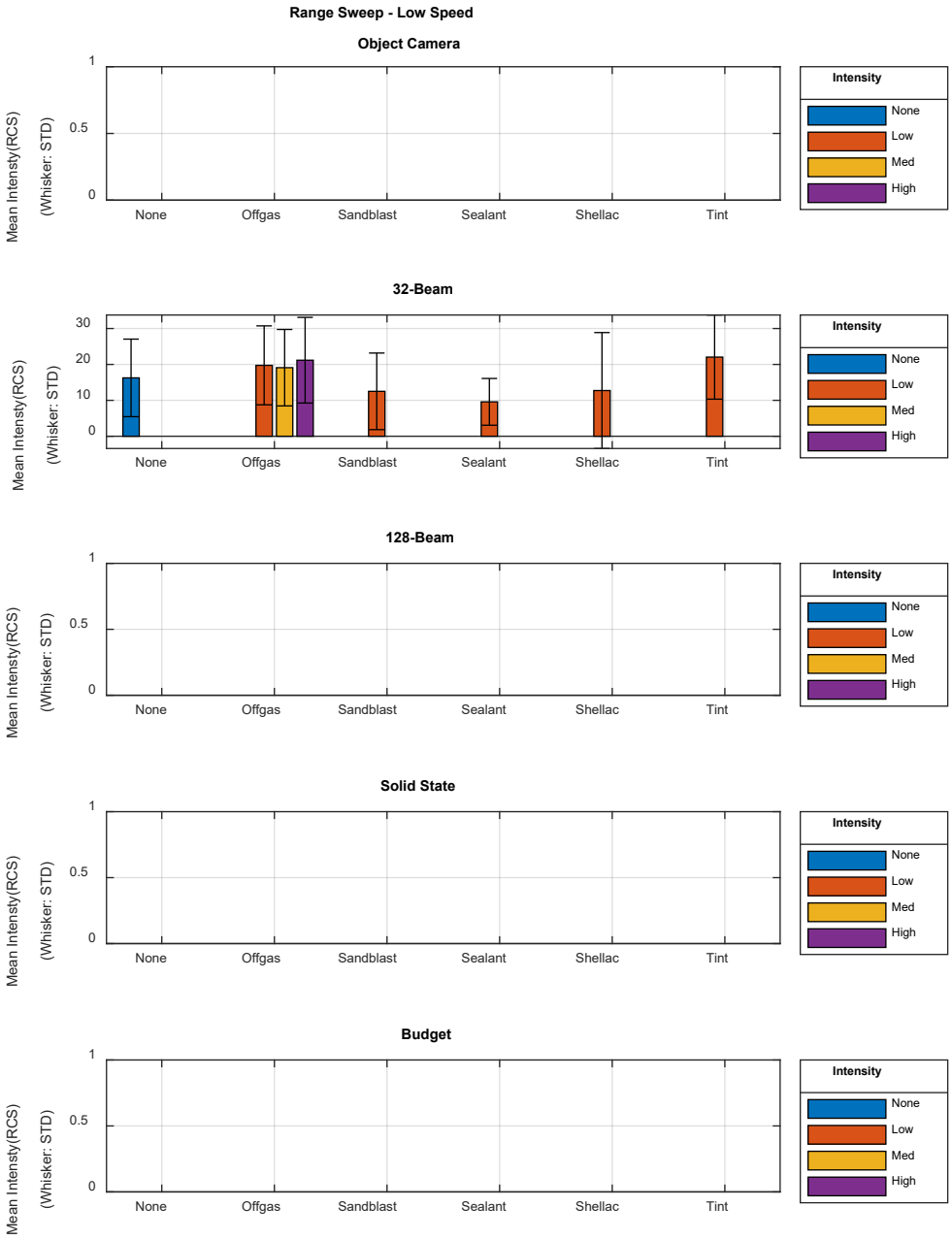

Figure 105. Mean intensity for range sweep at low speed: Camera and lidars

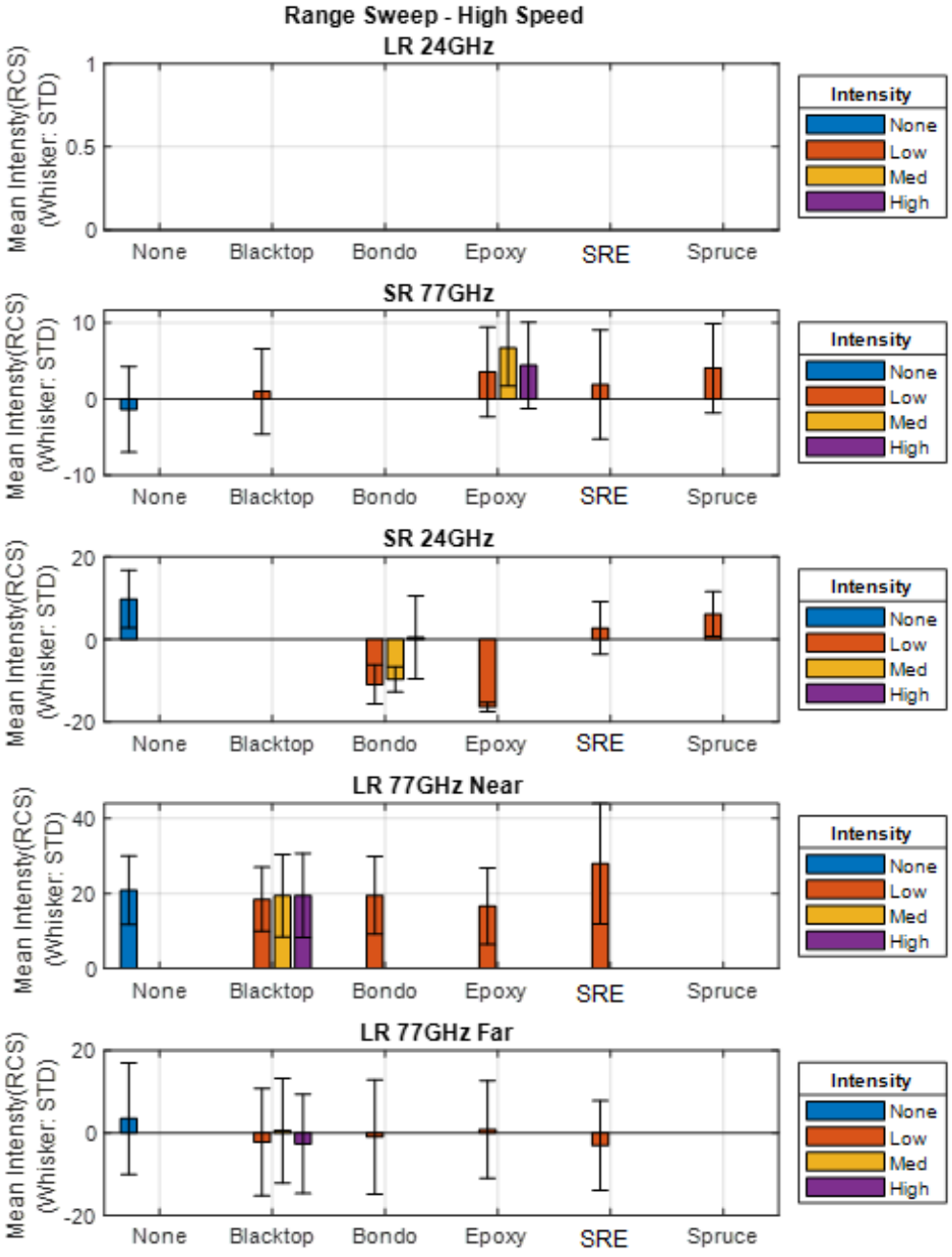

Figure 106. Mean intensity for range sweep at high speed: Radars

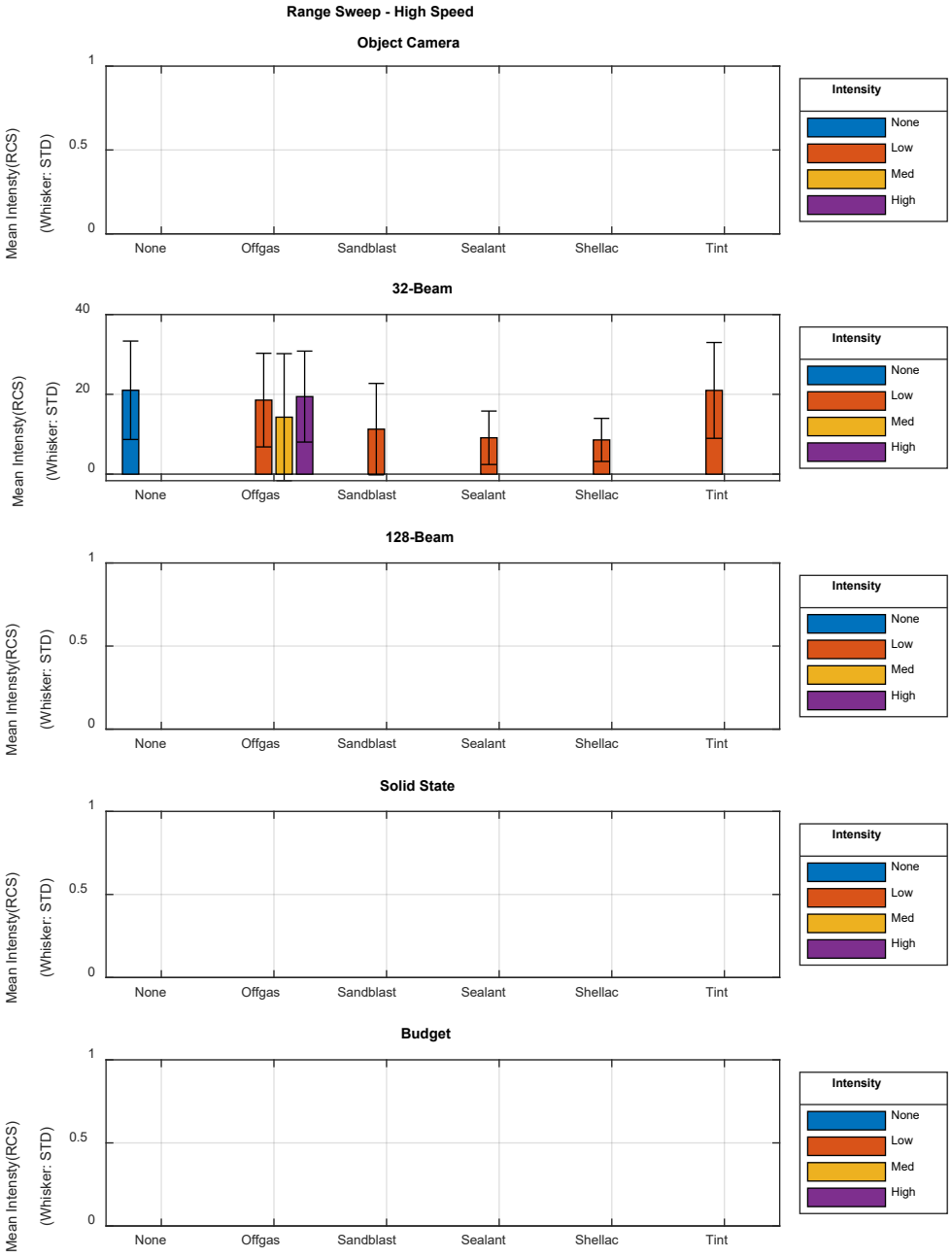

Figure 107. Mean intensity for range sweep at high speed: Camera and lidars

Appendix J: System Level Test Procedures

References and Standards used for ADAS Testing

- Longitudinal
  - Adaptive Cruise Control
    - ISO, 2018, *15622, Intelligent transport systems — Adaptive cruise control systems — Performance requirements and test procedures.*
    - Shin, 2013, *The Development of the ACC System Performance Evaluation Using VRS.*
  - Forward Collision Warning
    - SAE International, 2015a, *J3029, Forward Collision Warning and Mitigation Vehicle Test Procedure - Truck and Bus.*
    - NHTSA, 2013a, *Forward Collision Warning System Confirmation Test.*
  - Automatic Emergency Braking
    - SAE International, 2017, J3087, *Automatic Emergency Braking (AEB) System Performance Testing.*
    - IIHS, 2013, *Autonomous Emergency Braking Test Protocol* (Version I).
    - IIHS, 2018. *Pedestrian Autonomous Emergency Braking Test Protocol* (Version I).
    - IIHS, 2019b, *Pedestrian Autonomous Emergency Braking Test Protocol* (Version II).
    - Siddiqui, 2020, *Empirical Study of the Braking Performance of Pedestrian Autonomous Emergency Braking* (P-AEB).
- Lateral
  - Lane Centering Assist
    - Euro-NCAP, 2018, *Test Protocol - Lane Support Systems*.
  - Lane Departure Warning
    - SAE International,J3045, 2018, *Truck and Bus Lane Departure Warning Systems Test Procedure and Minimum Performance Requirements.*
    - NHTSA, 2013b, *Lane Departure Warning System Confirmation Test and Lane Keeping Support Performance Documentation*.
  - Lane Keep Assist
    - ISO, 2020, *11270, Intelligent transport systems — Lane keeping assistance systems (LKAS) — Performance requirements and test procedures.*
    - NHTSA, 2013b. *Lane Departure Warning System Confirmation Test and Lane Keeping Support Performance Documentation.*

Longitudinal Test Procedures

Longitudinal test procedures were developed from a combination of existing ADAS test procedures: (ISO, 2018; NHTSA, 2013a; SAE International, 2017). The evaluation signals are from the VRS and internal to the FlexDAS to eliminate the need to integrate any data output from the test vehicles.

1) Parameters
    a) TTC (time-to-collision) at FCW alert and AEB activation
        i) Following distance and SV-TV speed difference
    b) Speed reduction at collision with AEB
    c) Acceleration during AEB
    d) Distance from target when stopped AEB
    e) Error from set following distance and speed during ACC
    f) Acceleration during ACC
    g) Activation time and response time to cut-in during ACC
2) Equipment
    a) VRS
    b) DAS
    c) SV
    d) Targets (target vehicle and crash vehicle)
    e) Distance measuring device (tape measure, wheel odometer)
3) Setup
    a) Prepare vehicles and VRS
        i) Check vehicle fluids and pressures
        ii) Warm up vehicles if dynamic test
        iii) Ensure VRS reading within test space
        iv) Validate stationary VRS accuracy using a different distance measuring device
    b) Capture environmental and lighting conditions
        i) Track every minute and/or record before each test segment
        ii) Avoid unwanted glare conditions
    c) Capture test track
        i) Use a VRS receiver to capture reference points of the test track
            (1) Static signs/objects
            (2) Reference points of lane lines
                (a) Straight line: minimum of once every X m
                (b) Curved line: minimum of once every X m
                (c) Broken line: include line breaks if required for evaluation
4) Procedures
    a) ***FCW*** (NHTSA, 2013a)
        i) Stopped target vehicle
            (1) Execute test on a straight road.
            (2) TV is at a complete stop.
            (3) Drive SV at a constant speed (45 mph) towards the rear of the target vehicle.

(4) Reference figure. Note: TV corresponds to the POV is the reference figure.

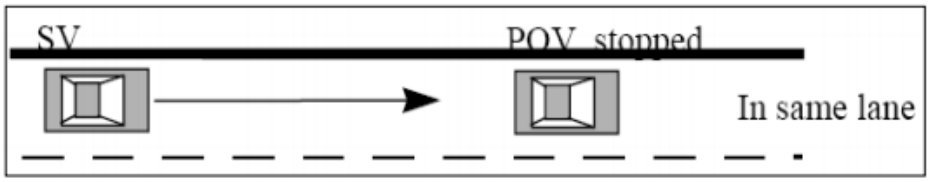

(NHTSA, 2013a)

ii) Slower target vehicle

(1) Execute test on a straight road.

(2) Target vehicle travels at a constant speed (e.g. 20 mph).

(3) Drive SV behind the target vehicle at a constant speed higher than the speed of the target vehicle (e.g. 45 mph).

(4) Reference figure. Note: target vehicle corresponds to the POV is the reference figure.

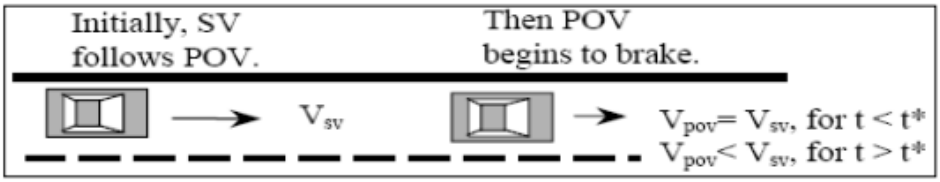

(NHTSA, 2013a)

iii) Decelerating target vehicle

(1) Execute test on a straight road.

(2) Target vehicle travels at a constant speed.

(3) Drive SV following the TV to match speed.

(4) Target vehicle starts to decelerate.

(5) Reference figure. Note: TV corresponds to the POV is the reference figure.

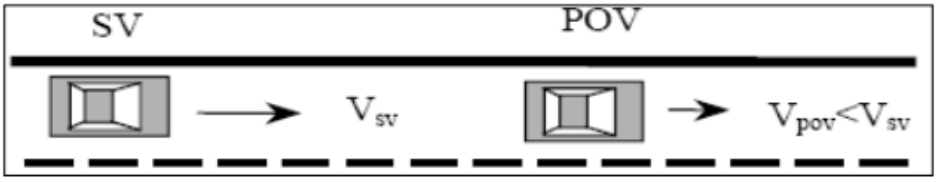

(NHTSA, 2013a)

b) ***AEB*** (NHTSA, 2013a)

i) The same procedures as those mentioned for FCW will be followed.

c) ***ACC*** (ISO, 2010)

i) Target vehicle constant speed

(1) Time gap to target vehicle procedure

(a) Execute test on a straight road (curvature less than *X* m)

(i) Drive SV and TV at constant speed, in target range of ACC and engage ACC. Increase set speed above TV speed.

(ii) The lateral displacement of the longitudinal centerline of the SV relative to the longitudinal centerline of the target vehicle shall be less than 0.5 m

ii) Target vehicle variable speed

(1) Time gap to target vehicle procedure
(a) Execute test on a straight road (curvature less than *X* m)
(i) Drive SV and TV at constant speed, in target range of ACC and engage ACC. Increase set speed to 25 percent above TV speed.
(ii) The lateral displacement of the longitudinal centerline of the SV relative to the longitudinal centerline of the target vehicle shall be less than 0.5 m.
(iii) Vary TV speed by $\pm$20 percent of target speed. Each run should consist of 3 cycles of different levels of accel/decel: e.g., low (1-2 m/s^2), medium (2-3 m/s^2), high (>3 m/s^2).

5) Evaluation
a) Baseline signal evaluation can be done for each scenario and ADAS function:
i) Metrics
(1) Standard deviation
(2) Absolute max
(3) Absolute mean
ii) Plots
(1) Time histories
(2) Histograms
(3) Power spectral density and fast Fourier transform
(4) Cross correlation
b) Function specific evaluation
i) FCW
(1) Distance at onset of warning(s)
(2) TTC for warning(s)
(a) Use the SV and TV VRS data to calculate the time to collision.
(b) $TTC = \frac{Distance_{SV-TV}}{Speed_{SV}-Speed_{TV}}, Assumes\ Heading_{SV} = Heading_{RV}$
ii) AEB
(1) Distance at onset of braking
(2) Final (stopped) distance from target
(3) TTC
(4) Speed Reduction if collision
iii) ACC
(1) Standard deviation of speed and acceleration
(2) Frequency (PSD/FFT) of speed and acceleration

Lateral Test Procedures

Lateral test procedures were based on existing ADAS test procedures: (Euro-NCAP, 2019; NHTSA, 2013b). The evaluation signals are from the VRS and internal to the FlexDAS to eliminate the need to integrate any data output from the test vehicles.

1) Parameters
   a) Lateral distance at LDW alert
   b) Lateral distance at LKA activation
   c) Acceleration during LKA
2) Equipment
   a) VRS
   b) DAS
   c) SV
   d) Distance measuring device (tape measure, wheel odometer)
3) Setup
   a) Prepare vehicles and VRS
      i) Check vehicle fluids and pressures.
      ii) Warm up vehicles if dynamic test.
      iii) Ensure VRS reading within test space.
      iv) Validate stationary VRS accuracy using a different distance measuring device.
   b) Capture environmental and lighting conditions
      i) Track every X minutes and/or record before each test segment.
      ii) Avoid unwanted glare conditions.
   c) Capture test track
      i) Use a VRS receiver to capture reference points of the test track.
         (1) Static signs/objects
         (2) Reference points of lane lines
            (a) Straight line: minimum of once every X m.
            (b) Curved line: minimum of once every X m.
            (c) Broken line: include line breaks if required for evaluation.
4) Procedures
   a) ***LDW*** (NHTSA, 2013b)
      i) Execute test on a straight road
         (1) Left lane departure
            (a) Drive SV at a constant speed parallel to left lane marker.
            (b) Driver steers the vehicle to initiate a left lane departure (with a target lateral velocity of 1.6 ft/s (0.5 m/s) with respect to the lane line).
            (c) Test different styles of roadway markings as appropriate (e.g., continuous white lines, discontinuous yellow lines, and discontinuous Botts dot raised pavement markers).
         (2) Right lane departure
            (a) Drive SV at a constant speed parallel to right lane marker.

(b) Driver steers the vehicle to initiate a right lane departure (with a target lateral velocity of 1.6 ft/s (0.5 m/s) with respect to the lane line).
(c) Test different styles of roadway markings as appropriate (e.g., continuous white lines, discontinuous yellow lines, and discontinuous Botts dot raised pavement markers).

b) ***LKA*** (NHTSA, 2013b)
   i) The same procedures as those mentioned for LDW will be followed.

5) Evaluation
   a) Baseline signal evaluation can be done for each scenario and ADAS function:
      i) Metrics
         (1) Standard deviation
         (2) Absolute max
         (3) Absolute mean
      ii) Plots
         (1) Time histories
         (2) Histograms
         (3) PSD/FFT
         (4) Cross correlation
   b) Function specific evaluation
      i) Calculate Lateral Distance:
         (1) Use the SV position data and reference lane data to calculate lateral distance between vehicle center and target lane line.
      ii) LDW
         (1) Lateral distance to lane edge at LDW alert.
      iii) LKA
         (1) Lateral distance to lane edge at LKA activation.

DOT HS 813 740
December 2025

U.S. Department
of Transportation

**National Highway
Traffic Safety
Administration**

16708-120525-v6